12th BCRRA 2026 Slovenia

12th International Conference
on the Bearing Capacity of Roads, Railways and Airfields

LJUBLJANA, CANKARJEV DOM, 22–24 JUNE 2026

BOOK OF EXTENDED ABSTRACTS

ORGANISERS

DRI
DRI, Investment Management Ltd.

ZAG
SLOVENIAN NATIONAL BUILDING AND CIVIL ENGINEERING INSTITUTE

DRC
ROAD AND TRANSPORTATION RESEARCH ASSOCIATION OF SLOVENIA

UNIVERSITY OF LJUBLJANA | FGG Faculty of Civil and Geodetic Engineering

IN COOPERATION WITH

IZS

12th BCRRA 2026
Slovenia

12th International Conference
on the Bearing Capacity of Roads,
Railways and Airfields

22–24 JUNE 2026, LJUBLJANA ▪ CANKARJEV DOM ▪ SLOVENIA

BOOK OF EXTENDED ABSTRACTS

DRAFT VERSION,
REUSE NOT ALLOWED

EDITED BY
Doron Hekič
Suzana Svetličič
Aleš Žnidarič

LJUBLJANA, SLOVENIA, 2026

Book of Extended Abstracts

12th International Conference on the Bearing Capacity of Roads, Railways and Airfields

Ljubljana, Cankarjev dom, Slovenia ▪ 22–24 June 2026

EDITED BY
dr. Doron Hekič, Suzana Svetličič, dr. Aleš Žnidarič

PUBLISHED BY
Slovenian National Building and Civil Engineering Institute
DRI Investment Management, Ltd.
Ljubljana, Slovenia, 2026

CONFERENCE ORGANIZERS
DRI Investment Management, Ltd.
Slovenian National Building and Civil Engineering Institute
University of Ljubljana, Faculty of Civil and Geodetic Engineering
DRC, Road and Transportation Research Association of Slovenia, Ltd.
in cooperation with IZS, Slovenian Chamber of Engineers

UNDER THE PATRONAGE OF
Ministry of Infrastructure of the Republic of Slovenia
Forum of European National Highway Research Laboratories (FEHRL)

WITH THE SUPPORT OF
The City of Ljubljana

REVIEWED BY
The 12th BCRRA International Scientific Committee

FRONT MATTER DESIGN LAYOUT BY
Sonja Eržen (Studio Aleja)

EDITORIAL SUPPORT BY
Lucija Nared, Metka Ljubešek, dr. Mateja Košir, Klemen Klemenčič

Foreword

Dear Readers,

We are pleased to present this book of extended abstracts from the 12th International Conference on Bearing Capacity of Roads, Railways, and Airfields (12th BCRRA 2026), held in Ljubljana, Slovenia, from 22 to 24 June 2026. Alongside the full-length contributions, the conference welcomed a large number of extended abstracts, allowing researchers and practitioners to share work in progress, focused findings, and practical experiences in a more concise format. This volume gathers the 51 extended abstracts that were presented at the conference and accepted for publication, complementing the full papers selected for the dedicated special issue of Transportation Research Procedia.

Each extended abstract was subjected to peer review by the International Scientific Committee, ensuring the scientific quality of the contributions. Although more concise than the full-length contributions, they span the full breadth of the conference and were delivered as both oral and poster presentations by authors from more than twenty countries across Europe, North America, Asia, Africa and Oceania, reflecting the international character of the BCRRA community.

The extended abstracts are organised into groups reflecting the same major thematic areas that structure the conference, allowing readers to navigate the two volumes in parallel.

The first group, with five contributions, addresses subgrade soils, unbound granular materials, and geotechnical considerations, presenting work on the resilient behaviour of crushable marginal subgrades, the integration of soil compaction and bearing-capacity characterisation, subgrade optimisation for transport infrastructure, discrete-element analysis of unbound granular response, and the use of geotechnical asset data to enhance road-network resilience.

The second group, comprising ten abstracts on asphalt and concrete materials, covers the technical evaluation of wearing-course layers, an alternative approach to low-temperature behaviour, balanced design tested in the field, fracture characterisation using cored Brazil-disk geometry, practical experiences with warm-mix asphalt, low-temperature cracking potential, rheological behaviour, recycled asphalt mixtures across laboratory, plant, and field, and durability questions for concrete pavements, including sustainable concrete with manganese steel slag and corrosion development on dowel bars.

The third group, with three abstracts on structural design methods, features VegDim, a digital system for pavement design and analysis, macro- and microscopic dynamic responses of coupled train-track systems, and advances in mechanistic-empirical design using AASHTOWare Pavement ME.

The fourth group, with five abstracts on in situ evaluation and performance prediction, presents numerical investigations of the influence of curve radius, monitoring of the behaviour of full-scale pavements under load, random-vibration analysis of three-dimensional high-speed track, monitoring of railway structures with bituminous layers, and risk assessment of rockfall events.

The fifth group, with two abstracts on recycled materials and technologies, examines fracture, cracking, and self-healing mechanisms of cement-treated materials and green mixtures for backfilling trenches beneath trafficable surfaces.

The sixth group, comprising five abstracts on rehabilitation and maintenance, addresses GPR-based railway ballast monitoring, improvement of the bearing capacity of pavements, quantitative prediction of ballast particle abrasion, a damaged-moduli approach within the MEPDG, and the assessment of structural reserves under the ACR–PCR framework.

The seventh and largest group, with ten abstracts, focuses on the measurement of traffic loading and the evaluation of deflection, including Falling Weight Deflectometer (FWD) applications and deflection at road traffic speed. The contributions span the evaluation of real traffic loading, seasonal load spectra, precision analyses of deflection measurements in FWD proficiency tests, the influence of moisture content on light-weight deflectometer results, temperature-correction sensitivity, the evaluation of visco-elastic behaviour, load-deflection linearity, global initiatives to advance deflection testing, and outcomes from the EU FWD Users Group and the DaRTS initiative on deflection at road traffic speed.

The eighth group, with two abstracts on climate change and infrastructure resilience, considers real-time rockfall monitoring for street safety using pulse-Doppler radar and the impact of wetting and drying cycles associated with climate change on pavement behaviour.

The ninth group, with four abstracts on intelligent construction, big data, and artificial intelligence, demonstrates how a Markov decision process for GPR-optimised assessment, the analysis of thermal data collected during accelerated pavement testing, improved pavement structural assessment with advanced data tools, and the domain adaptation of modern large language models are increasingly shaping evaluation and decision-making.

Finally, the tenth group, with five abstracts on construction practices and case histories, offers practical insights from real-world projects, including the influence of reduced lateral wandering by connected and automated vehicles, main apron renovation works at Ljubljana Airport, karst phenomena and the use of BIM in tunnelling, the change in the state of defects on airport pavements, and an investigation of structural capacity and surface defects.

The Editors would like to express their sincere gratitude to all authors, reviewers, and the local organising team in Slovenia for their dedication and support. We also extend our heartfelt thanks to the sponsors, supporters, and patrons of the conference, whose generous contributions made the event and this publication possible. We hope that these extended abstracts, complemented by the full papers in the accompanying special issue of Transportation Research Procedia, will foster continued innovation and collaboration towards resilient, sustainable transportation infrastructure.

The Editors
dr. Doron Hekič, Suzana Svetličič, dr. Aleš Žnidarič

Ljubljana, June 2026

Committees

National Organising Committee

CONFERENCE CHAIRS

- Suzana Svetličič, Conference Chair, DRI Investment Management, Ltd.
- Aleš Žnidarič, Scientific Committee Chair, Slovenian National Building and Civil Engineering Institute
- Vojkan Jovičić, Scientific Committee Co-Chair, University of Ljubljana, Faculty of Civil and Geodetic Engineering
- Doron Hekič, Slovenian National Building and Civil Engineering Institute

TECHNICAL COMMITTEE

- Evstahij Drmota, Chair, DRC, Road and Transportation Research Association of Slovenia, Ltd.
- Matija Mavrič, Co-Chair, Cestel
- Anja Kožuh, Cestel
- Darja Šemrov, University of Ljubljana, Faculty of Civil and Geodetic Engineering
- Sara Žerko, Cestel
- Sonja Eržen, Studio Aleja
- Uroš Parazajda, Parsis

International Advisory Committee – IAC BCRRA

- Albert Lau, Norwegian University of Science and Technology, Norway
- Alessandra Bianchini, United States Air Force, USA
- Aleš Žnidarič, Slovenian National Building and Civil Engineering Institute, Slovenia
- Andreas Loizos, National Technical University of Athens (NTUA), Greece
- Antonio Gomes Correia, University of Minho, Department of Civil Engineering, Portugal
- Asmus S. Kristiansen, Technical University of Denmark, Denmark
- Audrius Vaitkus, Vilnius Gediminas Technical University (VGTU), Lithuania
- Benjamin Worel, USA
- Berthe Dongmo-Engeland, Oslo Metropolitan University, Norway
- Christina Plati, National Technical University of Athens (NTUA), Greece
- Daba Gedafa, University of North Dakota (UND), USA
- David R. Brill, Federal Aviation Administration, USA
- Ephrem Taddesse, Norwegian Public Roads Administration, Norway
- Erol Tutumluer, University of Illinois at Urbana-Champaign, USA
- Gabrielle Tebaldi, University of Parma, Italy
- Greg White, University of the Sunshine Coast (USC), Australia
- Helge Mork, Norwegian University of Science and Technology, Norway
- Imad L. Al-Qadi, Illinois Center for Transportation, USA
- Inge Hoff, Norwegian University of Science and Technology, Norway
- James Maina, University of Pretoria, South Africa
- Jean-Pascal Bilodeau, Université Laval, Quebec, Canada
- Kjell Arne Skoglund, Statens vegvesen, Norwegian Public Roads Administration, Norway
- Leif Bakløkk, Statens vegvesen, Norwegian Public Roads Administration, Norway
- Lisa T. Hannasvik, Vianova, Norway
- Liu Gang, Wuhan University of Technology (WHUT), China
- Nadarajah Sivaneswaran, U.S. Department of Transportation (DOT), USA
- Pauli Kolisoja, Tampere University of Technology, Finland
- Pierre Hornych, Gustave Eiffel University, France
- Rabbira Saba, Statens vegvesen, Norwegian Public Roads Administration, Norway
- Rolf Dollevoet, Delft University of Technology (TU Delft), The Netherlands
- Sabine Leischner, Technische Universität Dresden, Germany
- Sigurdur Erlingsson, University of Iceland, Iceland
- Silvia Caro, Universidad de los Andes, Colombia
- Suzana Svetličič, DRI Investment Management, Ltd., Slovenia
- Ted Sussmann, University of Hartford, USA
- Tom Scarpas, Delft University of Technology (TU Delft), The Netherlands
- Tomas Winnerholt, Trafikverket, Swedish Transport Administration, Sweden
- Wu Shaopeng, Wuhan University of Technology, China
- Xinglong Wang

International Scientific Committee

- Gordon Airey, The University of Nottingham, United Kingdom
- Jostein Aksnes, Norwegian Public Roads Administration, Norway
- Imad Al-Qadi, Illinois Center for Transportation, UIUC, USA
- Andrej Anžlin, Slovenian National Building and Civil Engineering Institute, Slovenia
- Angeliki Armeni, National Technical University of Athens, Greece
- Joralf Aurstad, Norwegian Public Roads Administration, Norway
- Robert Braber, Infralab SA, Switzerland
- Francesco Canestrari, Università Politecnica delle Marche, Italy
- Jorge Carnerero Manzano, Transport Research Centre, CEDEX, Spain
- Silvia Caro, Universidad de los Andes, Colombia
- Jorge Carvalho Pais, University of Minho, Portugal
- George Chang, The Transtec Group, USA
- Asmus Christiansen, Technical University of Denmark, Denmark
- Erdem Coleri, Oregon State University, USA
- Felipe Collazos Arias, PIARC, Spain
- Marko Čičković, Fraport AG, Germany
- Herve Di Benedetto, University of Lyon ENTPE, France
- Josipa Domitrović, University of Zagreb, Faculty of Civil Engineering, Croatia
- Nikos Economou, Technical University of Crete, Greece
- Sigurdur Erlingsson, University of Iceland & VTI, Iceland
- Karmen Fifer Bizjak, Slovenian National Building and Civil Engineering Institute, Slovenia
- Simona Fontul, National Laboratory for Civil Engineering (LNEC), Portugal
- Eduardo Fortunato, National Laboratory for Civil Engineering (LNEC), Portugal
- Navneet Garg, Federal Aviation Administration (FAA), USA
- Konstantina Georgouli, University of Peloponnese, Greece
- Konstantinos Gkyrtis, Democritus University of Thrace (DUTh), Greece
- Antonio Gomes Correia, University of Minho, Portugal
- Neža Gošte, Slovenian National Building and Civil Engineering Institute, Slovenia
- Elie Hajj, University of Nevada Reno, USA
- Araz Hasheminezhad, Iowa State University, USA
- Doron Hekič, Slovenian National Building and Civil Engineering Institute, Slovenia
- Inge Hoff, Norwegian University of Science and Technology, Norway
- Pierre Hornych, Gustave Eiffel University, France
- Amine Ihamouten, Gustave Eiffel University, France
- Tatsuya Ishikawa, Hokkaido University, Japan
- Sean Jamieson, University of the Sunshine Coast, Australia
- Dirk Jansen, Federal Highway and Transport Research Institute (BASt), Germany
- Sanja Jocković, University of Belgrade, Faculty of Civil Engineering, Serbia
- Milorad Jovanovski, Macedonian Association for Geotechnics, Macedonia
- Vojkan Jovičić, University of Ljubljana, Faculty of Civil and Geodetic Engineering, Slovenia
- Mitja Jurgele, DRI Investment Management, Ltd.
- Wynand JvdM Steyn, University of Pretoria, South Africa
- Mehdi Kalantari, Federal Highway and Transport Research Institute (BASt), Germany
- Edina Koch, Széchenyi István University, Hungary
- Darko Kokot, Slovenian National Building and Civil Engineering Institute, Slovenia
- Pauli Kolisoja, Tampere University, Finland
- Mirko Kosič, Slovenian National Building and Civil Engineering Institute, Slovenia
- Maja Kreslin, Slovenian National Building and Civil Engineering Institute, Slovenia

- Claudio Lantieri, University of Bologna, Italy
- Albert Lau, Norwegian University of Science and Technology, Norway
- Sabine Leischner, TU Dresden, Germany
- Paulina Leiva-Padilla, ESTP, France
- Stanislav Lenart, Slovenian National Building and Civil Engineering Institute, Slovenia
- Peter Lipar, University of Ljubljana, Faculty of Civil and Geodetic Engineering, Slovenia
- Janko Logar, University of Ljubljana, Faculty of Civil and Geodetic Engineering, Slovenia
- Andreas Loizos, National Technical University of Athens (NTUA), Greece
- James Maina, University of Pretoria, South Africa
- Evangelos Manthos, Aristotle University of Thessaloniki, Greece
- Andre Martinez Costa, Infraestruturas de Portugal, Portugal
- Pavlo Maruschak, Ternopil Ivan Puluj National Technical University, Ukraine
- Alenka Mauko Pranjić, Slovenian National Building and Civil Engineering Institute, Slovenia
- Yusuf Mehta, Rowan University, USA
- Miomir Miljković, Slovenian National Building and Civil Engineering Institute, Slovenia
- Goran Mladenović, University of Belgrade, Faculty of Civil Engineering, Serbia
- Yoshitsugu Momoya, Railway Technical Research Institute, Japan
- Helge Mork, Norwegian University of Science and Technology, Norway
- Soheil Nazarian, University of Texas at El Paso, USA
- José Neves, University of Lisbon, Portugal
- Primož Oprčkal, Slovenian National Building and Civil Engineering Institute, Slovenia
- Michael P. Wistuba, TU Braunschweig, Germany
- Jovan Papić, Ss. Cyril and Methodius University in Skopje, North Macedonia
- Jean Pascal Bilodeau, Université Laval, Canada
- Marco Pasetto, University of Padova, Italy
- Margherita Pazzini, University of Bologna, Italy
- Andrei Petriaev, Emperor Alexander I St. Petersburg State Transport University, Russia
- Christina Plati, National Technical University of Athens (NTUA), Greece
- Filippo Pratico, Mediterranean University of Reggio Calabria, Italy
- David R. Brill, Federal Aviation Administration, USA
- Christiane Raab, EMPA, Switzerland
- Marko Renčelj, University of Maribor, Slovenia
- Robert Rijavec, Faculty of Civil and Geodetic Engineering, University of Ljubljana (UL FGG), Slovenia
- Lidija Ržek, Slovenian National Building and Civil Engineering Institute, Slovenia
- Rabbira Saba, Norwegian Public Roads Administration, Norway
- Mofreh Saleh, University of Canterbury, New Zealand
- Elena Scibilia, Norwegian University of Science and Technology, Norway
- Jean-Michel Simonin, Gustave Eiffel University, France
- Nadarajah Sivaneswaran, US Department of Transportation (DOT), USA
- Pahirangan Sivapatham, Bergische University of Wuppertal, Germany
- Brynhild Snilsberg, Norwegian Public Roads Administration, Norway
- Even Sund, Norwegian Public Roads Administration, Norway
- Ted Sussmann, University of Hartford, USA
- Suzana Svetličič, DRI Investment Management, Ltd., Slovenia
- Aljoša Šajna, Slovenian National Building and Civil Engineering Institute, Slovenia
- Darja Šemrov, University of Ljubljana, Faculty of Civil and Geodetic Engineering, Slovenia
- Lisa T. Hannasvik, Vianova, Norway
- Nader Tabatabaee, Sharif University of Technology, Iran
- Ephrem Taddesse, Norwegian Public Roads Administration, Norway
- Gabrielle Tebaldi, University of Parma, Italy

- Serdal Terzi, Suleyman Demirel University, Turkey
- Fabio Tosti, University of West London, United Kingdom
- Erol Tutumluer, University of Illinois at Urbana-Champaign, USA
- Shane Underwood, North Carolina State University, USA
- Carl Van Geem, Belgian Road Research Centre, Belgium
- Christ Van Gurp, Weetvanwegen, The Netherlands
- Julio Vaquero, Transport Research Centre, CEDEX, Spain
- Rok Vezočnik, Slovenian National Building and Civil Engineering Institute, Slovenia
- Greg White, University of the Sunshine Coast (USC), Australia
- Tomas Winnerholt, Trafikverket, Swedish Transport Administration, Sweden
- Mike Winter, Mike Winter Associates Limited, UK
- Martin Wiström, Ramboll Sweden AB, Sweden
- Benjamin Worel, Minnesota Department of Transportation (MnDOT), USA
- Yuanjie Xiao, Central South University, China
- George Yannis, National Technical University of Athens, Greece
- Sonja Zlatović, Croatian Geotechnical Society, Croatia
- Adam Zofka, Vilnius Gediminas Technical University (VGTU), Lithuania
- Aleš Žnidarič, Slovenian National Building and Civil Engineering Institute, Slovenia

Organisers

DRI
DRI, Investment Management Ltd.

ZAG
SLOVENIAN NATIONAL BUILDING AND CIVIL ENGINEERING INSTITUTE

DRC
ROAD AND TRANSPORTATION RESEARCH ASSOCIATION OF SLOVENIA

UNIVERSITY OF LJUBLJANA
FGG
Faculty of Civil and Geodetic Engineering

IN COOPERATION WITH

I Z S
INŽENIRSKA ZBORNICA SLOVENIJE

UNDER THE PATRONAGE OF

REPUBLIKA SLOVENIJA
MINISTRSTVO ZA INFRASTRUKTURO IN ENERGETIKO

FEHRL

WITH THE SUPPORT OF

Sponsors

DRI
DRI, Investment Management Ltd.

ZAG
SLOVENIAN NATIONAL BUILDING AND CIVIL ENGINEERING INSTITUTE

CESTEL

Ljubljana
Ljubljana Tourism
Konzorcij KUL

Alpacem

IRGO Consulting d.o.o.

KASKADER
ZAHTEVNA TERENSKA DELA d.o.o.

Rincent
ND TECHNOLOGIES

Table of contents

Evaluating the resilient behaviour of crushable marginal subgrade soil

Samuel Kingangai
Tatsuya Ishikawa
Faculty of Engineering, Hokkaido University, Kita 13, Nishi 8, Kita-Ku, Sapporo 060-8628, Japan
Tetsuya Tokoro
Faculty of Engineering, Hokkai-Gakuen University, 1-1, Minami 26, Nishi 11, Chuo-ku, Sapporo 064-0926, Japan

Abstract

Marginal soils, particularly volcanic soils, cover approximately 40% of Hokkaido, Japan. These volcanic soils are considered problematic soils as they exhibit markedly different behaviour from other soils resulting from their microstructure, developed during their geological formation. This study aims to make a contribution to the understanding of volcanic soils and practical design of pavements built on marginal subgrade soils. The Resilient Modulus (Mr) has been proven to be a fundamental mechanical property for assessing, and predicting pavement deterioration. However, most existing studies of the resilient modulus do not account for the influence of particle crushing. In this study, a series of resilient modulus (Mr) tests were conducted on crushable volcanic coarse-grained soil, in various water content and wheel loading conditions. Furthermore, the test results were fitted by predictive models to verify the applicability and to identify an appropriate method for predicting the resilient modulus of crushable marginal subgrade soil under different conditions.

Keywords: volcanic soils; resilient modulus; particle crushing; marginal subgrade soils; pavement design

1 Introduction

Mechanistic-Empirical Pavement Design Guide (AASHTO, 2008) adopted the Universal Model for predicting M_r under different stress conditions. However, the universal model does not factor in the effects of moisture content on the stiffness of the pavement. Ng et al. (2013) solved this drawback by treating the soil suction (ψ) as one of the stress tensors and proposed a model using cyclic deviator stress (q_{cyc}) and mean stress (σ_{net}). However, in order to maintain consistency with AASHTO's Universal Model, Ng's model can be modified to incorporate the octahedral shear stress (τ_{oct}) as shown below;

$$M_r = k_1 p_a \left(\frac{\theta}{p_a}\right)^{k_2} \left(\frac{\tau_{oct}}{p_a} + 1\right)^{k_3} \left(\frac{\psi}{\sigma_{net}} + 1\right)^{k_4},$$

Where:

- $\mathrm{k_1}$, $\mathrm{k_2}$, $\mathrm{k_3}$ and $\mathrm{k_4}$ – regression parameters;
- θ – bulk stress = $\sigma_1 + \sigma_2 + \sigma_3$;
- σ_1, σ_2, and σ_3 - major, intermediate, and minor principal stress respectively;
- τ_{oct} – octahedral shear stress = $\frac{1}{3}\sqrt{(\sigma_1 - \sigma_2)^2 + (\sigma_1 - \sigma_3)^2 + (\sigma_2 - \sigma_3)^2}$;
- $\mathrm{p_a}$ - atmospheric pressure (set as 101 kPa in this study);
- σ_{net} - net mean stress, defined as ($\frac{\theta}{3} - \mathrm{u_a}$).

In this study, a series of resilient modulus (M_r) tests were conducted on a crushable volcanic coarse-grained soil and non-crushable Japanese standard sand, in various water content and wheel loading conditions; the test results were analysed and fitted by regression analysis using Ng's model. The objective of this study was to improve the understanding on the mechanical characteristics of unsaturated crushable marginal subgrade soil during cyclic loading.

2 Material and Testing Method

2.1 Test Material

Table 1 below summarises the soil properties of the two types of soils utilised in this study: Japanese standard sand, Toyoura sand and subgrade soil sampled from Komaoka district, Hokkaido, Japan.

***Table 1**: Komaoka soil properties.*

Material	Soil Classification (ASTM)	Soil particle density (g/cm³)	Max dry density (g/cm³)	Opt. water content (%)	Mean Size (mm)
Komaoka soil	Silty Sand with gravel (SM)	2.512	1.06	40.5	0.30
Toyoura sand	Poorly graded sand (SP)	2.650	1.63	14.0	0.18

2.2 Testing Method

A cylindrical specimen with a 70mm Diameter by 170mm Height was prepared with a target dry density ≥ 95% of Maximum Dry Density to satisfy the quality control of the subgrade layer in asphalt pavement (Japan Road Association, 2006). The resilient modulus (M_r) tests conducted in this study are based on AASHTO 307-99 (AASHTO, 2008), with slight modification due to the limitation of the test equipment employed as explained by Lin et al. (2022). Influence of water content on the stiffness of the subgrade is investigated by comparing results of fully Saturated Test ('S-Test') to Unsaturated Test ('U-Test'), whereby a matric suction (ψ) is introduced to simulate suction at the subgrade soil surface during U-Test. Matric suction of 3.75 kPa is applied to Toyoura while 5kPa is applied to Komaoka soil to simulate the field condition. The influence of wheel loading conditions was considered based on the stress transmitted to the surface of the subgrade by a standard 49-KN wheel load on a typical pavement structure in the Japanese design guide (Japan Road Association, 2006). During Saturated Wheel Load Test ('SW-Test') and Unsaturated Wheel Load Test ('UW-Test) the loading frequency and waveform were the same as in the resilient modulus (M_r) test, and the loading number was 1,000 cycles. Sieve analysis was performed with due care after each test to determine the extent of particle breakage. The increment of fines content (ΔF_c) was utilised as the indicator of the degree of particle breakage induced from the cyclic loading process (Miura & Yagi, 1997).

3 Test Results and Discussion

As shown in Figure 1(a), resilient modulus (M_r) increases with the increment of the effective confining pressure (σ_c) while decreases with the increment of the deviator stress *(q)*. The test results were fitted to Ng's model and the regression parameters summarised in Table 2.

Table 2: *Regression analysis results.*

Regression Parameter	Komaoka Soil				Toyoura Sand			
	S-Test	U-Test	SW-Test	UW-Test	S-Test	U-Test	SW-Test	UW-Test
k_1	0.562	0.118	0.895	1.465	1.657	2.089	0.615	1.75
k_2	1.039	1.318	0.951	0.918	1.070	1.057	1.249	1.088
k_3	-2.800	-2.101	-2.437	-2.869	-5.661	-4.437	-6.304	-4.916
k_4	1.000	3.411	1.000	-0.396	1.000	1.692	1.000	3.639
R^2	0.9891	0.999	0.994	0.991	0.956	0.948	0.866	0.905

The matric suction (ψ) induces an apparent cohesion between the soil particles resulting in a positive influence of on the resilient characteristics of the subgrade. Therefore, increase in moisture content greatly degrades the subgrade layer stiffness resulting in larger permanent strains. Figure 1(b), shows that during the first few cycles of loading, there was accelerated plastic deformation in Komaoka soil as compared to Toyoura sand due to particle breakage and restructuring of the particles. Although the permanent axial strain of Komaoka increases with the increment of the number of loading cycles in the initial stages, the increasing rate converges to a constant in the later stage of the test. Figure 1(c), shows that at the final stages of the wheel loading process there was a significant decrease in the resilient modulus of Toyoura sand indicating the increase in cyclic loading resulted in greater permanent strains in Toyoura, particularly in saturated conditions. Whereas Komaoka soil attained a stable structure to resist further deformation during wheel loading.

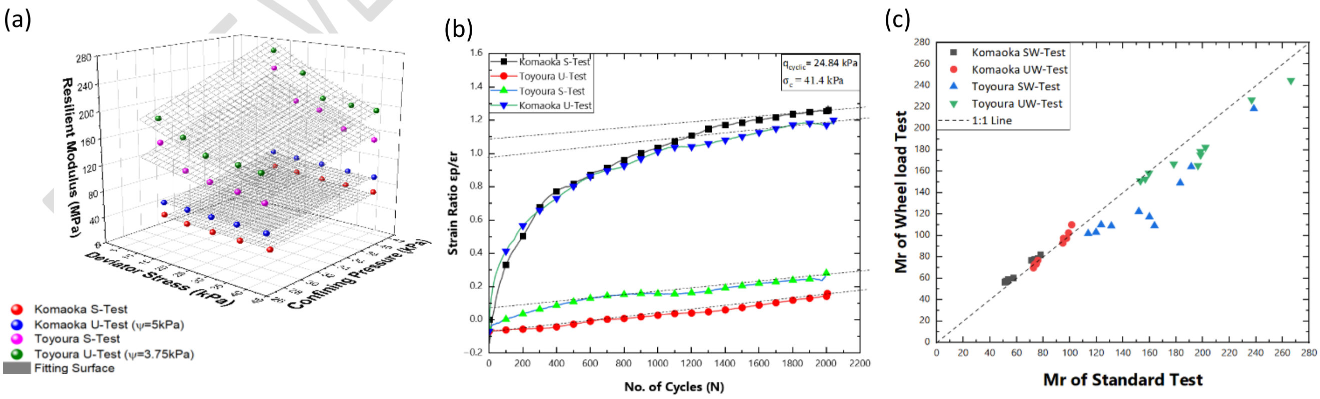

Figure 1: *(a) Influence of water content on resilient modulus (b) Change in permanent axial strain to resilient strain ratio ($\varepsilon_p/\varepsilon_r$) with increase in number of loading cycles (c) Influence of wheel loading on resilient modulus of subgrade soil.*

Moreover, as captured in Figure 2, saturated conditions soften the soil grains allowing for greater amount of abrasion of the grain edges to occur in crushable marginal subgrade soil. The SW-Tests registered the highest degree of particle breakage, since more energy is imparted by cyclic loading which triggered more particle degradation during wheel loading until a stable structure is attained.

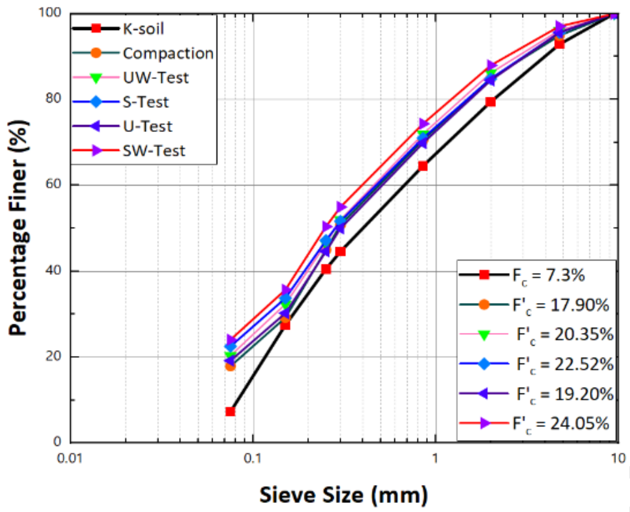

Figure 2: *Sieve Analysis results after Mr Tests.*

4 Conclusions

This study demonstrates that, although the crushable volcanic soil exhibited large deformations during the initial stages of cyclic, the soil structure gradually stabilized, reducing the long-term influence of wheel loading on resilient modulus. Future research should investigate the progressive accumulation of particle breakage during different stages of cyclic loading, rather than only pre- and post-test conditions. Additionally, development and validation of cyclic constitutive models that factor in particle crushing will allow for more reliable predictions of resilient behaviour of pavements built on crushable subgrade soils.

5 References

AASHTO. 2008. Mechanistic-empirical pavement design guide: A manual of practice. AASHTO, ISBN: 978-1-56051-423-7.

Japan Road Association. 2006. Pavement Design Manual. Maruzen Publishing. Japan Road Association, Tokyo.

Lin, T., Ishikawa, T., Yang, J., & Tokoro, T. 2022. Evaluation of climate effect on resilient modulus of granular subgrade material. Cold Regions Science and Technology, 194.

Miura, S., & Yagi, K. 1997. Particle breakage of volcanic coarse-grained soils and its evaluation. Society of Civil Engineers Paper, 1997(561), 257–269.

Ng, C. W. W., Zhou, C., Yuan, Q., & Xu, J. 2013. Resilient modulus of unsaturated subgrade soil: Experimental and theoretical investigations. Canadian Geotechnical Journal, 50(2).

Integrating soil compaction and bearing capacity characterization through a new laboratory-based approach

Samuel Valencia-Díaz
Departamento de Ingeniería Civil, Universidad de Las Palmas de Gran Canaria (ULPGC), Campus de Tafira, 35017 Las Palmas de Gran Canaria, Spain.
Jacob D. R. Bordón
Instituto Universitario de Sistemas Inteligentes y Aplicaciones Numéricas en Ingeniería, Universidad de Las Palmas de Gran Canaria (ULPGC), Campus de Tafira, 35017 Las Palmas de Gran Canaria, Spain.
Jorge Yepes
Departamento de Ingeniería Civil – IOCAG, Universidad de Las Palmas de Gran Canaria (ULPGC), Campus de Tafira, 35017 Las Palmas de Gran Canaria, Spain.
Juan J. Aznárez
Instituto Universitario de Sistemas Inteligentes y Aplicaciones Numéricas en Ingeniería, Universidad de Las Palmas de Gran Canaria (ULPGC), Campus de Tafira, 35017 Las Palmas de Gran Canaria, Spain.
Miguel A. Franesqui
Grupo de Fabricación Integrada y Avanzada – Departamento de Ingeniería Civil, Universidad de Las Palmas de Gran Canaria (ULPGC), Campus de Tafira, 35017 Las Palmas de Gran Canaria, Spain.

Abstract

Transportation infrastructure requires the use of large quantities of compacted geomaterials, resulting in significant economic and environmental impacts that must be considered throughout all stages of a project. A novel laboratory procedure is proposed for assessing the stiffness of embankments, capping layers, unbound base courses, and subbase layers. The use of well-established and simple testing equipment enables a practical and cost-effective methodology that combines the compaction procedure of the Modified Proctor test with the loading scheme of a repeated static plate load test, adapted to the reduced geometry of the newly developed miniature Plate Load Test (mPLT). This approach allows both compaction characteristics and the vertical deformation modulus to be determined within a single test.

Subsequently, the elastic modulus required for analytical pavement design is obtained through back-calculation using a numerical model. Soil specimens were tested under varying gradations, compaction energies, and moisture contents to develop regression surfaces relating the investigated variables. Furthermore, the laboratory deformation modulus obtained from the mPLT was compared with full-scale static plate load tests conducted in the field.

The results indicate that this methodology has the potential to become an important reference test for supporting both the design and quality control of compacted embankments and pavement foundation layers in transportation engineering applications.

Keywords: soil strain modulus, soil bearing capacity, compacted fill, subgrade design, laboratory test

1 Introduction

Transport infrastructure relies heavily on compacted geomaterials for embankments, subgrades, and pavement granular layers, often representing a substantial portion of construction costs and environmental impact. Accurate prediction of the stiffness and bearing capacity is therefore essential for design optimisation. Modern pavement design increasingly follows a Mechanistic-Empirical framework, combining analytical modelling with experimentally derived material properties. However, estimating elastic parameters remains challenging due to the complex interactions among moisture content, dry density, degree of saturation, and soil structure, particularly in partially saturated granular fills (Tatsuoka et al., 2021; Latimer et al., 2023). Existing laboratory and field tests such as cyclic triaxial tests and static plate load tests (PLT) are time-consuming, costly, and difficult to perform. These limitations highlight the need for simpler, faster, and more economical procedures capable of capturing the influence of soil state variables on stiffness while providing parameters suitable for analytical pavement design.

2 Materials and Methods

2.1 Materials and laboratory testing

Volcanic geomaterials from a construction site in Gran Canaria (Canary Islands, Spain) were processed into four gradations (García-González et al., 2020) with maximum size of 20 mm. A total of 92 miniature plate load tests (mPLT) were performed. This novel laboratory test method integrates the compaction stage of a Modified Proctor (MP) test with a reduced-scale repetitive static loading sequence following PLT procedure. Specimens were compacted at five compaction energies (25-125% of MP effort) and moisture contents between 2% and 12%, then loaded using a 50 mm CBR piston. First and second cycle strain moduli (E_{mPLT1}, E_{mPLT2}) and the k-ratio ($k = E_{mPLT2} / E_{mPLT1}$) were computed from secant stiffnesses between 30% and 70% of the applied stress. Moisture content and dry density were determined immediately after testing.

2.2 Numerical model

Because the mPLT is performed within a rigid mould, a numerical model was developed to quantify confinement effects and relate E_{mPLT2} to the Young's modulus (E) required for analytical design. A linear-elastic boundary element model was implemented using MultiFEBE (Bordón et al., 2022) and Gmsh© along with MATLAB codes. Boundary conditions reproduced the physical test configuration. Numerical simulations enabled the derivation of a dimensionless function dependent on Poisson's ratio and an analytical expression linking E_{mPLT2} to Young's modulus (E), accounting for geometric and boundary-condition differences between the mPLT and the standard PLT (Adam at al., 2009).

3 Results and Discussion

3.1 Statistical analysis

Correlation analysis showed that moisture content and degree of saturation exert the strongest influence on the EmPLT2 strain modulus, whereas dry density and void ratio exhibit weaker and more complex relationships due to coupling effects (Pacheco and Nazarian, 2011). Kruskal-Wallis testing demonstrated that compaction energy significantly affects dry density, void ratio, and strain modulus.

3.2 Relations between stiffness and state properties: geometrical interpretation of mPLT surfaces

E_{mPLT2} correlates strongly with moisture content and saturation ratio, following parabolic trends associated with capillary suction loss at very low and very high moisture contents (MC). No clear direct relationship between E_{mPLT2} and dry density (DD) or void ratio is observed in two-dimensional plots, but meaningful patterns emerge when data are analysed in a three-dimensional MC-DD-E_{mPLT2} space.

Polynomial regression surfaces were generated to represent E_{mPLT2} and k-ratio as functions of moisture content and dry density as shown in Figure 1 for a natural soil of maximum size 20 mm. These surfaces show increasing stiffness and decreasing k-ratio toward the theoretical maximum dry density and reveals that for a given soil and compaction energy, both the maximum strain modulus and the minimum k-ratio occur at specific moisture-density states located on the dry side of the Modified Proctor curve. These surfaces provide a practical tool for identifying stiffness trends and selecting state conditions that optimise modulus values for design.

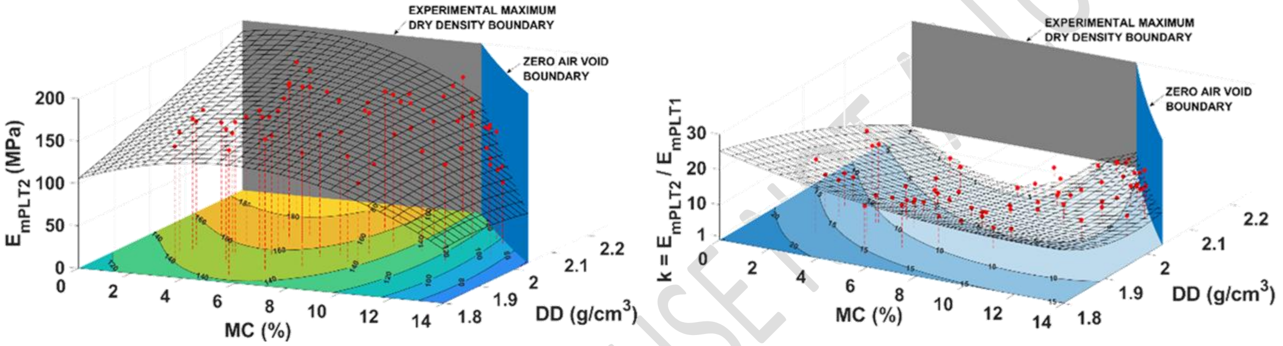

(a) (b)

***Figure 1**: mPLT surfaces. **(a)** E_{mPLT2} – MC – DD surface and boundaries; **(b)** k-ratio – MC – DD surface and boundaries.*

3.3 Correlation between laboratory and field strain modulus

Field static PLTs performed on an embankment built with the same material validated the laboratory method. Using field moisture and density conditions, corresponding E_{mPLT2} values were obtained from the regression surface. A strong linear correlation was found between laboratory E_{mPLT2} and field E_{v2}, consistent with previous PLT-CBR-modulus relationships (Plati and Tsakoumaki, 2023). Laboratory values were slightly higher due to mould confinement effects partially offset using half-space theory in modulus calculation.

3.4 Practical application

The proposed methodology can be applied during design by: (1) performing an MP test for each soil; (2) conducting an mPLT on each specimen to obtain E_{mPLT2} for the corresponding DD-MC pair; (3) selecting a design modulus from the specification-compliant DD-MC domain while verifying k-ratio limits; and (4) converting E_{mPLT2} to design Young's modulus (E) using the derived analytical expression (Figure 2). The mPLT can also support construction quality control by identifying moisture ranges that simultaneously satisfy stiffness, k-ratio, and density requirements.

4 Conclusions

The mPLT provides a simple, low-cost method to obtain moisture content, dry density, and strain modulus relationships in a single test, capturing the coupled influence of state variables on stiffness. Stiffness increases and k-ratio decreases toward the theoretical maximum dry density and the maximum modulus and minimum k-ratio occur always on the dry side of the Proctor curve. The numerical model enables conversion of laboratory strain modulus to Young's modulus for analytical pavement design.

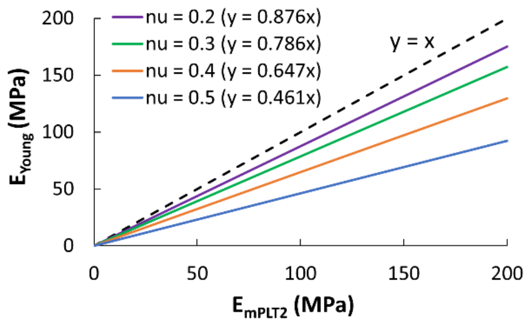

***Figure 2**: Young's modulus vs. E_{mPLT2} from the numerical modelling for various Poisson's ratios.*

The strong correlation observed between laboratory and field moduli highlights the practical applicability of the proposed method. This approach represents a valuable tool for both the design and quality control of compacted geomaterials with improved performance, reduced construction costs, and lower environmental impact. For future research, it would be beneficial to extend the study to a wider range of soil types to verify whether the proposed response surfaces maintain the global trends identified here. Additionally, comparing the outcomes of this new laboratory test with those obtained from traditional methods —such as the California Bearing Ratio (CBR) and cyclic triaxial tests— would provide further insight into its relative performance and potential advantages.

5 References

Adam, C., Adam, D., Kopf, F., & Paulmichl, I. 2009. Computational validation of static and dynamic plate load testing. Acta Geotechnica, 4, 35-55.

Bordón, J. D., Álamo, G. M., Padrón, L. A., Aznárez, J. J., & Maeso, O. 2022. MultiFEBE: A multi-domain finite element–boundary element solver for linear mixed-dimensional mechanical problems. SoftwareX, 20, 101265.

García-González, C., Yepes, J., Franesqui, M. A. 2020. Geomechanical characterization of volcanic aggregates for paving construction applications and correlation with the rock properties. Transportation Geotechnics, 24, 100383.

Pacheco, L. G., & Nazarian, S. 2011. Impact of moisture content and density on stiffness-based acceptance of geomaterials. Transportation research record, 2212(1), 1-13.

Plati, C., & Tsakoumaki, M. 2023. A critical comparison of correlations for rapid estimation of subgrade stiffness in pavement design and construction. Construction Materials, 3(1), 127-142.

Latimer, R., Airey, D., & Tatsuoka, F. 2023. Expected stiffness changes during compaction in laboratory and field. Transportation Geotechnics, 43, 101136.

Tatsuoka, F., Hashimoto, T., Tateyama, K. 2021. Soil stiffness as a function of dry density and the degree of saturation for compaction control. Soils and Foundations 61, 989–1002.

Subgrade optimisation for transport infrastructure: a mechanistic-economic framework

Samuel Valencia-Díaz
Departamento de Ingeniería Civil, Universidad de Las Palmas de Gran Canaria (ULPGC), Campus de Tafira, 35017 Las Palmas de Gran Canaria, Spain.
Jacob D. R. Bordón
Juan J. Aznárez
Instituto Universitario de Sistemas Inteligentes y Aplicaciones Numéricas en Ingeniería, Universidad de Las Palmas de Gran Canaria (ULPGC), Campus de Tafira, 35017 Las Palmas de Gran Canaria, Spain.
Miguel A. Franesqui
Grupo de Fabricación Integrada y Avanzada – Departamento de Ingeniería Civil, Universidad de Las Palmas de Gran Canaria (ULPGC), Campus de Tafira, 35017 Las Palmas de Gran Canaria, Spain.

Abstract

This paper presents a mechanistic–economic framework for the optimization of transportation infrastructure subgrades by integrating a deterministic mechanical solver with an explicit and traceable parametric cost formulation. Mechanical behavior is evaluated using the Boundary Element Method (BEM), in which the supporting soil is modeled as a series of compacted layers reflecting actual construction practices and quality control procedures in the field.

For natural soils, the intrinsic Young's modulus of the material is adjusted for each layer using the Dormon–Metcalf (1965) compatibility criterion, thereby accounting for the interaction between a layer and its underlying support. Stabilized soils are represented as engineered materials whose modulus is highly dependent on binder dosage and is therefore largely independent of the underlying structure.

The analysis comprises two complementary phases: a global sensitivity study based on relative costs under representative logistical conditions, and a local application conducted in accordance with Spanish standards across three design scenarios. An exhaustive search procedure is employed to map the Pareto frontier between vertical settlement and construction costs, avoiding stochastic or data-driven approaches and ensuring complete traceability of the optimization process.

The results identify optimal configurations and clarify the conditions under which stabilized alternatives become economically advantageous, thereby supporting decision-making across different transportation sectors. The framework remains adaptable to regional market conditions, as cost parameters can be updated without modifying the underlying mechanical model. Furthermore, the same mechanistic–economic logic can be extended to pavement structures, enabling integrated optimization of both foundation and pavement layers.

Keywords: subgrade optimization, pavement foundation, construction costs, multilayer systems, BEM

1 Introduction

Subgrade stiffness governs settlement, stress distribution, and long-term performance in transport infrastructure, and modern mechanistic-empirical design relies on multilayer elastic theory to represent stratified natural and stabilised soils (Burmister, 1945). Natural soils are constrained by the Dormon–Metcalf compatibility criterion (Dormon and Metcalf, 1965), while stiffness – CBR relationships support modulus assignment (Heukelom and Klomp, 1962). The static response is recovered using a quasi-static harmonic Boundary Element Method implemented in MultiFEBE (Bordón et al., 2022), with the Gazetas parameter $a_0 \approx 0.01$, ensuring quasi-static conditions (Gazetas, 1983).

Material behaviour is represented through natural soils governed by compatibility limits and stabilised soils whose stiffness scales with binder dosage (Puppala, 2016). Economic behaviour is captured through material-specific cost laws: natural soils follow a logarithmic cost–modulus trend reflecting haulage penalties, while stabilised soils follow linear increments proportional to binder content. Coupling these laws with deterministic multi-objective optimisation enables explicit exploration of cost – soil settlement deterministic trade-offs.

The framework is evaluated through a global sensitivity analysis and a local application under Spanish road specifications (technical codes PG-3 and 6.1 IC), providing a unified mechanistic–economic basis for subgrade optimisation across transport sectors.

2 Methodology

2.1 Design space and mechanical modelling

Two subgrade families were generated: Monomat systems (single material) and Bimat systems (combinations of natural and/or stabilised soils). Natural soils are classified as S-IN, S-0, S-1, S-2, S-3 and S-4 following PG-3 (being the associated Young's moduli 20, 30, 50, 100 and 300 MPa, respectively). The S-IN soil has only been considered as a possible support for the subgrade, but not as a fill soil. S-ST1, S-ST2 and S-ST3 (with 150, 300 and 1000 MPa) are the stabilised soils with increasing binder content (Puppala, 2016). All these types of soils and stiffnesses can be considered representative of the geomaterials that are used for infrastructure construction in most region around the world. Field-realistic lift thicknesses produced 580 *Monomat* and 5248 *Bimat* feasible analysis configurations. Therefore, finding the optimal solutions is of utmost importance.

Mechanical response was computed using MultiFEBE 3D harmonic BEM solver under quasi-static conditions. Natural soil lifts were adjusted using the Dormon–Metcalf rule, while stabilised layers retained fixed modulus values. The loading configuration reproduced the 300 mm plate load test.

2.2 Cost function formulation, logistic scenarios and optimisation

Cost laws were calibrated from Spanish construction price data. Natural soils follow a logarithmic cost–modulus trend reflecting haulage effort, while stabilised soils follow a linear law consistent with binder-controlled stiffness. Total cost was expressed in relative units anchored to soil type S-0.

In order to make this study universally aplicable, three global cost scenarios (A, B and C) were studied, from surplus-material to resource-scarce contexts, informed by international infrastructure cost studies (CE Delft, 2019).

A full factorial evaluation computed subgrade settlement and cost for every feasible layer configuration, extracting non-dominated solutions and generating cluster, Pareto, and competitive-interval plots.

3 Results and Discussion

3.1 Global sensitivity analysis

Across all global scenarios, settlement and cost follow a clear inverse pattern governed by half-space stiffness: weak undelaying supports (S-IN, S-0) generate large settlements and high costs, while stiffer supports (S-1 to S-3) shift the design space toward lower settlements and more favourable cost-performance behaviour. *Monomat* systems show widening cost dispersion as global logistic penalties increase, whereas *Bimat* configurations remain tightly clustered and structurally more stable. Stabilisation state patterns separate cleanly: fully stabilised *Monomats* achieve the lowest settlements but become prohibitively expensive under high-cost regimes, while partially stabilised *Bimats* consistently occupy the intermediate region and adapt best to rising costs. Material-class trends reveal strict stiffness-cost trade-offs for *Monomats*, especially over soft foundations, whereas *Bimats* gain flexibility by combining natural and stabilised layers, aligning along asymptotic branches that reflect mechanical limits. Across cost scenarios, *Bimats* prove more resilient to escalation, maintaining competitiveness where *Monomats* become constrained. Pareto fronts reinforce that foundation stiffness dictates the feasible design space, with soft half-spaces restricting options and stiffer ones enabling broader, more robust envelopes. Competitive intervals show that stabilised soils dominate over weak foundations and at low settlement targets, while natural soils become increasingly competitive as the supporting layer stiffens.

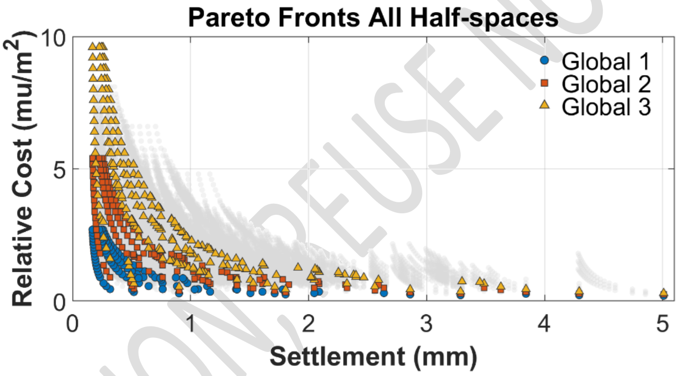

Figure 3*: Pareto fronts grouped by global cost scenario. (On the background the rest of the design space points are represented)*

3.2 Local application (Spanish context)

Adapting the framework to Spanish PG-3 specifications incorporates regional material availability, market pricing, and settlement limits, producing Pareto fronts consistent with Spain-specific economic behaviour. Once regulatory constraints are applied, foundation stiffness again governs feasible solutions: over S-IN, strict settlement limits and rising costs eliminate most alternatives, leaving only heavily stabilised options, whereas over S-1 and especially S-3, the stiff half-space absorbs mechanical and economic demand, widening the competitive interval and allowing natural soils to re-enter the optimal region on the basis of cost.

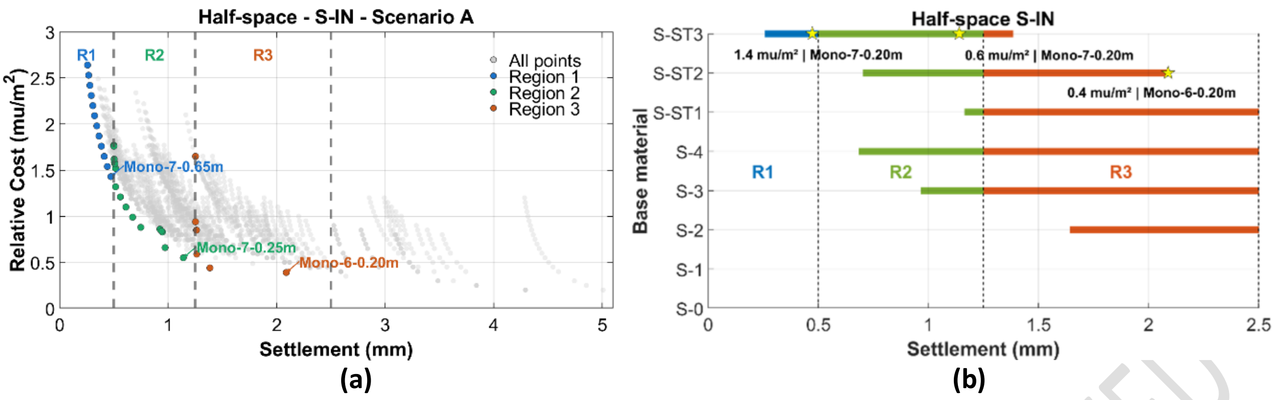

Figure 4: *Local analysis plots. (a) Pareto front showing design constraints; (b) Competitive intervals*

4 Conclusions

This study presents a unified mechanistic–economic framework for improved subgrade optimisation, that finds the set of optimal solutions for a given project, integrating multilayer elastic modelling with material-specific cost laws to identify Pareto-efficient designs. Natural soils follow logarithmic cost-stiffness trends with diminishing returns, while stabilised materials exhibit near-linear cost increments tied to binder dosage. Global and local analyses show that the underlaying support stiffness is the dominant factor shaping feasible solutions: soft foundations restrict the design space to high-modulus stabilised layers, whereas stiff foundations allow natural or lightly improved soils to become optimal. Regulatory settlement limits further narrow the feasible region, especially over weak supports, producing a predictable material hierarchy. The framework is adaptable to regional markets and provides a transparent basis for evaluating mechanical feasibility and economic efficiency. Future work should extend the approach to full pavement systems and explore data-driven enhancements.

5 References

Bordón, J. D., Álamo, G. M., Padrón, L. A., Aznárez, J. J., & Maeso, O. (2022). MultiFEBE: A multi-domain finite element–boundary element solver for linear mixed-dimensional mechanical problems. SoftwareX, 20, 101265.

Burmister, D. M. (1945). The general theory of stresses and displacements in layered systems. Journal of Applied Physics, 16(2), 89-94.

CE Delft. (2019). Infrastructure costs: Rail, road, waterways and airports. Delft, The Netherlands.

Dormon, G. M., & Metcalf, C. T. (1965). Design curves for flexible pavements based on layered system theory. Highway Research Record, 71, 1–40.

Gazetas, G. (1983). Analysis of machine foundation vibrations: state of the art. Soil Dynamics and Earthquake Engineering, 2(1), 2-42.

Heukelom, W., & Klomp, A. J. G. (1962). Dynamic testing as a means of controlling pavements during and after construction. Proceedings of the International Conference on the Structural Design of Asphalt Pavements, Ann Arbor, 667–679.

Ministerio de Transportes, Movilidad y Agenda Urbana. Pliego de Prescripciones Técnicas Generales para Obras de Carreteras y Puentes (PG-3). Madrid, Spain.

Puppala, A. J. (2016). Stabilization of subgrade soils using additives. Transportation Research Board, National Academies Press.

Discrete Element Analysis of the Response of Unbound Granular Materials Consisting Marginal Road Materials under Triaxial Loading

M. Kaan Etikan
Department of Civil and Architectural Engineering, KTH Royal Institute of Technology
Denis Jelagin
Department of Civil and Architectural Engineering, KTH Royal Institute of Technology
Erik Olsson
Department of Engineering Sciences and Mathematics, Luleå University of Technology
Manfred N. Partl
Department of Civil and Architectural Engineering, KTH Royal Institute of Technology

Abstract

Aggregate crushing in unbound granular materials (UGMs) significantly influences their strength, stiffness, and deformation characteristics, potentially leading to pavement distresses such as rutting and reduced service life. This study investigates the effect of aggregate fracture on the mechanical behaviour of UGMs composed of marginal-quality aggregates under triaxial loading conditions. To evaluate the fracture a Discrete Element Method (DEM) model, incorporating a granular mechanics-based contact law and a statistical fracture model, is employed as it enables detailed representation of particle-scale interactions and fracture processes. The model parameters are derived from previous studies and validated through uniaxial monotonic compression experiments conducted on crushed brick aggregates with particle sizes ranging from 2 - 16 mm, ensuring the reliability of the numerical approach. Building on this validated framework, the DEM model is then used to analyse the response of densely graded brick UGMs under triaxial loading, both with and without considering particle fracture, allowing direct assessment of fracture effects, thereby extending the approach to marginal-quality aggregates. Furthermore, the results are compared with granite UGMs of identical gradation to evaluate the influence of aggregate type on mechanical performance. The findings indicate that the DEM model successfully captures the macroscopic behaviour of UGMs with good agreement to experimental data, while inclusion of particle fracture reduces the maximum deviatoric stress by approximately 15% across all confining stress levels, highlighting the necessity of considering aggregate breakage when assessing the suitability of marginal materials in pavement applications.

Keywords: unbound granular materials; discrete element method; aggregate fracture; triaxial loading; crushed brick; marginal aggregates.

1 Introduction

Incorporating marginal-quality aggregates in unbound granular materials (UGMs) in road structures may significantly affect the performance of the UGM due to aggregate fracture. Aggregate fracture in UGMs may cause excessive deformations as well as compromise UGM strength and stiffness. Excessive aggregate damages may result in pavement distresses such as rutting, and surface deterioration (Colagrande et al., 2011; Zeghal, 2009), ultimately reducing the service life and durability of the pavement. Therefore, a more comprehensive understanding of the crushing mechanics of marginal aggregates within UGMs is essential for assessing their suitability in pavement applications and ensuring long-term structural performance.

To evaluate aggregate fracture, this study employs the DEM framework developed by Etikan et al. (2025a), which was previously applied to investigate the influence of particle fracture on the triaxial response of UGMs under different confining stress levels (Etikan et al., 2025b). The present study extends this approach to UGMs incorporating marginal-quality crushed brick aggregates, thereby addressing an aggregate type not considered in earlier applications of the framework. The main contribution of this work lies in isolating the influence of aggregate quality on fracture development and triaxial response through a direct comparison between crushed brick and granite UGMs of identical gradation. This provides new insight into the mechanical implications of using marginal aggregates in road base materials.

2 Methodology

The DEM model incorporates granular mechanics-based particle contact law and aggregate fracture model, as proposed by Olsson et al. (2019) and Etikan et al. (2025a), to accurately capture the effect of aggregate fracture. The parameters for contact law and aggregate fracture model obtained in Etikan et al. (2025a) and validated through experimental results are used.

Uniaxial monotonic compression tests are conducted on UGMs composed of crushed brick aggregates with a particle size range of 2 – 16 mm, under two loading magnitudes. Based on these experiments, a corresponding DEM model is developed. Three repetitions are conducted for each test and simulation. The macromechanical behaviour of the simulated UGMs are then compared with that of the experimental results.

Finally, a DEM model is used to evaluate aggregate fracture behaviour of a densely graded Brick UGM under triaxial loading, with and without fracture, at two confining stress levels of 10 and 20 kPa. The results are compared with each other and with the corresponding results for granite UGMs with same gradation obtained in Etikan et al. (2025b), to investigate the respective influences of particle fracture and aggregate type on the maximum achievable deviatoric stress.

3 Results and Discussion

To evaluate the predictive capability of the DEM model under triaxial loading conditions, results for granite UGMs reported in Etikan et al. (2025b), are compared against the measurements in Erlingsson and Rahman (2013), demonstrating that the DEM model captures the strain at maximum deviatoric stress with a deviation not exceeding 0.1%. The deviatoric stress obtained from the DEM model aligns well with the measurements for a confining stress of 10 kPa, while for confining stress of 20 kPa deviations up to 1.5 times are observed.

The DEM model of uniaxial monotonic compression captures the behaviour of the measurements of Brick UGM (2 – 16) well, with minor deviations at higher load levels, as presented in Figure 1. For triaxial loading, the DEM model provides a qualitative comparison between simulations with and without the fracture model, showing the maximum achievable deviatoric stress is reduced by approximately 15% across all confining stress levels when fracture is included. Additionally, the DEM model allows comparative analysis between UGMs of different aggregate types. Furthermore, the model provides insights into amount of fracture with respect to applied stress.

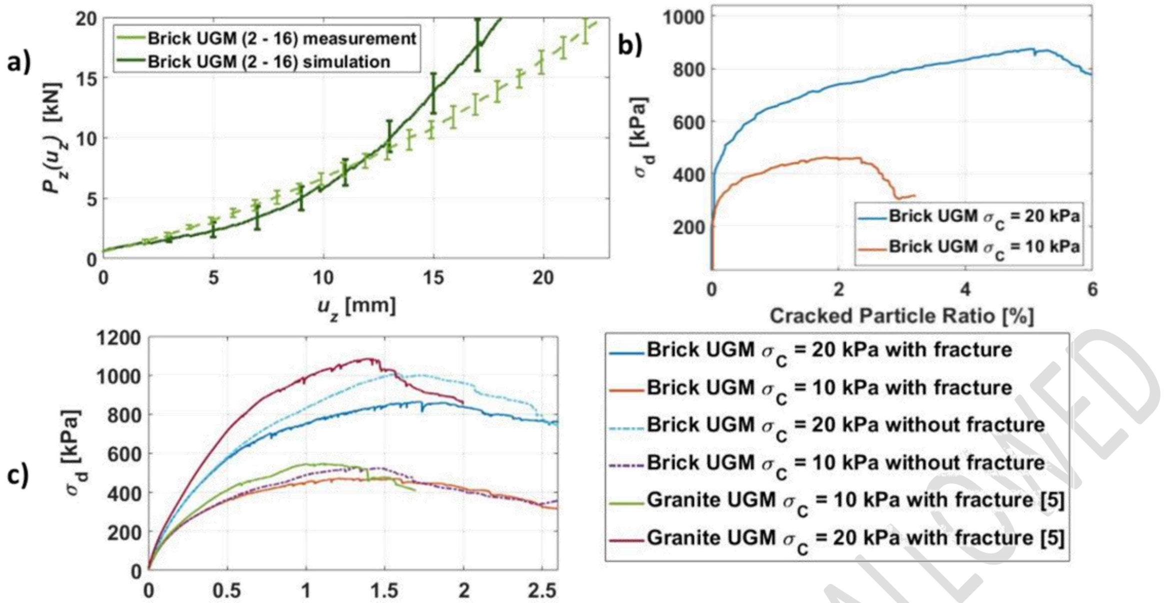

Figure 1: *a) Uniaxial monotonic compression tests on Brick UGM (2 - 16), Results of triaxial loading test on Brick UGM against Granite UGM [5]: b) Fractured particle ratio vs. deviatoric stress, c) Deviatoric stress vs. axial strain of the loading head.*

4 Conclusions

The study demonstrates that the DEM model of uniaxial monotonic compression captures the behaviour of the measurements of Brick UGM (2 – 16) well, with minor deviations at higher load levels. For triaxial loading, the inclusion of particle fracture reduces the maximum achievable deviatoric stress by approximately 15% across all confining stress levels. Additionally, the DEM model allows comparative analysis between UGMs of different aggregate types and provides insights into amount of fracture with respect to applied stress. The results highlight the potential of the DEM framework for evaluating performance limitations of marginal aggregates in road base materials.

References

Colagrande, S., Ranalli, D., & Tallini, M. (2011). Ground Penetrating Radar Assessment of Flexible Road Pavement Degradation. International Journal of Geophysics, 2011(1), 989136.

Erlingsson, S., & Rahman, M. S. (2013). Evaluation of Permanent Deformation Characteristics of Unbound Granular Materials by Means of Multistage Repeated-Load Triaxial Tests. Transp. Res. Rec, 2369(1), 11-19.

Etikan, M. K., Jelagin, D., Olsson, E., & Partl, M. N. (2025a). A new statistical fracture model for particles in unbound road materials. Materials and Structures, 58(6), 228.

Etikan, M. K., Jelagin, D., Partl, M. N., & Olsson, E. (2025b). A Numerical Study of the Effect of Aggregate Fracture on the Unbound Granular Materials Response under Triaxial Loading. Advances in Materials and Pavement Performance Prediction IV (AM3P 2025).

Olsson, E., Jelagin, D., & Forquin, P. A. (2019). Computational framework for analysis of contact-induced damage in brittle rocks. International Journal of Solids and Structures, 167, 24-35.

Zeghal, M. (2009). The Impact of Grain Crushing on Road Performance. Geotechnical and Geological Engineering, 27(4), 549-558.

Geotechnical Asset Data to Enhance Road Network Resilience

Tanja Waaser
Transport Scotland, Glasgow, United Kingdom
Mike G. Winter
Winter Associates Limited, Kirknewton, Scotland, United Kingdom

Abstract

Transport Scotland is responsible for the 3,739 km Trunk Road and Motorway Network (TRN) in Scotland. Contained within that are extensive earthworks and other geotechnical assets. The consequences of climate change present major hazards to Scotland's transport infrastructure including floods and landslides, which, in turn, present major risks. Climate projections for the next 30 years, indicate that the hazards and impacts currently seen are likely to escalate. A managed adaptation of these assets is required, not least to ensure that we maintain a transport system that is safe, reliable, and resilient. This includes the specific targeting of geotechnical, drainage and environmental hazards to ensure that adjacent slopes are stabilised where necessary, that third-party slope instability is managed, surface water is controlled, and the potential for flooding is reduced. Identifying the locations of vulnerable assets and environmental hazards, reviewing the effectiveness of management and maintenance processes, and developing appropriate adaptation, and hazard and risk reduction measures is essential to the avoidance of undue and increased failure and associated disruption and risk. In recognition of the challenge of climate change and the consequent need for adaptation and enhanced resilience at asset, route and network levels, work is ongoing to address the above issues using a data-led approach. In this paper we will report progress on ongoing work to assess the impact of climate change on our geotechnical assets and outline the current technical approach to managing and maintaining such assets. This paper sets out the background to this need.

Keywords: roads; geotechnical; asset; data; network; resilience

1 Introduction

The consequences of climate change present major hazards, including floods and landslides, to Scotland's transport infrastructure. Such infrastructure is vulnerable to these hazards, and therefore major risks are presented to the operation of the network. Projected climate trends show future impacts are likely to be more severe than experienced to date. Further, the UK Climate Change Risk Independent Assessment (CCRA3, 2021a) identifies seven key climate risks that relate to transport infrastructure, many of which directly relate to geotechnical assets. Therefore, a managed adaptation of the assets is required, not least to ensure that the transport system is maintained and is sufficiently safe, reliable and resilient.

Scotland's transport infrastructure networks are fundamental to our nation's communities, businesses, and visitors. They offer critical connections between people and places and are vital in providing access to economic opportunities and vital services. The 3,739 km Scottish Trunk Road Network (TRN) is one of the most critical transport networks and is illustrated in Figure 1.

Road infrastructure geotechnical assets (e.g. embankments, cuttings, and strengthening systems,), are often viewed as secondary, ancillary or 'child' assets in the portfolio. While this view recognises their essential function in supporting the primary assets (e.g. the road pavement) it could be argued that it fails to recognise their fundamental role in ensuring the resilience and accessibility of the TRN. While drainage and the effects of flooding are being taken forward under separate arrangements, the important link between the performance of geotechnical assets and the provision of adequate drainage must be borne in mind.

The National Transport Strategy (NTS2) (Transport Scotland, 2020) committed to taking climate action, including adapting the transport system to the impacts of climate change. In this context, there is a need to specifically target geotechnical assets on the TRN to ensure that their maintenance is subject to targeted procedures that are underlined by an in-depth knowledge of their behaviour, condition and performance. This would allow a proactive approach to preventative maintenance to be adopted, rather than the present reactive approach to asset failure.

2 Climate change

Key changes to Scotland's climate are highlighted by CCRA3 (2021b):

- Scotland's 10 warmest years on record have all occurred since 1997. The average temperature in the last decade (2010-2019) was 0.69°C warmer than the 1961-1990 average, and the warmest year on record was 2014.
- There has been an increase in rainfall over Scotland in the past few decades (with an increasing proportion of rainfall coming from heavy rainfall events). The annual average rainfall in the last decade (2010-2019) was 9 % wetter than the 1961-1990 average, with winters 19% wetter.
- Mean sea level around the UK has risen by approximately 1.4 mm a year from the start of the 20^{th} century.

Probabilistic predictions of future change are, of course, dependent upon the scenario selected but typically suggest decreased summer rainfall of as much as -6% and increased winter rainfall of up to 16 % for the RCP6.0 (50^{th} Percentile) for 2080 along with temperature increase of up to 2°C. Although climate models are not best suited to predicting storm events, the available evidence for climate change does point to an increase in such short duration, high intensity rainfall events, even in summer (Winter et al., 2019).

The relatively long lifespan of transport infrastructure assets in relation to climate changes must be considered for existing and new infrastructure. This will be important as Scotland moves toward Net Zero emissions, presenting an opportunity to build climate resilience into future infrastructure. These changes to cli-mate clearly signal the increased potential for instability and landslides, for example. While the increased hazards are likely to exhibit the greatest increases in the winter months, when the land is already saturated and unable to adsorb any further water Winter et al. (2005, 2008) particularly highlighted the increase in such hazards as a result of drier summers.

The impacts of climate change are already seen to cause significant delay to road users as a result of land-slides, and fluvial, pluvial and coastal flooding. The coastal floods experienced on the southwest coast lead to diversions of significant length as well as damage to the ageing infrastructure. Such effects are forecast to increase, and increased traffic will exacerbate their effect. Until 2014 the event frequency at the A83 Rest and be Thankful site (Fiddes et al., 2023) was around 0.9/year with a typical magnitude of less than 1,000m3 (Winter & Wong, 2020) whereas current evaluations suggest that in 2020 the total amount of debris that reached the road was around 20 times that in any previous year.

An unpublished study by AECOM found that the number of routes with the highest level of vulnerability to flooding will more than double by the 2030s. Without significant investment in drainage assets these figures are likely to increase significantly. Analysis of the available climate and climate change trends along with their impacts suggest that landslide hazards and risks are also likely to increase considerably (Winter et al., 2010; Winter & Shearer, 2013).

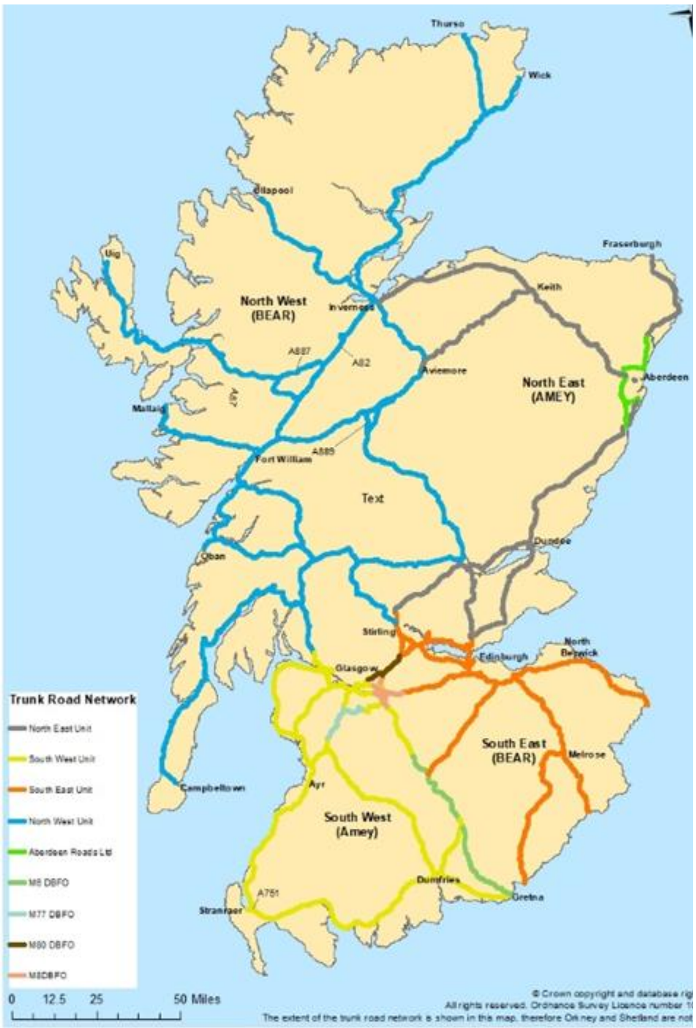

Figure 1: *Scottish Trunk Road Network Map.*

3 Adaptation and resilience

More investment will be needed to ensure that projected increases in, for example, heavy rainfall are factored into maintenance, adaptation, and longer-term renewal programmes. Additional adaptation actions were proposed by CCRA3 (2021a) including data-led monitoring, inspection, analysis and characterisation programmes; greater use of ‘soft’ engineering techniques; and enhanced drainage capacity. Such actions are particularly relevant to geotechnical assets and geohazards that are particularly vulnerable to the action of water and therefore to the effects of increased rainfall, whether by runoff and erosion, infiltration and strength reduction, or the action of flood water.

Of the four forms of resilience, redundancy and recovery apply to the network while resistance and reliability are arguably more relevant to geotechnical assets and geohazard events. The change in event recurrence period (frequency), allied with increased event magnitude, at the A83 Rest and be Thankful has been such that the situation is threatening to become one of reduced resilience (Winter, 2024) and much larger scale actions are planned with a new route currently in planning, design and procurement.

One of the purposes of the current work is to begin the process of assessing need, and placing values, costs and priorities on the required interventions to increase the resilience of the TRN through a managed adaptation plan applied to the geotechnical asset base (Figure 2).

Transport Scotland's short- and long-term asset management practices include the asset register, identification and planning of works that provide best value for money, and procedures for assessing and mitigating risk. The asset register is well-developed but, in the case of geotechnical assets, some work is required to ensure that is adequately populated facilitating further work within the new Asset Management System.

The behaviour and performance of earthworks and other geotechnical assets are particularly complex, as is the determination and prediction of their condition. This is reflected in the most important long-term asset management objectives of ensuring that the asset is:

- managed and maintained such that its condition remains fit-for-purpose,
- that deterioration is detected and quantified, and
- that intervention occurs prior to failure.

Such proactive responses can minimise reactive or responsive interventions and the associated unplanned disruption and other risks associated with failure. Guidance will be needed for Transport Scotland's agents to ensure that full value is achieved from adaptation interventions. Such guidance should be nonprescriptive, indicating the framework and form of adaptation measures that provide acceptable resilience. It should draw upon successfully implemented examples from the TRN and the wider national and international context and consider design, specification, maintenance and operation of geotechnical assets and especially focus on their interaction with drainage.

Figure 2: *Route from adaptation to resilience whether through maintenance and renewal, new construction or other opportunities.*

4 Vulnerable locations

The adaptation of the TRN to climate change is facilitated by Transport Scotland (2023) the purpose of which is as follows:

- Review current climate change adaptation and resilience activities, through identification and baselining of on-going work across all modes.
- Provide recommendations on how to further enhance adaptation and resilience across the Transport Scotland portfolio.
- Set the strategic direction for adaptation and resilience activity for Transport Scotland and outline supporting actions for those areas where we have an influence and/or can provide leadership.
- Enable the establishment of an appropriate and proportionate governance structure to oversee adaptation and resilience activity within Transport Scotland.

This document is not intended to set out a plan or programme of specific actions. That is the function of the Vulnerable Locations Group (VLG) which was set-up to drive Transport Scotland's strategic approach to climate change and adaptation. The Vulnerable Locations Operations Group (VLOG) is, in turn and as the name suggests, to implement the direction(s) determined by the VLG on the Trunk Road Network. This work in in progress with a number of sites having been identified and proposals are in development to allow their further assessment, remediation and adaption to provide enhanced local and network resilience.

5 Conclusions

Climate change presents significant challenges to road network operation, and these are particularly great when it comes to geotechnical (and drainage) assets and associated natural (or third party) slopes. In this short communication we have outlines the problem and Transport Scotland's approach to ensuring adequate resilience through strategic, targeted and data-led adaptation.

While this short communication predominately focusses on the effects of rainfall on geotechnical and drainage assets the effects of climate change are, of course, much wider and include inter alia those of temperature, wind, sea level rise on other asset types.

6 References

CCRA3. 2021a. Findings from the UK third Climate Change Risk Assessment, Transport Briefing. https://www.ukclimaterisk.org/wp-content/uploads/2021/06/CCRA3-Briefing-Transport.pdf

CCRA3. 2021b. Evidence for the third UK Climate Change Risk Assessment, Summary for Scotland. https://www.ukclimaterisk.org/wp-content/uploads/2021/06/CCRA-Evidence-Report-Scotland-Summary-Final-1.pdf.

Fiddes, G., Waaser, T. & Winter, M. G. 2023. Operating a major road at the Rest and be Thankful landslide site. Proceedings, XXVIIth World Road Congress, Session 14, Paper IP0469, Prague.

Transport Scotland. 2020. National Transport Strategy: Protecting our climate and improving lives. https://www.transport.gov.scot/media/47052/national-transport-strategy.pdf

Transport Scotland. 2023. Transport Scotland's Approach to Climate Change Adaptation and Resilience (ACCAR). https://www.transport.gov.scot/media/53779/ts-approach-to-climate-change-adaptation-and-resilience-accar.pdf

Winter, M. G. 2024. The John Mitchell Lecture 2023: road asset, socioeconomic and fatality risk from debris flow. Quarterly Journal of Engineering Geology and Hydrogeology, 57(2), 1-23.

Winter, M. G. & Shearer, B. 2013. Climate change and landslide hazard and risk - a Scottish perspective. Published Project Report PPR 650. Transport Research Laboratory, Wokingham.

Winter, M. G. & Wong, J. C. F. 2020. The assessment of quantitative risk to road users from debris flow. Geoenvironmental Disasters, 7(4), 1-19.

Winter, M. G., Macgregor, F. & Shackman, L. (Editors) 2005. Scottish Road Network landslides study, 119p. Trunk Roads: Network Management Division Published Report Series. The Scottish Executive, Edinburgh.

Winter, M. G., Macgregor, F. & Shackman, L. (Editors) 2008. Scottish Road Network landslides study: implementation, 278p. Transport Scotland Published Report Series. Transport Scotland, Edinburgh.

Winter, M. G., Dent, J., Macgregor, F., Dempsey, P., Motion, A. & Shackman, L. 2010. Debris flow, rainfall and climate change in Scotland. Quarterly Journal of Engineering Geology & Hydrogeology, 43(4), 429-446.

Winter, M. G., Ognissanto, F. & Martin, L. A. 2019. Rainfall thresholds for landslides: deterministic and probabilistic approaches. Published Project Report PPR 991. Transport Research Laboratory, Wokingham.

Technical evaluation of wearing course layer containing 40% RAP on the national roadway network

Mathieu Galiana
Christophe Ropert
Cédric Petiteau
Michel Dauvergne
Université Gustave Eiffel, France
Ciryle Some
Vincent Daniel
Cerema, France
Maxime Hordeaux
DIRO, France
Jean-Noël Ivry
DiRIF, France

Abstract

A technical evaluation of two wearing layer mixtures containing 40% Reclaimed Asphalt Pavement (RAP) was conducted between 2022 and 2024. The aim was not only to apply specifications outlined in the French guideline "Recycling of RAP in Hot Mix Asphalt (HMA)" published in 2021 but also to provide a feedback on recycling. The study focused on two national roadway sections: one in the west of France, near Nantes (RN137) and another near Paris (RN184). Standard tests were performed on both bitumen and mixtures sampled from the field including HMA containing 40% RAP as well as reference materials (containing either 10 or 20% RAP). Additionally, some specific tests were carried out: oxidation levels of bitumen were measured; thermal stress restrained specimen tests (TSRST) were performed on mixtures to assess their resistance to low temperatures; and surface characteristics of HMA relevant to road safety, such as Friction after Polishing (FAP) and skid resistance, … were evaluated. Finaly, an environmental assessment was performed for one of the cases. This article presents a synthesis of the results obtained for all these aspects.

1 Introduction - Context and objectives

In 2021, IDRRIM and Cerema published a french book devoted to the use of Reclaimed Asphalt Pavement (RAP) in hot mixes asphalt (HMA) (IDRRIM and Cerema, 2021). The book deals with HMA containing RAP with a rate until 40%. As recommendations, feedback was needed for higher rate (between 30 and 40% RAP) in order to consolidate the technical guidelines for wearing courses. This article analyses two sections of the french national road network where HMA containing 40% RAP have been implemented:

- RN184 Exterior from PR 13+300 to 14+700 (DiRIF road network). Wearing course layer in HMA R40 (named BBSG with 40% RAP in France). Construction site carried out in August 2022.
- RN 137 (Rennes-Nantes) from PR 11+200 to 10+600 (DIRO road network). Wearing course layer in HMA R40 (named BBMA with 40% RAP in France). Construction site carried out in June 2023.

The study was realized by University Gustave Eiffel and Cerema. And it was financed by the Ministry of Ecology and Sustainable Development in France.

2 Methodology and tests performed

Standard and specific tests were performed on aggregates, bitumens and on mixtures sampled from the field including HMA containing 40% RAP as well as reference materials (containing either 10 or 20% RAP). A list of specific tests is given in the following table.

Table 1: *List of specific tests.*

Specific tests	Objectives for the study	Standard reference
Bitumens		
FTIR (Fourier-transform infrared spectroscopy)	To know oxidation level and polymer content	ME LPC n°69 and n°71 (Mouillet et al., 2010; Farcas and Mouillet, 2009)
Complex modulus Métravib	To know rheological behaviour	XP T 66-065
BBR (Bending Beam Rheometer)	To know behaviour for low temperatures	NF EN 14 771
Aggregates		
PSV (Polished stone values)	To know resistance of aggregates to the polished action	NF EN 1097-8
Mixtures “HMA”		
Crack propagation by semi-circular bending test (SCB)	To know the capacity of HMA to resist to existing cracking propagation (fracture toughness KIC)	NF EN 12697-44
Thermal stress restrained specimen tests (TSRST)	To know the capacity of HMA to resist low temperatures (mean failure stress and failure temperature)	NF EN 12697-46
Sequenced binder recovery test	To evaluate the homogeneity of the HMA.	Method based on Navaro thesis (Navaro, 2011)
Surface characteristics in accordance to road safety		
Skid resistance tester	To know the skid resistance on a wet pavement	NF EN 13 036-4
DFT	To have a friction curve between 0 and 80km/h	ASTM E1911
T2GO	To know the uniformity of skid resistance on the section.	ASTM E3304-22
FAP (Wehner and Schulze)	To know skid resistance after polishing in the lab	NF EN 12697-49

3 Results

Bitumens modified with polymers were used as virgin bitumen and PSV properties of virgin aggregates were very satisfactory (PSV>54). Bitumen recovered from RAP were hard (softening point > 80°C for one site).

Normative values of mixtures were respected (stiffness modulus, resistance to rutting). The materials sampled from the RN137 and RN184 construction sites were also subjected to TSRST and SCB tests. As a result, density has effects on HMA properties for low temperatures. The higher the void content, the lower the stress at the failure. In terms of fracture behavior, the BBSG R40 mixture displays higher fracture toughness and a lower fracture temperature, indicating superior resistance to internal stresses induced by shrinkage. In contrast, the BBMA R40 mixture, with a higher air void content (7.8% compared to 5.6%), exhibits increased risk of early cracking for lower temperatures.

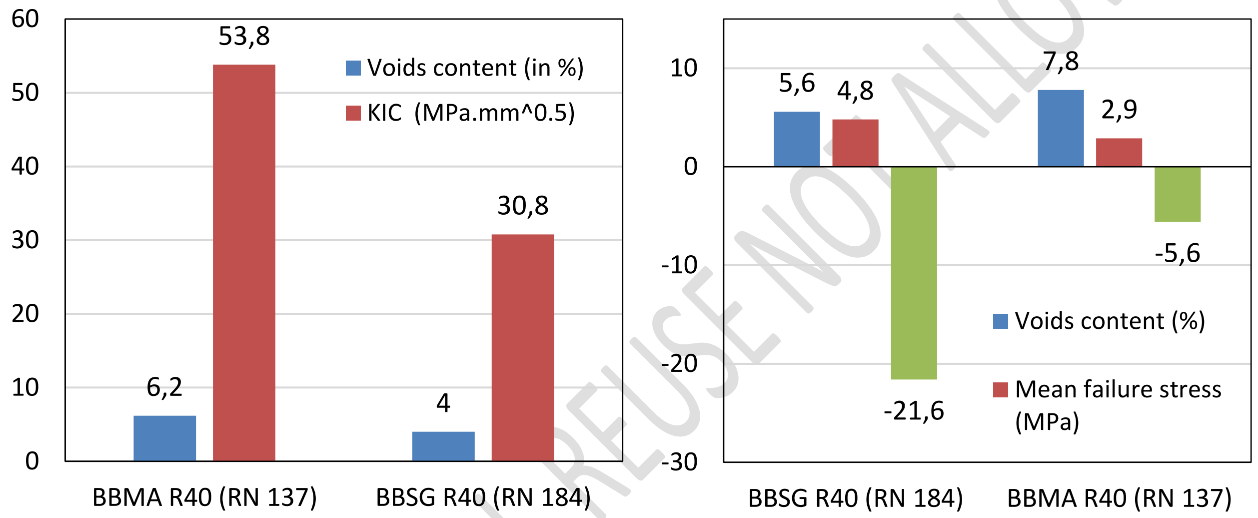

Results of SCB tests on HMA with 40% RAP: BBMA R40 and BBSG R40

Results of TSRST on HMA with 40% RAP: BBMA R40 and BBSG R40

***Figure 1**: Results on mixtures (SCB test and TSRST).*

Tests performed on bitumens recovered from the HMA shown that bitumen were hard and the polymer contend could drop during the mixing in the plant.

As a result of sequenced binder recovery tests, the mixture of virgin bitumen and old bitumen coming from RAP is satisfactory. On the bitumen recovered from HMA manufactured in asphalt plants and heated up in lab to get samples for TSRST, significant oxidation of the binder film on the surface was observed, most likely due to overheating in lab.

Evaluation of the surface characteristics in accordance to road safety shown that the differences in friction coefficients between the 40% formulas and the reference formulas are very small on the two sites. FAP tests shown that the final level remained satisfactory for all tested materials.

Finally, an environmental assessment was performed for the works on RN137 by using gas consumption, daily tonnages of HMA and data from SEVE TP[1]. An estimation of carbon emissions shown that the environmental impact of a HMA with 40%RAP is more interesting than a HMA with 10%RAP. It is interesting recycling to save resources but during manufacturing, formulae with higher rate of RAP get higher carbon emissions. This result is positive for formulae with higher rate of RAP. There is a gap around 15 %.

[1] SEVE TP : french eco comparateur (https://www.seve-tp.com/) – Version 6.1, June, 2025

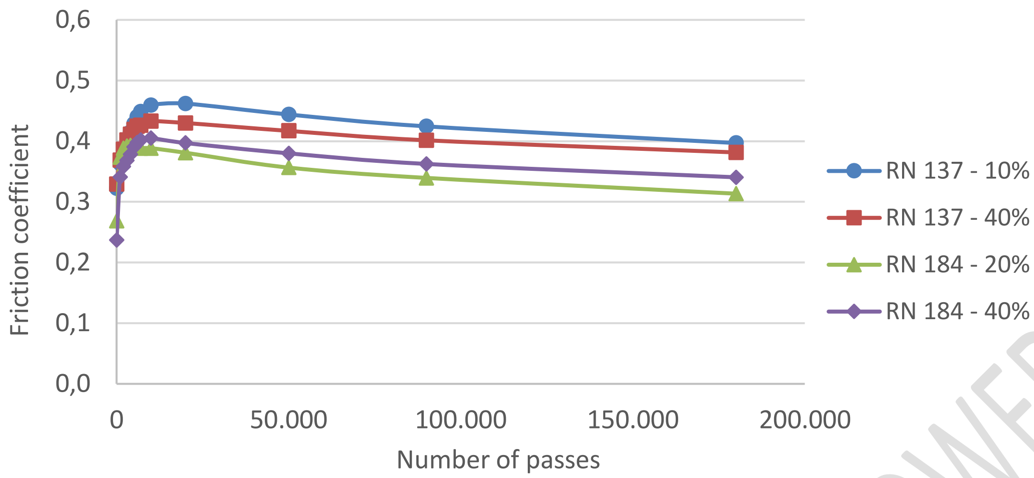

***Figure 2**: FAP on mixtures from RN137 and RN184 (results for R40 and reference mixtures).*

***Table 2:** Environmental assessment on RN137 (comparison between HMA 40% RAP and 10% RAP).*

Carbon emissions (t eq CO2) Calculation for 1 tonne of HMA	**HMA with 40% RAP (t eq CO2)**	**HMA with 10 % RAP (t eq CO2)**	**Gap between both technics (R40 / R10)**
Constituents manufacturing (virgin bitumen, aggregates, RAP)	0.022	0.032	-32 %
Manufacturing in plant (HMA)	0.014	0.010	38%
Total	0.036	0.042	-16%

4 Conclusions

Normative values were respected for HMA containing 40% RAP. Performance mechanics and surface characteristics in accordance to road safety were comparable between technics with high and low rate of RAP. Some points need to be investigated in future studies: resistance to existing cracking propagation; level of bitumen oxidation; evolution of polymer rate during manufacturing. To get information on durability, it could be interesting to follow technics on the field and to expand feedback to different climatic contexts.

5 Acknowledgments

The authors thank the Ministry of Ecology and Sustainable Development in France for financing this study. The authors express their gratitude to all the partners involved in this research project: technicians, researchers and engineers involved in the lab tests (Gustave Eiffel University; Cerema; DIRO; DIRIF) and the staff from the road companies (COLAS and KERAVIS) for their assistance in collecting bituminous materials and constituents during the construction phase.

6 References

IDRRIM & Cerema. 2021. Recyclage des agrégats d'enrobés dans les mélanges bitumineux à chaud. État de l'art et recommandations. Bron. Cerema. (in French)

Mouillet, V., Farcas, F., Battaglia, V., Besson, S., Petiteau, P. & Le Cunff, F. 2010. Identification et dosage des fonctions oxygénées présentes dans les liants bitumineux. Analyses par spectrométrie infrarouge à transformée de Fourier. Méthode d'essai n° 69. Paris. Laboratoire Central des Ponts et Chaussées (LCPC). (in French).

Farcas, F. & Mouillet, V. 2009. Identification et dosage par spectrométrie infrarouge à transformée de Fourier des copolymères SBS et EVA dans les liants bitumineux. Méthode d'essai n° 71. Paris. Laboratoire Central des Ponts et Chaussées. (in French).

Navaro, J. 2011. Cinétique de mélange des enrobés recyclés et influence sur les performances mécaniques. PhD thesis. Art et Métiers ParisTech. (in French).

An alternative approach to the low temperature performance of High Viscous Asphalt – a South Korean perspective

Kang Il Whan
Korea Institute of Civil Engineering and Building Technology, South Korea
Moon Ki Hoon
Korea Expressway Corporation, South Korea
Fan Zhang
Yuxuan Sun
Aalto University, Finland
Augusto Cannone Falchetto
University of Padua, Italy

Abstract

High Viscous Asphalt (HVA) binders are increasingly used in mixtures such as Stone Mastic Asphalt (SMA) and porous asphalt due to their proven rutting resistance at elevated temperatures, also in South Korea. While their performance in hot climates is well established, limited attention has been given to their behavior under low-temperature conditions, which may affect long-term durability in colder regions. This study evaluates the low-temperature performance of several HVA binders. Binders were characterized using the bending beam procedure specified in Korean standards. Despite sharing the same Performance Grade (PG), the binders exhibited distinct low-temperature responses. To capture these differences, exponential-logarithmic functions were fitted to the experimental data, leading to the development of two new indicators: the Low Temperature Performance Area Factor (LTPAF) and the Low Temperature Performance Slope Factor (LTPSF). The proposed approach offers an alternative framework for differentiating the low-temperature performance of HVA binders, providing a basis for more reliable material selection in cold climates.

Keywords: high viscous asphalt (HVA), low-temperature performance, predictive modeling

1 Introduction

High-viscosity asphalt (HVA) binders enhance pavement durability through their elevated viscosity and cohesive properties, making them suitable for heavily trafficked sections and high-performance mixtures such as Stone Mastic Asphalt (SMA) and porous asphalt (Huang et al., 2023). Compared with conventional binders, HVAs offer improved resistance to cracking and rutting, potentially reducing pavement thickness, lowering CO_2 emissions during production and transport, and decreasing life cycle costs (Zhu et al., 2023). A distinctive feature of HVAs is their ability to retain flexibility at low temperatures, improving thermal cracking resistance and extending use to colder climates (Zhu et al., 2023). A reliable evaluation of their performance across the entire temperature spectrum requires accurate testing methods and advanced analytical approaches. The current Performance Grade (PG) system, developed under the SHRP, classifies binders based on their temperature-dependent performance. However, the key PG parameters for low-temperature evaluation often fail to capture the behavior of modified binders. This limitation is evident when binders with identical PG grades exhibit distinct cracking responses. Several HVAs classified as PG XX–22, for example, may show markedly different low-temperature performance depending on the modifier type and dosage, resulting in variability among manufacturers (Korean Asphalt Institute, 2024). The 6 °C grading interval may therefore be insufficient to distinguish meaningful performance differences. Alternative methods have been proposed to close this gap. The Japanese flexural test, for instance, is widely recognized for its ease of use and capacity to highlight low-temperature characteristics of HVAs (Japan Road Association, 2010). Yet, while helpful for material discrimination, such a test remains limited in predictive capability across a wide range of conditions. This highlights the need for complementary approaches to describe binder response more robustly and support improved material selection in cold climates.

2 Objective and research approach

The objective of this study is to propose an alternative framework for evaluating the low-temperature performance of high-viscosity asphalt (HVA) binders. Building on conventional flexural testing, the approach combines experimental data with simple data fitting to better capture binder-specific differences that are often overlooked by the PG system. Two new performance indicators are introduced to discriminate low-temperature behavior more effectively, providing a basis for improved binder selection and design practices in cold climate applications.

3 Materials and testing

High-viscosity asphalt binders from four domestic (Korean) companies (A–D) and one Japanese company (E) were used. Companies A–C supplied premix binders with varying PG grades, while D and E provided plant-mix binders prepared by adding SBS modifiers to PG 58-22 and 64-22 bases and mixed at 180 °C. Rheological properties varied across manufacturers, even for the same PG grade. Specimens (120 × 20 × 20 mm) were prepared. Flexure tests were conducted on a PAF-100 tester at controlled low temperatures, with initial loading rates of 2 mm/min and subsequently increasing to 100 mm/min (Figure 1, left). The response depended on temperature and PG grade, ranging from multiple fragmentation to localized cracking or flexural deformation (see Figure 1, right).

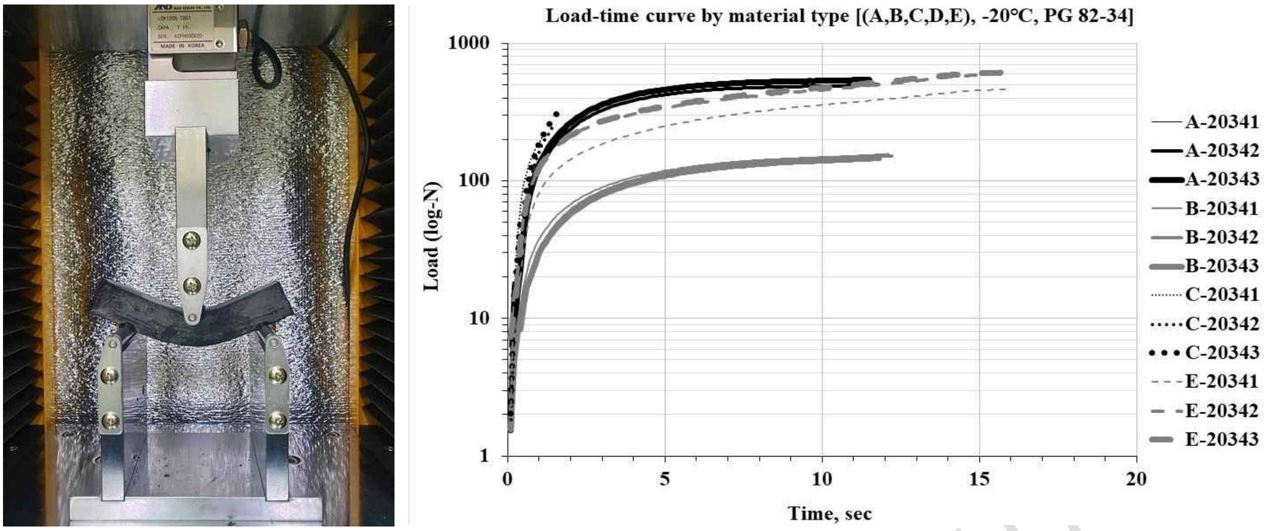

Figure 1: *Left - Testing device; right – Example of test results across original binders (A-E) for HAV binder PG 82-34.*

4 Alternative low-temperature performance prediction methods

To predict low-temperature performance beyond simple parameter comparisons of low-temperature behavior, four exponential-logarithm expressions (not detailed here for conciseness) were coupled to two new factors: the Low Temperature Performance Area Factor (LTPAF) and the Low Temperature Performance Slope Factor (LTPSF). See Figure 2. LTPAF can be defined as the area under the load-time prediction model curve up to the time of maximum load, representing the magnitude of resistance to low-temperature cracking. LTPSF represents the slope of the load-time prediction model, signifying the crack propagation rate at low temperatures. In the low-temperature region, a relationship between decreasing temperature and LTPAF was observed for all materials except Material C, though the increase was minimal. The maximum LTPAF magnitude was calculated as 503 N·s of deformation energy. Since all PG 82-22 grade specimens, regardless of re-examination status, exhibited bending failure during the bending test, this confirmed that LTPAF effectively reflects such behavior. Regarding LTPSF, since failure occurred rapidly upon reaching the maximum critical load, the parameter value was initially very large immediately after load application and then decreased sharply as time increased. This trend confirmed that LTPSF also accurately reflects the bending test results (initial loading phase → increasing phase → steady state due to failure).

5 Conclusions

This study investigated the response of High Viscous Asphalt (HVA) binders at low temperatures under bending beam tests. The proposed Low Temperature Performance Area Factor (LTPAF) and Slope Factor (LTPSF) have the potential to effectively differentiate binders by capturing energy storage and load evolution. Failing specimens exhibit low LTPAF and steep LTPSF drops, while non-failing ones display higher and steadier values. Both indicators consistently reflected temperature effects and flexural outcomes, confirming their role as complementary tools for modeling binder behavior. These findings highlight that PG grading alone is insufficient and that refined evaluation methods are needed to ensure the reliable low-temperature performance of modified HVA binders in cold climates.

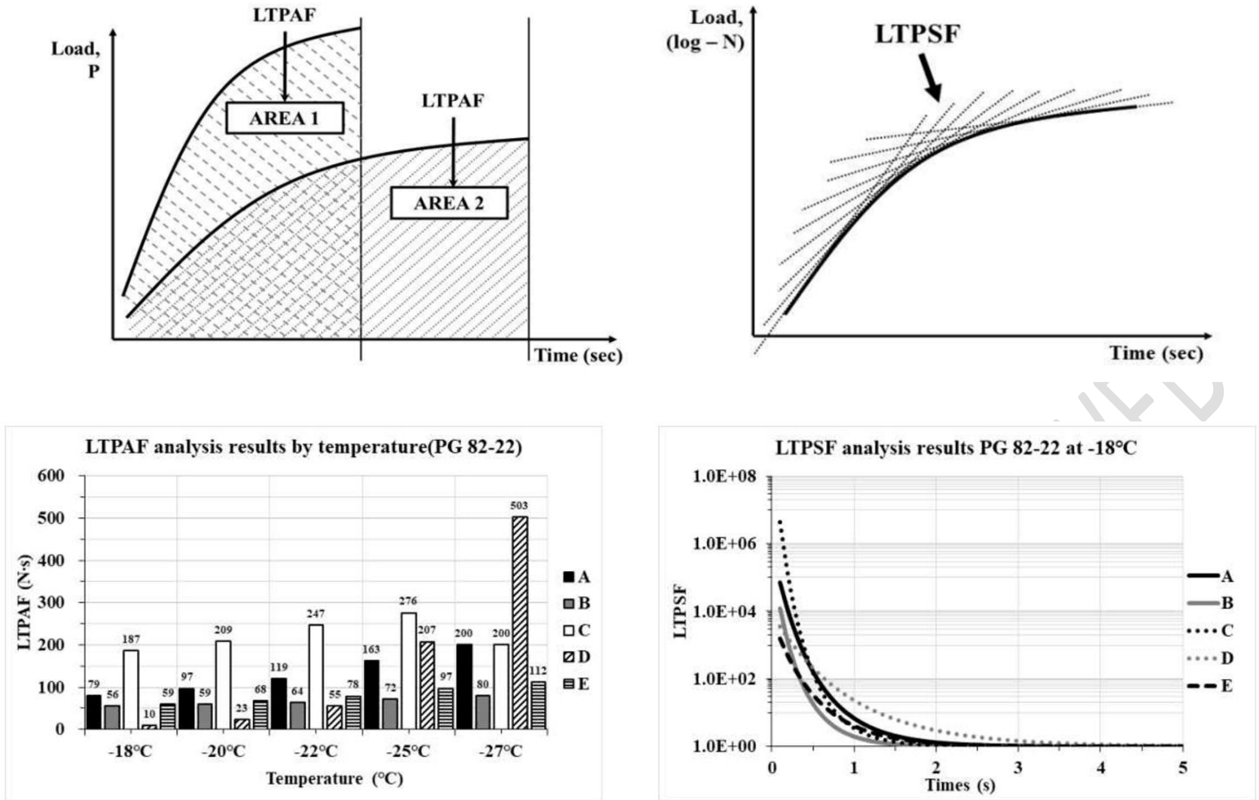

***Figure 2**: Left-top: Low Temperature Performance Area Factor (LTPAF); Right-top: Low Temperature Performance Slope Factor (LTPSF); Left-bottom: sample results of LTPAF for binder PG82-22; Right-Bottom: LTPSF for binder PG82-22.*

6 References

Huang, Z., et al. 2023. Research on high- and low-temperature rheological properties of high-viscosity modified asphalt binder. Buildings, 13(4), 1077.

Zhu, S., Li, Y., Zhang, Y. 2023. Thermal aging degradation of high-viscosity asphalt binder. Polymers, 16(11), 1489.

Korean Asphalt Institute. 2024. Annual Report on asphalt binder performance and classification. Seoul: Korean Asphalt Institute.

Japan Road Association (JRA). 2010. Manual for Pavement Design and Construction with High Viscosity Modified Asphalt. Tokyo, 2010.

Verifying Balanced Design in the Field

Carl Lenngren
AFRY Infrastructure

Abstract

The concept of "Balanced Design" is based on laboratory testing, but there is a need to get field performance, especially for performance contracting and long-time warranty programs. The Falling Weight Deflectometer has been used for decades to assess strains at critical points in the structure, which can be related to the traditional design parameters such as stress and strain. However, only the maximum deflections and load are used in the linear elastic layer model. If the entire time-history of each sensor is evaluated one may derive the initial crack energy for fatigue and permanent deformation as well. The present paper describes how the data can be handled and suggests how a database built on neural networks can be built.

Keywords: balanced design; FWD evaluation; FWD time histories

1 Introduction

Over half a century ago a mix design procedure emerged based on the stiffness of the bitumen binder. It was understood that a soft binder ensured good fatigue properties, but less resistance to rutting. Conversely, a hard binder was better for resisting deformation, but it fatigued early. Load frequencies and temperatures also affected properties. Later, additives like polymers improved their performance for a wider temperature range. With polymers and recycled pavements gaining popularity, it became necessary to change the mix design entirely. Super Pave led the way by assessing a temperature range for the binders needed for any given climate. Later, rheology and Balanced Design were used to optimize the binder for rutting and fatigue cracking as well, during any circumstance. In recent years, asphalt recycling implicating a severe change of binder stiffness imposes better models for achieving control of fatigue and rutting parameters. The Balanced Mix Design (BMD) is based on laboratory testing. Typical tests include a wheel tracker, a fatigue apparatus and moisture testing. The testing is both short-term and long-term as well. Hence, accelerated ageing is needed. As in other design procedures, traffic, climate and existing conditions must be assessed. Zhou et al. 2006 described early an BMD procedure for overlay pavements. And in the forthcoming years several U.S. states gained much experience and feedback of BMD. A comprehensive study of follow-ups and suggestions was conducted by Hajj et al, 2022.

Pavement criteria may be strict, adjustable and tested in the field. Usually, functional parameters like rutting and roughness are used. However, these measures reveal history, and not so much the prediction of the forthcoming years. A thorough structural analysis is a better tool for this purpose.

2 Objective

The objective of the present paper is a feasibility study to find and suggest useful parameters for evaluating BMD in the field.

3 Scope

Only existing parameters from previous pavement dynamic research with a falling weight deflectometer (FWD) are investigated.

4 FWD Research

The FWD is traditionally used for pavement mechanistic parameters, like assessing strain for a given load, so that fatigue life can be determined. Further, the top of subgrade strain correlates fairly with the rutting rate, has been used since the 1960:ies. That is fine of course, but the latter criterion is based on rutting in all layers, so how could we improve on assessing the rutting in separate layers? Originally, the FWD represents a defined load of a standard axle passing by at a constant speed. The stiffness of the asphalt layer is then adjusted to a reference temperature. Thus, results are comparable from time to time, and for different subjects.

5 FWD Dynamic Analysis

In 1992 software was presented to back calculate viscoelastic properties by using the entire load and deflection histories in a single test, Magnuson et al 1992. Typically, the application worked best on thick asphalt pavements. A few years later, high speed rolling deflectometers appeared moving along at traffic speeds. As the conditions varied, it was necessary to calibrate the dissipation caused by trucks with FWD time history data. It became clear that not only the bitumen viscoelastic properties, but also damping in unbound layers, internal friction, water movement and fracture mechanics all affected the deflection time histories. The potential energy from the drop ends up as heat. By plotting the load versus the deflection, it is possible to assess the dissipation. This is interesting as the elastic response will be altered if there is a relatively big loss, which in turn affects the linear elastic layer response. For improving on the vehicle rolling resistance, the dissipation should be minimized. However, the total dissipation derived from the center sensor is the combined effect of all the reasons mentioned above. Thus, there is a mix of apples, oranges and other fruits contributing to the dissipation.

6 Dissipation in Various Layers

The dissipation in bound layers consists of the fracture mechanics energy leading to crack propagation and finally fatigue cracking. This process was clarified by Rowe (1996).

In recent years, new backcalculation techniques have been developed. Thus, the total dissipation can be sorted by looking at all sensors' displacements much like the process for backcalculating the elastic modulus of different layers. A method to derive the cracking energy in a concrete pavement from FWD time histories was presented by Lenngren et al. (2024).

For asphalt bound pavements the influence of temperature is strong on the dissipation in the layer, due to viscoelastic response governed by the master curve for the material in question. At first thought one would assume that the fatigue is constant regardless of temperature. However, as the energy from the drop is consumed by the viscoelastic reaction, the crack energy will likely be diminished at higher temperatures. It seems that data on the master curve are most valuable. Luckily, most FWD tests proceed over some time, so that a data set is collected with some variability of temperatures. If the temperature stays the same, it is possible to use a different frequency when performing the test. Typically, a load mode for airport runways produces a much shorter load rise time, which can be used for the purpose, as demonstrated by the author, Lenngren 1994.

7 Analysis

The software TIMEHIST can be used to evaluate each sensor's response. Figure 1 shows an example from an intermediate asphalt layer road. The top diagram shows the load deformation curves, and the bottom diagram shows the load and deformations in the time domain. The outer dissipation. Thus, the dissipation in the asphalt layer is the area in the red loop minus the area in the green loop.

Figure 2 shows two curves from two different pavements. The narrow curve is from a cold pavement on a motorway at a few degrees Celsius. The shape of the curve resembles tests on Portland cement concrete and similar materials. The fat curve is from a thick asphalt pavement at 40 degrees Celsius. The shape of the curve is formed by the viscoelastic effects, with a clear delay of the response.

8 Conclusions

By evaluating time history curves, it is possible to assess the dissipation in various layers from an FWD load.

Over the years, various investigations have been conducted from rolling resistance to fracture mechanics and viscoelastic evaluation. Balanced Mix Design has been used by several state agencies over some time by now. It is primarily based on laboratory testing, but with a few exceptions, there are few studies on the actual behaviour of these pavements in the field. There is a need for feedback, especially when performance contracts and/or extended warranties are employed.

The present feasibility study shows that it is indeed possible to assess the mechanistic parameters that govern fatigue and permanent deformation as well by analysing FWD dynamic data. For each test the variation of temperature helps in correctly assess the master curve. As more projects are being analysed, they should be included in a data base for Artificial Intelligence evaluation, even if current data bases already are substantial in size for this purpose.

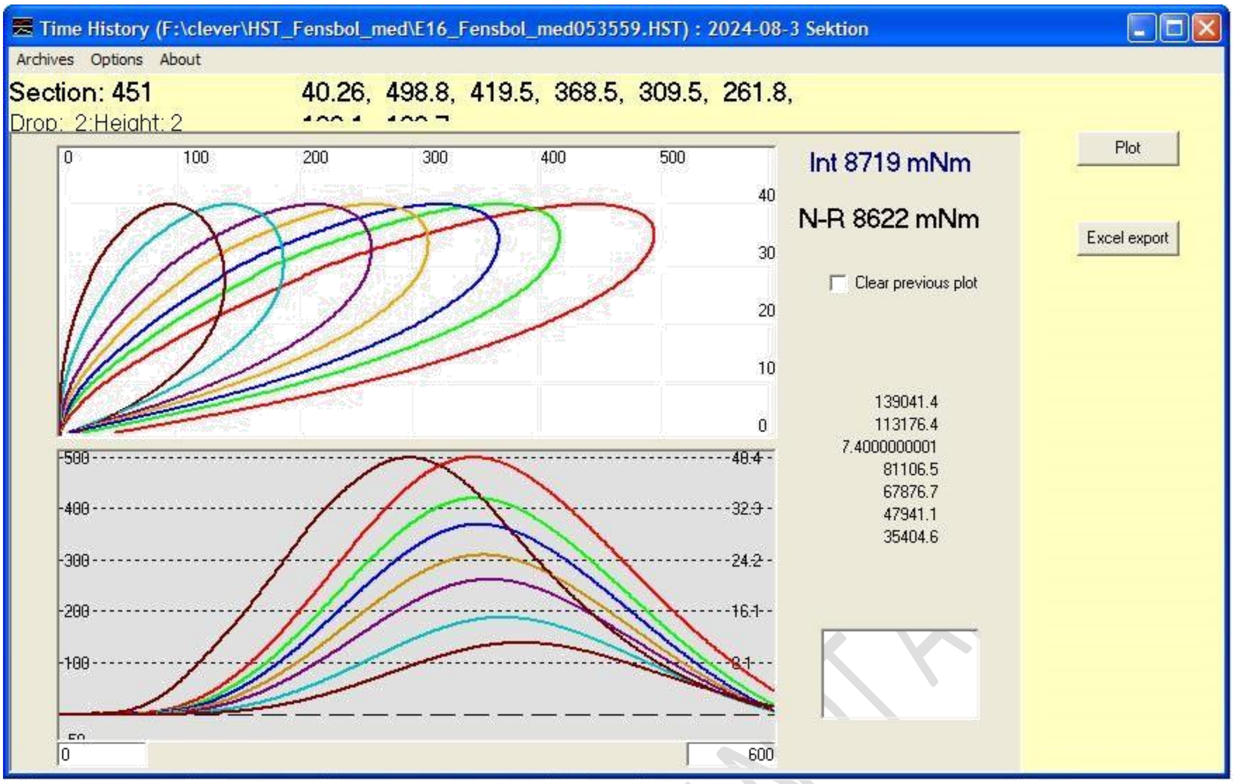

Figure 1: *Output from the TIMEHIST software.*

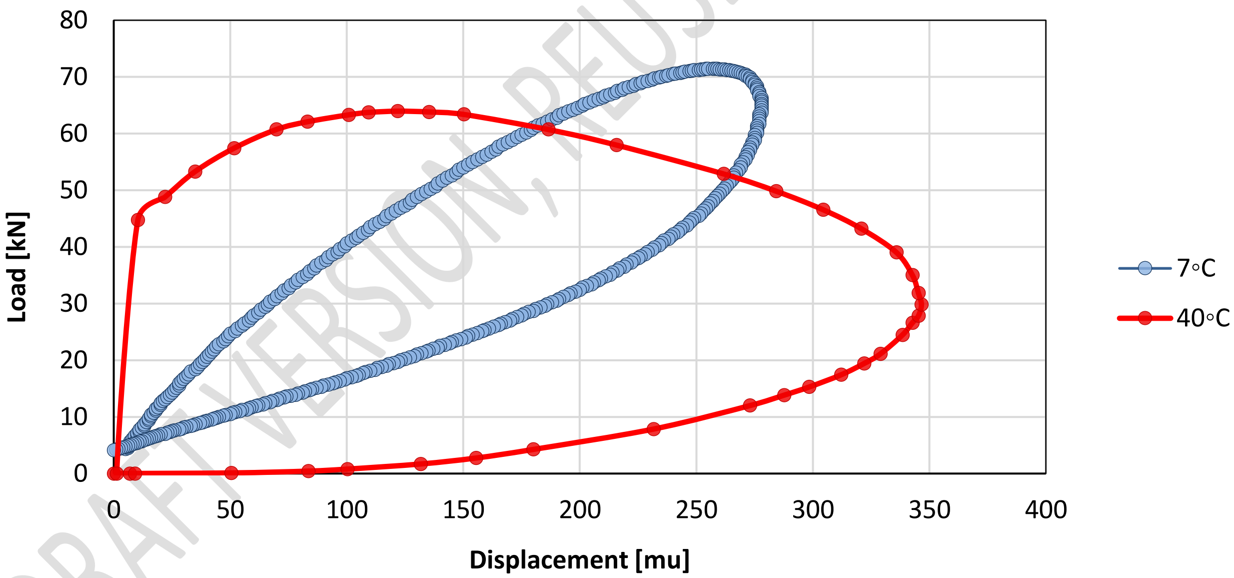

Figure 2: *Two different behaviours at different temperatures.*

9 References

Zhou, F. et al. 2007. A Balanced HMA Mix Design Procedure for Overlays. Journal of the Association of Asphalt Paving Technology, Volume 76. Pp. 823-848.

Hajj, E. Y., Aschenbrener, T.B., Nener-Plante, D. 2022 Positive Practices, Lessons Learned, and Challenges When Implementing Balanced Design of Asphalt Mixtures: Site Visits, WRSC-TR-22-11 March 2022 Pavement Engineering & Science Program University of Nevada, Reno

Magnuson, A.H., et al. 1991 Comparison of Computer Predictions and Field Data for Dynamic Analysis of Falling Weight Deflectometer Data. In Transportation Research Record 1293, pp. 61-71

Rowe, G.M.: 1996. Application of the Dissipated Energy Concept to Failure Cracking in Asphalt Pavement. PhD Thesis, University of Nottingham

Lenngren, C., Salini, R., Hernandez, M. 2024. Employing Field Energy Attenuation in Portland Cement Concrete Pavements as a Design Parameter . *Proceedings of the International Conference on Concrete Pavements*. 13, 1 (Aug. 2024), 149–161.

Lenngren C.A., 1994. Non-Destructive Testing Utilizing Controlled Variable Rise Time, Proceedings Fourth International Conference on Bearing Capacity of Roads and Airfields, Vol. 1, pp 467-490, 1994.

Fracture Characteristics of Cored Brazil Disk Geometry

Akash Bajaj
Imad L. Al-Qadi
Illinois Center for Transportation, Grainger College of Engineering, USA
University of Illinois Urbana Champaign, Rantoul, Illinois, USA
John Lambros
Department of Aerospace Engineering, Grainger College of Engineering,
University of Illinois Urbana-Champaign, USA

Abstract

Performance tests have become a vital tool for accurately assessing the damage potential of asphalt concrete (AC) as part of balance mix design philosophy. Geometries like semi-circular bend (SCB) and Brazil disk have been traditionally used to test the ultimate failure strength. Fracture mechanics principles have proven effective in describing AC cracking behavior by considering material properties, loading conditions, and the impact of geometry on stress distribution and ultimate cracking. Given the heterogeneous composition and viscoelastic nature of AC, energy losses constitute a significant portion for strength testing at room temperature.

While a notch in the SCB geometry has been used to concentrate stress at the tip and thus localize energy dissipation, no similar modification has been applied to the Brazil disk geometry for AC. This study addresses that gap by introducing a circular core into the Brazil disk specimen to create localized stress concentration. The resulting centrally cored disk (CCD) was evaluated under various configurations using a universal testing machine.

Fracture mechanics was used to quantify the cracking potential of AC mixes. Digital image correlation was employed during testing to capture both local and global strain fields, as well as crack tip opening displacements. A preliminary cracking index parameter, derived from the far-field applied load-displacement curve, was developed for practical applications. Ultimately, the study demonstrates the practical utility of the CCD geometry in effectively characterizing cracking in AC mixes and the prediction of AC fracture energy.

Keywords: asphalt concrete; fracture; Brazil disc; I-FIT; IDEAL-CT; DIC

1 Introduction

Asphalt concrete (AC) mix design was traditionally relied on volumetric properties like air voids (AV), voids in mineral aggregates (VMA) and binder content, as these were assumed to be reliable indicator of field performance. With the increasing use of recycled materials, rejuvenators, highly polymer modified binders, and novel additives, the design process has moved towards the performance driven philosophy of balance mix design (BMD). BMD incorporates lab-based performance testing for common AC pavements distresses, like rutting and cracking, in AC mix design and production stages to ensure a superior mix for use in pavements. As contractors and agencies try to increase pavement durability and reduce the global footprint of construction, BMD offers cost effective way to ensure longer lasting pavements. While BMD methodologies highlight the importance of performance-based testing, current FAA specifications primarily address rutting resistance, leaving a critical gap in evaluating the cracking potential of AC mixes.

The Illinois Flexibility Index Test (I-FIT) and Cracking Tolerance Index (CT_{index}) test, also called the IDEAL-CT, are widely used for characterizing cracking potential of AC mixes due to their rapid and cost-effective nature along with ease of implementation for a BMD protocol. I-FIT is performed on a semi-circular bend (SCB) specimen with a notch to act as stress concentration and, therefore, progresses as a true fracture test. On the other hand, a Brazil disk geometry is used for CTindex making it more like a strength test due to lack of any stress concentration (Al-Qadi et al., 2022).

The results from the FAA test lanes showed that the Flexibility Index (FI) measured with I-FIT was able to discern the cracking potential of AC when compared with CTindex as shown in Figure 1. Comparison of PMLC and LMLC specimen results showcased that the CT_{index} was significantly influenced by the aggregate skeleton while binder type and quantity contribute more significantly to the FI values. Both FI and CTindex increased with increase in AV and dropped after LTOA as expected. A threshold of 7 for STOA and 4 for LTOA for FI was recommended for airfield mixes during design and quality assurance process. No such threshold for CT_{index} was able to be validated (Bajaj et al., 2025).

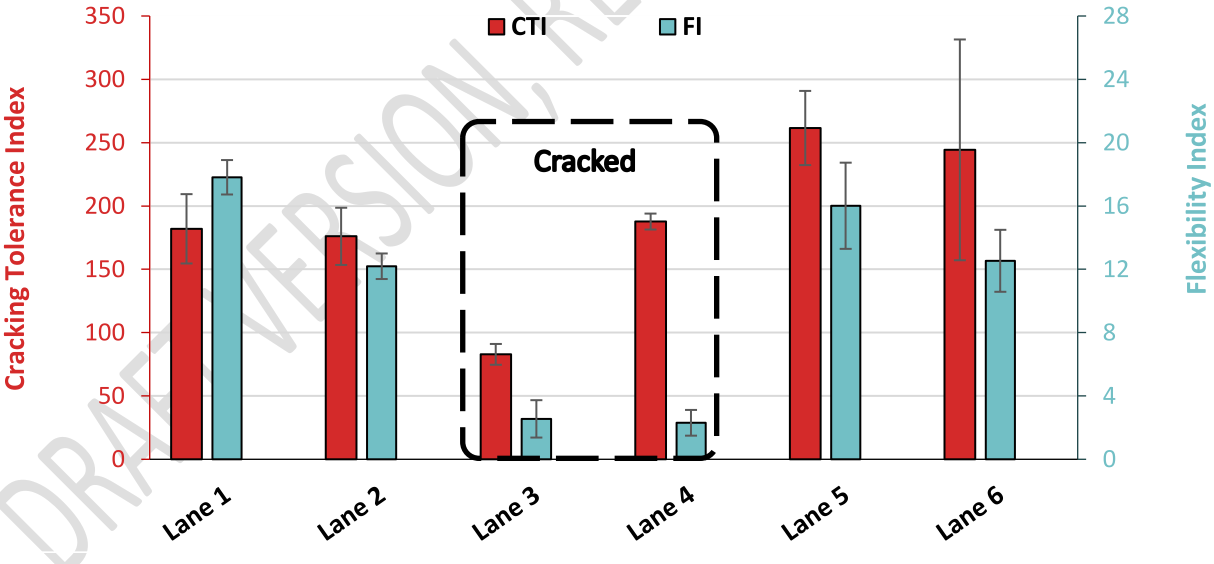

Figure 1: *Flexibility index and CT index values for FAA test lanes.*

Due to ease of fabrication, easy implementation and historical knowledge of IDT testing, the CT_{index} is a relatively popular test but it fails to isolate the fracture response. Digital image correlation (DIC) was used to capture the full-field response during the test, as shown in Figure 2 (a), and showcases significant plastic deformation, crushing at loading strips and bulk dissipation of energy during the test. This stress test was converted to a fracture test with the introduction of a stress concentration hole in the center of the disk. This idea of a central hole was previously explored by (Roque et al., 1999) for low temperature IDT. This cored Brazil Disk test was able to better access the fracture properties of AC mixes due to localization of macrocracking in specimen and reduction in non-fracture related energy during the test, as can be clearly seen in Figure 2 (b).

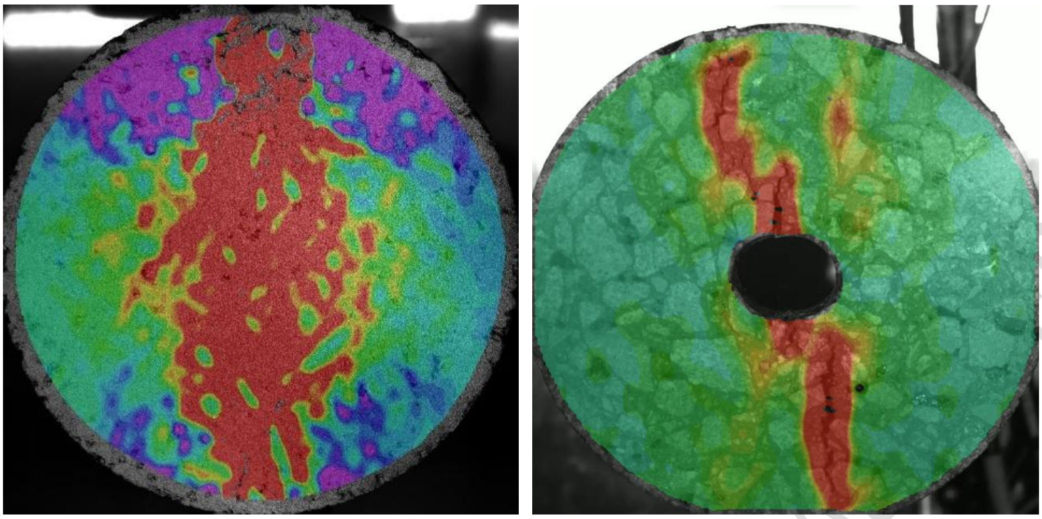

(a) *(b)*

Figure 2: *Full-field strain response during (a) CT index test and (b) centrally cored disk test.*

2 Summary and Conclusions

The study explored the optimization of testing condition (loading rate, specimen thickness, loading strip geometry) in order to minimize all non-fracture energy supplied during the test. A fracture-mechanics based index is developed to properly capture the cracking process for AC that is both practical and scientific. The study characterizes the fracture and strength metrics of various AC mixes and showed strong relationship between AC fracture properties and in-field cracking at service temperature. Impact of various mix design parameters like AV and binder type is studied and a recommended threshold is developed for implementation.

3 References

Al-Qadi, I. L., Said, I. M., Ali, U. M., & Kaddo, J. R. (2022). Cracking prediction of asphalt concrete using fracture and strength tests. International Journal of Pavement Engineering, 23(10), 3333–3345. https://doi.org/10.1080/10298436.2021.1892108

Bajaj, A., Gangidi, N., Al-Qadi, I. L., & Pine, W. J. (2025). Fracture and Strength Tests for Airfield Balance Mix Design. Presented at the ASCE T&DI International Airfield and Highway Conference 2025.

Roque, R., Zhang, Z., & Sankar, B. (1999). Determination of Crack Growth Rate Parameters Of Asphalt Mixtures Using the Superpave IDT. Journal of the Association of Asphalt Paving Technologists, 68, 404–433. https://trid.trb.org/View/639717

Comparative Evaluation of Virgin and Recovered Binders from Hot Mix Asphalt and Warm Mix Asphalt with Foamed Bitumen

dr. Dejan Hribar
STRABAG d.o.o. Ljubljana, Laboratory TPA, Slovenia
dr. Lidija Ržek
Slovenian National Building and Civil Engineering Institute, Ljubljana, Slovenia

Abstract

In this study, warm mix asphalt (WMA) with foamed polymer-modified bitumen was compared with conventional hot mix asphalt (HMA). The investigation focused on the properties of the original binder and the binders recovered from both WMA and HMA produced in a full-scale motorway trial in Slovenia. The characterisation of the binder included empirical tests (penetration, softening point, Fraass breaking point, ductility) and rheological analyses using a dynamic shear rheometer. The results indicate age-related stiffening in all the recovered binders, with WMA showing less ageing compared to HMA. While WMA exhibited slightly lower rutting resistance (G/sin δ), it showed better elastic recovery. Overall, the results confirm that WMA with foamed bitumen can achieve binder performance comparable to HMA, which supports its application in sustainable pavement construction.*

Keywords: warm mix asphalt; foamed bitumen; rheology

1 Introduction

Since the late 1990s, several warm mix asphalt (WMA) technologies have been developed to improve the workability of the binder at lower production temperatures (Cheraghian et al., 2020). The introduction of WMA is closely linked to the European Union's climate policy, which aims to reduce greenhouse gas emissions by 55 by 2030 and achieve climate neutrality by 2050 (Commission, 2021). The switch from con-ventional hot-mix asphalt (HMA) to WMA contributes to these goals by reducing energy requirements and CO_2 emissions during asphalt production and paving.

WMA is usually produced at temperatures about 30 °C lower than those used for HMA, which significantly reduces the consumption of thermal energy. Most of the energy used in asphalt production is consumed in the rotary drum, where the aggregate is simultaneously dried and heated, and in the heating of the binder (Androjić et al., 2020), (Hasan et al., 2017), (Milad et al., 2022). Depending on the technology and plant settings, energy savings of 20–75 % have been reported for WMA compared to HMA (Milad et al., 2022), (Sukhija et al., 2022).

A full-scale test of asphalt mixture AC 22 bin PmB 45/80-65 was carried out in October 2024 by Strabag on a section of motorway in Slovenia:

- a conventionally produced reference HMA and
- a WMA with foamed bitumen.

In the laboratory, both virgin and recovered binders were tested using standard empirical methods (softening point, penetration at 25 °C, Fraass breaking point and ductility at 5 °C and 10 °C for virgin and recovered bitumen respectively). The rheological properties of the binders were evaluated using a dynamic shear rheometer to assess the elastic recovery and non-recoverable creep and to characterize the elastic–viscous behavior.

2 Results and Discussion of bitumen testing

The basic physical bitumen properties are presented in Table 1. The softening point increased in both recovered binders, especially in the WMA sample, possibly due to a concentration of the polymer network or oxidized components. The penetration values of the recovered binders were lower compared to the virgin binder, indicating bitumen hardening during asphalt production. However, the recovered binder from the WMA exhibited a slightly higher penetration value than that from the HMA, suggesting reduced ageing due to the lower production temperature. The Fraass breaking point was similar for all samples, indicating satisfactory performance at low temperatures. The virgin binder tested at 5 °C achieved a total elongation of 445 mm, which is comparable to the elongation of the recovered binders tested at 10 °C. The highest maximum force and cohesive energy were found for the virgin binder, confirming its higher tensile strength. The recovered WMA binder exhibited slightly higher elongation and reference energy than the HMA binder, again indicating reduced hardening during production.

Table 1: *Basic properties of the virgin and recovered binders.*

Property	Test method	Unit	Virgin PmB	Recovered HMA	Recovered WMA
Penetration at 25 °C	SIST EN 1426:2015	1/10 mm	58	36	44
Softening Point (R&B)	SIST EN 1427:2015	°C	70.0	70.8	80.0
Fraass Breaking Point	SIST EN 12593:2015	°C	-18	-17	-18
Total elongation	SIST EN 13589:2018	mm	444.89	462.28	485.33
Maximum force	SIST EN 13589:2018	N	59.18	50.58	36.96
Total energy	SIST EN 13589:2018	J/cm²	14.23	10.86	11.34
Reference energy $E_s' = E_{0.4}' - E_{0.2}'$	SIST EN 13589:2018	J/cm²	6.58	4.40	4.78

The rheological evaluation (Table 2) confirms the age-related stiffening of both recovered binders compared to the virgin polymer modified bitumen (PmB 45/80-65), as evidenced by higher critical temperatures (T at G* = 15 kPa) and lower phase angles (δ), indicating increased stiffness and elasticity due to ageing. The susceptibility to rutting was assessed using the rutting parameter G/sinδ determined for the recovered binders. The binder extracted from the HMA mixture exhibited a higher G/sinδ value at the reference value of 2.2 kPa for short-term aged binders, indicating higher stiffness and potentially better resistance to permanent deformation compared to the WMA binder. The binder recovered from HMA is the stiffest and most stable under load (lowest J_{nr} and R_{diff}), but may exhibit increased brittleness due to lower flexibility. The WMA binder, on the other hand, has slightly lower stiffness and better elastic recovery (highest R-values), suggesting better resistance to fatigue and cracking. While both recovered binders have better rutting resistance than the virgin binder (lower J_{nr} value), the WMA binder offers a more favorable balance between elasticity and stiffness at high service temperatures, making it potentially better suited for long-term performance.

Table 2: *Rheological properties of the virgin and recovered binders.*

Property	Test method	Unit	Virgin PmB	Recovered HMA	Recovered WMA
T at G*=15 kPa	SIST EN 17643:2022	°C	54.6	62.4	58.8
δ at $T_{G^*=15\ kPa}$	SIST EN 17643:2022	°	61.4	58.4	58.0
T at G*/ sinδ>2,2 kPa	SIST EN 17643:2022	°	/	83.6	80.3
$R_{0,1\ kPa}$	SIST EN 16659:2016	%	74.4	74.6	80.7
$R_{3,2\ kPa}$	SIST EN 16659:2016	%	59.3	70.8	74.1
R_{diff}	SIST EN 16659:2016	%	20.4	5.1	8.2
$J_{nr\ 0,1\ kPa}$	SIST EN 16659:2016	kPa-1	0.197	0.074	0.082
$J_{nr\ 3,2\ kPa}$	SIST EN 16659:2016	kPa-1	0.340	0.088	0.118
$J_{nr\text{-}diff}$	SIST EN 16659:2016	%	72.5	19.6	43.3

3 Conclusions

In this study, a comparative evaluation of hot mix asphalt (HMA) and warm mix asphalt (WMA) was carried out on the basis of a full-scale field trial and comprehensive laboratory tests. The results of the binder and asphalt mixture tests show that WMA has comparable mechanical properties to HMA. While the recovered binder from the WMA mixture exhibits slightly lower rutting resistance based on the parameter G*/sinδ, it shows higher fatigue resistance. Field data confirms that WMA produced at significantly lower temperatures achieves uniform compaction and layer thickness, supporting its practical feasibility. These results underpin the potential of WMA as a sustainable alternative to conventional HMA, combining environmental benefits with satisfactory mechanical performance.

Continuous monitoring of the experimental section is recommended to evaluate the long-term performance of WMA under traffic and environmental loading. Further research should investigate the incorporation of reclaimed asphalt pavement (RAP) into WMA mixtures to enhance sustainability and support circular economy principles.

4 References

Androjić , I., Dolaček Alduk, Z., Dimter, S., & Rukavina, T. (2020). Analysis of impact of aggregate moisture content on energy demand during the production of hot mix asphalt (HMA). Journal of Cleaner Production, 244(118868).

Cheraghian, G., Falchetto, A. Y., You, Z., Chen, S., Kim, Y., Westerhoff, J., Wistuba , M. (2020). Warm mix asphalt technology: An up to date review. Journal of Cleaner Production, 268. doi:https://doi.org/10.1016/j.jclepro.2020.122128

Commission, E. (2021). 'Fit for 55': delivering the EU's 2030 Climate Target on the way to climate neutrality. Retrieved 7 31, 2025, from https://eur-lex.europa.eu/legal-content/EN/TXT/?uri=CELEX%3A52021DC0550

Hasan, M., You, Z., & Yang, X. (2017). A comprehensive review of theory, development, and implementation of warm mix asphalt using foaming techniques. Construction and Building Materials, 152, 115-133.

Milad, A., Babalghaith, A. M., Al-Sabaeei, A., Dulaimi, A., Ali, A., Reddy, S. S., Yusoff, N. I. (2022). A Comparative Review of Hot and Warm Mix Asphalt Technologies from Environmental and Economic Perspectives: Towards a Sustainable Asphalt Pavement. International Journal Environmental Research and Public Health. doi:https://doi.org/10.3390/ijerph192214863

Prediction Asphalt Airfield Pavement Low Temperature Cracking Potential

Akash Bajaj
Illinois Center for Transportation, Grainger College of Engineering, University of Illinois Urbana Champaign, Rantoul, Illinois, USA
Shubham Modi
Department of Civil and Environmental Engineering, University of New Hampshire, Durham, New Hampshire, USA
Imad L. Al-Qadi
Illinois Center for Transportation, Grainger College of Engineering, University of Illinois Urbana Champaign, Rantoul, Illinois, USA
Eshan Dave
Department of Civil and Environmental Engineering, University of New Hampshire, Durham, New Hampshire, USA
Jo Sias
Department of Civil and Environmental Engineering, University of New Hampshire, Durham, New Hampshire, USA

Abstract

The US Federal Aviation Authority (FAA) Advisory Circular AC 150/5370-10H details the specifications for asphalt concrete (AC) mix designs using both Marshall and Superpave methods. Currently, the specifications dictate the volumetric properties of AC mix designs (e.g., air voids, Voids in Mineral Aggregate (VMA), and number of blows/gyrations). With current spotlight on using balance mix design (BMD) philosophy, there has been an increasing interest in incorporating performance tests, in addition to volumetric properties. FAA specifications currently include performance tests for rutting and moisture susceptibility, but tests to characterize cracking potential are overlooked.

The aim of this study was to develop a protocol to characterize AC cracking potential. The protocol is practical, scientifically rigorous, and easy to implement. Cracking in AC is usually present in two distinct regions: i) Crack initiation, which includes microcrack nucleation and agglomeration, and ii) crack propagation, which evolves as a macrocrack grows with successive load applications. The study included testing of lab-mix lab-compacted, plant-mix lab-compacted, and field cores specimens obtained from 10 airports and the FAA National Airport Pavement and Materials Research Center facility.

Testing was conducted in three domains: Low temperature cracking, room temperature cracking, and fatigue cracking. In this paper, the low temperature cracking part is presented. The testing utilized a simplified low temperature semi-circular bend (SLT-SCB) test method, and test results were correlated to crack initiation. The SLT-SCB test results were successfully used to distinguish mix performance. Hence, the test deemed practical for application during mix design and quality assurance phase. The impact of various mix design parameters like air voids, asphalt binder content and type, aggregate gradation and lithology were also quantified. A testing protocol, with thresholds for mixes, was developed.

Keywords: asphalt concrete; low temperature cracking; FAA; airfield

1 Objective and Scope

The objective of this study was to develop and validate a simplified low-temperature SCB (SLT-SCB) protocol for assessing asphalt concrete (AC) for low-temperature cracking potential. The protocol was designed to be rigorous, rapid, and reliable for inclusion in a BMD framework and be applicable for adoption within P-401/403 specifications of the FAA. An SCB geometry was chosen for its simple fabrication and widespread laboratory use. Key testing parameters of the AASHTO T 394 were modified, including the selection of site-specific test temperature, operation in load-line displacement control, and loading rate, mainly to enhance the practicality of the test.

AC mixes were collected from seven airfield pavements across the United States with diverse location climates, mix designs, and components to ensure real-world relevance and were tested according to the SLT-SCB protocols. The protocol was validated using field cores from two in-service airfields and the FAA's National Airport Pavement and Materials Research Center (NAPMRC).

2 Simplified Low Temperature SCB (SLT-SCB) Test Protocol

2.1 Loading Rate Selection

Previous research has established that a crack mouth opening displacement (CMOD) rate of 0.7 mm/min in SCB geometry is analogous to a 1 mm/min CMOD rate in the DCT geometry (Dave & Behnia, 2018). Therefore, experimental trials were performed for three AC mixtures with varying nominal maximum aggregate size (NMAS), ranging from 4.75 to 19mm, to establish the load line displacement (LLD) rate necessary for maintaining the target CMOD rate of ≤0.7 mm/min at a test temperature of -12°C. Among these, a 4.75mm NMAS AC highway mixture, selected to account for smaller NMAS AC mixes. The procedure suggests a loading rate of 0.19 mm/min for 19mm NMAS (Newark Liberty International Airport), 0.21 mm/min for 12.5mm NMAS (Teterboro Airport), and 0.23 mm/min for 4.75mm NMAS to match a CMOD rate of ≤0.7 mm/min. The results indicated that the LLD rate required to achieve the target CMOD rate was influenced by the NMAS of the AC mixture. Specifically, the LLD rate was inversely proportional to the NMAS of the mixtures, varying from 0.17 mm/min to 0.23 mm/min. Therefore, a 0.15 mm/min LLD rate was selected for the study to ensure a CMOD rate of ≤0.7 mm/min across all airfield mixtures. The selected loading rate effectively reduces the likelihood of plastic deformation, creep effects, and softening behavior of the material that could occur at slower loading rates, while also mitigating the risk of sudden failure associated with faster loading rates.

2.2 Load-LLD Plot Parameters

Figure 1(a) shows a typical load-LLD plot for an LLD-controlled test. In the LLD case, an initial curvature is observed upon loading, resulting from the seating of the specimen on the supports and the development of the contact area, followed by the material's linear behavior. Finally, a sudden drop in load is observed due to the release of bulk-response (pre-fracture overall stress build-up in the specimen) energy stored in a specimen at such a low temperature.

At low temperatures, AC mixtures behave predominantly in an elastic manner with limited viscous dissipation, especially at a higher loading rate, and crack initiation becomes the dominant factor in fracture response. By monitoring CMOD measurements as a measure of crack growth, the CMOD-time plot shown in Figure 1(b) exhibits a sharp uptick near the peak load, marking a transition from crack initiation to propagation. For practicality and ease of implementation, the study approximates the initiation energy by calculating the pre-peak area under the load–LLD curve.

In addition to pre-peak fracture energy, the study considers the loading characteristics of the AC mix during testing by measuring loading stiffness. This particular stiffness measure was calculated from the linear portion of the load-LLD curve at the mid 50% pre-peak region using a sliding window regression enhanced with a chi-square penalty term (α).

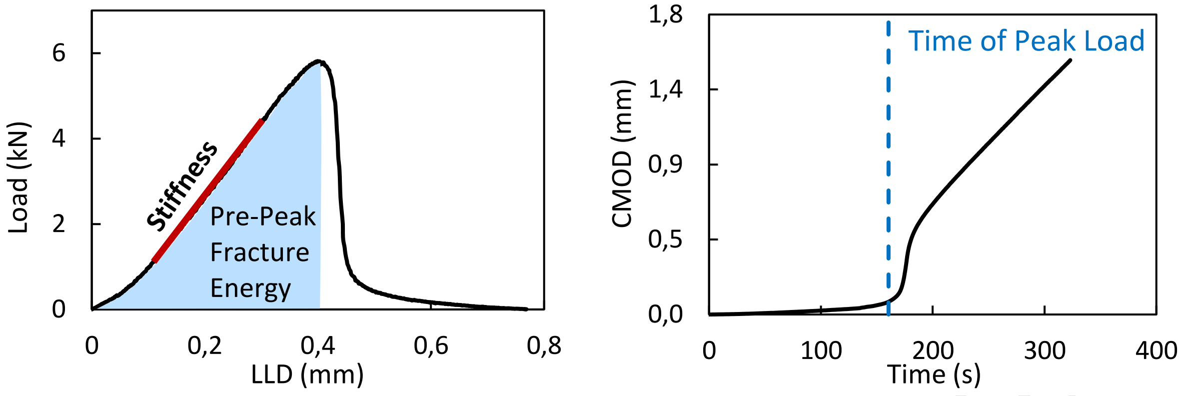

(a) *(b)*

Figure 1: *A typical (a) load-LLD and (b) CMOD-time plots for SLT-SCB.*

To provide a single index parameter, the study proposes Low-Temperature Cracking Index (LCI) as a metric to assess AC cracking potential at low temperatures. LCI was defined as the ratio of pre-peak fracture energy (PFE) to the measured stiffness (S) from the SLT-SCB test, as shown in the equation below. A higher LCI indicates higher energy required for crack initiation, or lower stiffness, implying an increased strain tolerance before fracture for materials with similar fracture energies. A higher LCI of an AC mixture would thus signify better resistance against low-temperature cracking.

$$LCI = G_{f-pre}/S,$$

Where:

- LCI– Low-Temperature Cracking Index;
- Gf-pre – Pre-peak Fracture Energy (J/m2);
- S – Stiffness (kN/mm).

2.3 Test Temperature Selection

The recommended testing temperature was selected based on site-specific low-temperature data which reflects the actual in-service geographical conditions of the AC mixtures. The rationale for this deviation from using low temperature PG for testing lies in the inherent limitations of PG-based selection, which prevents contractors from using a softer binder in a mix. From the data, the 50th percentile low temperature is a practical and effective choice, as it aligns well with the binder grade selection traditionally used for airfield pavements. An upper limit of -12°C is proposed to avoid creep effects for mixtures from warmer regions, in line with the FAA's requirement for a minimum binder grade of PG XX-22. Final test temperature was selected as 10°C warmer than the 50th percentile low temperature.

3 Results and Discussion

Figure 2 presents the results of the SLT-SCB test conducted on field cores obtained from three locations—Willard Airport (CMI), Kansas City International Airport (MCI), and six FAA test lanes at the NAPMRC. Among the FAA test lanes (all constructed in 2019), L3 and L4 exhibited cracking after accelerated loading(Alvarez et al., 2024). The cracks were believed to originate due to loading below the pavement surface. During the first winter cycle, the cracks became more prominent and propagated to the surface, indicating a higher cracking potential of L3 and L4. The SLT-SCB results aligned with the observations, as both L3 and L4 had notably lower LCI values, confirming their higher susceptibility to low-temperature cracking.

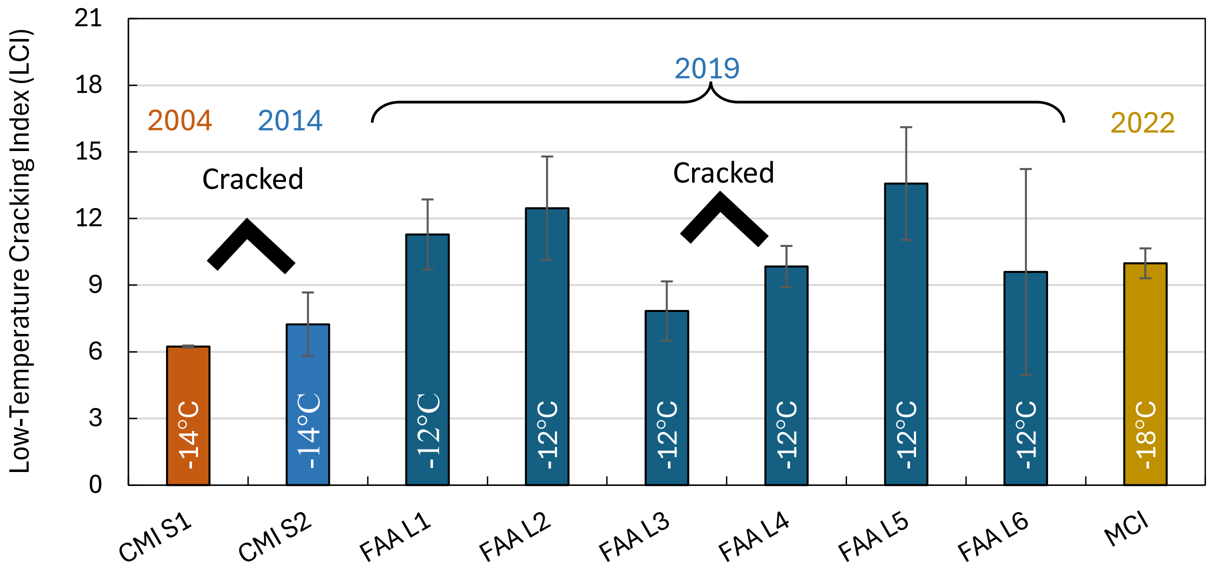

Figure 2: *LCI values of field cores (bars show test temperature).*

Both CMI sections exhibited low LCI values, consistent with the expected an increase in cracking potential of AC mixtures with aging in older surfaces. During the most recent condition assessment before reconstruction, both CMI pavement sections exhibited medium-severity cracking, including longitudinal, transverse, alligator, and block types (Illinois 2022-2024 IDEA. Meanwhile, the MCI cores, collected from a newly resurfaced pavement in 2022, showed a better LCI value compared to CMI cores, even at a lower test temperature (-18°C), reflecting its satisfactory performance. Collectively, the findings confirm that the SLT-SCB test, and its associated LCI, can reliably differentiate AC mixtures by their susceptibility to low-temperature cracking.

4 Summary and Conclusions

The study presents an SLT-SCB test protocol to assess the low-temperature cracking potential of airfield AC mixtures. The protocol is a modification of the existing AASHTO T 394 standard procedure. The SLT-SCB is a scientific, rapid, repeatable, and practical test that could be easily incorporated into the BMD framework with standard laboratory fixtures. Therefore, integrating the SLT-SCB into FAA Advisory Circular AC 150/5370-10H would provide airfield engineers with a tool to incorporate low-temperature cracking potential into design considerations alongside volumetrics, rutting criteria, and possibly in-service cracking.

5 References

Alvarez, D. B., Kazmee, H., & Garg, N. (2024). Laboratory and Field Performance Evaluation of Cracking of Airfield Warm Mix Asphalt with Reclaimed Asphalt Pavement at the National Airport Pavement and Materials Research Center. Transportation Research Record, 2678(11), 530–546. https://doi.org/10.1177/03611981241242071

Dave, E. V., & Behnia, B. (2018). Cohesive zone fracture modelling of asphalt pavements with applications to design of high-performance asphalt overlays. International Journal of Pavement Engineering, 19(3), 319–337. https://doi.org/10.1080/10298436.2017.1353393

Illinois 2022-2024 IDEA — Airport Details. https://idea.appliedpavement.com/hosting/illinois/airport-details/airport-details.html

Performance Characteristics of Rheological Behaviour and Chemical Properties for Recovered Asphalt Binders

Min-Chih Liao
Department of Civil and Construction Engineering, National Taiwan University of Science and Technology, Taipei, Taiwan R.O.C.

Abstract

As a critical binding material in paving mixtures, asphalt's rheological properties and chemical characteristics considerably affect the stability and durability of the pavements. Therefore, evaluating the short- and long-term aging behaviour of recovered asphalt is crucial for predicting pavement durability. Asphalt sampling as well as coring from two trial road sections were conducted in this study. AC20 unmodified and Type IV-F polymer modified asphalt binders were extracted and then recovered from asphalt mixtures to investigate their performance characteristics that occur during 0-8 months of in-service HMA pavements. The binders tested in this study include virgin, short-term aged and early-stage aged asphalt binders. Test results revealed a rapid increase in stiffness for asphalt binders during 1 month of in-service HMA pavement, while recovery performance was observed after 4 months. Regarding rheological behaviour, the modified asphalt binder showed a greater decline in elasticity and toughness under low- to medium-temperature aging conditions, while the AC20 binder exhibited more variation at intermediate to high temperatures and demonstrated better recovery over time. Observing the aging response over time, the aging indices of AC20 binder mostly fell between 2.0 and 2.5 during months 4 to 8, whereas those of the modified binder reached between 2 and 4. It is found that the presence of modifiers may result in more pronounced aging effects compared to unmodified asphalt. Furthermore, the CTindex^b of the binder showed a high correlation ($R^2 = 0.84$) with the CTindex of the mixture, highlighting its potential as a predictive indicator of crack resistance. This study contributes to have a better understanding of asphalt binder aging that occurs at early age of in-service HMA pavement, but long-term monitoring is needed in order to validate aging behaviour of asphalt.

Keywords: rheology; aging ; CT$_{index}$; RT$_{index}$; balanced performance

1 Introduction

Due to the recent dramatic growth of traffic intensity and higher axle loads, newly rehabilitated pavements on many of the national freeways in Taiwan show signs of distress such as rutting and cracking. Pavement rutting is of concern to road users because ruts may trap water, leading to hydroplaning. Cracking is also related to traffic stress, as potholes of various sizes can occur in the wheel paths due to water penetrating into the cracks during the rainy season (Islam et al., 2024). Balanced performance evaluation is the practice of assessing asphalt mixtures to account for aging, traffic, environment, and location within the pavement system so that several forms of distress can be mitigated (Zhou et al., 2021).

This study focused on assessing the field rutting and fatigue cracking of asphalt specimens after different ageing times due to the need for life cycle analysis of asphalt pavements in Taiwan. The objectives of the study were to: (1) evaluate the degree of ageing of the asphalt binders, (2) assess the aging degree of the asphalt mixtures, and (3) establish the balanced performance of the mixtures.

2 Methodology

The three types of asphalt mixtures used in this study were produced using aggregate from a limestone quarry. The experimental program included three combinations of nominal maximum aggregate size (NMAS), RAP content and asphalt binder type. as listed in Table 1. In addition, the asphalt plant-mix was collected from the spreader auger on paver during the laying process. In addition, the newly rehabilitated asphalt pavement was cored after 4-month construction. The field cores were taken for the IDEAL-CT and IDEAL-RT (Leavitt et al., 2024). The short-term and long-term aged binders were then extracted and recovered from the loose mixes and field cores, respectively, for further binder rheological tests (Poulikakos et al., 2014).

***Table 1**: Test trial sections and designations for asphalt mixtures.*

Mixture ID	Highway	Location	AADT (One-way)	NMAS (mm)	RAP Content (%)	Virgin Asphalt
25 mm AC20	No.1	Taoyuan County	11.400	25	0	AC20
19 mm AC10	No.6	Miaoli County	5.000	19	27	AC10
19 mm PMA	No.29	Kaohsiung County	5.900	19	0	PMA

3 Results and Discussion

As seen in the quadrant diagram in Figure 1, a soft mix, a super mix, a poor mix and a stiff mix can be identified based on rutting and cracking performance. The AC10 mix which contained 27% RAP, as expected, showed the highest rutting resistance and the lowest cracking resistance. As expected, the cracking resistance decreased as adding the RAP, but the mixtures became more rut-resistant. In general, the addition of RAP (without rejuvenator) would enhance the rutting performance. However, concern should be raised with the fatigue cracking resistance. Based on the performance space diagram, the unmodified asphalt mixtures with AC20 binder were found to lie on the top-left section of Figure 1 which implies they can be used for cracking-controlled pavement. The PMA asphalt mixtures were regarded as super mixes, which could be used as heavy-duty paving materials. With the sufficient thickness for the base layer, the occurrence of bottom-up or top-down cracking would not be an issue. It is also interesting to note that the trend of the rutting-cracking relationship tended toward the bottom right section with increasing service time. However, it is still needed to keep monitoring the long-term balanced performance in this ongoing project (Hu et al., 2023).

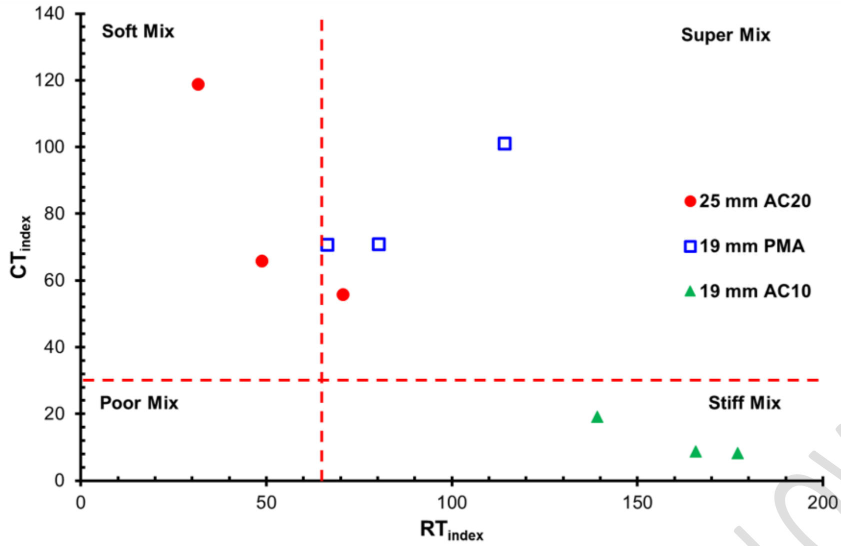

***Figure 1**: Performance space diagram for asphalt mixtures.*

4 Conclusions

This paper evaluates the binder aging behaviour and mixture balanced performance of the short-term plant mixes and field cores. It should be noted that the results de-scribed in this paper are confined to the materials, procedures and equipment used in this study. The following conclusions based on the laboratory and field results can be made:

- In terms of the performance space diagram, the AC 10 mix which contained 27% RAP showed the highest rutting resistance and the lowest cracking resistance.
- the cracking resistance decreased as adding the RAP, but the mixtures became more rut-resistant. In general, the addition of RAP (without rejuvenator) would enhance the rutting performance, but concern should be raised with the fatigue cracking resistance.
- The trend of the rutting-cracking relationship tended toward the bottom right section with increasing service time. However, it is still needed to keep monitoring the long-term balanced performance in this ongoing project for the life cycle analysis of pavements in the future.

5 References

Hu, Y. P., Xia, W., Xue, Y., Zhao, P. X., Wen, X. Y., Si, W., Wang, H. P., Zhou, L. & Airey, G. D. 2023. *Evaluating the ageing degrees of bitumen by rheological and chemical indices*. Road Materials and Pavement Design, 24, pp. 19-36.

Islam, M. R., Salomon, D. & Wasiuddin, N. M. 2024. *Investigation of oxidative aging of field-extracted asphalt binders at various conditions using carbonyl index*. Construction and Building Materials, 415, 134969.

Leavitt, A., Martin, A. E. & Arámbula, E. 2024. *Model for evaluating cracking performance of asphalt pavements with field aging based on IDEAL-CT parameters*. Transportation Research Record, 2678(10), pp. 14-25.

Poulikakos, L. D., dos Santos, S., Bueno, M., Kuentzel, S., Hugener, M. & Partl, M. N. 2014. *Influence of short and long term aging on chemical, microstructural and macro-mechanical properties of recycled asphalt mixtures*. Construction and Building Materials, 51, pp. 414-423.

Zhou, F., Steger, R. & Mogawer, W. 2021. *Development of a coherent framework for balanced mix design and production quality control and quality acceptance*. Construction and Building Materials, 287, 123020.

Recycled Asphalt Mixtures: Lab, Plant, and Field Properties

Jian-Shiuh Chen
Yu-Ming Cheng
Department of Civil Engineering, National Cheng Kung University, Tainan, Taiwan

Abstract

Reclaimed asphalt pavement (RAP) offers environmental and economic benefits by reducing natural re-source consumption, lowering construction costs, and mitigating the disposal of milled materials. However, the constraints of traditional Marshall mix design in incorporating virgin asphalt into recycled asphalt concrete frequently impede the concurrent optimization of rutting and cracking resistance. To surmount these limitations, this study implemented a balanced mix design (BMD) methodology. Dense-graded recycled asphalt concrete (RAC) incorporating 20% and 30% RAP, blended with natural aggregates and virgin binders, was fabricated. Performance assessments were conducted at three pivotal stages: laboratory mix design, plant-mixed/laboratory-compacted samples, and field cores. Cracking and rutting resistance were quantitatively assessed using the cracking index (CTindex) and rutting index (RTindex), respectively. The findings underscored substantial variability in performance across the different stages, thereby indicating the inadequacy of a singular benchmark value. Consequently, the proposition is to establish stage-specific thresholds for laboratory design, plant production, and field cores to ensure long-term pavement integrity.

Keywords: balanced mix design (BMD); recycled asphalt concrete (RAC); cracking index (CTindex)

1 Introduction

Traditional Marshall mix design is conducted under the assumption that virgin bitumen fully blends with the aged binder from reclaimed asphalt pavement (RAP) (Hand et al., 2020; Kaseer et al., 2020). This could lead to underestimating the amount of virgin binders needed, potentially causing premature cracking in pavements (Tran et al., 2017; Sobieski et al., 2022). To counter this, balanced mix design (BMD) incorpo-rates performance tests, specifically the cracking (CTindex) and rutting (RTindex) resistance indices, to determine the optimal binder content (Montañez et al., 2025; Vivanco Sala et al., 2022). Implementing BMD requires evaluating engineering properties at three distinct stages: lab mix design specimens, plant-mixed samples, and field cores (Duarte et al., 2025). This study compares the CTindex and RTindex across these three stages to identify performance differences and propose benchmark values for each.

2 Materials and Methods

This study utilized polymer-modified bitumen (PMB), reclaimed asphalt pavement (RAP) containing natural aggregate, and reclaimed asphalt pavement incorporating basic oxygen furnace (BOF_RAP). Four asphalt mixtures were produced: virgin mix (denoted as R_0), mixes with 20% and 30% RAP (denoted as R_20 and R_30), and a mix with 20% BOF_RAP (denoted as B_20). Materials were sourced from two distinct field locations. Performance tests including IDEAL-CT, IDEAL-RT, and tensile strength ratio (TSR) were conducted to evaluate cracking resistance (CTindex), rutting resistance (RTindex), and water resistance, respectively, across the three stages.

3 Results and Discussion

3.1 Mixture Composition

Gradation curves for R_0, R_20, and R_30 mixtures were consistent across design, plant, and field stages, while B_20 field cores exhibited finer gradation, likely due to BOF_RAP variability. In contrast, asphalt content varied significantly among the mix design, field core, and lab-compacted stages. Variations in air voids across these stages may be attributed to differences in compaction methods.

3.2 Performance Evaluation

As shown in Table 1, the cracking resistance index (CTindex) for field cores was significantly higher than those observed during the mix design and lab-compaction stages. These discrepancies are likely attributable to variations in asphalt content, compaction methods, air void distribution, and aggregate skeleton structure. This study evaluated three potential reference thresholds: the average CTindex value of virgin mixtures, group mean (M), and the group mean minus one standard deviation (M - σ). The mean minus one standard deviation is recommended as the CTindex reference indicator across all treatment stages. This threshold represents the 16th percentile, ensuring that 84% of the evaluated data complies with the suggested limit. Given the practical requirements of quality control, the mix design and field core stages should be prioritized as the critical phases for performance compliance.

Table 1: *CTindex performance indicators for each treatment stage.*

Treatment	Virgin mix	Group mean (M)	M - σ	Recommendation
Mix design	43	49	43	43
Lab compacted	75	70	55	55
Field core	307	283	182	182

Table 2 presents the rutting resistance index (RTindex) values. The lower RTindex observed in field cores is likely attributable to the discrepancy between roller and Marshall compaction methods. For practical application, the mean minus one standard deviation (M - σ) is recommended as the RTindex reference indicator across treatments. Furthermore, the tensile strength ratio (TSR) values exceeded requirements, confirming their resistance against moisture damage.

Table 2: *RTindex performance indicators for each treatment stage.*

Treatment	Virgin mix	Group mean (M)	M - σ	Recommendation
Mix design	126	130	126	126
Lab compacted	102	97	77	77
Field core	64	50	39	39

3.3 Performance Indices

The differences in CTindex values across all stages indicate that a single CTindex threshold cannot be universally applied. Likewise, significant variation in RTindex values between stages suggests the establishment of stage-specific thresholds.

4 Conclusions

No significant differences were observed in the gradation curves of R_0, R_20, and R_30 between the mix design, and plant-mixed samples. Notably, field cores consistently showed higher CTindex values than lab samples, potentially resulting from differences in asphalt content, compaction methods, and aggregate structure. Conversely, RTindex varied significantly, with lower rutting resistance observed in field cores, likely due to their compactions methods. These discrepancies highlight that a single performance criterion is inadequate across all stages. Therefore, distinct CTindex thresholds are proposed as follows: ≥43 for mix design, ≥55 for lab-compacted samples, and ≥182 for field cores. Correspondingly, RTindex thresholds are recommended as ≥126 for mix design, ≥77 for lab-compacted samples, and ≥39 for field cores. All mixtures demonstrated excellent moisture resistance, with tensile strength ratio (TSR) values exceeding specifications, indicating sufficient virgin binder content. In cases where field core performance is impacted by porosity or binder content, using lab-compacted samples with similar characteristics are recommended for evaluation. Future studies should investigate the effects of different fresh binder types and RAP contents on these performance indices across various stages.

5 References

Duarte, G.M., Xie, W. & Castorena, C. 2025. Variability of plant-produced high recycled content asphalt mixtures within a state. Transportation Research Record, 2679(6), pp. 351–363.

Hand, A. J. T., Aschenbrener, T. & Cooper, S. 2020. A field review: successful practices and lessons learned when using reclaimed asphalt shingles in asphalt mixtures. Report No. WRSC-TR-20-01, 2020, Western Regional Superpave Center, University of Nevada Reno.

Kaseer, F., Ara´mbula-Mercado, E., Cucalon, L.G. & Martin, A.E. 2020. Performance of Asphalt Mixtures with High Recycled Materials Content and Recycling Agents. International Journal of Pavement Engineering, 21(7), pp. 863–877.

Montañez, J., Martin, A.E., Arámbula-Mercado, E., Bairgi, B.K., Verma, M., Tran, N., Yin, F., Moraes, R. & Rodezno, C. 2025. Durability evaluation of high recycled binder ratio asphalt mixtures. Transportation Re-search Record, 2679(6), pp. 426–449.

Sobieski, T., Ara´mbula-Mercado, E. & Martin, A.E. 2022. A method for characterising RAP degree of binder activity. Road Materials and Pavement Design, 23(10), pp. 2250–2270.

Tran, N., Xie, Z., Julian, G., Taylor, A., Willis, R., Robbins, M. & Buchanan, S. 2017. Effect of a recycling agent on the performance of high-RAP and high-RAS mixtures: field and lab experiments. Journal of Ma-trials in Civil Engineering, 29(1), 04016178.

Vivanco Sala, D., N. Tran, N., Yin, F. & Bowers, B.F. 2022. Evaluating Impact of corrected optimum asphalt content and benchmarking cracking resistance of Georgia mixtures for balanced mix design implementation. Transportation Research Record, 2676(5), pp. 13–29.

Enhancing Sustainable Concrete with Manganese Steel Slag Aggregates: Performance, Durability, and Economic Viability

T Vezi
Sustainable Transportation Research Group, Civil Engineering, University of KwaZulu-Natal
AIE Engineering, Australia
MMH Mostafa
Sustainable Transportation Research Group, Civil Engineering, University of KwaZulu-Natal

Abstract

The global construction industry faces growing demand for infrastructure alongside environmental pressures from aggregate extraction and waste disposal. In South Africa, manganese steel slag (MSS), a by-product of steelmaking, accumulates in large stockpiles with limited reuse. This study examines MSS as a partial replacement for natural tillite aggregates in concrete for transport infrastructure. An experimental programme assessed mechanical properties, durability, and life cycle costs at varying water-to-cement ratios. At 60% replacement, MSS mixes achieved up to 20% higher compressive strength and 12% higher flexural strength than controls, with enhanced resistance to chloride ingress and lower oxygen permeability. Workability reductions were offset by superplasticisers. Life cycle cost analysis showed 20% savings in aggregate procurement and 15% lower maintenance costs. MSS is therefore a technically viable and economically advantageous concrete aggregate, with significant potential for sustainable road, railway, and airfield pavements construction.

Keywords: manganese steel slag; sustainable concrete; durability; infrastructure; circular

1 Introduction

Sustainable infrastructure development is a pressing global priority, particularly as governments and industries strive to meet ambitious climate and environmental targets. Concrete, as the most widely consumed man-made material, lies at the heart of this challenge. Accounting for an estimated 30 billion tonnes produced annually worldwide, concrete's environmental footprint is largely tied to cement production and aggregate consumption (Cota et al., 2023). Aggregates constitute 60–75% of concrete volume, and their extraction places severe pressure on land resources, ecosystems, and communities located near quarries. In regions such as South Africa, tillite is a widely used natural aggregate, yet quarrying has resulted in escalating costs, land use conflicts, and environmental degradation. Simultaneously, the steel industry generates vast volumes of slag, a by-product of smelting and refining processes. Manganese steel slag (MSS), in particular, accumulates in significant quantities due to South Africa's position as a global leader in manganese ore production. Traditionally, this slag has been landfilled, creating waste management challenges including leachate risks, dust generation, and land occupation (Buruiana et al., 2021). The lack of industrial reuse pathways contributes to growing environmental burdens, while construction industries remain heavily dependent on virgin aggregate extraction.

Research into industrial by-product utilisation in concrete has shown promising results with materials such as blast furnace slag, copper slag, and fly ash, many of which have already been incorporated into standards and construction practices. However, manganese slag remains relatively underexplored, despite its potentially advantageous physical and chemical characteristics. MSS typically exhibits high density, angular particle shapes, and chemical stability, suggesting that it could enhance particle interlock, mechanical strength, and durability when used as an aggregate (Nath et al., 2022). Yet systematic investigations are limited, and very few studies address MSS's potential in infrastructure requiring high load-bearing capacity, such as roads, railways, and airfields. This study aims to fill that gap by evaluating the technical, durability, and economic performance of MSS as a partial replacement for natural tillite aggregates. By focusing on applications in transport infrastructure, where concrete must withstand heavy loading and aggressive environments, the research aligns material innovation with practical engineering demands.

2 Literature Review

The utilisation of industrial by-products in concrete has gained considerable attention over the past two decades as a means to improve sustainability. Blast furnace slag, for example, is widely recognised for enhancing durability and reducing chloride ingress in marine environments, while copper slag has been used to increase strength in high-performance concrete. Recycled concrete aggregates also represent a growing area of research, though concerns about variability and long-term performance remain. Recent studies have specifically examined manganese slag and its variants. Xu et al. (2024) investigated the influence of manganese slag on ultra-high-performance concrete (UHPC) and found significant improvements in compressive strength and durability, as well as minimised risks of toxic leaching. Similarly, Shen et al. (2024) assessed electrolytic manganese slag in ready-mixed concrete, reporting strong mechanical performance and high durability, provided that leaching risks were managed. Wu et al. (2024) explored synergistic combinations of electrolytic manganese residue with steel slag and ground granulated blast furnace slag, achieving superior mechanical strength and improved environmental safety.

Kwon et al. (2025) evaluated silicon manganese slag as a fine aggregate substitute in shotcrete mortar, demonstrating enhanced strength and durability, which supports its potential in high-performance applications. Complementing these experimental studies, Cota et al. (2023) presented a critical review of silico-manganese slag applications in alkali-activated materials, highlighting both environmental benefits and technical challenges. Nath et al. (2022) provided a broader review of silico-manganese slag properties, suggesting its suitability as both a binder and aggregate. On the environmental front, Buruiana et al. (2021) investigated silico-manganese slag reuse, confirming its potential for sustainable construction, provided that leaching risks are addressed through proper stabilisation. The literature therefore indicates that manganese slags can deliver mechanical and durability benefits comparable to or exceeding those of other industrial by-products. However, gaps remain in their systematic evaluation in transport infrastructure concrete, particularly in relation to heavy-duty pavements where durability and load-bearing are critical.

3 Methodology

The experimental programme was designed to compare the performance of MSStillite blends with control mixes composed of 100% tillite aggregates. Ordinary Portland cement (CEM I 42.5N) was used as the binder, and natural river sand was used as the fine aggregate. MSS was sourced from a South African steel manufacturer, with processing involving crushing and sieving to ensure comparable grading to natural tillite. Superplasticisers were incorporated to mitigate workability reductions associated with MSS's high absorption and angularity. Mix proportions were prepared with 0%, 20%, 40%, and 60% MSS replacement by mass of coarse aggregates. Each mix was evaluated at water-to-cement ratios ranging from 0.42 to 0.50, with a base optimum ratio of 0.46 identified from preliminary trials. Standardised testing procedures (SANS, ASTM, and EN equivalents) were adopted for consistency and comparability. Fresh concrete properties were assessed using the slump test to evaluate workability. Hardened concrete was subjected to compressive strength testing at 7, 28, and 90 days, alongside flexural strength testing at 28 days. Durability was evaluated through oxygen permeability index (OPI), chloride conductivity index (CCI), and sorptivity testing, representing resistance to carbonation, chloride ingress, and capillary absorption, respectively. An economic assessment was conducted through aggregate procurement cost comparisons and life cycle cost (LCC) modelling over a 50-year service life, incorporating both initial material savings and projected maintenance costs.

4 Results and Discussion

The mechanical performance of MSS concretes showed improved results in comparison to conventional concrete. At 28 days, the 60% MSS blend exhibited compressive strengths 20% higher than the control mix, while flexural strength improved by approximately 12%. These results align with Xu et al.'s (2024) findings that manganese slag enhances mechanical properties due to its high density and angular interlock, which improve load distribution and crack resistance. Early age strength gains were less pronounced, but long-term performance consistently surpassed that of conventional tillite concrete. Durability indicators demonstrated clear improvements with MSS incorporation. Chloride conductivity tests revealed lower diffusion coefficients in MSS concretes, suggesting enhanced resistance to chloride ingress, critical for airfields exposed to de-icing salts and coastal roads vulnerable to marine environments. Sorptivity results indicated reduced capillary absorption, lowering the risk of freeze-thaw deterioration. Oxygen permeability indices confirmed lower permeability in MSS blends, reducing carbonation risks and the likelihood of reinforcement corrosion. Workability challenges were observed in high-MSS mixes, with slump reductions due to angularity and water demand. However, targeted superplasticiser dosing successfully restored workable consistencies without compromising strength. The economic analysis demonstrated aggregate procurement cost reductions of approximately 20% by substituting MSS for tillite. More significantly, LCC modelling suggested that durability enhancements would translate into maintenance cost savings of around 15% over a 50-year design life.

The findings support the hypothesis that MSS is a technically viable substitute for natural aggregates in concrete, with mechanical and durability performance improvements that are particularly relevant to transport infrastructure. Compared with other industrial by-products, MSS offers distinct advantages in terms of angularity and density, which enhance mechanical interlock and strength. While workability reductions are consistent with previous studies on steel slags (Kwon et al., 2025), these can be effectively managed through admixtures. Durability improvements are of particular importance for transport applications. Roads, railways, and airfields are exposed to aggressive environmental conditions, including chloride-rich environments, freeze-thaw cycles, and carbonation. By reducing permeability and sorptivity, MSS concretes enhance resistance to these deteriorative mechanisms, extending service life and reducing maintenance frequency. This aligns with broader sustainability frameworks that emphasise the need to reduce both the environmental and economic costs of infrastructure over its lifecycle.

5 Conclusions and Recommendations

This study demonstrates that manganese steel slag is both a technically viable and economically advantageous partial replacement for natural tillite aggregates in concrete. Mechanical performance was enhanced, particularly at 60% MSS replacement, while durability indicators confirmed improved resistance to aggressive environmental conditions. Workability challenges were successfully addressed with admixtures, and economic analyses highlighted significant lifecycle cost savings. These findings establish MSS as a promising sustainable material for transport infrastructure, offering both environmental and economic benefits while supporting circular economy objectives.

Further research should focus on field trials to validate laboratory results under real-world loading and environmental conditions. Comprehensive leachate analyses are required to confirm long-term environmental safety, particularly with respect to heavy metal mobility. Collaboration with policymakers and standards bodies is essential to develop guidelines for MSS use in structural and pavement concrete, ensuring its safe and widespread adoption.

6 References

Buruiana, D.L., Obreja, C.D., Herbei, E.E. and Ghisman, V. (2021). Re-use of silico-manganese slag. *Sustainability*, 13(21), p.11771. Available at: https://www.mdpi.com/2071-1050/13/21/11771

Cota, T.G., Cheloni, L.M.M.S. and Guedes, J.J.M. (2023). Silico-manganese slag and its utilization into alkali-activated materials: A critical review. *Construction and Building Materials*, 381, 131248. Available at: https://www.sciencedirect.com/science/article/pii/S095006182302305X

Kwon, W.R., Lee, J.B., Yoon, B.M. and Kim, J.H.J. (2025). Performance evaluation of shotcrete mortar with silicon manganese slag as substitute for fine aggregate. *Materials*, 18(8), p.1754. Available at: https://www.mdpi.com/1996-1944/18/8/1754

Nath, S.K., Randhawa, N.S. and Kumar, S. (2022). A review on characteristics of silico-manganese slag and its utilization into construction materials. *Construction and Building Materials*, 330, 127274. Available at: https://www.sciencedirect.com/science/article/pii/S0921344921005553

Shen, N., Liu, Y., Li, X., Chen, W. and Zheng, Y. (2024). Green low-carbon evaluation study on the utilization of electrolytic manganese slag for ready-mixed concrete production. In: *Sustainable Civil Engineering Materials and Practices*. Springer, Singapore. Available at: https://link.springer.com/chapter/10.1007/978-981-96-2948-0_2

Wu, Z., Feng, Z., Pu, S., Zeng, C., Zhao, Y. and Chen, C. (2024). Mechanical properties and environmental characteristics of cementitious materials using electrolytic manganese residue, steel slag, and blast furnace slag. *Construction and Building Materials*, 414, 134228. Available at: https://www.sciencedirect.com/science/article/pii/S0950061823041995

Xu, W., Yu, J. and Wang, H. (2024). The influence of manganese slag on the properties of ultra-high-performance concrete. *Materials*, 17(2), p.497. Available at: https://www.mdpi.com/1996-1944/17/2/497

Evaluating Corrosion Development on Dowel Bars in Concrete Pavements

C.A. Donnelly
Texas A&M University, USA
J.M. Vandenbossche
University of Pittsburgh, USA

Abstract

Corrosion of metallic dowel bars in concrete pavements is a significant source of distress development. While a number of alternative dowel bar designs and materials are currently on the market, to date, there has been limited research performed to quantify the performance of the dowels against corrosion. In this study, a novel accelerated dowel corrosion setup is introduced. A range of dowel materials and coating types were evaluated over a 12-week accelerated corrosion test. Results indicate that corrosion varies as a function of exposure duration and coating type. One key finding from this study is that zinc-clad dowels exhibit a significant amount of surface oxidation that may lead to dowel seizing and spalling. The results from this study will be used to more accurately account for corrosion development in the current pavement performance models.

Keywords: dowel bar, corrosion, concrete pavements

1 Introduction

1.1 Dowel corrosion

Corrosion of metallic dowel bars in concrete pavements is commonly caused by exposure to deicing salts and precipitation. Loss of metal due to corrosion causes a reduction in the dowel cross-sectional area and a reduction in the long-term dowel performance. The industry standard dowel in the United States consists of solid steel with an epoxy coating for corrosion protection. However, corrosion frequently initiates at defects in the coating where the underlying steel is exposed. Although corrosion is known to be a common cause of decreased dowel performance, the rate of corrosion development is not directly accounted for in the current pavement design procedure (Khazanovich, Darter, & Yu, 2004). Additionally, only pavement sections with standard epoxy-coated steel dowels were included in the calibration dataset, and as a result, alternative dowels are not included. Currently, there are a variety of alternative dowels on the market, which offer corrosion resistant materials or coatings at a higher price compared to the industry standard. Alternative dowels include tubular, stainless steel, non-metallic, and steel dowels with multiple layers of epoxy coating. While these alternatives may offer mitigated corrosion development, it is not currently possible to justify the increased costs using the pavement design tool. Moreover, the mechanisms of dowel corrosion are not fully understood, which limits the capabilities of available design tools.

1.2 Gap in knowledge

Previous studies have evaluated corrosion development in dowel bars, including alternative dowels (Abo-Qudais & Al-Qadi 2000) (Lee 2018) (Mancio et al. 2005). These studies typically consist of laboratory analyses in which dowel specimens are subjected to cyclic wetting and drying in extreme salt solutions. Corrosion progression was evaluated using a variety of non-destructive tests as well as visual inspection of the dowels.

However, there are a number of limitations to these studies. First, the specimens in these studies were not subjected to vehicle loading, which decouples corrosion development from mechanical loading of the joint. Doweled joints in the field are exposed to constant fatigue from vehicle loads, which could accelerate corrosion due to ingression of chlorides into the embedded dowel. Secondly, the effect of the expansive corrosion byproducts on dowel performance was not considered. Oxidized metal, such as ferric oxide (i.e., rust), is known to be expansive in nature and causes high tensile stress when embedded in concrete (Broomfield 1997). Previous studies did not account for the potential of seizing of the dowels caused by corrosion development. Lastly, the durability of the coatings were not evaluated in previous studies. Corrosion is most likely to initiate at flaws in the coating, commonly referred to as holidays. While one study did place holidays on the dowel (Lee 2018), no study compared the durability of the coating types and their susceptibility to development of flaws.

1.3 Research scope

A novel accelerated dowel corrosion test setup is introduced in this study and used to evaluate a range of dowel bars that are currently available on the market. The purpose of this setup is to replicate corrosion exposure in transverse joints. The effect of corrosion on joint movement and dowel diameter can then be evaluated.

2 Laboratory Analysis

2.1 Dowel specimens

The following seven (7) dowels were included in this study: solid carbon steel dowels with 0.5-mm thick green (ASTM A775) and purple (ASTM A943) epoxy coating, Grade G90 zinc-galvanized tubular dowels with 0.25-

mm thick green (ASTM A775) and purple (ASTM A943) epoxy coating, tubular carbon steel dowels with a mechanically bonded 1-mm thick zinc cladding, solid fiber reinforced polymer (FRP) dowels, and tubular stainless steel dowels. Coating damage resistance testing was performed on each dowel. Abrasion resistance and impact resistance testing was performed per the specifications in ACPA T253 (ACPA 2021).

Abrasion testing consists of 10,000 double-strokes of a mortar block across the surface of the dowel to evalute the loss in coating thickness due to wear between the dowel and concrete caused by joint opening and closing. Impact testing consists of dropping a weighted tup, or rounded point, on the surface of the dowel at three (3) locations to evalaute the resistance of the coating to holiday formation, while handling the dowel prior to placement. The purpose of this this testing was to evaluate the potential for each type of coating (epoxy, zinc-cladding, etc) to be damaged from mechanical wear (abrasion) and localized contact points (impact).

Additionally, six (6) circle holidays were placed on each dowel at two (2) different diameters using a flat-tipped end mill. Three (3) holidays at each diameter were placed, and the diameters correspond to 1% and 2% of the surface area of the dowel. The holidays were placed to evaluate the potential for corrosion development at localizated areas of coating failure. After the coating testing and holiday placement was completed, each dowel was cast in the concrete specimen shown in Figure1.

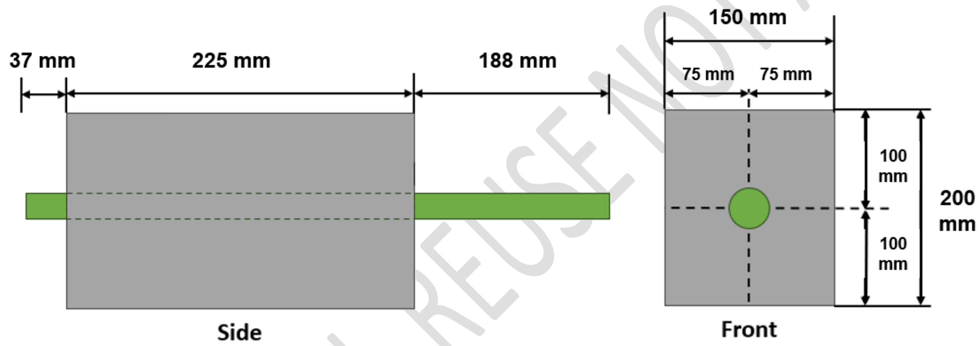

Figure 1: *Schematic of beam specimen.*

2.2 Accelerated corrosion setup

The accelerated corrosion setup consists of an exposure tank and a storage reservoir that were designed so that the 21 specimens (7 different dowel designs with 3 replicates each) tested could be simultaneously exposed to the same solution, thereby minimizing variability between specimens. The tank is filled with approximately 800 liters of 5% (wt) NaCl solution, which is used to simulate accelerated corrosive conditions. The laboratory setup is shown in Figure 2. The specimens are placed in the exposure tank with the dowels facing down so that the exposed portion of the dowels are submerged in the corrosion solution. A series of timer-controlled pumps cycle solution between the exposure and reservoir tanks to raise and lower the solution level, thus cyclically varying the saturation of the dowels. Each wetting/drying cycle consists of 30 minutes of full saturation followed by 2.5 hours of drying. The wetting/drying cycles are continuously run for a 12-week period. At two-week intervals throughout the exposure period, the dowel specimens are removed from the tank to evaluate corrosion development.

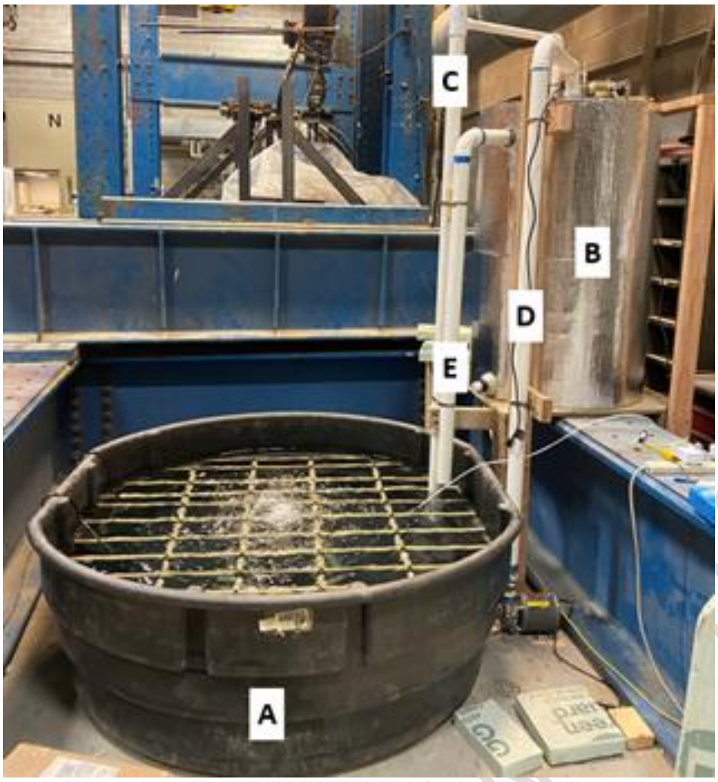

Figure 2: *Accelerated corrosion setup depicting A) exposure tank, B) reservoir, C-E) piping.*

2.3 Simulated joint opening and closing

Simulated joint movement was periodically conducted on each specimen to measure the bond strength between the dowel and surrounding concrete. The test performed in this study is a modified version of the pullout test described in ACPA T253 (ACPA 2021). A 25-kN actuator is used to apply a load parallel to the axis of the dowel. The actuator is operated in displacement control at a rate of 0.75 mm/min, and the applied load is recorded throughout the duration of the test. The test runs until the dowel moves 13 mm. The applied load and displacement is recorded at 10 Hz. A schematic of the pushout test is shown in Figure 3.

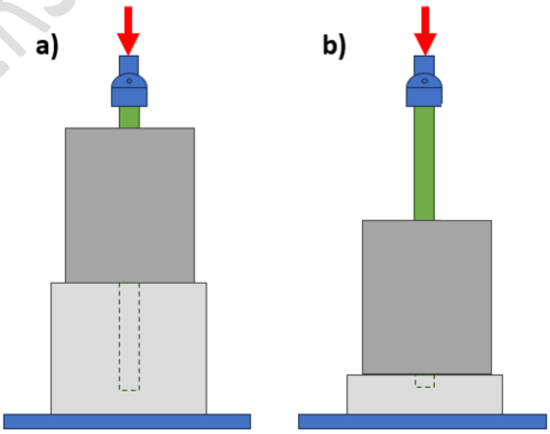

Figure 3: *Configuration for simulated joint a) opening and b) closing.*

The simulated joint opening and closing test replicates mobilization of slabs due to thermal changes in the concrete. There is the potential for this mobilization to result in coating damage and increase the mobilization of chloride further along the dowel, both of which would increase corrosion development. The effect of joint opening and closing was not considered in previous dowel corrosion studies but it is a critical mechanism for corrosion development in dowels.

2.4 Corrosion assessment

After simulated joint opening and closing testing is performed on each specimen, the corrosion progression is evaluated as a function of severity of corrosion on the exposed portion of the dowel. First, the dowel was visually inspected and documented with photographs. Second, the surface of the dowel is scanned using a Quantum Max FaroArm® 3D laser scanner to construct a high-resolution point cloud. By scanning the dowel periodically throughout the duration of testing, the scans can be overlaid to directly compare the progression of corrosion. The point clouds generated in this analysis are used to further evaluate the severity of corrosion development with specific interest in the holidays where the underlying metal is exposed.

3 Results

3.1 Coating evaluation

Upon completion of the abrasion and impact testing each dowel was inspected to identify any areas of compromised coating. Although some of the green- and purple epoxy-coated dowels exhibited a loss of approximately 0.07 mm of coating, none of the dowels exhibited full loss of coating due to abrasion. Critically, no areas of underlying metal were exposed for any dowels.

The only dowel type which exhibited damage during impact testing was the purple epoxy-coated steel dowels. The purple epoxy is stiffer than the green epoxy, and each dowel had at least one impact location at which partial failure of the coating was observed. An example of this is shown for one specimen in Figure 4. Although partial failure was observed, the underlying metal was not fully exposed.

Figure 4: *Partial coating failure due to impact testing.*

3.2 Simulated joint opening and closing

Simulated joint opening/closing was performed during Weeks 2 – 12 to characterize the effect of corrosion development on increases in force required to open or close the joint. The average joint opening force for each type of dowel either remained constant or decreased from Week 2 to Week 12 for most dowels evaluated. This can be explained by the fact that repeatedly simulating joint movement enabled easier mobilization of the dowel, despite any effects of local-ized corrosion. The one exception to this trend is the zinc-clad tubular dowels. After 2 weeks of corrosion exposure the average maximum joint opening force during testing was 2.5 kN. The joint opening force continuously in-creased after subsequent weeks of corrosion exposure for each zinc-clad specimen, as shown in Figure 5. The average force increased to 4.8 kN in Week 4, 6.9 kN in Week 6, 7.8 kN in Week 8, and 12.7 kN in Week 12, as shown in Figure 5. This is a 400% increase in mobilization force from Week 2 to Week 12 of corrosion exposure. The increase in joint opening force is likely due to the expansive zinc-oxide that formed on the dowel. An example is shown for one specimen after 6 weeks of exposure in Figure 6. This can lead to seizing of the dowel and concrete spalling around the dowel, which occurred on all zinc-clad dowel specimens.

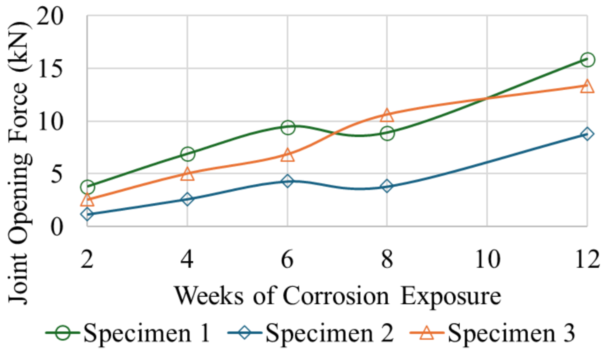

***Figure 5:** Joint opening force measured for each zinc-clad dowel specimen.*

***Figure 6:** Expansive zinc-oxide development on the surface of a zinc-clad dowel.*

3.3 Corrosion assessment

The scans performed throughout the duration of the corrosion program were compiled to evaluate the change in surface topography for each specimen due to the corrosion development. The focus of the analysis is on the areas with holidays placed on the dowel surface because these were the locations at which corrosion development was most likely to occur. With the exception of the zinc-clad dowels, corrosion was localized to the holidays placed on the dowel. No corrosion was observed throughout the duration of the corrosion test at any areas of impact or abrasion for all epoxy-coated dowels, including the purple epoxy-coated dowels with partial coating failure due to impact testing.

The point clouds generated using the scans were used to rate the severity of the corrosion progression at the holidays. An example of corrosion progression for a green epoxy-coated carbon steel dowel with increasingly severe corrosion rating assigned is shown in Figure 7. It was determined that the carbon steel dowels (both green and purple epoxy-coated) exhibit-ed the most severe corrosion development at the holidays after 12 weeks of corrosion testing. Corrosion was observed to progress from the center of the holiday, where the underlying steel was exposed, to the edge of the holiday. No corrosion or damage was observed in either the

FRP or stainless steel dowels. The zinc-clad dowels exhibited corrosion on the entire surface of the dowel, including the holidays. Lastly, the zinc-galvanized dowels were observed to have minimal corrosion development at the holidays. Galvanization appears to be an effective method for mitigating corrosion development even at locations where the epoxy coating is damaged.

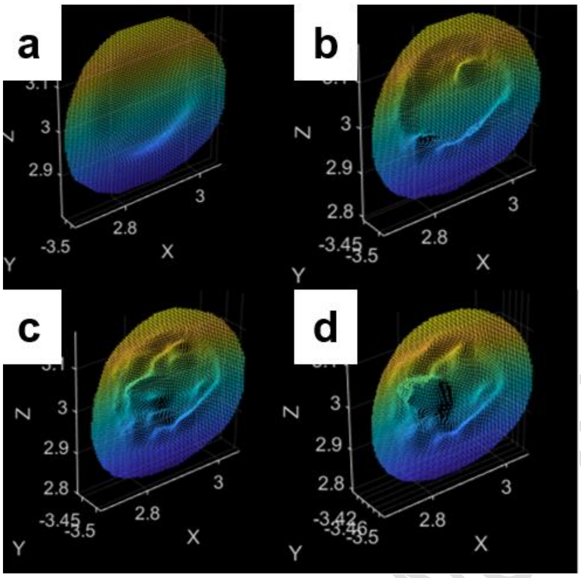

Figure 7: *Green epoxy-coated dowel with a) no, b) low, c) medium, and d) severe corrosion rating.*

4 Conclusions

The novel accelerated dowel corrosion test setup developed in this study was used to evaluate a range of dowels that are currently available on the market. This test setup replicates corrosion development at the transverse joint and accounts for the effect of joint opening and closing. All dowels evaluated met the criteria for coating performance after abrasion and impact testing. When comparing the development of corrosion at localized holidays, it was found that the severity of corrosion is a function of the duration of exposure and the underlying material. Carbon steel dowels, with either green or purple epoxy coating, was found to perform the worst. Zinc-based galvanization was found to provide significantly greater corrosion protection compared to carbon steel. Both the FRP and stainless steel dowels exhibited no measurable corrosion.

One key finding was that an expansive layer of zinc oxide formed on the entire surface of the zinc-clad dowels. This resulted in an increase in joint opening force and caused spalling around the dowel. Continued increase in joint opening force will result in further damage development in the concrete around the dowel, thus reducing the stiffness of the doweled system. Additionally, rapid oxidation of the zinc-cladding may result in a reduction of the cross-sectional area of the dowel, which would introduce additional looseness around the dowel.

The results from this study will be used to improve the current faulting prediction models. Current work is being performed to directly account for the development of corrosion as a function of key exposure and dowel material parameters. These improvements will enable pavement engineers to better account for design options, including alternative dowel bars.

References

Abo-Qudais, SA & Al-Qadi, IL 2000, 'Dowel bars corrosion in concrete pavement', Canadian journal of civil engineering, vol 27, no. 6, pp. 1240-1247.

ACPA 2021, 'Standard Method of test for Dowel Bars for Concrete Street and Highway Pavement'.

APTech 2009, 'Evaluation of Alternate Dowel Bar Materials: Revised Interim Report', Ohio Department of Transportation, Columbus, Ohio.

Broomfield, J 1997, Corrosion of Steel in Concrete, Taylor & Francis, New York.

Khazanovich, L, Darter, M & Yu, T 2004, 'Mechanistic-Empirical Model to Predict Transverse Joint Faulting', Transportation Research Board, vol 1896, pp. 34-45.

Lee, S-K 2018, 'Laboratory evaluation of corrosion resistance of various metallic dowel bars. No. FHWA-HRT-15-079.', Federal Highway Administration. Office of Infrastructure Research and Development.

Mancio, M, Carlos Jr, C, Zhang, J, Harvey, JT, Monteiro, PJ & Ali, A 2005, 'Laboratory Evaluation of Corrosion Resistance of Steel Dowels in Concrete Pavement', Institute of Transportation Studies, UC Davis.

VegDim: A Digital System for Pavement Design and Analysis

Brynhild Snilsberg
Norwegian Public Roads Administration
Rabbira Garba Saba
Norwegian Public Roads Administration
Tomas Winnerholt
Swedish Transport Administration
Sigurdur Erlingsson
The Swedish National Road and Transport Research Institute & University of Iceland

Abstract

VegDim (2018-2024) was a R&D project conducted by the Norwegian Public Roads Administration (NPRA) with the aim of developing and implementing a mechanistic-empirical (ME) pavement design and analysis system), which allows the prediction of pavement deterioration due to climate and traffic loads. The resulting tool, also named VegDim, is an adaptation of ERAPave PP, developed by the Swedish National Road and Transport Research Institute (VTI), to the Norwegian conditions. This included developing the material database, integration of climate data and improvement of traffic data. This work was conducted in collaboration with VTI and the Swedish Transport Administration (STA). To ensure a successful implementation of the system the work done in this project included calibration of the empirical performance models to Norwegian conditions. In addition, the ME pavement design method was harmonized with the Norwegian pavement design requirements and regulations and user training materials were developed. This extended abstract briefly summarizes the work that has been performed in VegDim to implement an entirely new pavement design system, incorporating new workflows and advanced models.

Keywords: mechanistic-empirical pavement design system; VegDim; ERAPave PP

1 Introduction

VegDim (2018-2024) was a R&D project conducted by the Norwegian Public Roads Administration (NPRA) and represents a significant advancement in the field of pavement design and analysis (Snilsberg, 2025). The project aimed to develop a digital pavement design system based on mechanistic-empirical (ME) principles, which allows for the prediction of pavement deterioration due to climate and traffic loads. Today, VegDim is available as a web-based platform (in Norwegian) that incorporates ME-models from ERAPave PP in addition to the existing empirical design method, providing a comprehensive tool for pavement design and analysis. The following sections describes the work done in the project to further develop and implement the system in Norway.

2 Background

The current regulatory framework for road construction in Norway is empirical. While the system is robust with respect to simplicity and provision of some safety margin, it lacks flexibility for the incorporation of new materials and for adapting to changes in traffic and climate conditions. It neither enables calculation of pavement performance, nor allows for the documentation of the effects of changes in materials, traffic loads, or climate variations. Furthermore, the system is manual, and there is no digital tool available to ensure compliance with the regulations. There is therefore a need for a new digital pavement design and analysis system.

Instead of creating an entirely new system for Norway, the project selected ERAPave PP (Elastic Analysis of Pavements – Performance Prediction), an ME system developed by the Swedish National Road and Transport Research Institute (VTI) in Sweden (Erlingsson and Ahmed, 2013). ERAPave PP was identified as the most suitable system for Norway (Saba, 2019) due to its ongoing development, relevance to local damage mechanisms like studded tyre wear, rutting and frost heave, and dual functionality as a design and analysis tool (Figure 1). Collaboration with VTI and the Swedish Transport Administration (STA) facilitated the adaptation of ERAPave PP to Norwegian conditions, ensuring the system's relevance and effectiveness. The system's performance models, some of which are quite similar to those used in AASHTOWare ME, have been validated through accelerated testing, ensuring reliability and confidence in its application.

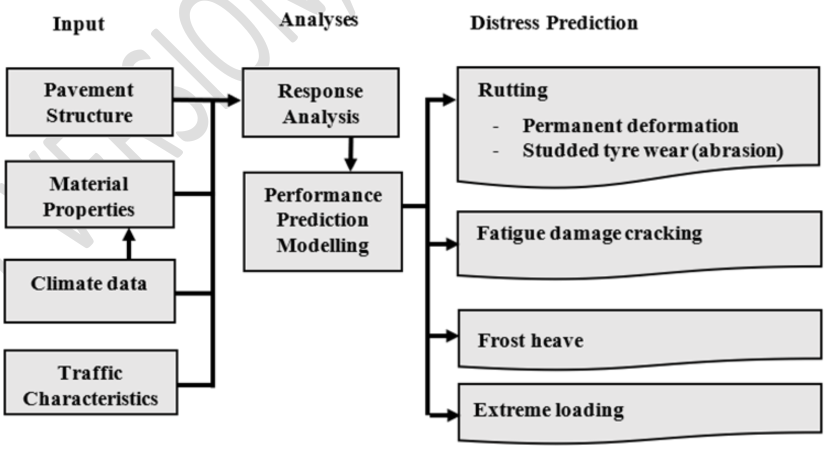

Figure 1*: Schematic description of ERAPave PP (VTI).*

3 Development and Implementation

The development and implementation of an entirely new pavement design and analysis system in Norway, incorporating new workflows and advanced models, necessitates substantial effort and is accompanied by a paradigm shift in both mindset and methodology. The project has therefore focused on:

- **Input data**: Acquiring data for materials of pavement structure, subgrade (Saba, 2025A), climate (Saba, 2025B), and traffic (Bakløkk, 2025).
- **Adaption of a frost model**: A model developed in Finland which calculates frost depth and frost heave was adapted (Skoglund and Berntsen, 2025).
- **Calibration:** Establishing reference sections to ensure that calculated values for performance agree with measured performance from field (Johansen et al., 2025).
- **Adjustment of design requirements:** Adapting the Norwegian requirements for road construction to the ME pavement design method (Skoglund and Dongmo-Engeland, 2025).
- **Training and information:** Creating courses and training materials for various user groups, as well as contributing to university and college education.
- **Web-based program:** Developing VegDim as a web-based tool for pavement design and analysis.

The work done in the VegDim project involved several key components, including the integration of material databases, climate data, and traffic data for Norwegian conditions into VegDim/ERAPave PP which is an essential component of an ME system. Access to such data is crucial for the successful implementation and reliability of the system. Consequently, the project has placed significant emphasis on acquiring material properties, climate data, and traffic data for Norway. Testing of commonly used asphalt materials and some subgrade materials were conducted in the laboratory. Material data was also collected from existing reports and some back-calculation of stiffness modulus for unbound materials were conducted using deflection measurements. A system for transfer of climate data from weather stations using a map-based solution to the VegDim/ERAPave PP system was established. Some data from WIM (weigh-in-motion) measurements were analysed to improve traffic data input to the system.

A frost model developed in Finland, called the SSR-model (Seppo-Saarelainen-Routanousu), was integrated into VegDim/ERAPave PP. The model calculates the frost depth and frost heave. The calculated critical frost heave is compared to the maximum allowed frost heave for a given road. This will ensure that there will not be excessive frost heave.

Calibration of VegDim/ERAPave PP to Norwegian conditions is crucial for ensuring reliable results and trust in the pavement performance models. Calibration involves comparing and adjusting calculated performance data to measured field data. Several calibration sections with diverse traffic, climate, materials, and ages were established to cover the variation in road types and loads. The work with calibration of performance models is ongoing. A preliminary calibration of the rutting models has been conducted, and incorporated into VegDim/ERAPave PP.

The Norwegian requirements for pavement design was revised and published in 2024, permitting the use of VegDim/ERAPave PP in pavement design. The input data and results from the pavement design using VegDim/ERAPave PP must be reviewed and approved by the NPRA to minimize risk and gain experience.

Creating training materials, both for ME-pavement design and VegDim/ERAPave PP, is also an ongoing activity and crucial for a successful implementation of the design system in Norway.

ERAPave PP was initially available only as a desktop application, requiring individual downloads. To enhance accessibility and usability, the development of a Norwegian web version VegDim (https://vegdim.atlas.vegvesen.no), was commenced in 2023. This web-based platform incorporates ME-models from ERAPave PP and a digital version of the existing empirical design method, providing a comprehensive tool for pavement design and analysis.

4 Collaboration and further development

The initial phase of VegDim focused on integrating the Norwegian conditions, requirements and practice into ERAPave PP. The work was conducted in collaboration with VTI and STA. Despite substantial progress, the nature of ME systems necessitates ongoing development and refinement. Recognizing this, a further collaboration was established through the NordFoU project NorDim (2025-2029) with the VTI and STA, ensuring continuous improvement and adaptation. Further development work will include improvement of the performance models as well as adaptation of the design system to rehabilitation design for existing roads.

5 Conclusions

This extended abstract presents the work conducted by NPRA in collaboration with VTI and STA to further develop and implement an ME pavement design and analysis system called VegDim/ERAPave PP. VegDim stands as a testament to the collaborative efforts between Norway and Sweden in advancing pavement technology. Many of the models used in ME systems are international, making collaboration between countries both important and resource efficient. The system's continuous development through projects like NorDim ensures its adaptability and effectiveness in addressing the dynamic challenges posed by climate and traffic conditions. VegDim's web-based platform offers an accessible and robust solution for pavement design and analysis, contributing to the sustainable management of Norway's road infrastructure.

6 References

Bakløkk, L. J. 2025. VegDim – Analysis of WIM (Weigh-In-Motion) data. NPRA report, 1092, 2025-10. [in Norwegian]

Erlingsson, S. & Ahmed, A. 2013. Fast layered elastic response program for the analysis of flexible pavement structures. Road Materials and Pavement Design. 14:1, 196-210, DOI: 10.1080/14680629.2012.757558.

Johansen, J. M., Evensen, R., Holen, Å. & Hannasvik, L. T. 2025. VegDim – Calibration of rutting model. ViaNova report 2025-04-11. [in Norwegian]

Saba, R. G. 2019. Analytical design of pavement structures: Evaluation and choice of a system for Norwegion conditions. NPRA report, 524, 2019-12. [in Norwegian]

Saba, R. G. 2025A. VegDim – Material data. NPRA report, 1067, 2025-06. [in Norwegian]

Saba, R. G. 2025B. VegDim – Climate data. NPRA report, 1066, 2025-06. [in Norwegian]

Skoglund, K. A. & Dongmo-Engeland, B. J. 2025. VegDim – Design requirements. NPRA report, 1094, 2025-10. [in Norwegian]

Skoglund, K. A. & Berntsen, G. 2025. VegDim – Modeling of frost penetration and frost heave. NPRA report, 1089, 2025-10. [in Norwegian]

Snilsberg, B. 2025. VegDim – Final report. NPRA report, 1100, 2025-11. [in Norwegian]

Macro- & microscopic dynamic responses of coupled train-ballasted track-subgrade system via hybrid MBD-DEM FDM method

Yuanjie Xiao
School of Civil Engineering, Central South University, Changsha 410075, China
Ministry of Education Key Laboratory of Engineering Structures of Heavy Haul Railway Central South University, Changsha 410075, China
Yiling Chen
Zehan Shen
School of Civil Engineering, Central South University, Changsha 410075, China
Pan Tan
School of Civil Engineering, Changsha University of Science & Technology, Changsha 410075, China

Abstract

With the growing complexity of high-speed railway operations, the train-ballasted track-subgrade system is increasingly subjected to intensified dynamic loads and operational demands, posing significant challenges to structural integrity and maintenance strategies. However, most existing numerical models treat the train, track, ballast, and subgrade as decoupled subsystems, thereby failing to capture the essential dynamic interactions within this integrated system. To address this limitation, this study proposes and develops a coupled multi-scale dynamic simulation framework that integrates a Multi-Body Dynamics (MBD) model for the train, a Discrete Element Method (DEM) model for ballast particles, and a Finite Difference Method (FDM) model for the continuous subgrade. This framework enables a comprehensive investigation of both macro- and micro-scale dynamic responses under varying train speeds ranging from 250 to 350 km/h. The results show that vertical acceleration of the train body increases by 25% as speed rises, while lateral acceleration and wheel-rail contact forces increase by 85.9% and 54.7%, respectively. Speed-dependent precursor displacements are observed in the rail and sleeper, and ballast deformation at 350 km/h increases by 144% compared to that at 250 km/h. At the granular scale, the proportion of sliding contacts among ballast particles increases by 64% when train speed exceeds 325 km/h, the force chain network becomes more dispersed, and up to 73% of the sleeper base load is carried by force chains. These findings suggest that 325 km/h may serve as a critical threshold for ballast maintenance, indicating the need for enhanced monitoring and more frequent ballast replenishment in key zones. The multi-scale modeling strategy proposed herein offers novel theoretical insights and methodological guidance for dynamic analysis and intelligent maintenance of high-speed railway infrastructure.

Keywords: train-ballasted track-subgrade system; multi-body dynamics; discrete element method; finite difference method; coupled modelling; macro-microscale dynamic response

1 Introduction

Ballasted tracks remain essential in some high-speed railways for their cost-effectiveness and easy maintenance, but repetitive train loads lead to ballast degradation, reduced stiffness, and failures such as mud pumping and loss, threatening stability. Therefore, it is imperative to develop a high-fidelity coupled train-track-subgrade system model to elucidate the underlying degradation mechanisms and inform the design and maintenance strategies of railway infrastructure. Existing studies employing CAE software (Zhong et al., 2024) or self-programmed codes often simplify the train subsystem into excitation functions (Zhai et al., 2019) or rely on limited software coupling (Liu et al., 2025). Although self-developed approaches have introduced nonlinear wheel-rail contact (Sun et al., 2022), dynamic substructuring (Kurhan et al., 2025), and track deterioration effects (Lu et al., 2025), the ballast layer is still commonly treated as a continuum or a mass-spring-damper system. Such simplifications overlook critical mesoscopic features, including particle geometry, random contact interactions, and micromechanical behaviors. By contrast, the DEM enables particle-scale analysis. Studies by Chen et al. (2016), Indraratna et al. (2019), and Qian et al. (2018) have revealed ballast kinematics and force chain evolution under cyclic loading. Recent efforts to couple MBD with DEM (Zhang et al., 2021) have advanced vehicle-ballast interaction modeling but are typically restricted to two dimensions or simplified load inputs. In summary, most existing studies have yet to realize fully coupled, three-dimensional, real-time simulations that integrate the train, track, and granular ballast subsystems. To bridge this gap, the present study proposes a comprehensive coupled dynamic simulation framework that integrates a MBD model for the vehicle subsystem, a DEM model for the granular ballast layer, and a FDM model for the continuous subgrade. Based on this integrated approach, a systematic analysis of both macro- and micro-scale dynamic responses is conducted under varying operating speeds (250~350 km/h). The findings provide novel theoretical insights and robust methodological support for the dynamic assessment and intelligent maintenance of high-speed railway infrastructure.

2 Method

This study establishes a multi-scale coupled framework for simulating the high-speed train-ballasted track-subgrade system by integrating MBD-DEM-FDM, see Figure 1. The train subsystem is modeled in MBD with 38 degrees of freedom, employing Hertzian contact for normal forcesand Kalker's linear creep theory for tangential forces, while track irregularities are introduced as excitations based on established spectral methods (Mao et al., 2021). The ballast bed is simulated in PFC3D using DEM, where aggregates are idealized as spheres governed by the Rolling Resistance Linear Model (Xiao et al., 2024), and staged compaction replicates tamping operations (Li et al., 2019). Sleepers and the subgrade are represented via FDM, with refined discretization according to wavelength criteria (Baghban et al., 2021).

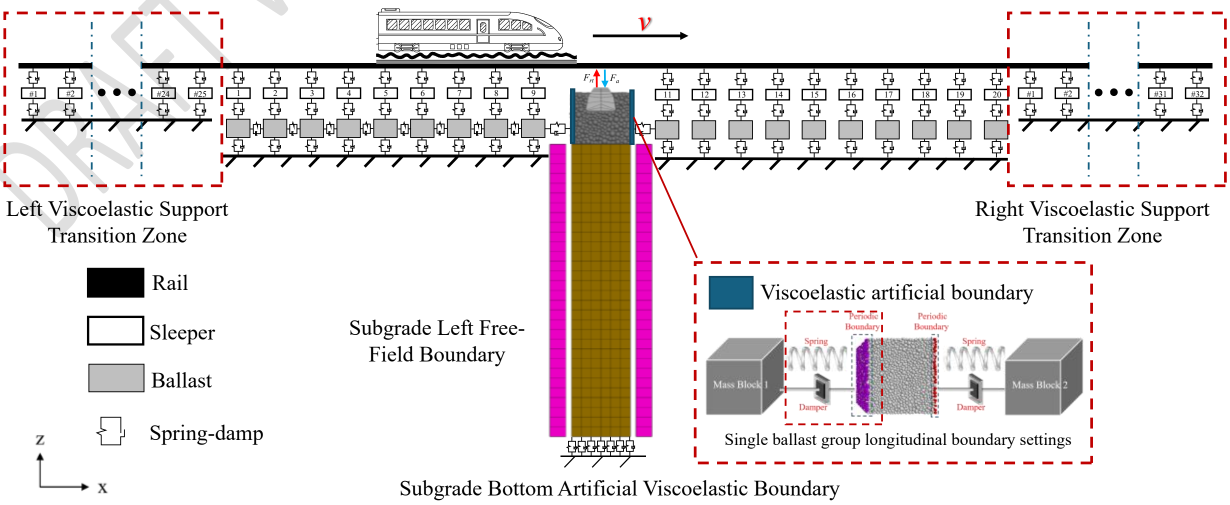

Figure 1: *Overall coupling model in the longitudinal direction.*

The specific coupling scheme is illustrated in Figure 2, where real-time bidirectional MBD-DEM-FEM coupling is implemented through the Service-link interface using Python. The Service-link interface consists of Rail-Fastener-Sleeper Coupling Module and the Ballast Particle-Mass Block Spring-Damper Coupling Module. Within the Rail-Fastener-Sleeper Coupling Module, the MBD module outputs the fastener force obtained from the previous time step and applies it to the FDM sleeper model. The sleeper then transfers the interaction forces to both the DEM ballast module and the FDM subgrade model through the Socket I/O interface provided by Itasca (2004). After completing the calculation for one time step, the reaction forces are returned to the MBD module, thereby achieving bidirectional coupling (Liu et al., 2023). It should be noted that the time step used in the simulation is 0.001 s, determined based on the Wilson-θ method time integration scheme (Wilson et al., 1973). Meanwhile, within the Ballast Particle-Mass Block Spring-Damper Coupling Module, the spring-damper forces of the ballast mass block elements calculated in the MBD module at the previous time step are equivalently discretized and applied to the boundary particles of the DEM ballast assembly. After the DEM calculation advances by one time step, the resultant spring-damper forces are recalculated based on the centroid displacement, velocity, and acceleration of the particle assembly and subsequently transmitted back to the MBD module (Zhang, 2016).

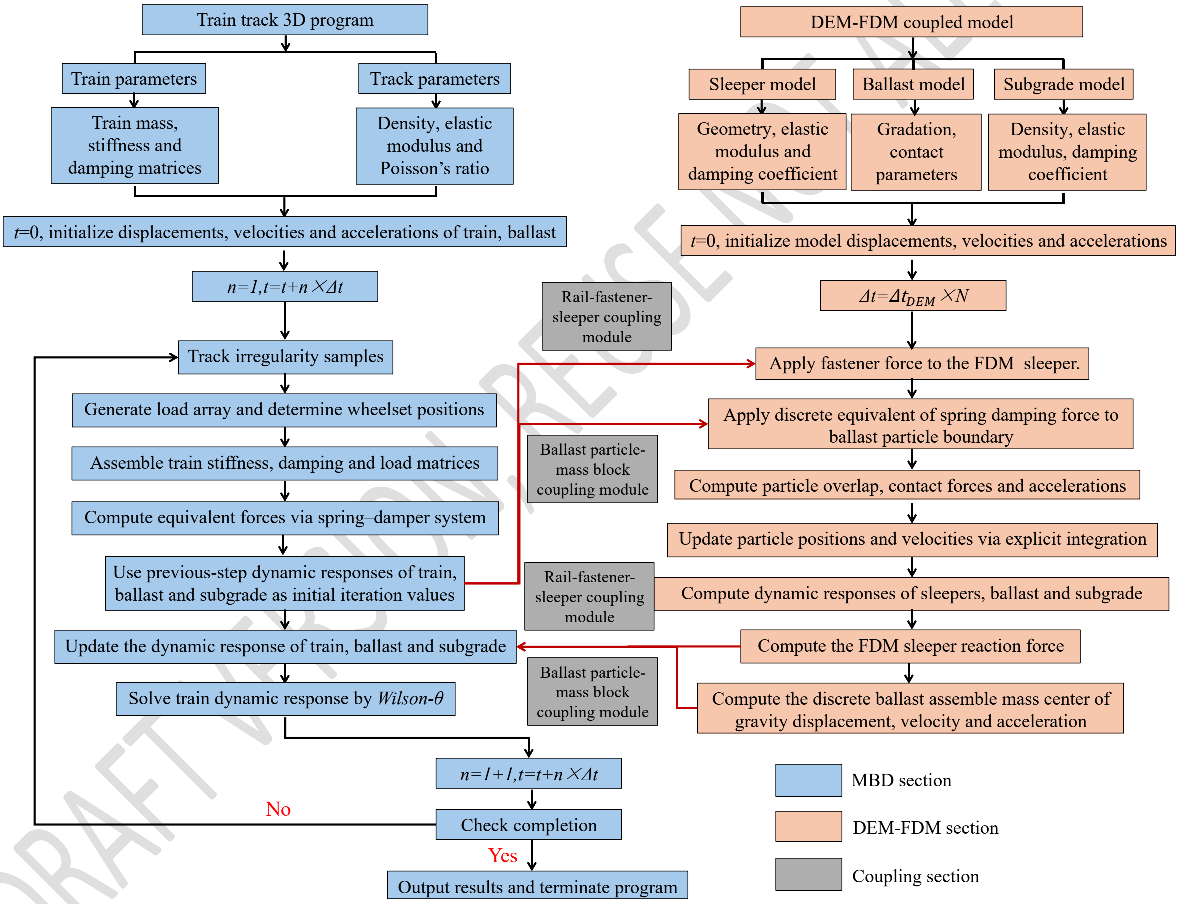

***Figure 2**: Overall coupling model in the longitudinal direction.*

3 Results

This study established a three-dimensional MBD-DEM-FDM coupled model to investigate the dynamic responses and micromechanical evolution of the high-speed train-ballasted track-subgrade system. The model achieved high fidelity in reproducing field-measured rail displacements and sleeper accelerations, outperforming continuum-based approaches in characterizing sleeper-ballast dynamics, see Figure 3. Results revealed that increasing train speed significantly amplifies dynamic responses: vertical and lateral accelerations rose by 25% and 85.9%, respectively, while lateral wheel-rail forces increased by 54.7%. Ballast deformation at 350 km/h was 144% higher than at 250 km/h, with a critical velocity limit predicted at 421.7 km/h, see Figure 4. Micromechanical analyses indicated a behavioral transition beyond 325 km/h, marked by reduced coordination number (-31.8%), higher sliding contact ratio (+64%), and accelerated force chain degradation, particularly beneath sleepers and at shoulders. Prolonged high-speed loading was shown to weaken contact networks, promote lateral instability, and exacerbate ballast deterioration, see Figure 4. Accordingly, a threshold of 325 km/h is identified as critical for maintenance intervention, with sub-sleeper and shoulder regions recommended as priority zones for monitoring and reinforcement to ensure structural stability and extend service life.

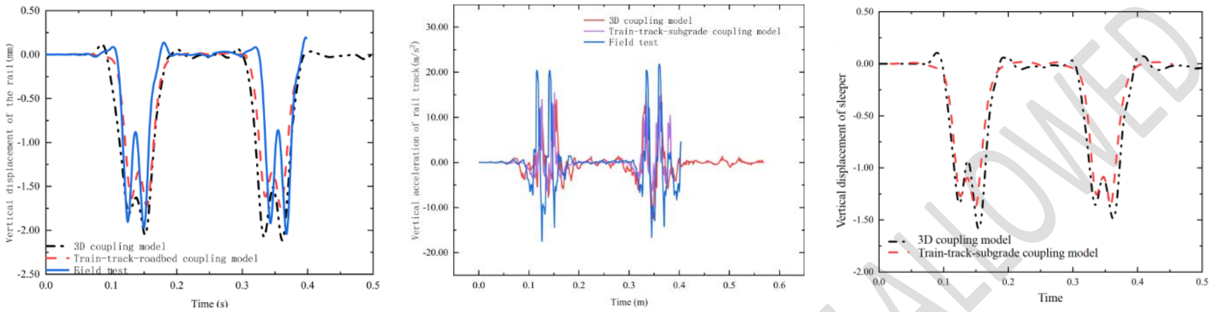

***Figure 3**: Comparison of statistical extremes of structural dynamic responses: (a) Vertical displacement of rail (b) Vertical acceleration of rail (c) Vertical displacement of sleeper.*

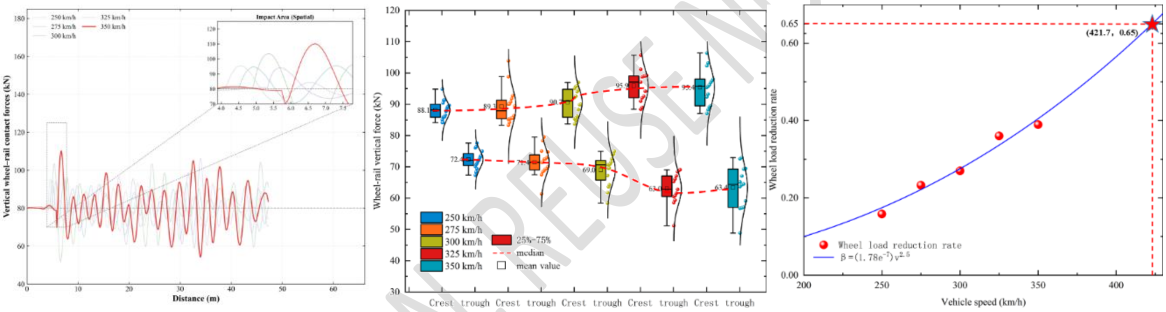

***Figure 4**: Vehicle dynamic response: (a) Distance-history curves of vertical wheel–rail contact forces. (b) Box plots of peak vertical wheel-rail contact forces. (c) Fitted curve of wheel load reduction ratio vs. train speed.*

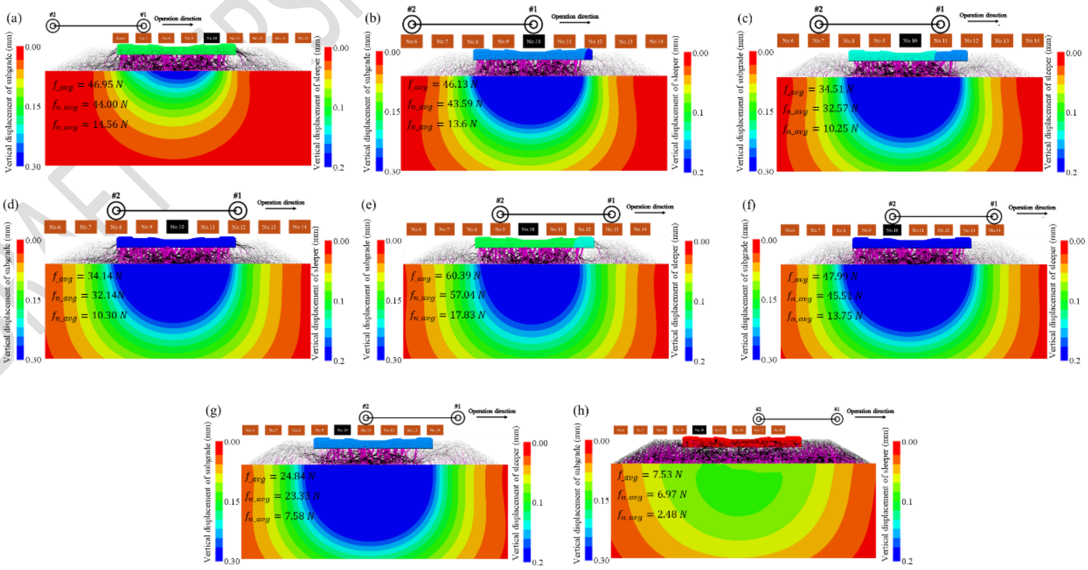

***Figure 5**: Cloud maps of ballast contact force chain distribution: (a) Initial State; (b) t=0.115s;(c) t=0.125s; (d) t=0.130s;(e) t=0.135s; (f) t=0.140 (g) t=0.145s; (h) t=0.150s;(i) t=0; (j) End of Train Passage.*

4 References

Zhong, K., Li, X., Zhou, Z., 2024. High-speed train-induced vibration of bridge–soft soil systems: observation and MTF-based ANSYS simulation. Buildings 14 (8), 2575.

Zhai, W., Han, Z., Chen, Z., Ling, L., Zhu, S., 2019. Train–track–bridge dynamic interaction: a state-of-the-art review. Vehicle System Dynamics 57 (7), 984–1027.

Liu, M., Gu, Q., Guo, W., Zhou, H., Wang, T., Chang, R., 2025. Numerical simulation for real-time hybrid testing of high-speed maglev train-track-bridge systems under complex loads. Structures 73, 108337.

Sun, Y., Ling, L., 2022. An optimal tangential contact model for wheel–rail non-Hertzian contact analysis and its application in railway vehicle dynamics simulation. Vehicle System Dynamics 60, 3240–3268.

Kurhan, D., Fischer, S., Khmelevskyi, V., 2025. Mathematical modeling of the rail track superstructure–subgrade system. Geotechnics 5 (1), 20.

Lu, Y., Xie, X., Ma, H., Xiang, P., 2025. Braking performance and response analysis of trains on bridges under seismic excitation. Applied Sciences 15, 6799.

Chen, C., McDowell, G.R., 2016. An investigation of the dynamic behaviour of track transition zones using discrete element modelling. Proceedings of the Institution of Mechanical Engineers, Part F: Journal of Rail and Rapid Transit 230 (1), 117–128.

Indraratna, B., Qi, Y., Ngo, T.N., Rujikiatkamjorn, C., Neville, T., Ferreira, F.B., Shahkolahi, A., 2019. Use of geogrids and recycled rubber in railroad infrastructure for enhanced performance. Geosciences 9 (1), 30.

Qian, Y., Lee, S.J., Tutumluer, E., Hashash, Y.M., Ghaboussi, J., 2018. Role of initial particle arrangement in ballast mechanical behavior. International Journal of Geomechanics 18 (3), 04017158.

Zhang, Z., Xiao, H., Wang, M., Zhang, M., Wang, J., 2021. Research on dynamic mechanical behavior of ballast bed in windblown sand railway based on dimensional analysis. Construction and Building Materials 287, 123052.

Mao, J.F., Xiao, Y.J., Yu, Z.W., Tutumluer, E., Zhu, Z.H., 2021. Probabilistic model and analysis of coupled train-ballasted track-subgrade system with uncertain structural parameters. Journal of Central South University 28 (7), 2238–2256.

Xiao, Y., Shen, Z., Tan, P., Hua, W., Wang, M., Jitsangiam, P., 2024. Evaluating enhancement effect of bottom groove shape on lateral resistance of frictional sleepers in ballasted railway track via hybrid DEM-FDM approach. Construction and Building Materials 436, 136755.

Li, L., Liu, W., Ma, M., Jing, G., Liu, W., 2019. Research on the dynamic behaviour of the railway ballast assembly subject to the low loading condition based on a tridimensional DEM-FDM coupled approach. Construction and Building Materials 218, 135–149.

Baghban, H., Arulrajah, A., Narsilio, G.A., Horpibulsuk, S., 2021. DEM simulation of the thermo-geomechanical effect of recycled concrete aggregate assemblies in geothermal pavement bases. Transportation Geotechnics 28, 100528.

Itasca Consulting Group Inc., 2004. Particle Flow Code. Software manual. Itasca Consulting Group Inc., Minneapolis.

Liu, Z., Feng, B., Tutumluer, E., 2023. Coupling train–track models with the discrete element method for realistic simulation of ballasted track dynamics. Transportation Research Record 2677, 414–427.

Wilson, E.L., Farhoomand, I., Bathe, K.J., 1973. Nonlinear dynamic analysis of complex structures. Earthquake Engineering and Structural Dynamics 1, 241–252.

Zhang, W., 2016. Study on vibration of subgrade-ballastless track-vehicle coupled system under irregularities condition. PhD thesis. Southwest Jiaotong University.

AASHTOWare Pavement ME Design: Advancing Pavement Performance Prediction with Models and Software Enhancements

Rami Chkaiban, PhD, PE
Applied Research Associates, Inc.

Abstract

The AASHTOWare® Pavement ME Design (PMED) software is widely used by transportation agencies for the mechanistic–empirical design of new and rehabilitated flexible and rigid pavements. With increasing demands for improved accuracy, transparency, and efficiency in pavement design, continuous advancements in both performance prediction models and software capabilities are essential. This extended abstract presents recent developments in PMED focusing on enhanced distress prediction models and improved user workflow functionalities.

Recent updates to performance models aim to improve predictions of key pavement distresses, including cracking, rutting, and surface roughness. Refined calibration methodologies and updated algorithms enable better representation of material variability, traffic loading spectra, and climatic effects. These improvements are particularly relevant in the European context, where the growing use of recycled materials and innovative binders requires more reliable long-term performance assessment.

In parallel, software enhancements such as the Structure Builder provide an intuitive interface for defining pavement layer configurations and evaluating design alternatives. This functionality improves workflow efficiency, reduces input errors, and facilitates scenario-based analysis. The combined advancements in modelling and software functionality contribute to more robust, transparent, and performance-based pavement design practices, supporting the development of durable and sustainable infrastructure.

Keywords: mechanistic–empirical design; pavement performance; AASHTOWare PMED; pavement modelling; sustainable pavements

1 Introduction

Pavement design methodologies have undergone significant evolution over the past several decades. Early design approaches were primarily empirical, relying heavily on relationships derived from the AASHO Road Test conducted in the mid-20th century. While these methods provided a practical foundation, they were limited in their ability to account for varying traffic conditions, material properties, and environmental influences.

To address these limitations, the mechanistic–empirical (ME) design framework was developed through collaborative efforts involving transportation agencies and research institutions. This led to the creation of the Mechanistic–Empirical Pavement Design Guide (MEPDG), which integrates mechanistic analysis of pavement responses with empirical performance models calibrated against field observations. The AASHTOWare Pavement ME Design (PMED) software represents the practical implementation of this framework and has been widely adopted since its release.

As pavement engineering continues to evolve, new challenges have emerged, including the need to incorporate sustainable materials, address climate variability, and improve prediction accuracy. These challenges necessitate ongoing updates to both the analytical models and the software environment used in pavement design.

2 PMED Methodology

2.1 Mechanistic–Empirical Framework

The PMED methodology is based on the calculation of pavement responses—such as stresses, strains, and deflections—under traffic and environmental loading conditions. These responses are computed using mechanistic models and are subsequently linked to pavement distresses through empirically calibrated relationships.

The design process is iterative and evaluates pavement performance over time by accumulating damage caused by repeated loading and environmental effects. Key performance indicators include rutting, fatigue cracking (both top-down and bottom-up), thermal cracking, and surface roughness, typically expressed as the International Roughness Index (IRI).

2.2 Iterative Design Process

The PMED procedure consists of three primary stages:

- **Stage 1: Evaluation** – Characterization of site conditions, material properties, traffic, and climate inputs.
- **Stage 2: Analysis** – Development and evaluation of trial pavement structures using mechanistic and empirical models.
- **Stage 3: Strategy Selection** – Comparison of viable design alternatives using engineering judgment and life-cycle cost analysis (performed outside PMED).

During the analysis stage, trial designs are iteratively refined until they meet predefined performance criteria at a selected reliability level. This approach allows engineers to systematically optimize pavement structures.

3 Recent Advancements in Performance Models

3.1 Enhanced Distress Prediction

Recent updates to PMED (pre and post Version 2.3) improved the prediction of key pavement distresses (e.g., top-down fatigue cracking). Enhanced cracking models provide better differentiation between fatigue mechanisms, while improved rutting models more accurately represent permanent deformation across pavement layers. Additionally, updates to roughness models (e.g., for Jointed Plain Concrete Pavement) enable more reliable prediction of long-term ride quality.

3.2 Improved Input Characterization

Advancements in material characterization have strengthened the reliability of model predictions. Updated approaches for asphalt mixtures consider temperature dependency, aging effects, and binder properties, while improvements in subgrade and unbound material modelling better capture moisture sensitivity and stiffness variations.

Traffic loading inputs have also been refined using axle load spectra and temporal distribution factors, allowing for a more realistic representation of field conditions.

3.3 Climate Modelling Enhancements

The Enhanced Integrated Climate Model (EICM) remains a core component of PMED, simulating temperature and moisture variations within pavement layers. Recent improvements enhance the integration of climatic data and better account for seasonal effects, freeze–thaw cycles, and extreme weather conditions. Adding the Modern-Era Retrospective analysis for Research and Applications, Version 2 (MERRA2) database through the Long-Term Pavement Performance (LTPP) program, which makes climatic data available across the globe

These developments are particularly significant in regions with diverse climates (e.g., Europe), where environmental considerations play a critical role in pavement design.

4 Software Enhancements and Workflow Improvements

4.1 Structure Builder Functionality

A major recent advancement in PMED is the introduction of the Structure Builder tool, which provides an intuitive interface for defining pavement layer configurations. This tool allows users to:

- Assemble pavement structures efficiently;
- Modify layer thicknesses and material properties;
- Evaluate multiple design alternatives within a unified environment.

The Structure Builder significantly improves usability and reduces the complexity associated with input data management.

4.2 Improved Design Workflow

The updated software environment enhances workflow efficiency by minimizing input errors and enabling rapid iteration of design scenarios. Designers can more easily compare alternatives and assess the impact of different materials and structural configurations on pavement performance.

These improvements support a more transparent and systematic design process, which is particularly beneficial for collaborative projects and standardized design practices.

5 Applications and Relevance to European Practice

The recent developments in PMED are highly relevant to the European pavement engineering context. Increasing emphasis on sustainability has led to greater use of recycled materials, such as reclaimed asphalt pavement (RAP), and innovative binders. These materials introduce additional variability that must be accurately captured in performance models.

The enhanced modelling capabilities of PMED enable more reliable evaluation of such materials, supporting performance-based design approaches aligned with European research and policy priorities. Furthermore, improved climate modelling supports adaptation to region-specific environmental conditions.

6 Conclusions

The continued development of AASHTOWare Pavement ME Design represents a significant advancement in pavement engineering practice. Enhanced performance models improve the accuracy of distress predictions, while software innovations such as the Structure Builder streamline the design process and enhance usability.

These advancements enable engineers to better evaluate alternative materials and design strategies, supporting more informed and reliable decision-making. The integration of improved modelling techniques with user-friendly tools contributes to the development of durable, resilient, and sustainable pavement infrastructure.

Future work should focus on further calibration of models for regional conditions, continued integration of emerging materials, and expansion of capabilities to address evolving transportation challenges.

7 References

American Association of State Highway and Transportation Officials (AASHTO). 2022. Washington, D.C. A*ASHTOWare Pavement ME Design User Guide (Version 3.0)*. AASHTO.

Numerical investigations on the influence of radius and track gauge on wheel-rail contact in narrow curves

Dominik Rudisch
Stephan Freudenstein
Chair and Institute of Road, Railway and Airfield Construction, Technical University of Munich, Germany

Abstract

Narrow curves are common in metro systems worldwide, even though the conventional rolling-radius steering becomes ineffective in them. Due to the small radius, an angle of attack occurs instead, steering the bogie under high dynamic forces through the curve, which often results in vibrations and increased wear. Field measurements along curves at the Milan Metro have indicated that the leading axle mainly drives gauge-widening effects. Based on these findings, this research aims to enhance the understanding of wheel-rail contact in narrow curves by conducting a simulation-based parameter study on the influence of curve radius and track gauge. A multibody simulation model was developed in SIMPACK and extended by Vtech CMCC's user subroutine CONTACT for full rolling contact theory. Simulations were performed with a radius varying from 200 m to 900 m, and in one scenario, with additional track gauge widening of 5 mm and 10 mm. For each scenario, the speed was chosen to fully compensate centrifugal acceleration for the constant superelevation, ensuring a balanced load distribution across all scenarios. The simulation results show that in narrow curves, large angles of attack result in flange contact at the outer wheel, leading to significant lateral creep forces. With an increasing curve radius, these lateral forces decrease — particularly on the outer rail — while longitudinal creep forces rise until roll-radius steering seems to become effective again. The maximum contact pressure trends differ: on the outer rail, pressures initially decrease and then increase with larger radii, likely due to changes in contact shape, position, and patch distribution. In contrast, maximum pressures on the inner rail remain high and largely independent of radius. Gauge widening primarily affects the inner contact by shifting it toward the rail center, causing lower pressure through a more favourable elliptical contact, while the outer contact remains mainly unaffected. Overall, moderate gauge widening of a softer fastening system implies that it can reduce pressure-related wear on the inner rail from a quasi-static perspective.

Keywords: wheel-rail contact; narrow curves; gauge widening; wheelset steering; multibody simulation

1 Introduction

Metro Systems worldwide have railway lines with narrow curves. When trains run through them, mutual excitations occur, which can manifest in the form of squeal noise and structure-borne sound as well as increased wear on wheels and rails. The reason for this dynamic vehicle-track interaction is that in small-radius curves, the rolling radius difference between inner and outer rails becomes inefficient. Instead, the wheelset experiences an angle of attack on the outer rail. As a result, the bogie is steered through the curve under high lateral forces, causing wear.

How curved tracks react to passing trains was intensely investigated in (Acquati et al., 2009). In collaboration between Metropolitana Milanese S.p.A. and the Chair and Institute for Road, Railway and Airfield Construction of the Technical University of Munich (TUM), field measurements were carried out in several curve sections with different installed fastening systems in the Milan Metro. They found that, in general, the leading axle generates the greatest horizontal forces on the rail head, causing a widening of the track gauge, whereas the trailing axle only leads to a minor reaction on the inner rail or none on the outer rail. Further, they noted that, under fully compensated lateral acceleration, the horizontal load on the outer side is accompanied by a load of similar magnitude on the inner side, which together contribute to widening the track gauge.

Based on these findings, this research conducts a simulation-based parameter study to investigate in depth how track gauge widening and radius affect the wheel-rail contact interaction in narrow curves. Only with a detailed understanding can the next future step be taken to efficiently research solutions for rail fastening systems that address the problems.

2 Multibody Simulation Workflow

To perform the parameter study, a three-dimensional multibody simulation model was developed in SIMPACK 2024x6. The model, as shown in Figure 1, consists of a train vehicle and an elastic track foundation moving along the defined track layout. The simplified vehicle model is based on the ERRI B176 benchmark vehicle 1 described in (Iwnicki, 1998), which can translate and rotate in all directions. The static wheel load is 5.56 t, the wheel profile geometry is S1002, and the axle distance within the bogies is 2.56 m. The used default track model can, in whole, translate in vertical z and lateral y direction, as well as rotate around the longitudinal x direction. Its values for stiffness and damping are listed in (Dassault Systèmes, 2024). As the focus of this research is on a detailed analysis of the wheel-rail contact, the model was further extended with a user subroutine for the online integration of the program CONTACT by Vtech CMCC. This subroutine replaces SIMPACK's internal algorithms for calculating wheel-rail contact with those of CONTACT, allowing access to Prof. J.J. Kalker's full theory for rolling contact (Vollebregt, 2024). A Poisson's ratio of 0.28 and a shear modulus of 82000 N/mm² were selected for the material properties of the wheel and rail. Coulomb's friction law was used with a friction coefficient of 0.4. For reasons of computation and later evaluation, the subroutine was applied at the leading bogie's wheelsets only.

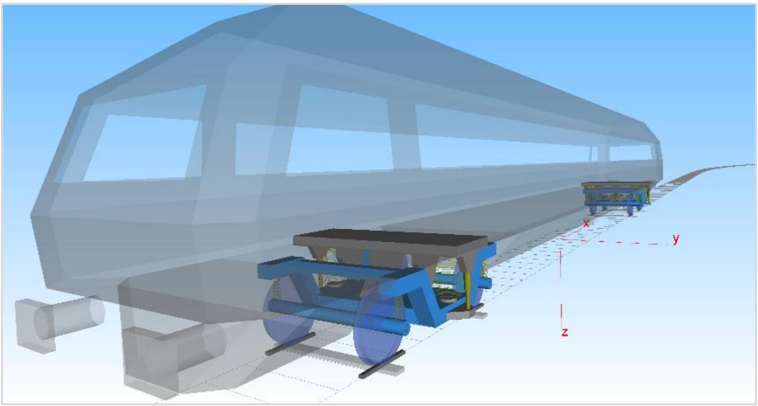

Figure 1: *Multibody simulation model for vehicle-track interaction in SIMPACK 2024x6.*

The parameter study was developed based on a track scenario in (Acquati et al., 2009) at the Milan Metro, where gauge widening was measured along a 259.2 m radius curve with a standard track gauge of 1435 mm. Hereafter referred to as the "reference scenario", the curve radius and track gauge were varied from there, enabling an analysis of their influence on wheel-rail contact. As listed in Table 1, the radius range was from 200 m to 900 m. Additionally, 5 mm and 10 mm of track gauge widening were simulated for the reference scenario, whereas it was kept constant at 1435 mm for the others.

Table 1: *Simulation overview with the reference scenario highlighted in blue.*

Radius [m]	Track gauge [mm]	Superelevation [mm]	Transition curve length [m]	Speed [km/h]
200	1435	85	50	37.96
259.2	1435, 1440 (+5), 1445 (+10)	85	50	43.21
300	1435	85	50	46.49
350	1435	85	50	50.21
400	1435	85	50	53.68
500	1435	85	70	60.01
600	1435	85	70	65.74
700	1435	85	70	71.01
800	1435	85	70	75.91
900	1435	85	70	80.99

In all scenarios, the train started on a straight track, entered a 150 m long right-hand curve with a constant superelevation of 85 mm, and then proceeded into a straight section. Between the straight sections and the curve, a 50 m long clothoid transition was applied for the radii 200 m to 400 m, and a 70 m long one for the higher radii. Within these transitions, the outer rail was lifted or lowered in the form of a linear ramp. For each radius, the train speed was adjusted in a way that the superelevation fully compensates the centrifugal acceleration, leaving no free lateral acceleration. This ensured a reasonably balanced load distribution across all scenarios. Consistent with the reference scenario, rail profile UIC60 with an inclination of 1:20 was used.

3 Analysis and discussion of the simulation results

The evaluation of the simulation results in this research concentrates on the train's leading wheelset only, following the investigations in (Acquati et al., 2009). While the raw results of the discussed parameters are fully presented in the distance domain for all simulations in the Appendix, the following analysis focuses in detail on the situation in the middle of the curve at x = 175 m, where the wheelset is fully sliding. First, the influence of radius r, and secondly, the influence of track gauge g on the wheel-rail contact, are investigated.

3.1 Influence of radius

As can be seen in the Appendix, the angle of attack ψ at the leading wheelset with decreasing curve radius rises from -2.2 mrad (r = 900 m) to -12.8 mrad (r = 200 m), resulting in different but fully saturated creep force situations summarised in Figure 2(a). In small-radius curves, due to the high angle of attack, the outer wheel in flange contact is steered through the curve, resulting in high lateral creep forces Ty. As the radius increases, the lateral creep forces decrease due to the lower angle of attack, on both rails, but more so on the outer rail. At the same time, the longitudinal creep forces Tx increase similarly on both rails until a radius of 700 m, after which a decreasing trend can be observed. This trend could be due to the smaller getting an angle of attack, leading to rolling-radius steering becoming effective again. Further, for very small radii, the vertical wheel-rail forces Q are not balanced between the inner and outer rails, even though the speeds were chosen to compensate for the centrifugal acceleration. Only for larger radii do the vertical forces approach each other, which suggests that the imbalance before is caused by the wheel flange running against the outer rail head at high angles of attack.

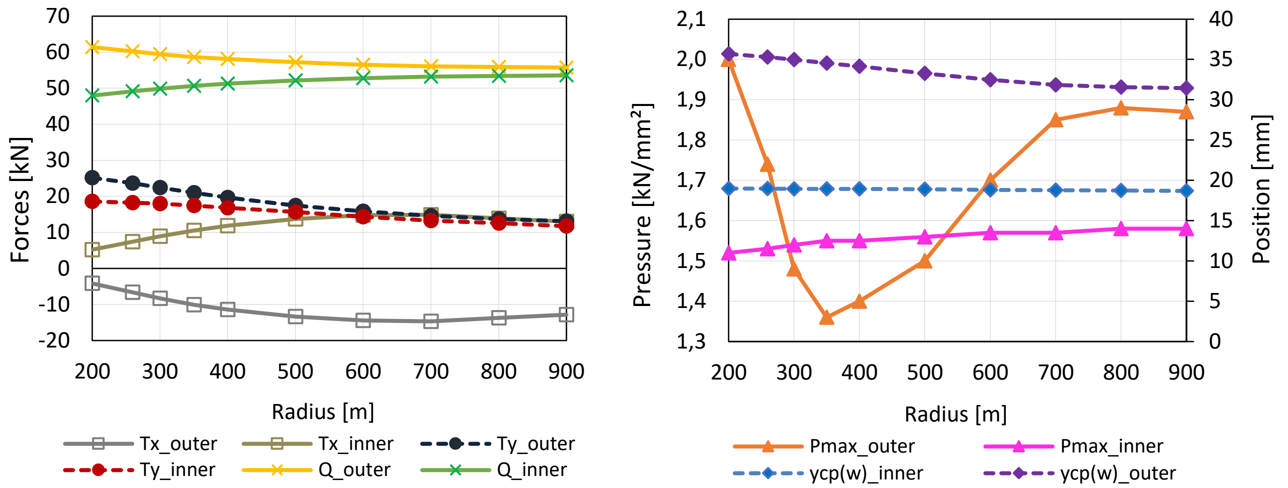

***Figure 2:** (a) Longitudinal Tx and lateral Ty creep forces, vertical wheel-rail force Q, as well as (b) maximum pressure Pmax and lateral contact position on the wheel ycp(w) in dependence of radius at inner and outer rail.*

For the maximum pressure Pmax acting in the wheel-rail contacts, the situation appears different. As illustrated in Figure 2(b), the maximum pressure of 2.0 kN/mm² for a radius of 200 m on the outer rail is initially reduced as the radius increases. However, above 350 m (Pmax = 1.36 kN/mm²), the maximum pressure rises again until reaching another peak of 1.88 kN/mm² at a radius of 800 m. This could be related to the different contact shapes occurring for the radii on the outer rail, as presented in Figure 3, where the positive y-direction is the track side and the negative the field side. At a very small radius of 200 m, the high pressures seem to be driven by the decisive wheel-flange contact. For the larger radii, the formation of further small contact patches on the rail top, as observed for 700 m, 800 m, and 900 m, may lead to a higher pressure concentration on the still more decisive patch on the track side (right patch).

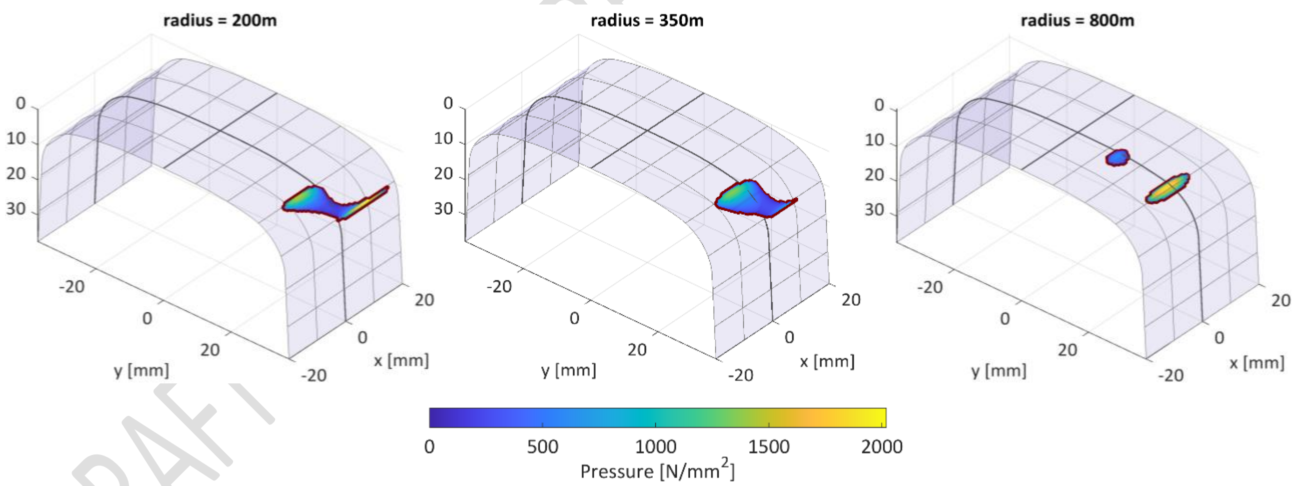

***Figure 3**: Normal Pressure on the outer rail for different radii, evaluated under the leading wheelset in the curve middle (x = 175 m).*

In contrast, the maximum pressure on the inner rail, at around 1.5–1.6 kN/mm², does not appear to be greatly influenced by the radius as visible in Figure 2(b). It slightly rises with increasing radius. A similar applies to the inner contact position on the wheel ycp(w), which remains nearly the same at the wheel tread's middle, around 19 mm. On the outer wheel, the lateral position of the decisive contact patch shifts in the flange root area about 5 mm from around 36 mm (r = 200 m) to 31 mm (r = 900 m) in field direction.

The results suggest that for a constant track gauge in narrow curves, regardless of the radius, the inner rail and wheel are loaded at the same contact position, and the pressure remains almost constant. The contact positions and shapes between the outer rail and wheel, on the other hand, are more dependent on the radius, which, in unfavorable combinations, can lead to extreme pressure causing increased rail wear.

3.2 Influence of track gauge

The reference scenario, with a radius of 259.2 m, was additionally simulated with track gauge widening of 5 mm (g = 1440 mm) and 10 mm (g = 1445 mm). Unlike for the radius, the saturated creep forces at the leading axle are hardly affected by a larger track gauge, as shown in Figure 4(a).

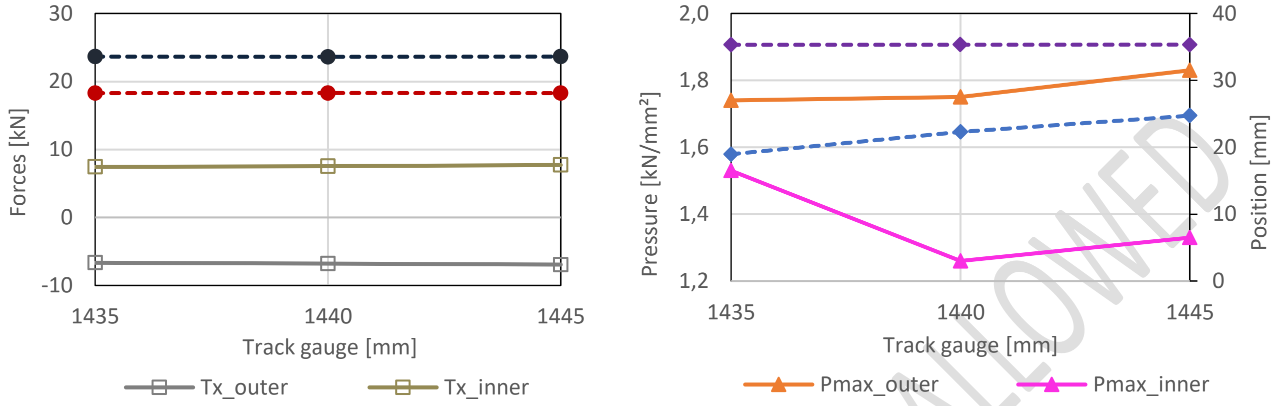

Figure 4: *Longitudinal Tx and lateral Ty creep forces, vertical wheel-rail force Q, as well as (b) maximum pressure Pmax and lateral contact position on the wheel ycp(w) in dependence of track gauge at inner and outer rail.*

The contact position and maximum pressure are more affected, as shown in Figure 4(b). With a widening track gauge, a greater lateral displacement of the wheelset y towards the outer rail occurs, as visible in the Appendix. This results in roughly the same contact situation between the outer rail head and the wheel flange root at a position of approximately 35 mm, regardless of the track gauge. Accordingly, the maximum pressure on the outer rail stays nearly the same, around 1.75 kN/mm². Only at a widening of 10 mm does it rise slightly, to 1.83 kN/mm². On the inner side, as the wheelset shifts laterally, the contact position of the inner wheel moves towards the field side, resulting in a smaller rolling radius. As depicted in Figure 4(b), the lateral contact position moves from 19 mm (g = 1435 mm) in the wheel tread middle by around 6 mm in the wheel field direction to 25 mm (g = 1445 mm). While the contact position on the inner wheel moves to the field side, on the inner rail, the contact moves with increasing track gauge in the track side direction towards the rail head middle. To better understand how this influences normal pressure, a closer look at the contact situations on the inner rail is provided for the three different track gauges in Figure 5. Again, the positive lateral y-direction is the field side, and the negative is the track side.

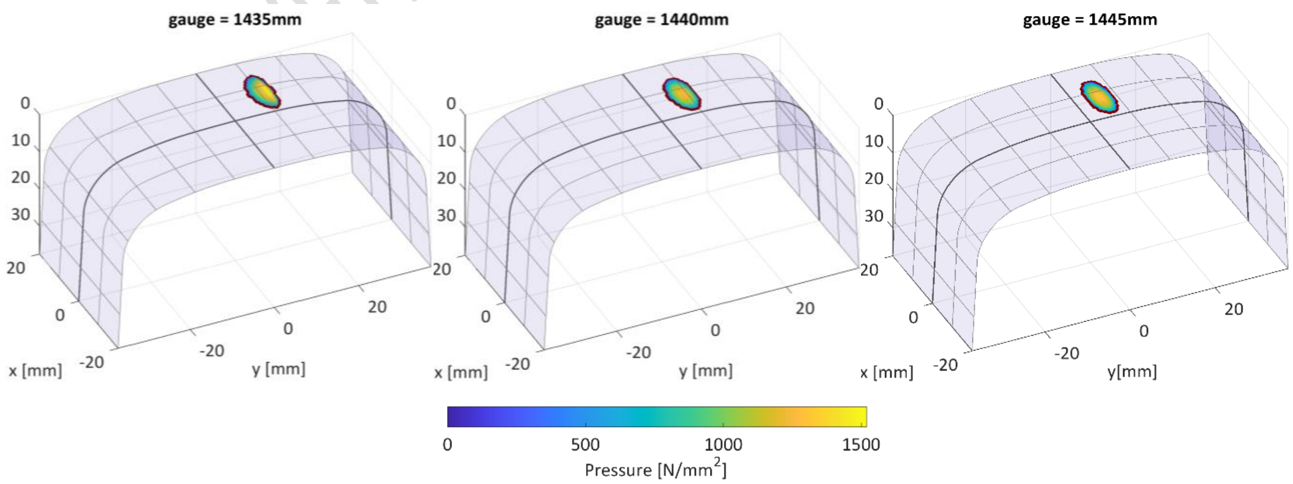

Figure 5: *Normal pressure on the inner rail for a radius of 259.2 m with three different track gauges, evaluated under the leading wheelset in the curve middle (x = 175 m).*

Apparently, not only the contact position, but also the contact shape and pressure distribution change on the inner rail with increasing track gauge. For the standard track gauge of 1435 mm, the contact has the largest eccentricity from the rail head middle. High pressure of up to 1.53 kN/mm² concentrates in a stripe shape (yellow), likely caused by a rather unfavorable combination of rail and wheel geometry curvatures at this point. The position shift toward the center of the rail with increasing track gauge seems to lead to a more favorable, elliptical pressure distribution. With a widening of 5 mm (1440 mm), the maximum pressure is reduced by 18% to 1.26 kN/mm², with a widening of 10 mm (1445 mm) by 13% to 1.33 kN/mm². This implies that, under the leading wheelset, a moderate track gauge widening in curves has little effect on the position and pressure in the outer wheel-rail contact but may be beneficial for the inner contact.

4 Conclusions

A multi-body simulation model was developed to conduct a parameter study on the influence of curve radius and track gauge on wheel-rail contact in narrow curves. On the basis of a scenario derived from a field measurement, curve radii ranging from 200 m to 900 m, and for one radius, the track gauge ranging from 1435 mm to 1445 mm, were simulated.

The numerical results show that in narrow curves, high angles of attack lead to flange contact at the outer wheel, generating large lateral creep forces. As the radius increases, lateral creep forces decrease, especially on the outer rail, while longitudinal creep forces rise until a point is reached where roll-radius steering, due to a lower angle of attack, seems to become effective again. The contact pressures behave differently. On the outer rail, the pressure initially drops, then increases again for higher radii. A closer look at the contacts revealed that this trend may be related to the varying contact shapes, positions, and patch numbers associated with different radius sizes. Whereas on the inner rail, the maximum pressure remains consistently high and more radius-independent. The contact positions change only slightly with the radius. Other for a gauge widening, which seems to primarily affect the inner wheel-rail contact, shifting the contact towards the rail center and reducing the maximum pressure through a more elliptical distribution. The outer wheel-rail contact and pressure remain relatively unchanged by the widening.

However, it must be noted that the multibody simulation model contains simplifications that can limit the results. Aside from contact determination, all bodies are rigid, which excludes consideration of the eigenmodes for the rail and wheelset in the dynamics. The rails themselves cannot move or rotate in the model. Therefore, load eccentricities as detected, which lead to rail tilting and thus to additional dynamic changes in track gauge, are neglected. Further, a constant coefficient of friction is applied, which under real conditions can vary, promoting stick-slip effects and vibrations. In addition, this research focuses on the leading wheelset, while the trailing wheelset, depending on the bogie construction and the properties of the primary suspension, also affects steering. To address these limitations, a co-simulation model is developed next to enable a more accurate investigation of wheel-rail contact dynamics in narrow curves.

Still, the results imply that in narrow curves, a moderate gauge widening could beneficially reduce the maximum contact pressure on the inner rail. Therefore, a softer fastening system could reduce pressure-related rail wear and safe maintenance costs from a quasi-static view.

5 References

Acquati, M., Cavagna, B., Lechner, B., Liu, J., & Stahl, W. 2009. London. Comparative procedure for assessing Wheel/Rail Contact Forces among different slab track formations in a Metro Tunnel Railway Engineering - 10th International Conference and Exhibition.

Iwnicki, S. 1998. Manchester Benchmarks for Rail Vehicle Simulation. Vehicle System Dynamics, 30(3-4), 295-313. https://doi.org/10.1080/00423119808969454

Dassault Systèmes. 2024. Vélizy-Villacoublay. SIMULIA User Assistance 2024x.

Vollebregt, E. 2024. Rotterdam. User-subroutine for on-line integration of CONTACT in Simpack Rail. Vtech CMCC, EV/M24.004, version 24.1.3.

Monitoring the behaviour of full-scale pavements under moving loads using distributed optical fiber sensors

Marina AlBacha
Mai-Lan Nguyen
Pierre Hornych
Olivier Chupin
Juliette Blanc
MAST-LAMES, Université Gustave Eiffel, Nantes Campus, F-44344, Bouguenais, France
Xavier Chapeleau
COSYS-SII, I4S Team (Inria), Université Gustave Eiffel, Nantes Campus, F-44344, Bouguenais, France

Abstract

Pavement behavior under moving loads can be assessed using full-scale instrumentation. Distributed optical fiber sensors (DOFS) are particularly suited for such applications, offering continuous strain measurements along the entire fiber length. Their lightweight, compact design and small diameter make them ideal for deployment in complex road environments. This study investigates the use of DOFS for strain monitoring in pavements under moving loads. Full-scale experiments were conducted with DOFS embedded at different pavement depths, and the results were compared to traditional strain gauge measurements. The results show that DOFS provide a much higher density of measurements, making it possible to capture strain variations in the bituminous layers more effectively.

Keywords: distributed optical fibers, strains measurements, full-scale pavement, moving loads

1 Introduction

DOFS are advanced tools increasingly used in road engineering for assessment of pavement behavior , including the measurement of strain, stress and displacement, temperature and other parameters (Kashaganova et al., 2023), and traffic monitoring (Tekinay et al., 2023). Given the large scale and heterogeneous nature of pavement structures, the ability to monitor large areas is essential for understanding structural behaviors and ensuring effective road construction, maintenance, and rehabilitation. Unlike traditional strain gauges, which provide localized measurements and have limited suitability for thin pavement layers (Davis et al., 2016), DOFS can capture continuous, distributed strain profiles along the entire fiber length. This allows for detailed mapping of strain variations, making it possible to track structural responses and detect damage initiation. DOFS also offer significant advantages due to their small diameter and lightweight design. Recent full-scale studies have successfully applied DOFS for strain monitoring under real traffic (Wang et al., 2020). This paper investigates the performance of DOFS embedded at different depths within bituminous pavements and compares their strain measurements with those obtained from traditional strain gauges. The experiments were conducted on a full-scale pavement, tested on the accelerated pavement testing (APT) facility at Université Gustave Eiffel. DOFS measurements were made using Rayleigh/OFDR technology (Soga and Luo, 2018), which allows for high-resolution strain measurements at a frequency of 100 Hz.

2 Full-scale test

The experiments presented in this study were part of the European funded project NEMO (Grant agreement ID: 860441), and started in November 2022. The APT track was divided into several pavement structures, with one 35-meter-long structure selected for analysis in this study. This structure was subjected to loading using single axles equipped with dual wheels, applying a load of 3.25 tons per wheel (Figure 1 (a)). The structure consisted of a 3.4 cm very thin bituminous surface layer (BBTM 0/4), a 13 cm bituminous base layer (GB3 0/14), a 30 cm granular subbase, and a sandy soil subgrade. Instrumentation was installed at three depths within the bituminous layers: the bottom of the surface layer, the top of the base layer, and the bottom of the base layer (Figure 1 (b)). At each depth, the instrumentation included one 10-meter-long optical fiber and 4 strain gauges (2 longitudinal and 2 transverse). DOFS strain data were collected every 2.6 mm along the fiber. Due to the acquisition frequency limitation, measurements were performed at a low loading speed of approximately 7 km/h. Each fiber included three measurement zones: one 2 m longitudinal section and two 1 m transverse sections (Figure 1(c)). In this study, the focus is on strain measurements in the longitudinal direction, performed at 50,000 load cycles and at a pavement temperature of 8°C.

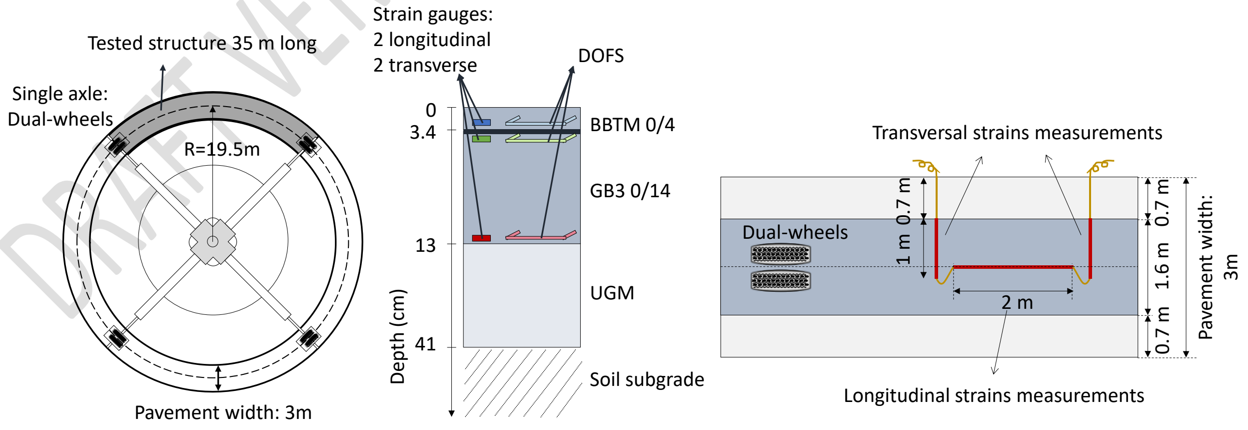

(a): Fatigue caroussel (b): Structure and vertical position of instrumentation (c): Top view of the instrumentation with DOFS

***Figure 1**: Top view of the instrumentation with DOFS for the pavement structures.*

3 Strain measurements

Figure 2 presents strain measurements obtained from the DOFS over a 1 m interest zone, avoiding the fiber curvature areas. The results show compressive strain values at the bottom of the surface layer and at the top of the base layer, averaging -97 and -95 µm/m, respectively. These similar values indicates good bonding between layers, and represents typical visco-elastic behavior of a pavement with bonded interface. At the bottom of the base layer, tensile strains were observed, as expected, averaging +128 µm/m. Such tensile strains will lead to fatigue-induced damage. As shown in the figure, fiber measurements display significant variability over a 1-meter length at a given level, which can be attributed to the material's heterogeneity. Strains recorded at the bottom of the base layer exhibit a wider range of variation than those in the surface layer, with values ranging from +102 µm/m to +260 µm/m (see Table 1). This high variability may be explained by the interface with the underlying unbound granular layer—which is generally more heterogeneous than the bituminous layers—as well as by the lower efficiency of compaction at the bottom of the base layer.

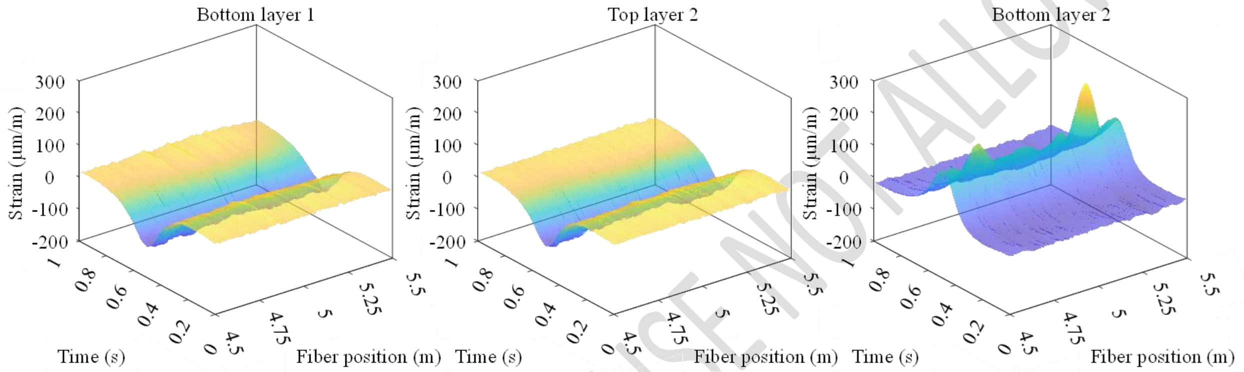

Figure 2: *3D representation of the DOFS measurements, at 3 levels (- for compression and + for extension).*

Napaka! Vira sklicevanja ni bilo mogoče najti. compares strain measurements from DOFS and strain gauges. The shaded areas represent the range of optical fiber signals along the fiber, while the solid and dashed lines correspond to gauge signals. The results show good agreement between the two measurement methods across all pavement levels, with similar signal shapes and average strain values (Table). This confirms the reliability of the DOFS measurements. Unlike strain gauges, DOFS provide a much higher measurement density, capturing detailed strain variability within the bituminous layers.

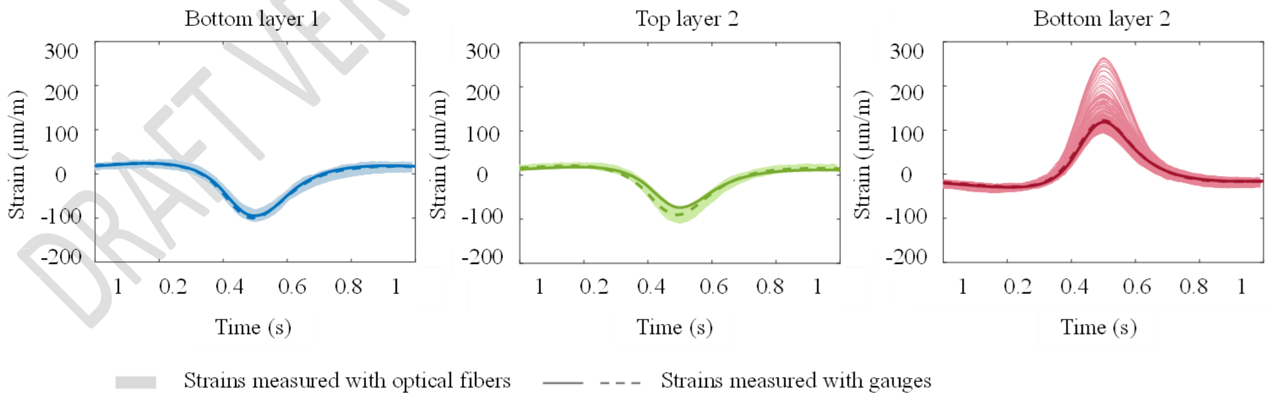

Figure 3: *Comparison of DOFS and strain gauge measurements, at 3 levels (- for compression and + for extension).*

Table 2: *Strain values obtained using DOFS and strain gauges, at 3 levels (- for compression and + for extension).*

	DOFS (over 1-m)			Strain gauges
Strain values (µm/m)	Average	Minimum	Maximum	Average
Bottom layer 1	-97	-108	-82	-98
Top layer 2	-95	-106	-80	-84
Bottom layer 2	+128	+102	+260	+120

4 Conclusions

This article presents a comparison of strain measurements in a bituminous pavement structure obtained using Distributed Optical Fiber Sensors (DOFS) and traditional strain gauges, installed at three different depths. The DOFS measurements were performed with Rayleigh/OFDR technology, which provides high-resolution strain data at sampling frequencies of up to 100 Hz. This approach allows continuous, distributed measurements every 2.6 mm along a 10-meter fibre under moving loads, thereby capturing the spatial variability of pavement strains. In contrast, strain gauges provide only localized measurements. The comparison between DOFS and strain-gauge data confirmed the reliability and accuracy of the DOFS method. Results also revealed significant strain variability within the bituminous layers, particularly at the bottom of the base layer. These findings demonstrate the potential of DOFS to improve predictions of pavement damage by identifying the zones where the highest strains occur.

5 References

Davis, C., Knowles, M., Rajic, N., Swanton, G., 2016. Evaluation of a Distributed Fibre Optic Strain Sensing System for Full-Scale Fatigue Testing. Procedia Structural Integrity 2, 3784–3791. https://doi.org/10.1016/j.prostr.2016.06.471

Kashaganova, G., Kozbakova, A., Kartbayev, T., Balbayev, G., Togzhanova, K., Alimseitova, Z., Orazaliyeva, S., 2023. Research of a Fiber Sensor Based on Fiber Bragg Grating for Road Surface Monitoring. Electronics 12, 2491. https://doi.org/10.3390/electronics12112491

Soga, K., Luo, L., 2018. Distributed fiber optics sensors for civil engineering infrastructure sensing. Journal of Structural Integrity and Maintenance 3, 1–21. https://doi.org/10.1080/24705314.2018.1426138

Tekinay, M., Sylvester, T., Brunton, M., Ganesh, T., 2023. Applications of fiber optic sensors in traffic monitoring: a review. Innov. Infrastruct. Solut. 8, 88. https://doi.org/10.1007/s41062-023-01057-1

Wang, H.-P., Xiang, P., Jiang, L.-Z., 2020. Optical fiber sensing technology for full-scale condition monitoring of pavement layers. Road Materials and Pavement Design 21, 1258–1273. https://doi.org/10.1080/14680629.2018.1547656

6 Appendix: Simulation results in the distance domain [m]

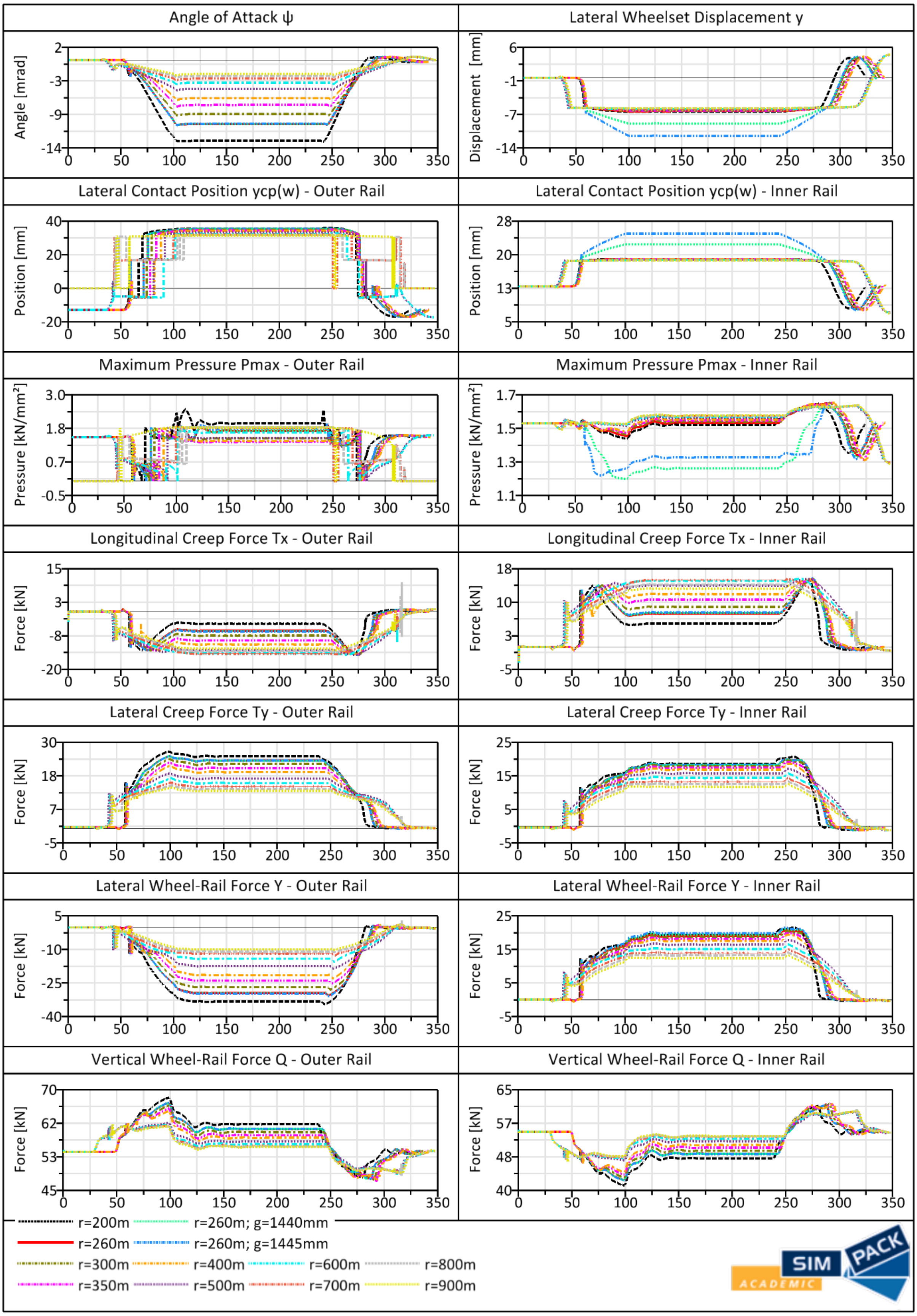

Random vibration analysis of three-dimensional high-speed train-ballasted track-subgrade coupling system based on PDEM

Yuanjie Xiao
School of Civil Engineering, Central South University, Changsha 410075, China
Ministry of Education Key Laboratory of Engineering Structures of Heavy Haul Railway Central South University, Changsha 410075, China
Zixuan Deng
School of Civil Engineering, Central South University, Changsha 410075, China

Abstract

With increasing railway operational speeds, train-induced vibrations exert substantial influences on substructures and the surrounding environment. To investigate the train-track-subgrade interaction mechanism and subgrade dynamic behavior under high-speed conditions, a three-dimensional coupled vibration model of the high-speed train-ballasted track-subgrade system was developed through integration of finite element method, elastoplastic mechanics theory, and multibody dynamics, implemented via an in-house MATLAB computational framework. The proposed model incorporates three-dimensional wheel-rail contact kinematics and elastoplastic constitutive relationships for subgrade soils, enabling comprehensive analysis of dynamic responses in high-speed ballasted track systems under operational loading conditions. Employing probability density evolution theory combined with random field characterization, a stochastic subgrade parameter field model was established, accompanied by formulation of probability density evolution equations for the coupled system under multivariable randomness, effectively characterizing the evolutionary patterns of stochastic vibration responses. Numerical results demonstrate that train velocity critically governs vehicular stability and vibration propagation through track layers. Spatial variability in subgrade parameters exhibits significant influence on stochastic dynamic responses, with response distributions demonstrating near-Gaussian characteristics. Parametric studies reveal that vehicle structural uncertainties, particularly random wheel-rail excitations, substantially affect system dynamics. Future investigations should incorporate discrete element modeling to resolve granular characteristics of ballast aggregates, facilitating more realistic simulation of train-track interaction mechanics and associated infrastructure responses.

Keywords: high-speed railway; nonlinear finite element method; random vibration; probability density evolution method (PDEM); running safety

1 Introduction

With the continuous development of high-speed railways and the increasing operational velocity, train-induced dynamic loads and vibrations have become more pronounced. These vibrations not only exert cumulative effects on the track structures and subgrade but may also pose adverse impacts on the surrounding environment. In ballasted track systems, the complex interactions among ballast, sleepers, and subgrade, as well as the diverse vibration transmission paths, render the train-track-subgrade system highly nonlinear. Meanwhile, substantial uncertainties inherently exist in the system, including fluctuations in vehicle loads, stochastic excitations at the wheel-rail interface, and the spatial variability of subgrade soil parameters. These random factors considerably affect the distribution characteristics of system responses, making traditional deterministic analyses inadequate for capturing the true dynamic behavior. Consequently, it is essential to introduce a stochastic analysis framework when investigating the dynamic responses of high-speed train-track-subgrade coupled systems. Such an approach enables the exploration of evolutionary patterns of system dynamics from a probabilistic perspective, providing not only theoretical insights into the coupling mechanisms under high-speed conditions but also practical guidance for infrastructure safety assessment and reliability-based design.

2 Method

To investigate the dynamic behavior of the high-speed train-ballasted track-subgrade system, a three-dimensional coupled vibration model was developed by integrating the finite element method, elastoplastic mechanics theory, and multibody dynamics. The model was implemented within an MATLAB computational framework, enabling efficient numerical simulations. In this model, the vehicle subsystem is represented using multibody dynamics, while the track and subgrade structures are discretized through the finite element method. The wheel-rail interaction is formulated based on three-dimensional contact kinematics, which provides an accurate description of the nonlinear coupling between the vehicle and track. Moreover, the elastoplastic constitutive relationships of subgrade soils are incorporated to capture the nonlinear deformation characteristics under repeated train-induced loads, thereby ensuring the model’s capability to reproduce realistic dynamic responses of the coupled system.

The stochastic analysis was conducted by combining random field characterization with the probability density evolution method (PDEM). First, the spatial variability of subgrade soil parameters was modeled using a random field approach, where statistical distributions and correlation structures were assigned to represent inherent material uncertainties. This random field was discretized and mapped into the finite element framework of the coupled train‑track‑subgrade system. Subsequently, the governing probability density evolution equations (PDEEs) were derived based on the system’s dynamic equations under stochastic excitations. The PDEEs were solved numerically using a finite-difference time-stepping scheme, which enables the propagation of probability densities over time. Through this procedure, the temporal evolution of response probability distributions was obtained directly, avoiding extensive sampling requirements typical of Monte Carlo simulations.

3 Result

The numerical simulations reveal several key characteristics of dynamic responses in the high-speed train-ballasted track-subgrade system. Train velocity is identified as the dominant factor influencing both vehicle stability and vibration propagation through the track-subgrade layers. Specifically, the increase in train speed from 200 km/h to 350 km/h leads to more than twofold amplification in vertical vibration amplitudes transmitted from the rail to the subgrade surface, while the lateral stability index of the vehicle decreases by approximately 15%.

The spatial variability of subgrade soil parameters exerts a significant impact on stochastic responses. When the coefficient of variation of soil stiffness increases from 0.1 to 0.3, the standard deviation of subgrade displacement responses rises by nearly 40%, and the probability density functions of acceleration responses exhibit increasingly dispersed distributions, although their overall shapes remain close to Gaussian. Furthermore, response kurtosis values remain within the range of 2.9-3.2, further confirming near-Gaussian characteristics.

Parametric studies also highlight the importance of vehicle structural uncertainties. Under random wheel-rail excitations with an imposed spectral density amplitude increased by 50%, the peak accelerations in the car body increase by nearly 35%, while the dynamic amplification factor of track displacement grows by around 20%. These quantitative results demonstrate that both operational parameters and stochastic factors have substantial effects on system dynamics, underscoring the necessity of incorporating randomness into the evaluation of high-speed railway performance.

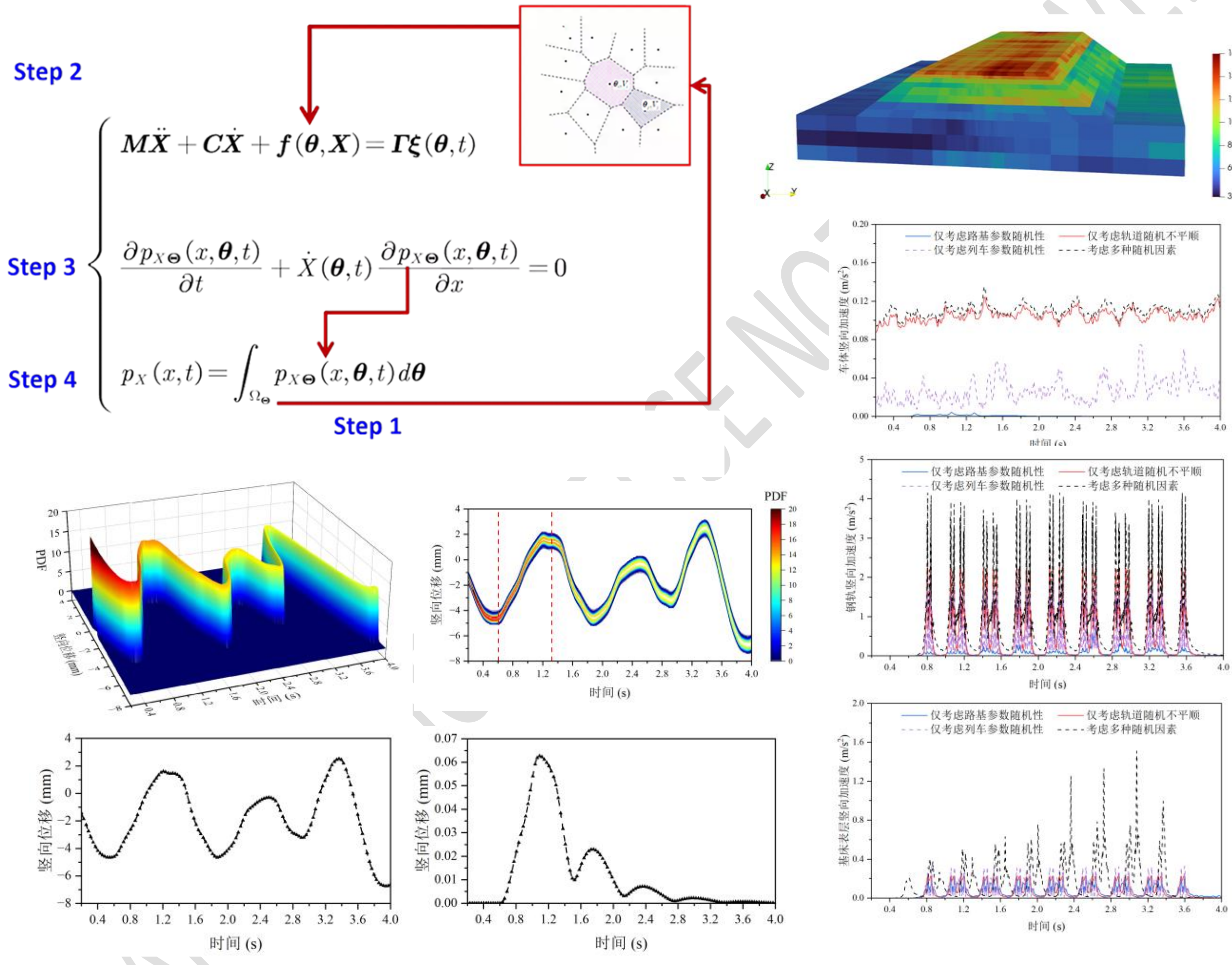

***Figure 1**: Solution process of probability density distribution of dynamic response.*

4 Conclusions

This study established a three-dimensional coupled dynamics framework for the high-speed train-ballasted track-subgrade system, integrating finite element modeling, elastoplastic constitutive theory, and multibody dynamics. By further incorporating random field characterization and probability density evolution theory, the stochastic nature of system responses under operational excitations was captured in a computationally efficient manner.

The findings demonstrate that operational speed, vehicle-track interaction, and subgrade spatial variability jointly govern the dynamic performance of the coupled system. Quantitative analyses confirm that variations in soil stiffness and random wheel-rail excitations substantially amplify response fluctuations, and that the statistical distributions of subgrade vibrations tend to approximate Gaussian forms. These results not only enrich the understanding of vibration transmission mechanisms in ballasted tracks but also provide a probabilistic framework for assessing railway infrastructure reliability.

Nevertheless, the current framework simplifies the granular behavior of ballast and neglects certain degradation processes occurring under long-term loading. Future research should incorporate discrete element modeling of ballast aggregates and investigate multi-scale coupling effects, with the aim of further enhancing the fidelity of train-track-subgrade simulations and supporting the development of more resilient high-speed railway systems.

5 References

Xiao Y, Zhou S, Chang Z, et al. 2023. Analysis of influence of differential subgrade settlement on dynamic responses of the three-dimensional train-ballasted track-subgrade coupled system. Journal of Central South University (Science and Technology), 54(12), pp. 4763–4776. (in Chinese)

Xiao Y, Chang Z, Mao J, et al. 2022. Evaluating the effect of rail fastener failure on dynamic responses of train-ballasted track-subgrade coupling system for smart track condition assessment. Materials, 15(7), p. 2675.

Mao J, Xiao Y, Yu Z, et al. 2021. Probabilistic model and analysis of coupled train-ballasted track-subgrade system with uncertain structural parameters. Journal of Central South University, 28(7), pp. 2238–2256.

Zhai W, Xia H, Cai C, et al. 2013. High-speed train–track–bridge dynamic interactions – Part I: theoretical model and numerical simulation. International Journal of Rail Transportation, 1(1-2), pp. 3–24.

Xu P, Cai C. 2011. Spatial dynamic model of train-ballast track-subgrade coupled system. Engineering Mechanics, 28(3), pp. 191–197. (in Chinese)

Zhai W, Stichel S, Ling L. 2025. Train–track coupled dynamics problems in heavy-haul rail transportation. Vehicle System Dynamics, pp. 1–54.

Chen Jianbing, Li Jie. 2011. Stochastic harmonic function and spectral representations. Chinese Journal of Theoretical and Applied Mechanics, 43(3), pp. 505–513. (in Chinese)

Rocha J M, Henriques A A, Calçada R. 2014. Probabilistic safety assessment of a short span high-speed railway bridge. Engineering Structures, 71, pp. 99–111.

Monitoring of railway structures with bituminous and granular sublayers: assessment after eight years of use

Johann Priou
Juliette Blanc
Université Gustave Eiffel, MAST-LAMES, France
Suzy Maddah
Eiffage Energie Systèmes, France
Thomas Attia
Eiffage Route, France
Amine Dhemaied
SNCF Réseau, France
Hélène Maugueret
SETEC, France, France
Juliette Deslavières
IRT Railenium, France

Abstract

Maintenance operations, such as tamping, and ballast wear due to dynamic loads result in frequent and costly maintenance. To mitigate these effects, the Bretagne-Pays de la Loire High-Speed Line (BPL HSL) has an innovative track structure that combines an asphalt concrete layer under the ballast. The track is designed to reduce the amplitude of the accelerations produced by passing high-speed trains (HST), which are the main cause of evolution of the track geometry parameters and therefore degradation of the sub-ballast layers. The BPL HSL includes 105 km of asphalt concrete layer under the ballast and 77 km of granular sub-base. In order to study the dynamic response of these different structures, some track sections have been instrumented with anchored deflectometers, accelerometers, strain gauges and temperature probes. The aim of this paper is to present the results obtained with the accelerometers after eight years of commercial traffic. The vertical acceleration peaks at the top of the sub-base are compared between the granular and bituminous track structures and show that there is no major evolution of the measurements during the eight years of monitoring. The study clearly shows that the presence of the asphalt layer in the structure reduces the accelerations under the ballast that cause its deterioration.

Keywords: high speed line; bituminous sublayer; granular sublayer; monitoring

1 Introduction

Ballast deterioration, under dynamic loads, remains an important issue on high-speed tracks that can lead to high maintenance costs. Several studies have shown that these settlements are related to the high accelerations produced in the ballast by high-speed trains. The use of asphalt sublayers under the ballast has been identified as a possible solution for improving track structures. By interposing a semi-rigid layer of asphalt concrete (GB) between the ballast and the Unbound Granular Material (UGM) layer, the behavior of the overall structure is greatly improved (Rose and Souleyrette, 2015).

The high-speed line (HSL) Bretagne-Pays de la Loire (BPL) (between Rennes and Le Mans, in the western France) is the first large-scale application of the asphalt concrete sublayer technique in France, with varying subgrade conditions, and using higher performance asphalt materials. The line has officially initiated its operations in July 2017 with trains travelling at a speed of 320 km/h.

The BPL HSL combines several platform compositions: 77 km of conventional track with a granular ballast sublayer and 105 km of bituminous underlayment. In order to study the dynamic response of these different structures, some track sections have been instrumented with anchored deflectometers, accelerometers, strain gauges and temperature probes. In this article, only the vertical acceleration measurements will be presented. Other results can be seen in (Khairallah et al., 2019; Khairallah et al., 2020 and Blanc et al., 2022). The objective of this study is to present the results after eight years of commercial traffic.

2 Structure and instrumentation

The innovative track structure consists of a 15 cm thick UGM adjustment layer reinforced by a 12 cm thick asphalt layer named GB4 (Grave Bitume in French). The standard track structure consists of a 35 cm thick treated soil reinforced by a 20-cm thick UGM capping layer. Both structures rest on a subgrade layer treated with lime and hydraulic binders. The different structures are shown in Figure 1. It is important to specify that the support layer of the bituminous structure is a soil treated with lime and hydraulic binders, with a minimum bearing capacity objective of 80 MPa. The treatment was very effective and the bearing capacity (EV2) on this layer was found to be higher than 250 MPa in most of the linear section (maximum level measurable by the dynamic device). This is also the case for the treated layer under the UGM in the area with a conventional structure. The soil beneath the earthwork treated layer is composed mainly of clay for Section 2 (granular sublayer) and for Section 4 (bituminous sublayer). Sections 2 and 4 are built on embankments.

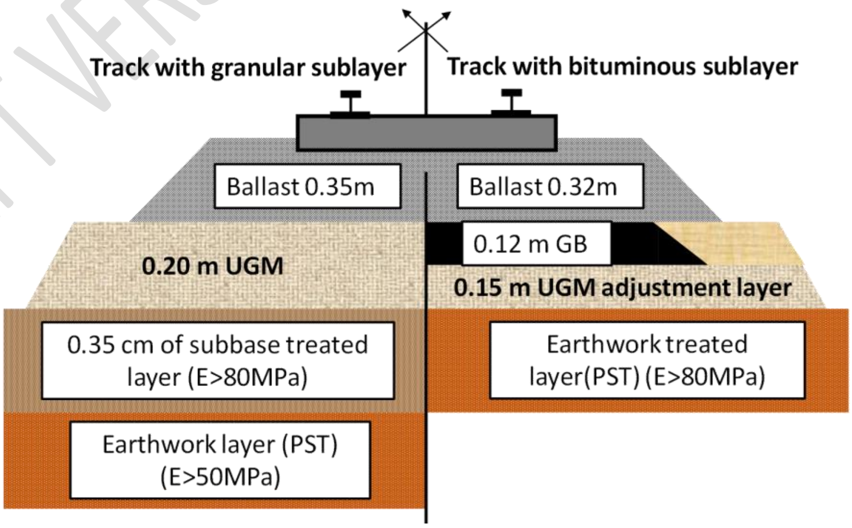

Figure 1: *The two experimental structures of the BPL high-speed line (adapted from Khairallah et al., 2019)***.**

The HSL track instrumentation is described in detail in (Khairallah et al., 2017) and in (Khairallah et al., 2019). Figure 2 presents the layout of the instrumentation for accelerometers and displacement sensors, for the two instrumented sections. Accelerometers (reference 2210-005 of Silicon Design brand) recorded the track's vertical dynamic behavior, with measurements at several levels: under the sleepers, at the top of the asphalt concrete layers and at the top of the granular layer. Measurements are recorded under each passage of trains. The signal acquisition frequency is 2000 Hz.

The train speed is first calculated, by calculating the time difference between signals of two accelerometers placed at different longitudinal positions, at the top of the sub-ballast layer. Then, low-pass filtering of the measurements, function of train speed, are performed to eliminate dynamic effects. The adjusted filter allows to extract the peaks of all sensor signals. Once signals are filtered, the number of bogies can be determined. 4 types of high-speed trains have been identified: simple trains with 13 and 15 bogies, and double trains with 26 and 30 bogies. For accelerometer signals, a positive and a negative peak (corresponding to upward and downward accelerations respectively) are determined. Only the measurement under trains with 13 bogies are presented here.

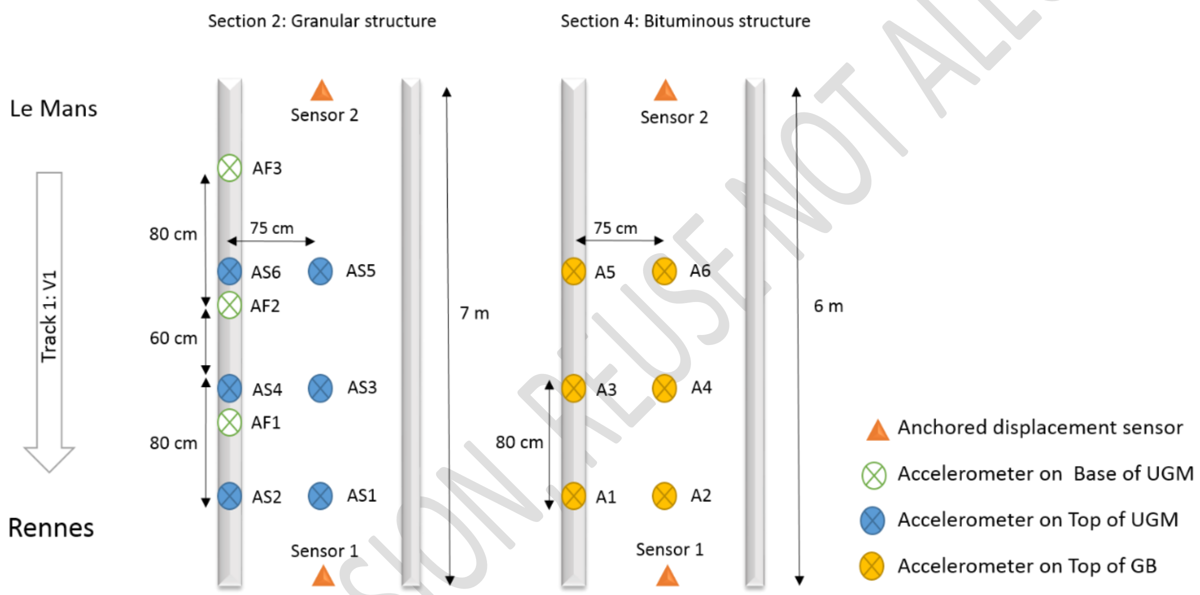

Figure 2: *Instrumentation of sections 2 (granular structure) and 4 (bituminous structure).*

3 Results

Accelerometers measurements obtained on section 2 with granular sub-layer and on section 4 with bituminous sub-layer, during the commercial phase are compared. Figure 3 shows a comparison of the minimum and maximum accelerations for accelerometers installed below the rail axis at the top of the sub-layer: AS2, AS4 and AS6 on section 2 with granular sub-layer and A1, A3 and A5 on section 4 with a bituminous sublayer. The results clearly show that acceleration peaks at the top of the GB4 sublayer are much lower than those measured at the top of the granular sublayer, both for upward and downward accelerations. It can be concluded that, during the commercial phase, even after eight years of commercial traffic, the presence of the GB layer reduces by a factor of about 2 the accelerations measured under the ballast.

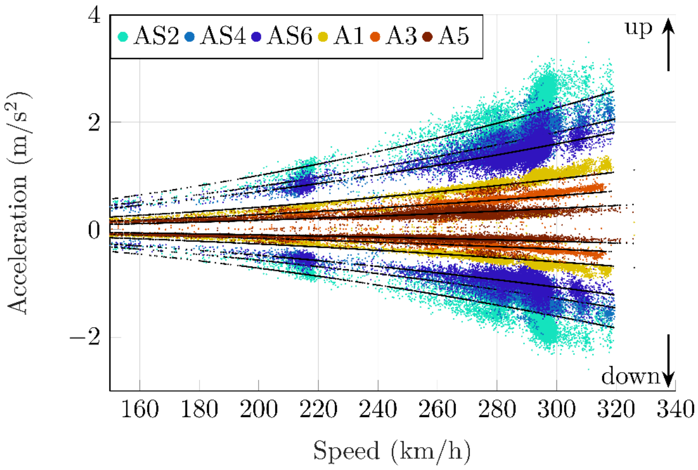

Figure 3: *Comparison of positive and negative vertical accelerations peaks measured by accelerometer AS2, AS4 and AS6 on section 2 with granular sub-layer and accelerometer A1, A3 and A5 on section 4 with bituminous sub-layer, during 8 years of commercial traffic.*

4 Conclusions

The BPL HSL consists of two different structures, with granular and bituminous sublayers. It was instrumented with more than 100 sensors during its construction, to monitor the response of the two types of structures. This paper treats data collected during the first 8 years of commercial traffic. The analysis of this phase therefore required the processing of a large number of measurement files. Only a small part of this data is presented in this paper, focusing on the evolution of maximum and minimum accelerations over the duration of the observation period.

The analysis of accelerations measured at the top of the sub-layers indicates significant reduction of accelerations on the bituminous sections, in comparison with the UGM section, by a factor of about 2.

5 Acknowledgments

The authors would like to thank all those who contributed to this project: Railenium, Eiffage, SNCF Réseau and Setec.

This research has received funding from the French Government under the France 2030 – CORIFER research and innovation program, in the framework on the MINERVE R&D project.

6 References

Blanc J., Khairallah D., Ramirez D., Chupin O., Pouget S., Ta Q.-A., Duval A., Hornych P., Benoist S., 2022. Monitoring of railway structures with bituminous and granular sub-layers: Assessment after four years of use, Construction and Building Materials, Vol 336, https://doi.org/10.1016/j.conbuildmat.2022.127515.

Khairallah, D., Blanc, J., Cottineau L.M., Hornych P., Piau J.-M., Pouget S., Hosseingholian M., Ducreau A., Savin F., 2019. Monitoring of railway structures of the high-speed line BPL with bituminous and granular sublayers. Construction and Building Materials 211, p337–348. doi.org/10.1016/j.conbuildmat.2019.03.084.

Khairallah D., Blanc J., Hornych P., Piau J.M., Cottineau L.M., Pouget S., Ducreau A., Savin F., Hossengholian M., 2020. Influence of the bituminous layer on temperature and water infiltration in railway structures of the BPL High Speed Line, Journal of Testing and Evaluation, 48(1), doi:10.1520/JTE20180894.

Rose J.G., Souleyrette R., 2015. Asphalt Railway Trackbeds: Recent Designs, Applications and Performances. AREMA. Proceedings of the 2015 AREMA Annual Conference. Minneapolis, MN.

Risk assessment rockfall events

Roberto Luis-Fonseca
Helene Lanter
Geobrugg AG
Carles Raïmat-Quintana
Geobrugg Iberica, SA
Tomaž Cej
Rejda Environmental Solutions

Abstract

Rockfall events represent a significant hazard to linear infrastructure, particularly in mountainous regions where unstable slopes pose risks to road users and assets. Accurate and efficient assessment methods are essential to prioritize mitigation measures and ensure safety. This work presents a simplified and updated procedure for evaluating rockfall hazards, derived from modifications to the traditional Rockfall Hazard Rating System (RHRS). The proposed method builds on earlier developments and incorporates refinements introduced in 2010 aimed at improving applicability, reproducibility, and usability in real-world engineering contexts. The improved framework evaluates key parameters related to slope instability, geomorphological conditions, and potential rockfall magnitudes. It integrates qualitative and quantitative indicators, enabling practitioners to classify hazardous road sections rapidly and consistently. By applying a scoring-based structure like RHRS, the method establishes clear priorities for intervention while maintaining simplicity for field use. Case studies demonstrate that this modified system effectively identifies high-risk areas that require urgent mitigation and provides a rational basis for allocating resources. Its adaptability makes it suitable for diverse geological environments and for multi-disciplinary teams working in road safety management, engineering geology, and environmental risk assessment. Overall, the method enhances decision-making in rockfall management and offers a practical tool for improving safety along roads and other linear projects exposed to slope instabilities.

Keywords: rockfall; risk assessment; rockfall hazard rating system; linear infrastructure projects

1 Introduction

The communication pathways (roads, railways and channels) of communication come affected by the dangerousness associated with the orography and the geology of the territory through which it runs, due to natural hazards (Varnes et al., 1984). Exposure to these risks is high on local roads that provide access to towns, or isolated mountainous areas or those with occasionally high IMDs, and that connect them to the networks. Regional or national roads with the highest vehicle traffic and with more populated urban centres that concentrate most services. Natural hazards affecting local roads, usually with narrow roadways and poor shoulders and gutters, can be classify into different types: rock blocks falling (from adjacent slopes, excavated embankments or tunnel entrances), instability of excavated embankments on slopes to create the route, impact on the road due to debris slides from the ravines that cross them, and locally and in dimensions high, avalanches that affect to the hillside path, roads and railways (Luis Fonseca, 2008). The current paper describes a simple method that constitutes an adjustment (Luis Fonseca, 2010) of the method RHRS (Rockfall Hazard Rating System; Pierson et al., 1990; Abbott and Bruce, 1998; Hoek, 2007) for potential dangers in sections of roads and establishes priority in actions.

2 ID of the danger's potential

The ID of the danger's potential shape performance using Rock Mechanics techniques. In many cases, the presence of unstable blocks at the top of slopes or high areas of the hillside makes the danger obvious. However, what is usually more dangerous is the occurrence of rockfalls (Figure 1) on slopes or hillsides whose faces are healthy. This usually occurs when forces that act in the planes of discontinuity or networks of joints, isolate a block from their neighbours. This is due to changes in water pressure at the joints or the reduction of the friction force between the planes due to the action of water. This phenomenon can cause detachment of blocks of significant size and, in extreme cases, loss of stability of large surfaces.

***Figure 1**: Block in the rebound and impact phases.*

In any case, it should not be assumed that it is safe, simply inspecting the face of the rock massifs, which are in good visual condition, looks to be free from the rockfall danger.

3 Criteria and method of assessment of risks

Risk assessment in the case of linear projects such as roads and railways undoubtedly constitutes a significant challenge for the engineers and geologists responsible for this work. It is evident that the amplitude of this kind of work is difficult to obtain enough information to conduct stability assessments of all slopes and hillsides along the route (Figure 2). This means that, except for those sections identified as particularly critical, most of the road slopes must be designed based on a rudimentary geotechnical analysis.

***Figure 1**: Rockfall in lineal project.*

This analysis aims at attempting to guarantee the overall stability of the slope against rockfalls, losses of stability, and either rockfalls that by importance could affect the operation of roads or railways. Except in densely populated areas in advanced countries, it is rare to find a detailed analysis of landslide hazards. Due to this major inconvenience and the economic importance of making some kind of forecast or classification, the use of a visual inspection method is proposed. The main objective is to identify which slopes or hillsides are at particular risk and what work needs to be done most urgently to efficiently correct or reduce these potential hazards. As already noted, the method described and proposed for use constitutes a systematization of the RHRS (Rockfall Hazard Rating System) method. After studying several proposals whose worth is cash to level international, the propose uses the following system evaluation of risks, which establishes categories in function of the assign values to each of the parameters to be inventoried: slope height; effectiveness of the interception ditch; presence of vehicles in the area; visibility distance; roadway width; geological characteristics; size of the block or volume of rockfall material; climatic conditions; presence of water and rockfall history. The assessment quantitative of these parameters could be summarize as follows:

4 Analysis of the rockfall risk on roads

The analysis of the risk of rockfalls on roads and their respective consequences, both material and human losses, has never had very extensive coverage in geotechnical literature. In general, the reports only refer to the probability of the phenomenon occurring and the damage it may cause. For contribute in rational way to analysis of the odds of risk potential and using as based the stated in the previous sections, it is proposed to carry out an evaluation based on the rational combination of the parameters indicated and obtain for the specific sections and for subsections in particular priority levels of action or, in other words, levels of danger. The modified RHRS (Rockfall Hazard Rating System; Pierson et al., 1990; Abbott and Bruce, 1998) method consists of applying additional weight (importance) to certain factors that are of greater influence and that allow, based on an analogous data collection process, to define hazard levels and establish action priorities. These additional weights are the result of the methodology application, during several years (Luis Fonseca, 2010).

5 Conclusions

The presented rockfall-risk assessment method is a straightforward quantitative instrument designed solely to assist in setting priorities and developing a rational, systematic strategy for action. These are very crude tools which can only be regarded as semi-quantitative, however combined with the evaluator's obvious common sense, allows for more solid criteria when considering corrective protection or stabilization measures and allocating a budget to implement them. In recent years, innovative photogrammetry and probabilistic approach techniques have allowed for the quasi-automatic and simple evaluation of geotechnical parameters of cuts and slopes, making fieldwork more efficient and precise. In any case, assigning weight or importance to these parameters adds objectivity to the evaluation, since not all parameters influence risk in the same way.

Table 1: *Recommended weight parameters.*

Weight	Parameter		Points	Range
2	slope height, SH [m]		5 - 80	7.5 – 30.0
1	ditch effectiveness, DE		5 - 80	good - no present
1	average vehicle, AV [%]		5 - 80	25 -100
2	visibility distance, VD [%]		5 - 80	100 - 40
1	roadway width, RW [m]		5 - 80	14 - 6
3	geological conditions, GC			
	case 1	structural	5 - 80	discontinuous, favorable – continuous unfavorable
		rock friction	5 - 80	rough - stuffed
	case 2	structural	5 - 80	slight erosion - severe erosion
		differential erosion	5 - 80	small - extreme
2	block size, BS [m]		5 - 80	0.3 - 1.2
	volume of material, BS [m3]		5 - 80	23.0 – 9.0
2	climate condition and water (rain), CC		5 - 80	low - high
1	rockfall history, RH		5 - 80	few - constant

$$\frac{2 \cdot SH + DE + AV + 2 \cdot VD + RW + 3 \cdot GC + 2 \cdot BS + 2 \cdot CC + RH}{15} = \boldsymbol{Index}\ [\%]$$

6 References

Abbott, B. & Bruce, I. 1998. A methodology for the assessment of rockfall hazard and risk along linear transportation corridors. Proceedings. 8th Congress of the International Association for Engineering Geology and the Environment.

Hoek, E. 2007. Toronto. Analysis of rockfall hazard. Rocscience.

Luis-Fonseca, R. 2008. Barcelona. Gestión sostenible de los riesgos naturales que afectan a las vías locales. Proceedings. Congress of Mobility and Territory.

Luis-Fonseca, R. 2010. Madrid. Aplicación de membranas flexibles para la prevención de riesgos naturales. Ropero.

Pierson, L. A., Davis, S. A. & Van Vickle, R. 1990. The Rockfall Hazard Rating System: Implementation manual. US Department of Transportation.

Varnes, D. J. 1984. Paris. Landslide hazard zonation: A review of principles and practice. Natural Hazards 3. UNESCO.

Investigation on fracture and healing mechanism of cement-treated recycled aggregate materials via Peridynamics

Yuanjie Xiao
School of Civil Engineering, Central South University, Changsha 410075, China
Ministry of Education Key Laboratory of Engineering Structures of Heavy Haul Railway, Central South University, Changsha 410075, China
Jiahui Zhou
School of Civil Engineering, Central South University, Changsha 410075, China
Ke Hou
Railway Engineering Research Institute, China Academy of Railway Science Corporation Limited, Beijing, 100081, China
Wenjun Hua
Department of Civil and Architectural Engineering, KTH Royal Institute of Technology, Stockholm 10044, Sweden

Abstract

Cement-treated recycled aggregate material (CRAM), derived from construction and demolition waste, is highly susceptible to cracking during service, which significantly undermines the integrity and stability of pavement structural layers. Microbially induced calcite precipitation (MICP) has emerged as a promising technique to enhance the durability of permeable CRAM. However, its effectiveness remains insufficiently validated. This study proposes a novel crack-healing characterization method based on Peridynamics (PD) to evaluate the mechanical recovery induced by MICP. Cement mortar treated with MICP was used as the model material, and numerical simulations were performed to evaluate the flexural strength of cement mortar incorporating crack-healing behavior, as well as the flexural strength of CRAM utilizing the same type of MICP-treated mortar. The results show that the proposed PD approach accurately captures the recovery of mechanical performance due to crack healing. While MICP treatment significantly restores the flexural strength of cement mortar, its effect on the flexural strength of permeable CRAM is limited. Moreover, reduced cement content markedly diminishes the healing efficiency; when the matrix filling ratio falls below 0.76, strength recovery becomes negligible even after 28 days of curing. Extending the healing-related curing time effectively enhances tensile strength recovery while mitigating crack branching. A minimum of 7 days of healing is recommended to ensure meaningful mechanical restoration through MICP.

Keywords: pavement engineering; crack propagation and healing; peridynamics; cement-treated recycled aggregate materials; microbially induced calcite precipitation

1 Introduction

The rising volume of construction and demolition waste has increased the demand for sustainable materials in transportation infrastructure. Cement-treated recycled aggregate material (CRAM) is a promising option for high-speed railway and urban road projects, but it is prone to cracking and rapid crack propagation, which accelerates structural deterioration and reduces durability (Achal et al.,2015, Hou et al., 2024). Effective healing strategies are therefore needed. Autogenous healing from unhydrated cement particles provides only limited recovery (Reinhardt et al., 2003). Alternative methods, such as fibre reinforcement (Larsen et al., 2020, Yu et al., 2021), encapsulated agents (Huang et al., 2021), and shape memory alloys (Konlan et al., 2022), improve crack resistance but face issues of compatibility, applicability, and replenishment (Jefferson et al., 2018). Microbially induced calcium carbonate precipitation (MICP) offers a sustainable alternative. Through urease-driven urea hydrolysis and Ca^{2+} adsorption on negatively charged cell surfaces, microbes induce $CaCO_3$ precipitation that fills cracks and restores mechanical integrity (Ma et al., 2020). Experimental studies confirm its effectiveness, focusing on microbial strains, nutrient conditions, and post-repair performance (Justo-reinoso et al., 2021). However, experiments capture only macroscopic behaviour and cannot reveal the coupled multiscale mechanisms. Modeling efforts have attempted to address this. Micro- and meso-scale approaches (Nguyen et al., 2018, Kunhi et al., 2022), including individual-based models (Jayathilake et al., 2018), simulate microbial dynamics but cannot predict macroscale recovery. At the structural level, BCH and BCHM models describe solute transport, permeability, and stress-strain evolution (Mehrabi et al., 2022, Wang et al., 2022), yet they neglect mineral product degradation. Discrete element methods (DEM) provide insights into fracture processes (Sun et al., 2022, Wu et al., 2023), but assumptions about pore structure limit their use in CRAM. This study proposes a peridynamics-based macroscale model for MICP healing in CRAM. A healing reset algorithm and κ - δ r parameter system are introduced to capture strength recovery and clarify the effects of matrix filling ratio and curing time. The framework overcomes limitations of existing models and offers theoretical guidance for repair design, supporting the sustainable use of recycled materials in infrastructure.

2 Method

This study establishes a peridynamics-based computational framework to evaluate the crack-healing performance of cement-treated recycled aggregate materials (CRAM) via microbially induced calcite precipitation (MICP). The PD model incorporates a novel crack-healing characterization method, where healing behavior is represented through the introduction of healing bonds within a defined healing horizon. The material system consists of cement mortar and CRAM, with the latter modelled as a meso-heterogeneous composite comprising cement matrix, natural aggregate, recycled mortar, and recycled brick, each with distinct material properties. Interface transition zones (ITZs) are explicitly modelled using an exponential softening law to capture nonlinear damage behaviour. The healing process is triggered upon reaching a pre-damage threshold, after which broken bonds within the healing radius are partially restored based on a healing recovery coefficient κ. Model parameters are calibrated against experimental flexural strength tests of cement mortar under varying healing durations (0-28 days). The framework enables simulation of crack initiation, propagation, and healing under mechanical loading, providing insights into the recovery of mechanical properties and the influence of matrix filling ratio and curing time on healing efficiency. The calculation process of peridynamics considering crack-healing behaviour is shown in Figure 1.

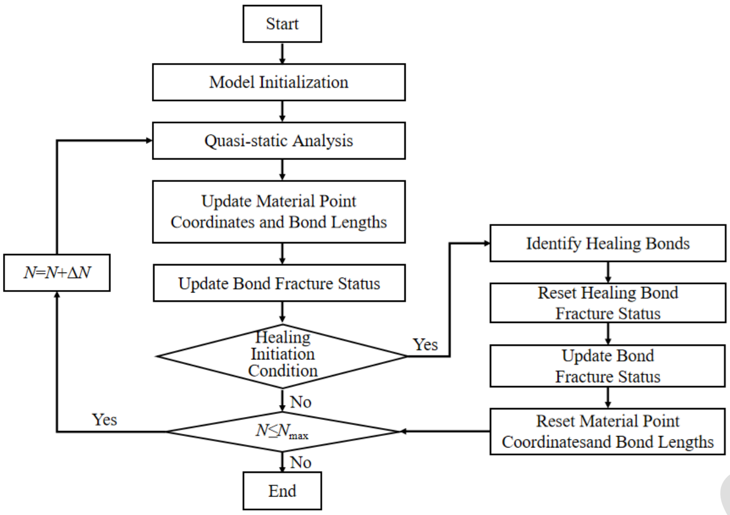

***Figure 1**: Computational Flowchart of Peridynamics Incorporating Self-healing Behavior.*

3 Conclusions

This study proposes a peridynamics-based framework to systematically evaluate the crack-healing performance of microbially induced calcite precipitation in permeable cement-treated recycled aggregate materials. The numerical model effectively reproduces the flexural response and damage evolution of CRAM, with the structural configuration and loading scheme clearly illustrated in Fig. 2, providing a reliable basis for simulating crack initiation, propagation, and healing processes. The pre-damage characteristics are strongly influenced by the matrix filling ratio, as shown in Fig. 3, where damage is primarily concentrated in the tensile zone and serves as the dominant factor controlling subsequent crack evolution. Quantitative analysis in Table 1 demonstrates that the flexural strength recovery ratio decreases markedly with decreasing matrix filling ratio, and becomes negligible when the ratio falls below 0.76 even under prolonged curing conditions, indicating a critical threshold for effective MICP-based healing. Furthermore, the post-healing damage evolution reveals that cracks tend to reinitiate from partially healed regions due to residual defects, followed by propagation and branching under loading, as illustrated in Fig. 4, highlighting the limited ability of MICP to fully restore structural integrity. The final damage patterns shown in Fig. 5 further confirm that increasing curing time promotes more localized crack propagation and reduces crack branching, whereas insufficient curing leads to more dispersed and complex fracture networks. Overall, while MICP exhibits certain healing potential, its effectiveness in permeable CRAM is significantly constrained by material heterogeneity and pore structure, emphasizing the necessity of adequate matrix filling ratio and curing duration to achieve meaningful mechanical recovery and providing important guidance for the design and application of self-healing recycled materials in pavement engineering.

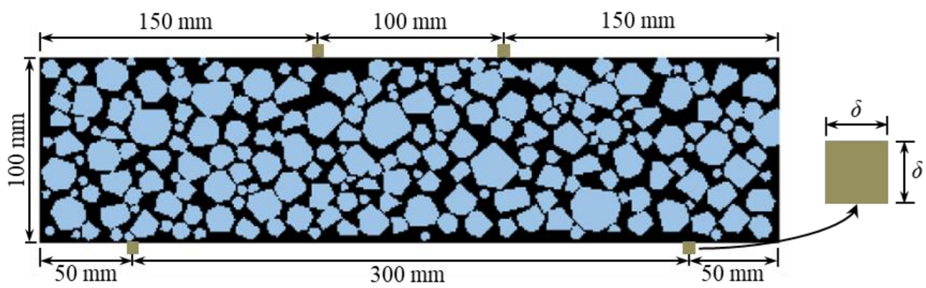

***Figure 2**: Schematic Diagram of the CRAM Flexural Strength Test Model.*

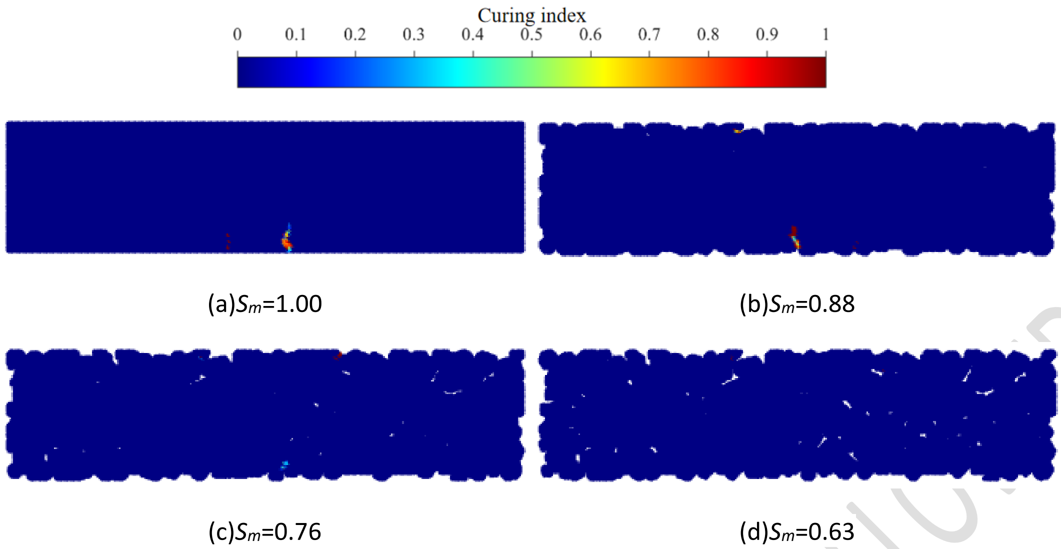

***Figure 3**: Healing Distribution Patterns under Different Matrix Filling Ratio.*

***Table 1**: Simulation Results and FLC under Different Matrix Filling Ratios.*

S_m	$R_{s,RS}$ /MPa	$R_{s,R0}$/MPa	$R_{s,R28}$/MPa	FLC/%
1.00	1.98	1.90	1.94	43.0
0.88	1.77	1.30	1.40	21.3
0.76	1.37	1.19	1.20	5.1
0.63	1.16	1.01	0.99	-6.0

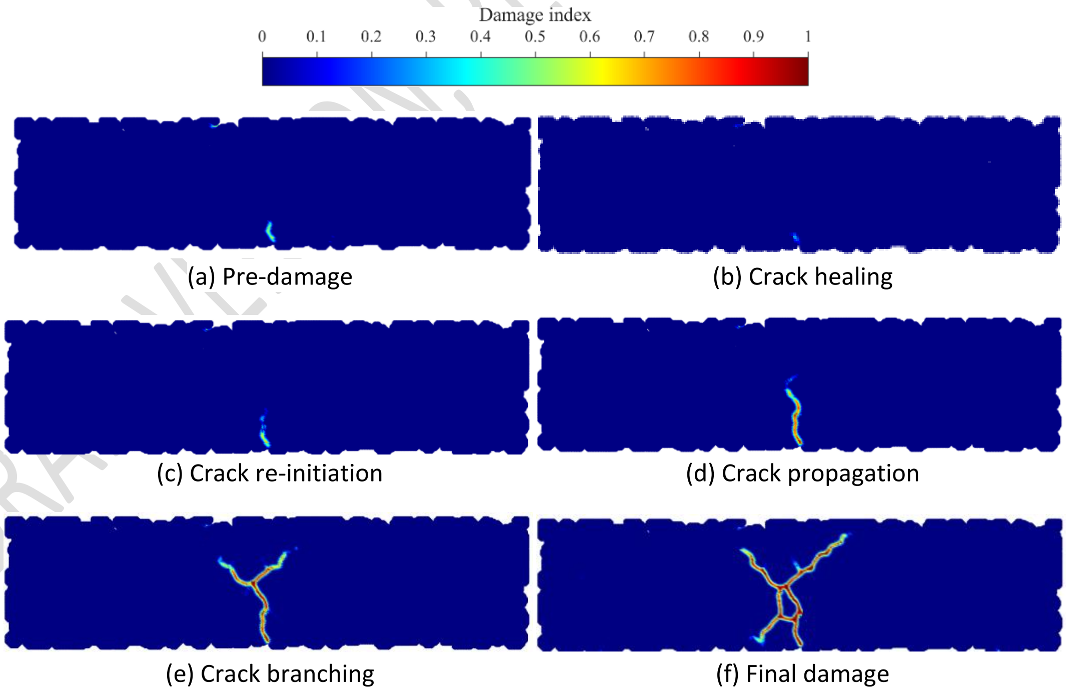

***Figure 4**: Damage Evolution Process at 28d Curing.*

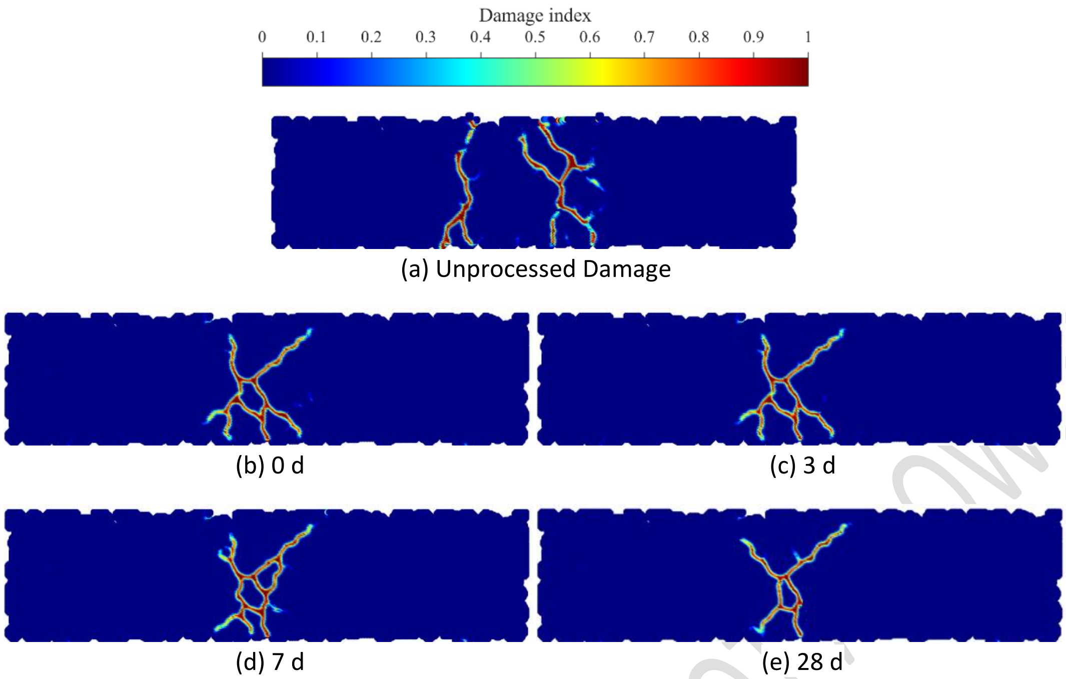

Figure 5*: Final Damage Distribution patterns under Different Curing Durations.*

4 References

Achal, V., Mukherjee, A., 2015. A review of microbial precipitation for sustainable construction. Construction and Building Materials 93, 1224–1235.

Hou, K., Hua, W. J., Xiao, Y. J., et al., 2024. Insights into the failure mechanisms of cement-treated recycled aggregate materials (CRAMs) under uniaxial compression via peridynamics. Construction and Building Materials 451, 138726.

Reinhardt, H. W., Jooss, M., 2003. Permeability and self-healing of cracked concrete as a function of temperature and crack width. Cement and Concrete Research 33 (7), 981–985.

Larsen, I. L., Thorstensen, R. T., 2020. The influence of steel fibres on compressive and tensile strength of ultra high performance concrete: A review. Construction and Building Materials 256, 119459.

Yu, K., Zhu, H., Hou, M., et al., 2021. Self-healing of PE-fiber reinforced lightweight high-strength engineered cementitious composite. Cement and Concrete Composites 123, 104209.

Huang, Y., Wang, X., Sheng, M., et al., 2021. Dynamic behavior of microcapsule-based self-healing concrete subjected to impact loading. Construction and Building Materials 301, 124322.

Konlan, J., Mensah, P., Ibekwe, S., et al., 2022. SMA z-pinned composite laminate with delamination healing capability. Encyclopedia of Materials: Plastics and Polymers 1–4, 395–415.

Jefferson, T., Javierre, E., Freeman, B., et al., 2018. Research progress on numerical models for self-healing cementitious materials. Advanced Materials Interfaces 5 (17), 1701378.

Ma, L., Pang, A. P., Luo, Y., et al., 2020. Beneficial factors for biomineralization by ureolytic bacterium Sporosarcina pasteurii. Microbial Cell Factories 19 (1), 12.

Justo-Reinoso, I., Heath, A., Gebhard, S., et al., 2021. Aerobic non-ureolytic bacteria-based self-healing cementitious composites: A comprehensive review. Journal of Building Engineering 42, 102834.

Nguyen, M. T., Wang, Z., Rod, K. A., et al., 2018. Atomic origins of the self-healing function in cement–polymer composites. ACS Applied Materials & Interfaces 10 (3), 3011–3019.

Kunhi Mohamed, A., Weckwerth, S. A., Mishra, R. K., et al., 2022. Molecular modeling of chemical admixtures: opportunities and challenges. Cement and Concrete Research 156, 106783.

Jayathilake, P. G., Gupta, P., Li, B., et al., 2017. A mechanistic individual-based model of microbial communities. PLOS ONE 12 (8), e0181965.

Mehrabi, R., Atefi-Monfared, K., 2022. A coupled bio-chemo-hydro-mechanical model for bio-cementation in porous media. Canadian Geotechnical Journal 59 (7), 1266–1280.

Wang, X., Nackenhorst, U., 2022. Micro-feature-motivated numerical analysis of the coupled bio-chemo-hydro-mechanical behaviour in MICP. Acta Geotechnica 17 (10), 4537–4553.

Sun, M., Cao, J., Cao, J., et al., 2022. Discrete element modeling of shear wave propagation in carbonate precipitate–cemented particles. Acta Geotechnica 17 (7), 2633–2649.

Wu, H., Wu, W., Liang, W., et al., 2023. 3D DEM modeling of biocemented sand with fines as cementing agents. International Journal for Numerical and Analytical Methods in Geomechanics 47 (2), 212–240.

Green Mixtures for Backfilling Trenches beneath Trafficable Areas: Bridging Laboratory Innovation and Real-World Application

Ehsan Yaghoubi
Zahra Kamali
Victoria University, Melbourne, Australia
Malindu Sandanayake
RMIT University, Melbourne, Australia
Ernie Gmehling
Ground Science Pty Ltd, Melbourne, Australia
Graham Holt
Greater Western Water, Melbourne, Australia

Abstract

This study presents the mix design, construction, and performance evaluation of green mixtures composed entirely of recycled aggregates for backfilling excavated pipeline trenches located in trafficable areas. Extensive laboratory investigations on 36 recycled blends incorporating recycled glass, plastic, recycled tire, and recycled concrete aggregates were undertaken to assess compaction, bearing capacity, and resilient modulus, leading to the selection of two optimal mixtures: a cement-stabilized bound blend and an unbound blend enhanced with recycled concrete. These mixtures were used in a full-scale field trial beneath an asphalted roadway, constructed alongside a conventional crushed rock control section. Field monitoring over several months using high-precision surveying techniques indicated that both recycled sections experienced comparable permanent deformation and stiffness to the control. The results validate the field applicability of recycled green mixtures and their potential to serve as sustainable alternatives to natural aggregates in trafficable trench backfilling.

Keywords: recycled aggregates; green trench backfills; trafficable areas; field performance; permanent deformation monitoring

1 Introduction

The growing scarcity of natural aggregates and the increasing emphasis on sustainable construction have accelerated the search for environmentally friendly backfilling alternatives for buried infrastructure. Conventional crushed rock (CR), while reliable, contributes to resource depletion and greenhouse gas emissions. Previous laboratory research by Victoria University demonstrated that mixtures composed entirely of recycled aggregates, namely recycled glass (RG), recycled plastic (RP), recycled tire (RT), and recycled concrete aggregate (RCA), can achieve mechanical properties comparable to natural materials for backfilling pipeline excavated trenches when properly designed and compacted (Al-Taie et al., 2023; Yaghoubi et al., 2023). However, limited evidence exists regarding their field performance under traffic loading. To address this gap, a full-scale field trial was undertaken in September 2024 to evaluate two optimized green mixtures developed from an extensive laboratory program. The objective was to validate the constructability and structural performance of these materials for backfilling purposes.

2 Materials and Laboratory Program

Thirty-six candidate blends were initially examined through laboratory testing that included compaction to determine the maximum Dry Density (MDD), California Bearing Ratio (CBR), and repeated load triaxial (RLT) tests. The results confirmed that several recycled combinations satisfied the minimum performance thresholds for use as structural backfill. Two superior blends were selected for field construction (Table 1):

- Bound Mix: A cement-stabilized combination of RG, RP, and RT.
- Unbound Mix: A blend of RG, RP, RT, and RCA.

Both blends were designed within VicRoads Class 4 crushed rock (CL4) gradation limits (VicRoads, 2013). These blends achieved comparable resilient modulus (Mr) and CBR values to conventional materials.

Table 1*: compositions and properties of the mixtures/materials used in the field trial.*

Mixture	Cement (%)	RG	RP	RT	RCA	MDD (Mg/m³)	CBR (%)	Mr (MPa)	Remarks
Bound	✓	✓	✓	✓	✕	1.80	79 (>20)	89	Cement-stabilized
Unbound	✕	✓	✓	✓	✓	1.68	41 (>20)	54	RCA-enhanced
CL4	✕	✕	✕	✕	✕	2.20	126 (>20)	76	Current practice

3 Field Trial Construction

The field trial was carried out at Harker Street, Sunbury, Victoria, Australia, within a Greater Western Water facility. Three adjacent trenches, each approximately 5m long, 1.2m wide, and 1.8 m deep, were excavated beneath an asphalted access road with an annual average daily traffic of approximately 150 (mostly trucks):

- Trench 1 – Control: Backfilled with natural Class 2 over Class 4 crushed rock.
- Trench 2 – Bound: Backfilled with natural Class 2 over the cement-stabilized RG + RP + RT blend.
- Trench 3 – Unbound: Backfilled with natural Class 2 over the RG + RP + RT + RCA blend.

According to the Australian specification (MWRA, 2013) for trenches excavated to a depth of >1.5 m, the 600 mm backfill beneath pavement layers should be 20 mm Class 2 CR and the remaining depth should be backfilled with 20 mm Class 4 (CL4) CR. Backfilling was performed in 0.5 m layers using a vibratory plate compactor. In-situ density and modulus verification were undertaken after each layer compaction using a Light Weight Deflectometer and a Nuclear Density Gauge for quality control. This was to ensure that at least 98% of the MDD obtained through the modified compaction effort is achieved. A geotextile layer was placed above and below the recycled backfills as a separation layer to allow future retrieval of the backfill if needed. Finally, all trenches were backfilled with a 0.6 m Class 2 CR to reach the subgrade level, and the surface was reinstated using a 150 mm thick base course and a 50 mm thick asphalt surface course.

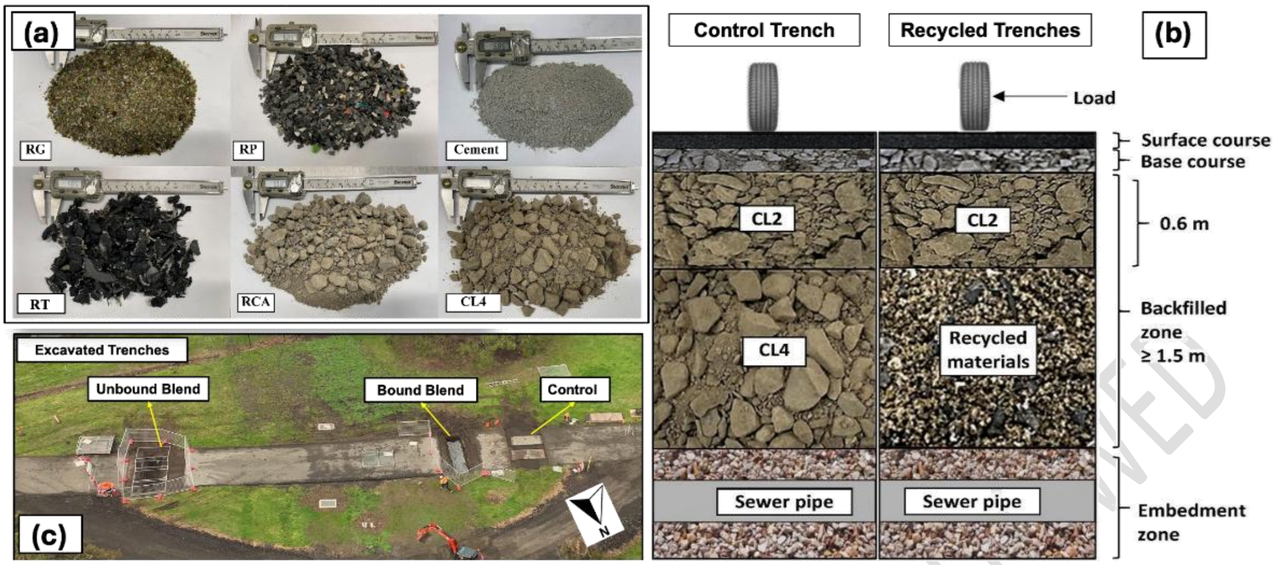

***Figure 1**: Images of (a) individual materials, (b) Cross-sectional layouts, and (c) bird view of the site with excavated trenches.*

4 Field Monitoring and Results

Monitoring of surface deformation was performed periodically over several months, between September 2024 and April 2025, using high-precision total-station surveying. Elevation points were established at fixed reference locations to capture differential settlement across all trench sections (Figure 2). The results, as presented in Figure 2, indicated that both recycled sections exhibited comparable settlement magnitudes to the Control trench and showed stable behavior over time. The Bound mix showed the smallest deformation, confirming that the inclusion of a small proportion of cement significantly improved stiffness and deformation resistance. These outcomes validate that recycled blends can be effectively compacted and maintain structural integrity comparable to crushed rock under real traffic conditions.

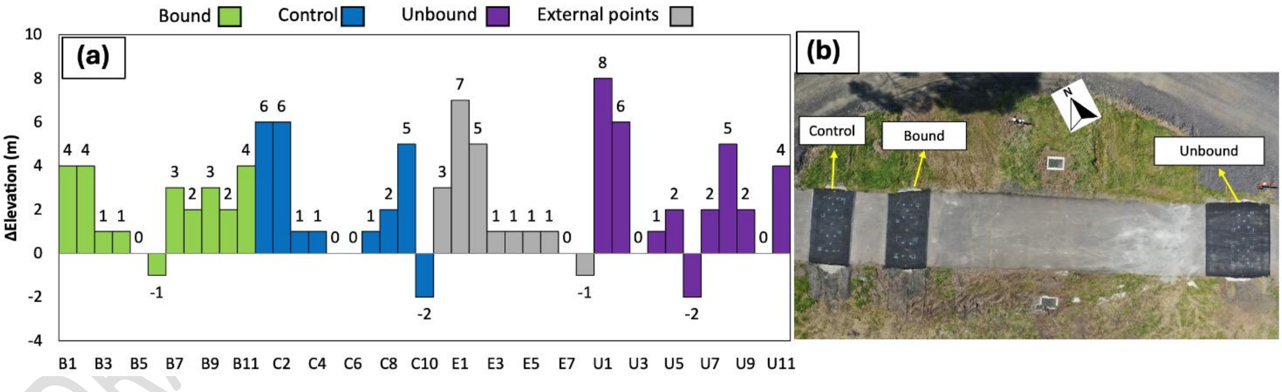

***Figure 2**: (a) Average permanent deformation of each trench section, and (b) reinstated surface with marked surveying points.*

To complement the current surveying program, future monitoring will include two advanced techniques:

- High-Precision Camera Imaging: A fixed high-resolution camera will be mounted on a custom-made frame to periodically capture images for crack detection, to quantify the propagation of cracks.
- Walking Profilometer Surveys: A portable surface profiler will be used to obtain detailed transverse elevation profiles to enable accurate quantification of rut depths along the wheel paths.

The future monitoring will continue for over two years to capture at least two wet and dry seasons.

5 Conclusions

This study demonstrated the successful application of 100% recycled aggregate blends in trafficable trench backfilling. Both the cement-stabilized and unbound mixtures achieved satisfactory compaction and strength characteristics in the laboratory and displayed stable deformation performance during field monitoring. Planned implementation of camera-based crack imaging and walking profilometer surveys will provide higher-resolution insights into surface integrity and deformation mechanisms. The results affirm that green recycled mixtures are viable, sustainable alternatives to natural aggregates for buried infrastructure beneath trafficable areas, supporting circular economy and long-term pavement resilience objectives.

6 References

Al-Taie, A., Yaghoubi, E., Gmehling, E., Fragomeni, S., Disfani, M. & Guerrieri, M. 2023. Recycled aggregate blends for backfilling deep trenches in trafficable areas. Construction and Building Materials, 401, 132942.

MRWA. 2013. Melbourne. Backfill Specification – Specification 04–03.2. Melbourne Water Retail Agencies.

VicRoads. 2013. Kew, VIC. Section 812: Crushed rock for pavement base and subbase. Australia.

Yaghoubi, E., Al-Taie, A., Disfani, M., Fragomeni, S., Guerrieri, M. & Gmehling, E. 2023. Cement and fly ash-treated recycled aggregate blends for backfilling trenches in trafficable areas. Transportation Geotechnics, 42, 101091.

Enhancing Railway Ballast Monitoring with GPR Attribute Analysis

Saeed Parnow
University of West London, UK
Luca Bianchini Ciampoli
Alessandro Calvi
Andrea Benedetto
Roma Tre University, Italy
Fabio Tosti
University of West London, UK

Abstract

Ground Penetrating Radar (GPR) is a well-established non-destructive technique for subsurface imaging. This study investigates the use of GPR attribute analysis, specifically the centroid frequency attribute, to monitor railway ballast condition, focusing on fragmentation and fouling as key indicators of track-bed health. GPR scans were conducted on a 30 m test-site railway section reproducing controlled ballast configurations ranging from clean to fouled, using 1 GHz and 2 GHz horn antennas under both dry and wet conditions. The centroid frequency attribute results were compared against conventional GPR processing. The attribute analysis revealed clear contrasts between clean and degraded ballast, offering higher sensitivity and improved interpretation of fouling and fragmentation than traditional methods. These findings support more targeted maintenance strategies and enhanced railway safety.

Keywords: ground penetrating radar; GPR; railway ballast; attribute analysis; centroid frequency; ballast fouling; non-destructive testing; track-bed monitoring

1 Introduction

Ground Penetrating Radar (GPR) is an established non-destructive technique for subsurface imaging applied in several fields. While GPR and attribute analysis have been effectively used for assessing internal anomalies in tree trunks, this study explores its potential application in railway infrastructure, specifically for railway ballast monitoring. We investigate the use of GPR and attribute-based imaging to evaluate ballast conditions, including fragmentation and fouling, which are critical indicators of the health of track-beds.

2 Experimental activity Introduction

The experimental campaign, conducted on a test-site railway section, involved GPR scans over controlled scenarios replicating several ballast conditions from healthy to highly polluted. Specifically, the test site was composed of a 30 m-long railway track with a thickness of 30 cm. The system was equipped with precompressed concrete sleepers equally spaced with a 60 cm interaxis distance. A detailed description of the test site is given in (Bianchini Ciampoli et al., 2019°). Plan view and cross-section of the test site are reported in Figure 1.

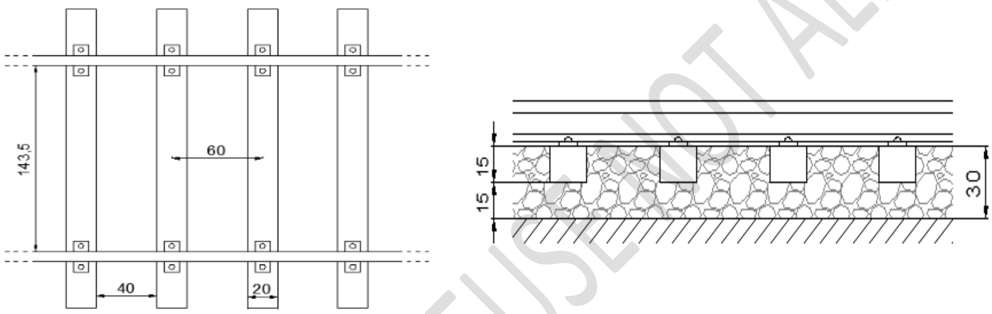

Figure 1: *Test site geometric and structure characteristics.*

The test site reproduced ten different ballast conditions with different levels of decay, involving both aggregates fragmentation and void pollution. Each decay condition was simulated by removing the ballast from a 1.80 m-long rail track section, and by filling it up again with the selected material. Out of the ten configurations, the configurations C2 and C4 were selected for the purpose of this study (see Figure 2). C2 is composed of clean ballast, whereas C4 is made of the same ballast but with voids filled with polluting soil, to replicate fouling.

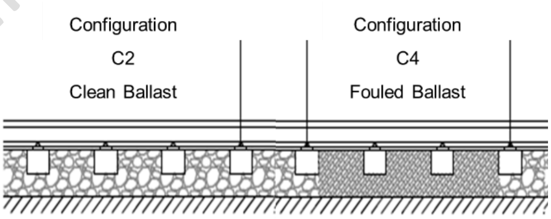

Figure 2: *Selected ballast configurations.*

GPR tests were conducted on the test site by using pulse radar systems equipped with 1000 MHz and 2000 MHz central frequency horn antennas, both manufactured by IDS Georadar (part of Hexagon). The GPR systems were towed along the rail track by using a dedicated rail cart carrying the radars on a cantilever beam. The beam was capable of maintaining the horn antenna at approximately 40 cm of height from the ballast surface.

Data was first collected in dry conditions. Data collection was repeated after water was poured onto the track bed to allow collection of same configurations in wet conditions.

3 Data processing and results

This research is based on the GPR attribute analysis methodology, utilising key textural attributes to improve the visualisation and interpretation of the subsurface structures within the railway ballast. In particular, the centroid frequency attribute analysis was used to process the GPR data and enhance visualisation of internal reflection patterns related to ballast decay (Zhang et al., 2023a), (Liu et al., 1998), (Zhang et al., 2023b). The results were compared to those obtained using a more conventional GPR data processing approach (Zhang et al., 2023b) (Figures 3-6).

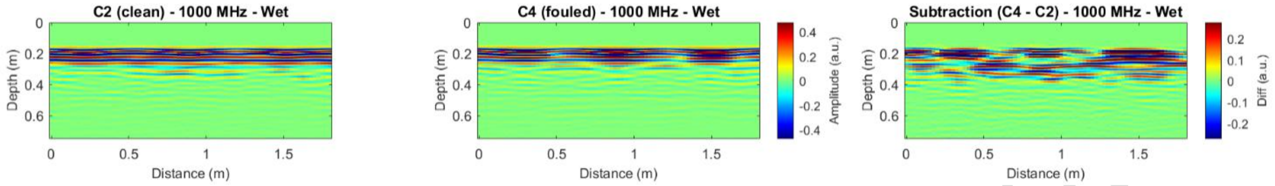

Figure 3: *GPR profiles acquired with the 1 GHz antenna. (a) Clean ballast; (b) fouled ballast; (c) section difference between clean and fouled configurations. Clear attenuation and scattering effects can be observed in the fouled ballast.*

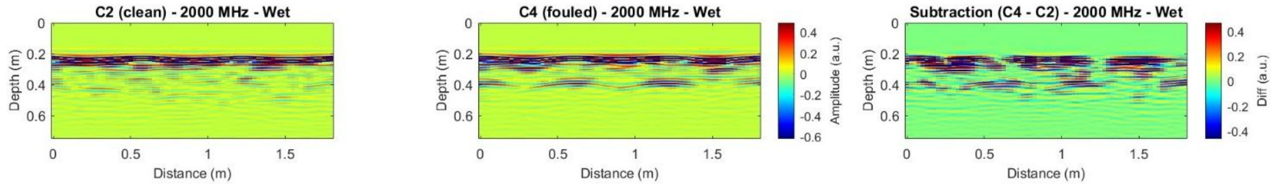

Figure 4: *GPR profiles acquired with the 2 GHz antenna. (a) Clean ballast; (b) fouled ballast; (c) section difference between clean and fouled configurations. Higher frequency provides enhanced resolution of shallow features and increased sensitivity to fouling.*

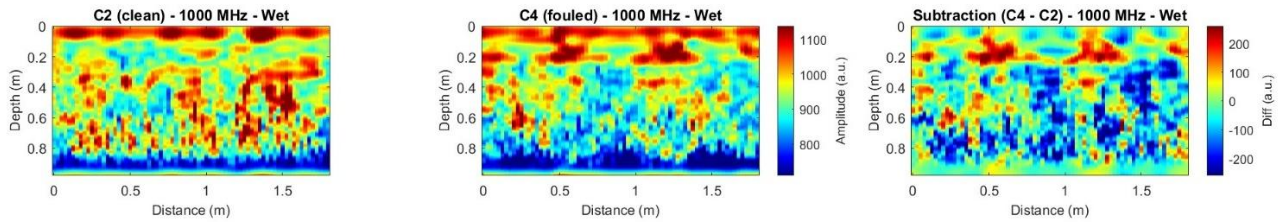

Figure 5: *Centroid frequency attribute results for the 1 GHz antenna. (a) Clean ballast; (b) fouled ballast; (c) section difference. Centroid frequency highlights subsurface contrasts between clean and degraded ballast, allowing improved visualisation and interpretation of fouling effects.*

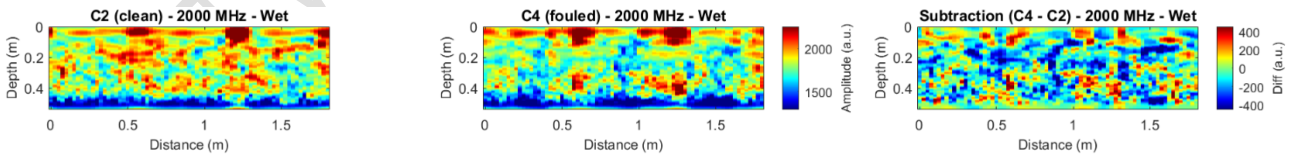

Figure 6: *Centroid frequency attribute results for the 2 GHz antenna. (a) Clean ballast; (b) fouled ballast; (c) section difference. Centroid frequency highlights subsurface contrasts between clean and degraded ballast, allowing improved visualisation and interpretation of fouling effects.*

4 Conclusions

This study showed that GPR attribute analysis, focused on the use of the centroid frequency, can effectively detect and locate ballast fouling and fragmentation. Controlled tests under dry and wet conditions high-lighted clear contrasts between clean and degraded ballast. Compared to traditional methods, the attribute analysis offers higher sensitivity and better interpretation of the ballast conditions, supporting more targeted maintenance strategies and improved railway safety.

5 References

L. Bianchini Ciampoli, A. Calvi e F. D'Amico , «Railway Ballast Monitoring by GPR: A Test-Site Investigation,» *Remote Sensing,* 2019a.

X. Zhang, X. Hu, Z. Qiu, X. Feng e Y. Qin, «Extraction of the GPR instantaneous centroid frequency based on the envelope derivative operator and ICEEMDAN,» *Remote Sensing Letters,* vol. 14, n. 5, 2023.

L. Liu, J. W. Lane e Y. Quan, «Radar attenuation tomography using the centroid frequency downshift method,» *Journal of Applied Geophysics,* vol. 40, n. 1-3, pp. 105-116, 1998.

X. Zhang, Z. Song, X. Feng, J. Zhou, Y. Yu e X. Hu, «the LPR Instantaneous Centroid Frequency Attribute Based on the 1D Higher-Order Differential Energy Operator,» *Remotre Sensing,* vol. 15, n. 5305, 2023.

L. Bianchini Ciampoli, F. Tosti, N. Economou e F. Benedetto, «Signal Processing of GPR Data for Road Surveys. Geosciences,» *Geosciences,* vol. 9, n. 2, 2019a.

Improving bearing capacities of pavements by stabilising concrete slabs with silicate resins

Tim Alte-Teigeler
OAT green tech solutions GmbH

Abstract

To extend the lifetime of traffic areas for many years it is very important to secure good bearing capacities. Loosely embedded concrete slabs, for example, should be stabilised and if necessary lifted in an early stadium to prevent further damage of those and the adjacent slabs. By a thorough full maintenance the amount of necessary severe repair works can be reduced. This leads to a longer service life, better conservation of value, less repair costs, saving of CO_2 emissions and a reduction of traffic obstructions. Especially voids underneath concrete slabs and unstable bearing conditions can cause cracking of slabs and a reduced durability of the entire pavement.

Long-lasting products for slab jacking and stabilisation with high strength and short curing times have been developed in the last decades. This is in particular silicate resin which is mainly used for stabilisation of pavements by filling hollows but also for lifting slabs.

This method is successfully applied in the German market since 15 years and listed in the German Standards (ZTV BEB). Silicate resin is hardening within 20 minutes, so just after finishing the works the traffic blocking can be removed. Therefore, maintenance works are accelerated and the traffic obstructions are reduced. This minimises the user delay costs and economical damage by preventing traffic jams. The method has a lower emission of GHG compared to replacement of concrete pavements and enables to postpone a renewal of pavements in higher scale. Consequently, it saves both carbon emissions as well as costs.

Keywords: concrete pavements; improved bearing capacities; silicate resin; reduced GHG; extend useful life; sustainability

1 Introduction

Maintaining optimal bearing capacities in road pavements and other traffic areas is critical to prolonging their lifespan, reducing repair costs, and minimising disruptions to traffic. Unstable concrete slabs on top of voided base course are a major cause of premature pavement failures, often resulting in cracks and reduced structural integrity. Early intervention through effective stabilisation not only safeguards the affect-ed slabs but also protects adjacent sections, helping prevent the need for extensive repairs. In recent years, silicate resin technologies have emerged as a robust solution for slab jacking and void filling, offering significant improvements in strength and remarkably short curing times. These advanced resins harden within minutes, enabling rapid reopening of traffic lanes and minimising user delay costs. The method has proven successful over the past 15 years in Germany and is integrated into national standards, attesting to its reliability. Furthermore, the lower GHG emissions associated with resin stabilisation, compared to full pavement replacement, underline its environmental advantages. This paper discusses the practical application, technical benefits, and sustainability impacts of silicate resin-based slab stabilisation according to German standards.

2 History of slab jacking and stabilisation in Germany

In earlier decades, the maintenance of concrete pavements in Germany addressed issues of faulting and void formation beneath slabs primarily through the injection of cementitious slurries. This method, standardised in past technical guidelines, involved pumping a mixture with relatively high viscosity underneath the affected slabs. The intention was to fill subsurface voids and restore uniform support, thereby mitigating further deterioration and prolonging the service life of the pavement.

However, practical application revealed several significant limitations of slurry injection. Due to their high viscosity, slurries sometimes failed to achieve broad and uniform distribution beneath the slabs. In certain instances, the injected material accumulated around the injection points, forming concentrated pillars colloquially referred to as "elephant feet." Rather than providing a continuous bearing layer, these pillars could create localised stress concentrations, potentially leading to new cracking or instability. Another drawback was the relatively long hardening time associated with traditional slurries. Extended curing periods delayed the reopening of traffic lanes and increased the duration of construction-related disruptions. These operational challenges highlighted the need for more efficient and reliable solutions.

3 Introduction of silicate resins and polyurethane foams in German Standards

In response to the operational challenges of traditional slurry injection, German pavement maintenance standards have embraced innovative materials and methods over the last decade. The 2015 revision of the ZTV BEB-StB (Standards for the maintenance and repair of concrete pavements) officially introduced silicate resins and polyurethane (PU) foams as approved solutions for slab jacking and stabilisation.

Polyurethane foams, mainly used for slab jacking, offer the advantage of expansion and therefore lower material consumption. It is not so easy to control them as the reaction is taking some time and, thus, still continue after stopping injection. Of course, this behaviour is influenced by the foaming factor which should be limited in order to improve the possibility of control. The expansion causes the slab to be lifted, and this has made them a popular choice for targeted lifting operations.

Silicate resins, however, have become the preferred method for both slab jacking and stabilisation across Germany. Valued for their exceptional durability, high strength and precise controllability during injection, silicate resins deliver reliable results in a wide range of pavement conditions. Their low viscosity ensures comprehensive penetration, allowing the material to fill even the smallest voids beneath concrete slabs. This capacity for complete void filling creates a homogeneous bearing layer, which not only stabilises but also significantly extends the life of the pavement structure.

The road authority's move toward silicate resin technology reflects its superior technical properties and long-term benefits. As a stabilising agent, silicate resin consistently outperforms other materials, delivering rapid curing times and reducing traffic obstructions to a minimum. Its adoption within the German standards – most notably the ZTV BEB-StB 2015 – demonstrates a clear commitment to durability, efficiency and sustainability in modern pavement maintenance.

Figure 1: *Drilling of injection holes (left); injection of silicate resin (right).*

4 Case study M180 in the UK: Economic and Ecologic savings

A 5 km stretch of the M180 nearby Doncaster required urgent refurbishment due to strong movements of the concrete pavement. The road authority considered a concrete bay replacement. This traditional method involves cutting and removing old concrete slabs, preparing the subbase and pouring new concrete. The process is labour-intensive and time-consuming, leading to significant roadwork disruptions. Finally, as an alternative, the innovative method of resin injection for slab stabilisation was chosen.

Instead of the estimated construction time of 12 month and the costs of 120 million GBP for the traditional method the project was finished within 4 month and total costs of 10 million GBP using the injection method which shows the huge potential of time and cost savings. By increasing the availability of the highway, in addition, user delay costs and risk of accidents were reduced tremendously.

Based on the project the Nottingham Trent University calculated the carbon emissions for both repair methods and figured that a concrete bay replacement would sum up in 11,827 tCO_2eq compared to 379 tCO_2eq in case of resin injection (Figure 2). That shows a carbon saving of 96.8 %. This reduction is primarily due to the lower carbon footprint of the materials and processes involved in the resin injection method.

Admitting that the resin injection does not completely replace a renewal of pavements on the long term it must be seen as a possibility to extend the useful life of the pavement by decades. The silicate resin has a durability of up to 30 years and gives the concrete pavement sufficient support to forward the loads of traffic securely into the bearing course. Thus, by postponing the replacement of the pavement for several years, huge carbon savings are still proven.

Item Description	Concrete Bay Replacement Method (A)	Resin Injection Method (B)	Difference in Values (A - B)
Total carbon emissions for all activities	11,827,033.7 $kgCO_2eq$	379,147.5 $kgCO_2eq$	11,447,886.20 $kgCO_2eq$
Total carbon emissions for all activities	11,827 tCO_2eq	379.1 tCO_2eq	11,447.90 tCO_2eq

Figure 2: *Results of carbon calculation by Nottingham Trent University (Boscoe-Wallace).*

5 Conclusions

The advancements in pavement maintenance, particularly the integration of silicate resins into German standards and international projects, mark a significant leap forward in both technical performance and sustainability. As demonstrated in recent revisions to the ZTV BEB-StB, these modern materials address many of the operational limitations of traditional methods, offering enhanced control, durability and efficiency. Silicate resins have set a new benchmark for concrete pavement stabilisation, providing reliable, long-lasting solutions with minimal disruption to traffic and substantial improvements in lifecycle performance.

The case study of the M180 in the UK exemplifies the transformative potential of resin injection methods when compared with conventional concrete bay replacement. The dramatic reductions in time, cost and carbon emissions underscore the environmental and economic advantages of adopting such innovative technologies. Specifically, the 96.8% decrease in carbon emissions, alongside a tenfold reduction in costs and a threefold acceleration in project delivery, clearly highlight the value of embracing resin injection in modern infrastructure management.

6 References

Boscoe-Wallace, A. 2025. Nottingham. Concrete Slab Stabilisation Report

FGSV. 2015. Cologne. Zusätzliche Technische Vertragsbedingungen und Richtlinien für die Bauliche Erhaltung von Verkehrsflächenbefestigungen – Betonbauweisen (ZTV BEB-StB)

Quantitative Prediction of Ballast Particle Abrasion Based on Surrogate Modeling and Machine Learning

Yuanjie Xiao
School of Civil Engineering, Central South University, Changsha 410075, China
Ministry of Education Key Laboratory of Engineering Structures of Heavy Haul Railway Central South University, Changsha 410075, China
Yifan Ning
School of Civil Engineering, Central South University, Changsha 410075, China

Abstract

Ballasted railways represent the dominant form of railway infrastructure in China and globally. During service, ballast beds inevitably experience particle abrasion and fragmentation, which alter the morphology of ballast particles. These morphological changes reduce interparticle interlock and packing efficiency, thereby compromising the strength and permeability of the ballast layer. However, particle shape characteristics are inherently geometric and visual in nature, making them difficult to quantify. Traditional evaluations have relied heavily on expert visual inspection and manual measurement, which are subjective and inefficient. This study proposed a methodology for quantifying ballast particle abrasion by extracting four shape-related indices, including sphericity, aspect ratio, roundness, and angularity, through image processing and computational geometry. These indices were correlated with abrasion levels determined via the Los Angeles (LA) abrasion test. Based on the extracted indices, a predictive framework was developed using Kriging surrogate modeling and neural networks to estimate ballast particle abrasion levels. The analysis of ballast particles under both dispersed and compacted arrangements revealed that the proposed multi-index-based algorithm exhibits strong predictive capability for dispersed particle distributions, with an average prediction error of 22.5 abrasion cycles. In contrast, performance was reduced under compacted conditions, yielding an average prediction error of 90.2 cycles. This work elucidates the evolution of shape indices under progressive abrasion and introduces a quantitative prediction method for ballast degradation. The findings hold practical significance for assessing the service life of ballast and guiding maintenance strategies for ballasted track infrastructure.

Keywords: ballast particle abrasion; shape indices; Los Angeles abrasion test; kriging surrogate modeling; computer vision

1 Introduction

Fragmentation and abrasion are two critical aspects of the degradation of individual ballast particles. Fragmentation primarily affects the particle size distribution, while abrasion is mainly reflected in changes to particle shape. Since the external morphology of particles is a visual characteristic, traditional evaluation methods largely rely on manual measurement by experts, which is not only time-consuming and subjective but also difficult to directly quantify. Consequently, digital image processing has emerged as a prominent approach in related studies.

Ballast particle shape analysis based on image processing can be broadly categorized into two types: (1) two-dimensional (2D) image processing techniques, as illustrated in Figure 1(a); and (2) three-dimensional (3D) image processing techniques, as shown in Figure 1(b). In the context of 2D image processing, previous studies have employed Fourier transform and related methods to analyze the two-dimensional contours of particles, and subsequently used computational geometry to quantitatively characterize contour-based shape features. This has laid the foundation for quantitatively assessing ballast particle abrasion through digital imaging. The principal advantages of 2D image processing lie in its simplicity of equipment, rapid image acquisition, and higher operational efficiency. In contrast, 3D imaging provides complete information on particle morphology, enabling more accurate shape characterization and has thus been widely applied in ballast shape evaluation. However, 3D image processing requires more sophisticated equipment, involves complex procedures, and generally suffers from lower efficiency.

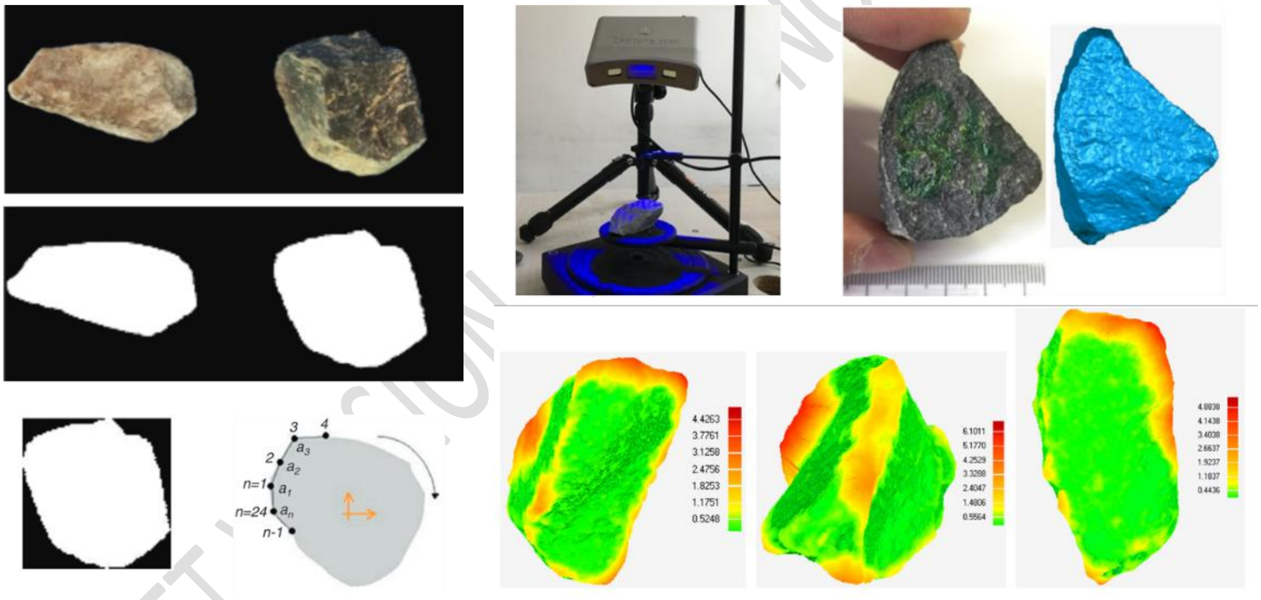

(a) Two-dimensional image processing *(b) Three-dimensional image processing*

Figure 1: *Schematic illustration of image-based ballast particle shape evaluation methods.*

In summary, both 2D and 3D image-based approaches for ballast abrasion assessment have established solid research foundations. While 2D image processing offers greater simplicity and efficiency, 3D image processing enables more precise morphological characterization but is limited by higher equipment complexity and operational constraints. Nevertheless, existing studies have predominantly focused on qualitative analyses of shape index variations under different abrasion levels or correlations between abrasion degree and shape index changes. There remains a notable gap in research regarding the direct quantitative evaluation of abrasion degree based on shape indices.

2 Method

This study focuses on the abrasion behaviour of individual ballast particles, with experimental samples obtained at different abrasion stages through the Los Angeles abrasion test. Multiple abrasion cycles were set to capture the evolutionary process from the initial state to gradual rounding of the particles. To ensure the representativeness of the dataset, particle images were acquired under both dispersed and aggregated conditions: the dispersed state minimized occlusion between particles, enabling precise extraction of particle contours, whereas the aggregated state better reflected real engineering scenarios by characterizing the collective morphological features of particle assemblies.

For image processing and shape characterization, a multi-index evaluation framework was established, incorporating roundness, sphericity, aspect ratio, and angularity. Roundness was defined as the ratio of particle projected area to the squared perimeter of the equivalent circle, representing the degree of similarity to a perfect circle. Sphericity was quantified as the ratio of particle volume to the volume of an equivalent sphere, describing the uniformity of morphology in three-dimensional space. The aspect ratio was determined from the ratio of the major to minor axes of the best-fit ellipse, indicating the elongation and flatness of particles. Angularity was extracted using a combination of Fourier contour fitting and local gradient variation analysis, which effectively captured the disappearance of sharp edges and the progressive rounding of corners during abrasion. The results of image segmentation are shown in Figure 2.

***Figure 2**: Schematic illustration of particle contour extraction through image segmentation: segmentation of particles in dispersed state (left) and segmentation of particles in densely packed state (right).*

In terms of statistical modelling, the study systematically fitted the frequency distributions of each shape index under varying abrasion levels. Candidate models included the normal, Weibull, exponential, and lognormal distributions, with the optimal fit selected based on goodness-of-fit evaluations. Furthermore, considering the limited number of experimental samples and the discrete nature of abrasion cycles, a Kriging surrogate model was introduced to establish the mapping between abrasion cycles and shape indices. This approach not only enabled high-accuracy nonlinear interpolation but also provided predictive uncertainty intervals, thereby offering more comprehensive data support and methodological rigor for the subsequent development of machine learning-based prediction models of ballast abrasion.

3 Results

The results demonstrate that, across different abrasion stages, the shape indices of ballast particles exhibit relatively stable statistical distribution characteristics. Specifically, the distributions of roundness, sphericity, and aspect ratio are generally consistent with normal or lognormal distributions, while angularity tends to display skewed patterns that are better captured by Weibull or exponential distributions. This indicates that the morphological evolution of particles is not entirely random but follows discernible statistical regularities, with the distribution type remaining consistent throughout the abrasion process and only the distribution parameters undergoing systematic shifts.

Regarding the specific abrasion effects, an increase in abrasion cycles leads to a progressive rise in both roundness and sphericity, reflecting the trend of particle morphology becoming increasingly regular and uniform. Conversely, the aspect ratio and angularity decrease with abrasion progression, signifying the gradual smoothing of sharp edges and the transition of particle geometry from irregular to rounded forms. This trend is in strong agreement with the degradation mechanism of ballast subjected to long-term train loading and inter-particle friction, thereby confirming both the rationality of the experimental methodology and the engineering relevance of the results.

The predictive analysis based on the Kriging surrogate model further revealed that this approach accurately captures the variation trajectories of shape indices with abrasion cycles, while also compensating for data deficiencies in certain abrasion stages. The model not only provided high-fidelity mean predictions but also quantified prediction variance and confidence intervals, thereby supplying more comprehensive inputs for subsequent machine learning–based modelling. The extended dataset generated through this method demonstrated that the relationship between shape indices and abrasion cycles is markedly nonlinear: during the initial stage, abrasion exerts a pronounced influence on particle morphology, leading to rapid changes, whereas at higher abrasion levels, shape indices converge towards stability, indicating a saturation of the rounding effect.

In summary, this study establishes a complete methodological framework encompassing experimental acquisition, image-based analysis, statistical modelling, and surrogate modelling. The findings reveal the statistical regularities and evolutionary patterns of ballast particle abrasion, thereby providing a robust theoretical and data foundation for future quantitative prediction of ballast degradation using machine learning approaches.

4 References

Fu, Z., Cai, C., Xu, P., et al., 2013. Method to quantify realistic particle shape angularity and texture of high-speed railway ballast aggregate.

Moaveni, M., Wang, S., Hart, J.M., et al., 2013. Evaluation of aggregate size and shape by means of segmentation techniques and aggregate image processing algorithms. Transportation Research Record 2335 (1), 50–59.

Okonta, F.N., 2014. Relationships between abrasion index and shape properties of progressively abraded dolerite railway ballasts. Rock Mechanics and Rock Engineering 47 (4), 1335–1344.

Wang, L., Wang, X., Mohammad, L., et al., 2005. Unified method to quantify aggregate shape angularity and texture using Fourier analysis. Journal of Materials in Civil Engineering 17 (5), 498–504.

Su, D., Yan, W.M., 2018. Quantification of angularity of general-shape particles by using Fourier series and a gradient-based approach. Construction and Building Materials 161, 547–554.

Qian, Y., Boler, H., Moaveni, M., et al., 2014. Characterizing ballast degradation through Los Angeles abrasion test and image analysis. Transportation Research Record 2448 (1), 142–151.

Qian, Y., Boler, H., Moaveni, M., et al., 2017. Degradation-related changes in ballast gradation and aggregate particle morphology. Journal of Geotechnical and Geoenvironmental Engineering 143 (8), 04017032.

Kim, J., Park, B.S., Woo, S.I., et al., 2020. Evaluation of ballasted-track condition based on aggregate-shape characterization. Construction and Building Materials 232, 117082.

Koohmishi, M., Palassi, M., 2020. Degradation of railway ballast under impact loading considering the morphological properties of aggregate. Transportation Geotechnics 25, 100398.

Guo, Y., Markine, V., Song, J., et al., 2018. Ballast degradation: effect of particle size and shape using Los Angeles abrasion test and image analysis. Construction and Building Materials 169, 414–424.

Rao, C., Tutumluer, E., Kim, I.T., 2002. Quantification of coarse aggregate angularity based on image analysis. Transportation Research Record 1787 (1), 117–124.

Bian, X., Shi, K., Li, W., et al., 2021. Quantification of railway ballast degradation by abrasion testing and computer-aided morphology analysis. Journal of Materials in Civil Engineering 33 (1), 04020411.

Chen, J., Gao, R., Liu, Y., 2019. Numerical study of particle morphology effect on the angle of repose for coarse assemblies using DEM. Advances in Materials Science and Engineering 2019, 1–15.

Zeng, Y.W., Jin, L., Du, X., et al., 2015. Refined modeling and movement characteristics analyses of irregularly shaped particles. International Journal for Numerical and Analytical Methods in Geomechanics 39 (4), 388–408.

Ferreira, T., Rasband, W., 2012. ImageJ user guide. ImageJ/Fiji 1, 155–161.

Altuhafi, F.N., Coop, M.R., Georgiannou, V.N., 2016. Effect of particle shape on the mechanical behavior of natural sands. Journal of Geotechnical and Geoenvironmental Engineering 142 (12), 04016071.

Fu, P., Walton, O.R., Harvey, J.T., 2012. Polyarc discrete element for efficiently simulating arbitrarily shaped 2D particles. International Journal for Numerical Methods in Engineering 89 (5), 599–617.

Feng, Y.T., Owen, D.R.J., 2004. A 2D polygon/polygon contact model: algorithmic aspects. Engineering Computations 21 (2–4), 265–277.

Fraige, F.Y., Langston, P.A., Matchett, A.J., et al., 2008. Vibration induced flow in hoppers: DEM 2D polygon model. Particuology 6 (6), 455–466.

Wang, L., Mohammad, L.N., 2003. Quantification of morphology characteristics of aggregate from profile images.

Yang, D., Wang, X., Zhang, H., et al., 2021. A Mask R-CNN based particle identification for quantitative shape evaluation of granular materials. Powder Technology 392, 296–305.

Oliver, M.A., Webster, R., 1990. Kriging: a method of interpolation for geographical information systems. International Journal of Geographical Information Systems 4 (3), 313–332.

Evaluation of MEPDG Damaged Moduli Approach Using Viscoelastic Backcalculated Damaged Moduli

Atish Nadkarni
Engineering & Software Consultants, LLC
Mahdi Nasimifar
Engineering & Software Consultants, LLC
Salar Zabihi
Federal Highway Administration
Nadarajah Sivaneswaran
Federal Highway Administration

Abstract

In the Mechanistic-Empirical Pavement Design Guide (MEPDG) overlay design for asphalt concrete (AC) flexible pavements, the field-damaged dynamic modulus is determined by applying a damage factor to the undamaged dynamic modulus estimated using Witczak predictive equation. The damage factor for level 1 input is derived from the damaged modulus backcalculated from falling weight deflectometer (FWD) data. While this approach evaluates damage through material behavior at a single test frequency, evaluation of multiple damage levels considering the viscoelastic behavior of asphalt mixtures is less explored. A degree of uncertainty remains regarding the ability of the MEPDG procedure to capture AC mixture behavior at the range of traffic-relevant frequencies as compared to viscoelastic procedures. This study compared the dynamic modulus master curves generated at two damage levels (0.5 and 4.0 encompassing near insignificant and high damages, respectively) using the MEPDG methodology with those derived from viscoelastic backcalculation. An undamaged master curve constructed using the Witczak predictive equation was used in a linear elastic forward calculation, consistent with most backcalculation procedures employed to estimate damaged modulus from FWD data and simulate an FWD deflection basin. Dynamic backcalculation was applied to this basin using the ViscoWave spreadsheet-based software, resulting in a revised undamaged reference master curve. The MEPDG approach was then applied to this reference curve to generate a set of master curves corresponding to two assumed damage levels—referred to as the input reference damaged set. The process of forward calculation and dynamic backcalculation was then repeated for each damage level, yielding a corresponding set of master curves—referred to as the output damaged set. Comparison across the traffic-relevant frequency range (0.1–100 Hz) revealed noticeable differences between the two approaches. Finally, using LTPP data for two projects, a validation exercise to compare the AC layer thickness requirement in rehabilitation design for one location across two damage levels to establish the validity of the viscoelastic analysis was conducted. The findings underscore the necessity of adapting the viscoelastic design approach, since variations in these approaches substantially affect pavement structure rehabilitation.

Keywords: overlay design; dynamic modulus; damage factor; viscoelastic backcalculation.

1 Introduction

Performance of AC pavements is significantly influenced by dynamic modulus, which in turn varies with traffic loading frequency and pavement temperature (Witczak and Fonseca, 1996). For overlay design for AC flexible pavements in level 1 of the MEPDG approach, first, the undamaged dynamic modulus of the existing layer can be calculated using the Witczak predictive equation (Kim et al., 2011). Next, the damage factor is estimated using the backcalculated AC modulus from the falling weight deflectometer (FWD) data for a single frequency (e.g. 30 Hz) and the corresponding modulus at that frequency from the undamaged dynamic modulus curve. Finally, the damaged modulus of the existing AC layer is calculated by applying the damage factor to the entire undamaged dynamic modulus curve. However, uncertainty remains regarding how well the MEPDG procedure captures AC behavior across multiple loading frequencies, since evaluation is typically conducted at a single frequency, typically around 30 Hz frequency. This approach limits consideration of the full viscoelastic behavior of the existing AC layer. This research presents a methodical case study and illustrates the dynamic modulus as a pavement damage assessor by leveraging viscoelastic principles.

2 Methodology

The approach defined above is implemented through a case study of a Long-Term Pavement Performance (LTPP) repository section. The section used is at a location 10.82 miles north-west of I-287, between Doremus Road and Paradise Road, 0.82 miles North-East of Jefferson, New Jersey. The binder used was PG 70-22. Suitable assumptions and approximations were made regarding material classification. For the purpose of analysis and design, all LTPP material descriptions were converted into equivalent Unified Soil Classification System (USCS) classification.

An undamaged deflection basin is simulated through linear elastic forward calculations, using the undamaged dynamic modulus (|E*|) at 30 Hz from the Witczak predictive equation. Next, applying viscoelastic backcalculation to this deflection basin, the equivalent undamaged master curve is generated. To this, two arbitrary damage factors (d_{ac}) values (0.5 and 4.0, representing minimal and extensive damage levels, respectively) are applied to generate the “input reference damaged set” (Ayyala et al., 2018). Using |E*| at 30 Hz from the input reference damaged set, the whole process is then repeated to generate two equivalent damaged master curves (“output damaged set”). These curves are then assessed qualitatively and quantitatively to portray the differences that arise in rehabilitation design. Finally, two rehabilitation designs using input and output damaged set are compared. The linear elastic forward simulations were conducted using spreadsheet-based software program EVERSTRESS (WSDOT, 2005). A typical single wheel load of 9,000 lb and a plate radius of 5.9 inches (representing the tire–pavement contact surface radius) were assumed. For the viscoelastic backcalculation, a spreadsheet-based finite layer program, ViscoWave, was utilized (Lee, 2023).

3 Results

The input reference and the output damaged sets were then assessed qualitatively and quantitatively to highlight the differences that arise in rehabilitation design of AC pavements with respect to material modeling. Figure 1 below illustrates the two sets. In the figure, “MEPDG-VW Normalized Dynamic Modulus” represents the input reference damaged set, while “VW Calculated Dynamic Modulus” represents the output damaged set. At damage level of 0.5, the modulus at 30 Hz was 997 and 1150 ksi for input and output set, respectively; while at damage level of 4.0, the same was 76 and 99 ksi, respectively.

Since the output set is generated by backcalculation using viscoelastic principles and by converting time-based relaxation modulus sigmoidal coefficients into frequency-based dynamic modulus sigmoidal coefficients, it represents the viscoelastic-equivalent response that would produce the same damaged deflection basin as represented by the input set. In the absence of a physical basis for consistency in their quantitative comparison, the key finding of this research is the perceivable difference, allowing for a generalized understanding of the potential variations in the moduli.

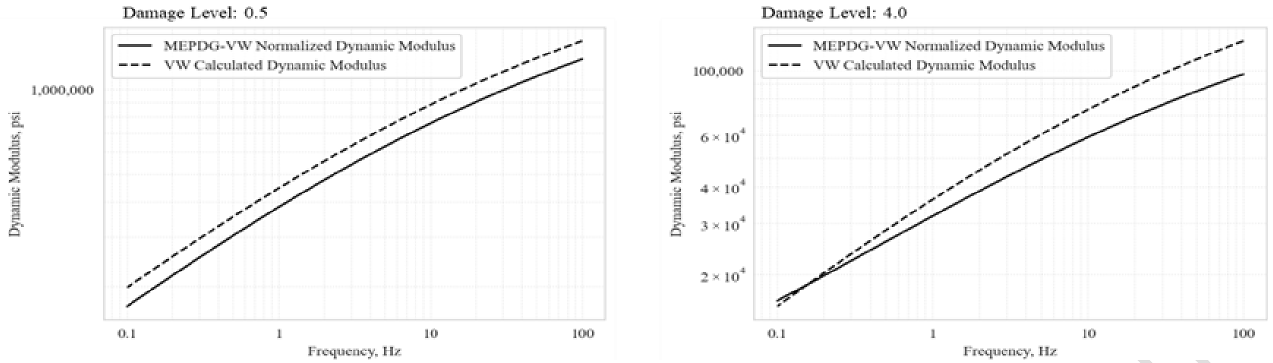

Figure 1: *Input reference and output damaged sets at 0.5 and 4.0 damage level.*

Finally, the AASHTOWare Pavement ME Design (PMED) software was used to design a trial pavement section for this LTPP section. Two design options were explored: (a) design option 1: linear elastic backcalculation; and (b) design option 2: linear viscoelastic backcalculation.

Linear elastic backward simulations were conducted on the FWD deflection drop data for design option 1. The backcalculated resilient modulus was used as the AC modulus input. Design option 2 was conducted using FWD time series data with a haversine loading history from LTPP and involved computation of AC sigmoidal frequency-dependent dynamic modulus. For the time series data, the 8th drop was chosen to improve analysis accuracy, since the load and the applied pressure match closest to the actual loading conditions on a highway pavement. ViscoWave was utilized to perform viscoelastic backcalculation. For the FWD simulation, a single wheel load of 9,000 lb and a plate radius of 5.9 inches was considered, closely approximating actual loading conditions. The analysis was run by incrementing the AC overlay thickness until all the pass reliability criteria (such as for the International Roughness Index (IRI), and other major rutting and cracking distresses) were met. Design option 1 met all the criteria at 5-inch overlay thickness while design option 2 met the criteria at 4-inch thickness.

4 Conclusion

This researched explored the degree of uncertainty in how closely the MEPDG procedure captures AC mixture behavior at the range of traffic-relevant frequencies, compared to viscoelastic procedures. Dynamic modulus master curves generated at two damage levels using the MEPDG methodology were compared with those derived from viscoelastic backcalculation. Perceivable differences were observed in the moduli derived using the MEPDG elastic method and those derived using the viscoelastic approach using ViscoWave. Finally, two design strategies: linear elastic (utilizing the FWD drop data) and viscoelastic (utilizing the FWD time series data) were compared. The difference of 1 inch in the required overlay thickness between design options 1 and 2 revealed how potential occurrences of differences in the moduli can lead to differing outcomes and the effect of incorporating full viscoelastic behavior of the existing AC layer.

5 References

Witczak, M. W. & Fonseca, O. A. 1996. Revised predictive model for dynamic (complex) modulus of asphalt mixtures. Transportation Research Record, pp. 15–23.

Kim, Y. R., Underwood, B., Far, M. S., Jackson, N. & Puccinelli, J. 2011. LTPP computed parameter: dynamic modulus (No. FHWA-HRT-10-035). U.S. Department of Transportation, Federal Highway Administration.

Ayyala, D., Lee, H. & Von Quintus, H. L. 2018. Characterizing existing asphalt concrete layer damage for mechanistic pavement rehabilitation design (No. FHWA-HRT-17-059). U.S. Department of Transportation, Federal Highway Administration.

WSDOT. 2005. Pavement analysis computer software and case studies. Washington State Department of Transportation, Olympia, Washington.

Lee, H. S. 2023. ViscoWave. December 2023. [Online]. https://github.com/leehyu20/ViscoWave/tree/main.

AASHTO. 2008. Mechanistic-empirical pavement design guide: a manual of practice. Washington D. C.

Evaluating Structural Reserves under the ACR-PCR Framework: An Integrated NDT and Forensic Case Study

Ashish Walia
Satish Pandey
CSIR-Central Road Research Institute, New Delhi, India

Abstract

The operational continuity of high-intensity airfield infrastructure demands periodic and rigorous evaluation to manage ultra-heavy aircraft loading. This paper presents an integrated investigation of a runway which facilitates over 900 daily operations. The methodology synchronizes Non-Destructive Testing (NDT) via Heavy Weight Deflectometer (HWD) and Network Survey Vehicle (NSV) with forensic laboratory characterization of field-extracted cores. Structural analysis was performed using PCASE 7 software, employing a composite maximum traffic strategy to simulate a 20-year saturation envelope. Results indicate a Pavement Classification Rating (PCR) of 1944, compared against an Aircraft Classification Rating (ACR) of 555 for the critical fleet, yielding a robust ACR/PCR ratio of 0.3. Functional assessments revealed localized roughness (IRI > 2.5 m/km) at intersections and surface smoothening in touchdown zones. The study concludes that while the deep-strength pavement possesses massive structural reserve, maintenance must prioritize functional preservation to mitigate engine-ingestion risks from aggregate plucking.

Keywords: airfield; HWD; NSV; PCASE 7; ACR-PCR; IRI.

1 Introduction

An airport runway serves as the primary structural interface between heavy aircraft and the foundation soil, and functions as a critical component of airside infrastructure. The pavement structure is engineered as a multi-layered system, often a composite of flexible bituminous layers with other granular materials. The pavement design of airport runway should facilitate the efficient distribution of high vertical stresses from aircraft tires down to the natural subgrade. For high-intensity operational hubs, the structural and functional integrity of this system is fundamental to aviation safety. Beyond load distribution, the pavement surface must maintain specific frictional and geometric characteristics to ensure safe braking, prevent hydroplaning during adverse weather, and mitigate the risk of engine breakdown from Foreign Object Debris (FOD). Consequently, there is an imperative need for periodic evaluation because every aircraft pass consumes a portion of the pavement's finite structural life. Maintaining a robust Pavement Classification Rating (PCR) relative to the aircraft fleet's damaging effect is essential for preventing rapid structural degradation. The timely intervention shall ensure the unrestricted operational continuity under saturation traffic demands at much lesser cost in comparison to delayed rehabilitation measures.

Runway is the primary airside asset at any airport for handling safe operations, which becomes even more critical for the present runway handling more than 900 average operations daily. The runway pavement is expected to sustain operations of ultra-heavy wide-body aircraft including the Airbus A380 and Boeing 777-300ER. Geometrically, the runway extends 3,400 meters with an operational width of 60 meters. Historically, the pavement has undergone progressive strengthening since 1979, resulting in a massive cumulative crust thickness of 1,635 mm with more than 600 mm of bituminous thickness accumulated over the years. The most recent major rehabilitation in 2019-2020 involved a structural overlay of 100 mm of dense bituminous mix with Polymer Modified Bitumen (PMB) utilizing high-performance binder. This paper evaluates the structural adequacy of this complex multi-layered system under the transition from the legacy ACN-PCN system to the current ICAO ACR-PCR standards.

2 Experimental Programme

2.1 Field Investigation and NDT Methodology

The structural response was quantified using a Heavy Weight Deflectometer (HWD) in accordance with ASTM D 4694 and FAA Advisory Circular 150/5370-11B. To accurately simulate wide-body aircraft tire footprints, a 450 mm diameter segmented loading plate was used to apply transient impulse loads peaking at 250 kN. Testing was conducted in a systematic grid covering the central Keel Section, with specific test lines at 3 meters, 6 meters and 9 meters offsets to capture the critical load path of main gear repetitions. Functional characterization utilized a Network Survey Vehicle (NSV) equipped with high-precision laser profilometers. In accordance with ASTM D 5340, the system measured the International Roughness Index (IRI), Mean Texture Depth (MTD), and Rut Depth (RD) at operational speeds to assess riding quality and hydroplaning risks.

2.2 Forensic Laboratory Testing

In order to collect the actual field samples, a total of seven cylindrical cores of approximately 150 mm diameter were extracted in accordance with ASTM D 5361. Although the overall thickness of the bituminous layers was reported more than 700 mm as per previous design records, the cores were extracted for the total height in a range of 200 to 300 mm only. The field extracted core specimens were precision-sawed into segments (Layers A through D) to distinguish between the different layers laid at different service period. This segmentation allowed to evaluate the performance gradient of different layers obtained through it. The segmented core specimens were further evaluated in laboratory for different parameters as discussed subsequently.

2.2.1 Volumetric Analysis

This analysis establishes the internal structure of the asphalt mix, specifically the relationship between aggregate, binder, and air pockets. Bulk Specific Gravity (Gmb) was determined per ASTM D 2726, while Theoretical Maximum Specific Gravity (Gmm) was measured for loose bituminous mixtures per ASTM D 2041. The Air Voids (Va) percentage was then calculated by correlating Gmb with the void-free Gmm reference. The analysis revealed extremely low air voids (< 2.0%) across all samples, including those from non-trafficked shoulder areas. This confirms that the pavement has achieved refusal density, where the aggregate skeleton has reached its maximum possible state of consolidation. It also demonstrates that reaching near-refusal density ensures the pavement possesses an exceptionally tight stone-on-stone interlock, which maximizes resistance to water ingress and permanent deformation (rutting).

2.2.2 Mechanical Strength Characterization

The strength characterization testing was conducted in two sequential phases to ensure the material was characterized within its linear viscoelastic range without inducing premature failure. The indirect tensile strength (ITS) is a destructive through which the maximum tensile load the cores could sustain was measured. These values served as a control baseline to establish cyclic stress ratios for subsequent testing. The ITS values in Layer A were computed relatively higher which confirmed the use of high-performance mixes capable of resisting different distresses. The second test for strength characterization was conducted to measure resilient modulus (Mr) as per ASTM D 7369, which is a non-destructive dynamic test simulates the elastic rebound of the pavement under moving aircraft wheel loads. The target cyclic stress was limited to approximately 10% of the ITS peak load to stay within the viscoelastic range. The Mr values provide the foundational data needed to verify the back-calculated layer moduli derived from HWD surveys. Results showed a significant stiffness gradient, with the new overlay and aged historic layers both exceeding 5,000 MPa, creating a rigid upper crust.

2.2.3 Recovered Binder Rheology

The bituminous phase was isolated to evaluate how environmental exposure and oxidative aging have affected the binder's performance over time. Bitumen was recovered utilizing the Rotary Evaporator (Rotavapor) method as per ASTM D 5404. This vacuum-distillation process is superior to traditional centrifugal methods as it prevents artificial hardening or oxidation during extraction, ensuring the recovered binder represents its true in-situ condition. Apart from conventional binder tests such as penetration test, softening test and rotational viscosity, the Dynamic Shear Rheometer (DSR) was employed to determine the Performance Grade (PG) by evaluating the binder's elasticity and resistance to shear at high temperatures. The analysis confirmed the surface course (Layer A) retains a robust PG 84 rating, verifying an active polymer network capable of withstanding extreme runway shear stresses. However, Layer B was identified as PG 64, indicating a lack of effective polymer modification in that specific lift. Historical Layer C also tested at PG 84, though other tests indicated it has become brittle due to oxidative aging.

3 Data Analysis and Interpretation

3.1 Laboratory Findings

Volumetric analysis revealed extremely low air voids (< 2.0%) across all samples, confirming the mix has achieved refusal density. This signifies a robust stone-on-stone interlock that maximizes shear resistance. Rheological testing confirmed that the surface Layer A retains a PG 84 rating, ensuring superior resistance to surface shear and rutting. However, the 2010 historical Layer C, while stiff (Mr > 5,000 MPa), showed reduced ductility due to oxidative aging.

3.2 PCR Computation

Structural capacity was evaluated using PCASE 7 software utilizing the LEEP (Layered Elastic Evaluation Program) module. A composite maximum traffic model was developed by aggregating the peak annual frequency of each aircraft type between different years to simulate true saturation capacity. During back-calculation, a judicious limiting approach was adopted to obtain rational back calculated modulus values. The surface layer modulus was clamped at 7,000 MPa based on the maximum laboratory-determined Mr values to prevent mathematical overshoot caused by the extremely low field deflections (230–280 microns). Based on the frequency and gear configuration, the Airbus A330-200 was computed as critical aircraft. With respect to ACR of 555, the thick pavement structure with sufficient strength leads to PCR value of 1944. It meant that the ACR/PCR ration is only 0.3, which conveys that the anticipated traffic would consume only 30% of the pavement's current condition, indicating the runway is structurally quite sound for the current fleet.

3.3 Functional Performance

The Automated profiling collected through NSV indicated a smooth surface with IRI values predominantly below 2.0 m/km. Rut depths were negligible, ranging from 1.0 mm to 4.0 mm, far below the 13 mm maintenance threshold. MTD values generally exceeded the 0.80 mm safety threshold; however, reductions (0.90–1.10 mm) in touchdown zones corroborated visual logs of rubber vulcanization which fills surface voids and reduces wet skid resistance.

4 Conclusions

Runway is in excellent structural condition, with a PCR of 1944 providing a significant structural reserve (ACR/PCR = 0.3) for current and forecasted traffic.

The pavement structure can theoretically sustain over 2.2 million passes of the critical aircraft over a 20-year design life without fatigue failure.

Maintenance should focus on functional preservation, including periodic rubber removal in touchdown zones and localized milling and inlay (50-60 mm) using PMB binder to mitigate engine-ingestion risks from dislodged aggregates.

5 References

ASTM D2041. 2019. Standard Test Method for Theoretical Maximum Specific Gravity and Density of Bituminous Paving Mixtures. West Conshohocken, PA: ASTM International.

ASTM D2172. 2022. Standard Test Methods for Quantitative Extraction of Asphalt Binder from Asphalt Mixtures. West Conshohocken, PA: ASTM International.

ASTM D2726. 2021. Standard Test Method for Bulk Specific Gravity and Density of Non-Absorptive Compacted Asphalt Mixtures. West Conshohocken, PA: ASTM International.

ASTM D3549. 2018. Standard Test Method for Thickness or Height of Compacted Asphalt Mixture Specimens. West Conshohocken, PA: ASTM International.

ASTM D4694. 2020. Standard Test Method for Deflections with a Falling-Weight-Type Impulse Load Device. West Conshohocken, PA: ASTM International.

ASTM D5340. 2020. Standard Test Method for Airport Pavement Condition Index Surveys. West Conshohocken, PA: ASTM International.

ASTM D5361. 2021. Standard Practice for Sampling Compacted Asphalt Mixtures for Laboratory Testing. West Conshohocken, PA: ASTM International.

ASTM D5404. 2021. Standard Practice for Recovery of Asphalt from Solution Using the Rotary Evaporator. West Conshohocken, PA: ASTM International.

ASTM D7369. 2020. Standard Test Method for Determining Resilient Modulus of Bituminous Mixtures by Indirect Tension Test. West Conshohocken, PA: ASTM International.

CROW. 2006. Netherlands. Report 05-06: Guideline on PCN Assignment. Information and Technology Centre for Transport and Infrastructure.

Federal Aviation Administration. 2014. Advisory Circular 150/5335-5C: Standardized Method of Reporting Airport Pavement Strength - PCN. U.S. Department of Transportation.

Federal Aviation Administration. 2018. Advisory Circular 150/5370-10H: Standard Specifications for Construction of Airports. U.S. Department of Transportation.

Federal Aviation Administration. 2011. Advisory Circular 150/5370-11B: Use of Nondestructive Testing in the Evaluation of Airport Pavements. U.S. Department of Transportation.

International Civil Aviation Organization. 2018. Montreal, Canada. Annex 14 to the Convention on International Civil Aviation: Aerodromes, Volume I - Aerodrome Design and Operations, Eighth Edition.

International Civil Aviation Organization. 2013. Montreal, Canada. Aerodrome Design Manual, Part 3: Pavements (Doc 9157), Second Edition.

PCASE. 2023. Pavement-Transportation Computer Assisted Structural Engineering User Guide (Version 7.0.7). U.S. Army Corps of Engineers.

Evaluation of real traffic loading with the use of portable bridge WIM system and laser traffic counters

Martin Hauptman
Bajko Kulauzović
Cestel, Slovenia
Uroš Brumec
Slovenian Infrastructure Agency, Slovenia

Abstract

Data on axle loads of heavy goods vehicles (HGVs) is essential in pavement design. Weigh-in-motion (WIM) systems are the primary source of this data, but they have drawbacks related to the costs of installation and maintenance, which results in limited deployment of such systems. Because of that, there is a lack of data on actual traffic loads for most road sections, with this being especially pronounced on the lower ranking roads. The Slovenian Infrastructure Agency is using portable bridge weigh-in-motion systems coupled with laser traffic counters to broaden the usability of WIM data on the road sections adjacent to where the WIM measurement is taking place. The bridge WIM system is positioned on the main road, while the laser traffic counters detect vehicles on the roads which branch off the main road. The collected data shows a severe underestimation of the equivalency factors and traffic loading on many road sections when compared to the technical specifications for road design.

By combining outputs of WIM systems with other intelligent traffic systems, data on axle loads and GVW can be applied to wider parts of the road network. The article presents an example of such a type of measurement conducted by the Slovenian Infrastructure Agency.

The summary represents the description of the contribution. It should describe the key content of the paper, including the problem, purpose, method of addressing the problem, and key findings. The summary should not exceed 25 lines.

Keywords: weigh-in-motion; pavement design; intelligent traffic systems

1 Introduction

Weigh-in-motion stations are the preferred method of gathering traffic loading data for pavement design and performance prediction, but high installation and maintenance costs limit their deployment to motorways and roads of higher logistical importance (Faruk et al., 2016). This limitation is significant as regional, main, and local roads present the largest part of the road network, and in case of overloading, these roads are not designed for large traffic loads. A Canadian study compared the relative impact of regular HGVs on different types of roads and concluded that pavement damage costs for a typical truck are more than 100 times larger for a local street than for a high-standard motorway (Dey, 2014).

Among other responsibilities, the Slovenian Infrastructure Agency (Agency) is responsible for managing approximately 5900 km of Slovenian main and regional roads. The Slovenian road classification system divides these roads into five categories: G1 and G2 (main roads) and R1, R2, and R3 (regional roads). G1 main roads connect regional centers of population, while the lowest category of road under the management of the Agency, R3 regional roads, connects local communities, areas important for tourism, and areas close to the national border (Cestna infrastruktura, 2026).

When it comes to gathering statistical data on heavy traffic, the Agency relies on two technologies: portable bridge weigh-in-motion systems and permanent and portable traffic counters. Over 100 bridge WIM measurements of varying duration are performed on the Agency's road network each year - on some road sections, a bridge WIM system and mobile traffic counters are used simultaneously in order to assess the heavy traffic outflow to lower-ranking road sections.

2 Case study: traffic loading data collection in the Cerknica area

The town of Cerknica is located in the southwest part of Slovenia at the foot of the Bloke plateau, a heavily forested area with a significant presence of the lumber industry (E-občina , 2026). From the point of view of traffic loading, the transportation of lumber can be challenging as the high variability in the density and moisture of wood materials may contribute to the overloading of trucks (Trzciński et al., 2021).

In September 2023, the Agency conducted a one-week bridge WIM measurement in combination with traffic classification and counting measurement using two laser traffic counters. Figure 1 shows the positions of the measurement systems; the bridge WIM system was positioned on the R1 regional road in the town of Cerknica, which connects the town with the Bloke plateau. One traffic counter was positioned on the regional road of the same category going towards the town of Rakek and A1 motorway, while the second traffic counter was used to gather data on the R3 regional road from Cerknica towards the Rakitna plateau.

The measurement was done incognito; the bridge WIM system is not visible to drivers since its sensors are positioned on the soffit of the bridge, while the portable traffic counters are designed to look like guidepost.

2.1 Bridge WIM data

The bridge WIM system was used to classify HGVs, detect their gross vehicle weight (GVW), axle loads and determine their tire types. This was the input used to calculate equivalent single axle loads (ESAL) and equivalency factors (EF) for different vehicle classes. The concept of ESAL enables the conversion of the damage caused by axle loads of varying magnitudes and axle configurations to an equivalent standard single axle load. For practical purposes, it is more convenient to express the pavement damage for particular vehicles classes (equivalency factor), which is done by averaging the number of ESAL applications per vehicle class (Kim et al., 2021).

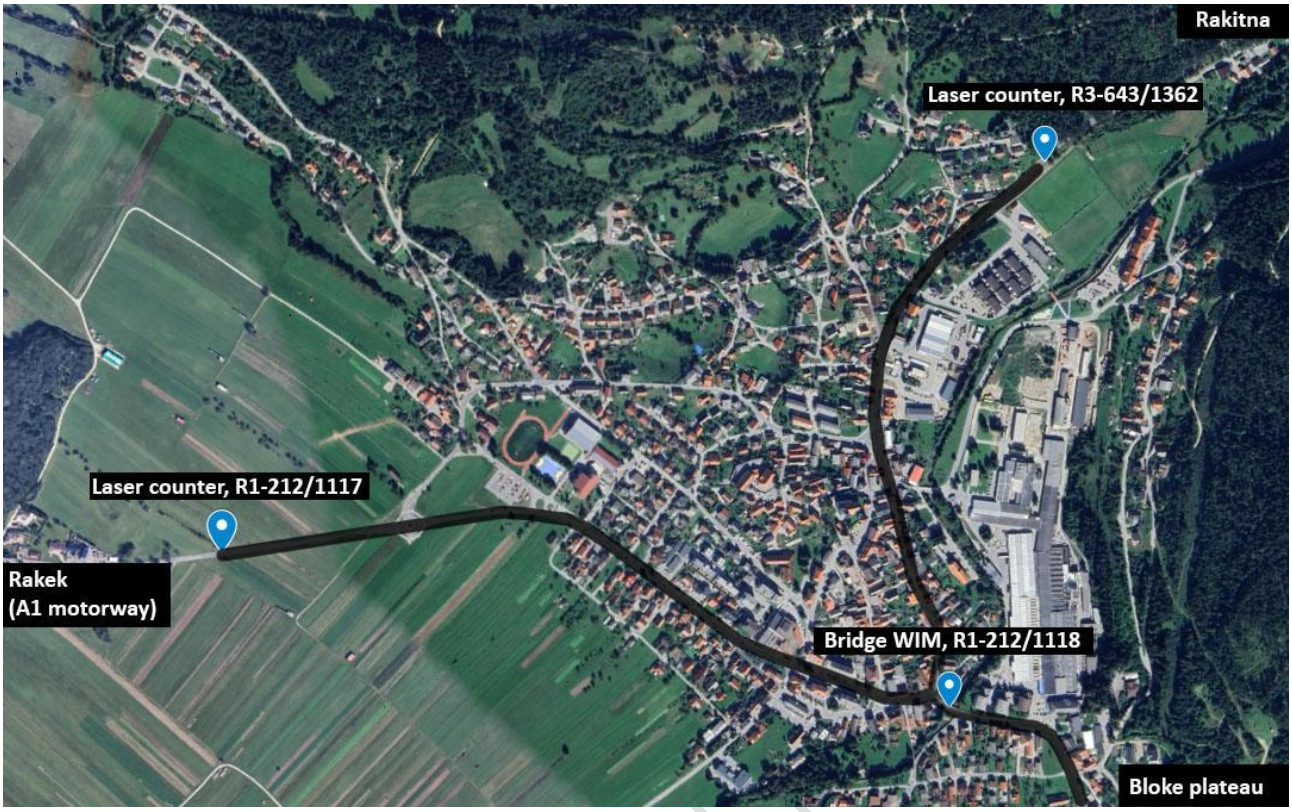

Figure 1: *Locations of the measurement equipment in and around the town of Cerknica – black marking denotes the relevant road sections.*

Table 1 gives the overview of the one-week bridge WIM measurement. Articulated 5-axle HGVs were the most numerous category of heavy vehicles, with the direction from the Bloke plateau toward Cerknica seeing the highest number of HGVs.

Table 1: *Average daily number of vehicles with GVW over 3,5.*

	Buses	Medium trucks (3 t to 7 t)	Heavy trucks (over 7 t)	Articulated HGVs
To Bloke plateau	27	66	23	81
To Cerknica	29	79	25	109

For each of the categories in Table 1, average EF values were calculated based on the data gathered by the bridge WIM system.

Table 2: *Average EF and ESAL values calculated from the bridge WIM data.*

	Buses	Medium trucks (3 t to 7 t)	Heavy trucks (over 7 t)	Articulated HGVs
To Bloke plateau	0.51	0.17	1.56	1.44
To Cerknica	0.56	0.17	0.76	1.99

When compared to the EF values calculated on the basis of the bridge WIM output, the EF found in the Slovenian Technical specifications for public roads (Direkcija Republike Slovenije za ceste, 2009) are lower for heavy trucks and articulated vehicles in the direction to the Bloke plateau and significantly lower for articulated HGVs in the direction to Cerknica (Table 3).

Table 3: *Comparison between EF found in the Slovenian Technical specifications for public roads and EF calculated based on the bridge WIM data.*

	Technical specifications (R1 and R2 roads)	Bridge WIM (to Bloke plateau)	Bridge WIM (to Cerknica)
Medium trucks	0.25	0.17	0.17
Heavy trucks	1	1.56	0.76
Articulated HGVs	1.25	1.44	1.99

2.2 Measurement of the traffic outflow and an assessment of traffic loading

The measurements with the bridge WIM system and both laser traffic counters were conducted in the same week.

Table 4 gives an overview of the number of HGVs detected by the laser traffic counters positioned on the road sections, which branch off from the location where the bridge WIM system was installed. Category medium and heavy rigid trucks is presented as a single value, since laser traffic counters cannot differentiate between vehicles based on their GVW. The average daily traffic loading was based on the EF from Table 2.

Table 4: *Data from laser traffic counters (their positions are marked in Figure 1).*

	Buses	Medium and heavy rigid trucks	Articulated HGVs	Average daily traffic loading
	R3-643/1362			
Rakitna - Cerknica	3	28	8	27 ESAL
Cerknica - Rakitna	4	26	7	24 ESAL
	R1-212/1117			
Rakek - Cerknica	25	133	105	235 ESAL
Cerknica - Rakek	31	125	125	305 ESAL

The average daily traffic loading on the R3-643/1362 road section falls under the lowest category (very light loading). On the R1-212/1117 road section, in the direction toward Cerknica, the traffic loading is in the medium category, while in the opposite direction, the traffic loading is in the heavy category, according to the Slovenian Technical specifications for public roads.

The data from the laser traffic counter shows that the majority of HGVs from the Bloke plateau continue in the direction of Rakek and the A1 motorway.

3 Conclusions

Based on the bridge WIM data, the real equivalency factors at the road section in question are higher than what is prescribed in the technical specifications for heavy rigid trucks and articulated HGVs. On the R1 main road presented in this article, the equivalency factors are in fact higher than the equivalency factors prescribed by the technical specifications for motorways (0,7 for heavy rigid trucks and 1,6 for articulated HGVs).

Data from laser traffic counters show that the majority of HGVs from the Bloke plateau continue their route towards the A1 motorway (Rakek). When we applied the EF from bridge WIM measurements to this road section, the average daily traffic loading was calculated at 305 ESAL. The R3 road section saw low traffic numbers, and the average daily traffic loading was very light.

The concept of combining portable WIM technology with portable traffic counters can help in determining traffic patterns and broaden the usability of WIM data to adjacent road sections.

4 References

Cestna infrastruktura. GOV.SI. (n.d.). Portal GOV.SI. https://www.gov.si/teme/cestna-infrastruktura/. Accessed 8 April 2026.

Dey, K. 2014. Minimizing bridge and pavement deterioration from large trucks: A policy analysis for damage recovery. TigerPrints (Clemson University).

E-Občina. Predstavitev občine - Občina Cerknica. 2026. https://www.cerknica.si/objave/175. Accessed 29 March 2026.

Faruk, A. N., Liu, W., Lee, S. I., Naik, B., Chen, D. H., & Walubita, L. F. (2016). Traffic volume and load data measurement using a portable weigh in motion system: A case study. International Journal of Pavement Research and Technology, 9(3), 202–213. https://doi.org/10.1016/j.ijprt.2016.05.004

Kim, S., Yang, J., Durham, S., Kim, I., Yaghoubi, N. T. (2021). Determination of Equivalent Single Axle Load (ESAL) Factor for Georgia Pavement Design. University of Georgia. College of Engineering. https://rosap.ntl.bts.gov/view/dot/57399.

Trzciński, G. Tymendorf, Ł. Kozakiewicz, P. 2021. Parameters of Trucks and Loads in the Transport of Scots Pine Wood Biomass Depending on the Season and Moisture Content of the Load. Forests 2021, 12, 223. https://doi.org/10.3390/f12020223

Direkcija Republike Slovenije za ceste. (2009). TSC 06.511: 2009 Prometne obremenitve – določitev in razvrstitev. Ministrstvo za promet. https://www.gov.si/assets/organi-v-sestavi/DRSI/Dokumenti-DRSI/Tehnicne-specifikacije/Ukinjene-TSC/TSC_06_511_2009_Prometne_obremenitve_Dolocitev_in_razvrstitev.pdf

Seasonal Load Spectra on Illinois Interstate Highways

Aditya Singh, Hong Lang and Imad L. Al-Qadi
Illinois Center for Transportation, Grainger College of Engineering, University of Illinois Urbana-Champaign, Rantoul, Illinois, USA

Abstract

Vehicle loading distribution is a critical input for mechanistic-empirical pavement design. In Illinois, traffic factor equations were last updated in 1983, before the legal axle load limit increased to 80,000 pounds. Since then, trucking patterns have evolved significantly (e.g., fewer empty trailers and heavier multiple-unit vehicles). This increased the cumulative damage to the pavement. Currently, Illinois operates a statewide weigh-in-motion (WIM) system that continuously records axle weight for each vehicle. The dataset provides a unique opportunity to develop a more accurate approach, particularly in high-traffic areas (e.g., industrial sites and multimodal hubs), where an average is no longer applicable. This study developed a data-driven framework to generate cluster-specific, seasonal axle load spectra as traffic inputs for pavement design. One year of quality-controlled WIM data from 18 permanent stations were organized and analyzed. Axle load distributions for front, single, tandem, and tridem axles were structured into a four-way tensor (station × vehicle class × axle load bin × month) for multiway analysis. A PARAFAC decomposition extracted station-level features, which were clustered using statistical criteria (silhouette index) to identify representative traffic regions. Within each region and season, non-negative mixture lognormal models were fitted to axle-group spectra, converting empirical histograms into smooth, closed-form distributions. The findings indicated that Illinois traffic could not be accurately represented by a single statewide factor. The proposed clustering approach captures seasonal and regional freight variation, providing traffic inputs tailored to design needs. This will allow to derive equivalent axle-load factors (EALFs) and evaluate design impacts with calibrated transfer functions.

Keywords: weigh in motion (WIM); axle-load; traffic factor; clustering; pavement design

1 Introduction

Accurate characterization of vehicle loading is essential for mechanistic–empirical (ME) pavement design, as axle weight distributions directly influence fatigue, rutting, and pavement service life predictions. In Illinois, traffic factor equations have remained unchanged since 1983, before the legal axle load limit was raised to 80,000 pounds. Over the past four decades, freight movement patterns have shifted significantly, with heavier multi-unit trucks, increased intermodal activity, and fewer empty trailers, leading to higher cumulative pavement loading. This gap between design inputs and current freight conditions highlights the need for a data-driven, scalable framework to better capture spatial and seasonal variations in traffic loading.

The statewide weigh-in-motion (WIM) network in Illinois continuously records axle weights, spacings, speeds, timestamps, and vehicle classes, providing a high-resolution dataset that reflects freight activity across diverse corridors (VI^{2}M, 2025). This dataset presents a unique opportunity to revise the single statewide factor, particularly in high-traffic corridors such as industrial hubs, multimodal hubs and freight-intensive highways. However, leveraging this resource for pavement design is challenging. The dataset's size and multidimensionality complicate its direct use in design, while a fully site-specific calibration for each project would be costly and impractical for statewide practice. Clustering approaches have been applied in other states to define the representative traffic factors. For example, Sayyady et al. (2010 applied hierarchical clustering in North Carolina, and Li et al. (2017) evaluated multiple clustering algorithms in Michigan. These studies have shown the potential of clustering, and this work extends it by developing seasonal, probabilistic axle load spectra for direct use in pavement design.

In this paper, a framework was developed that replaces a single statewide average with cluster-based, seasonal axle-load spectra. For each station, front, single, tandem, and tridem axle spectra were plotted to observe the differences. The data were then represented in a multiway array (vehicle class x axle-load bins x months x station), and station scores were extracted using the PARAFAC model. The scores were then clustered to define the representative loading regions. For each region and season, probabilistic spectra were generated for front, single, tandem, and tridem axle configurations.

2 Data and Methodology

This study analysed one year (2024) of WIM records collected from 18 permanent stations across Illinois. Data quality was verified using iQC diagnostics (iQC, 2025), and records containing sensor malfunctions, calibration drift, anomalous values, or other outliers were excluded to ensure reliability. As an initial step, axle-load spectra for the front axle, single axle, tandem axle, and tridem axle were plotted to visualize the traffic distribution across the stations. The cleaned dataset was structured into a four-way tensor (station × vehicle class × axle load bin × month) with 13 Federal Highway Administration (FHWA) vehicle classes, 80 axle-load bins and 12 months of data per station. A PARAFAC decomposition model was applied to this tensor to extract component loadings across vehicle class, axle load, and seasonal variations. The station mode scores obtained from the PARAFAC model summarised the key traffic-loading characteristics and served as input features for clustering.

Four clustering methods were evaluated: k-means, Ward's agglomerative clustering, spectral clustering, and density-based spatial clustering of applications with noise (DBSCAN). Clustering performance was evaluated using silhouette scores and elbow curves. After clusters were defined, axle-load spectra were generated for each cluster, separated by axle group (front, single, tandem, and tridem) and by seasons (winter, spring, summer, and fall). To provide smooth, design-ready representations, non-negative mixture lognormal models were fitted to these seasonal spectra, converting empirical histograms into closed-form probability distributions. The overall workflow is summarized in Figure 1.

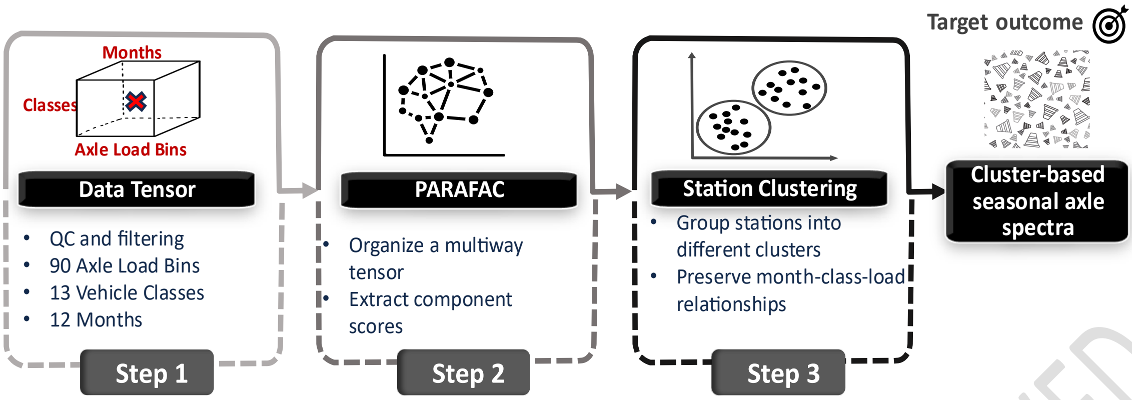

Figure 1: *Framework for developing cluster-based seasonal axle spectra.*

3 Results and Discussion

The four-way PARAFAC decomposition of the WIM records revealed two dominant loading patterns. The first pattern corresponds to heavy freight behavior, characterized by tandem axle loads concentrated around 32 kips and front axle loads near 12 kips, typical of FHWA Class 9. The second pattern represents lighter axle loading, with single axle loads near 6 kips, typical of FHWA Class 5. The patterns remained consistent throughout 2024, effectively separating freight-intensive corridors from routes with local or medium-duty traffic. Clustering was performed using the PARAFAC station mode scores. Silhouette analysis indicates a three-cluster (K = 3) k-means solution provided compact, well-separated clusters. The clusters are summarized as follows:

- Cluster 1: light loading (lower axle-load levels).
- Cluster 2: medium loading (intermediate axle-load levels).
- Cluster 3: heavy loading (heavier tandem/tridem axle-loads).

Geographically, heavy loading clusters align with the industrial and intermodal corridors, while light loading clusters were concentrated on rural and agricultural routes. For each cluster, seasonal axle-load spectra were generated by axle group. Mixture lognormal models ($R^2 > 0.94$) provided smooth, closed-form, non-negative distributions for tandem axle loads in Cluster 3 (heavy freight), as shown in Figure 2. Overall, the multiway clustering framework successfully captures regional and seasonal variations and yields cluster-specific, seasonal spectra suitable as traffic inputs for mechanistic-empirical pavement design, replacing the generalized statewide average.

4 Conclusion

This study developed a multiway clustering methodology for Illinois WIM data. PARAFAC decomposition was combined with multiple clustering techniques to group stations into distinct clusters. Each cluster was assigned to a seasonal probabilistic axle-load spectrum for front, single, tandem, and tridem axles. Results demonstrated that Illinois' traffic inputs cannot be adequately represented by a single statewide factor. Instead, cluster-based, seasonal spectra provide a practical and scalable improvement for mechanistic-empirical pavement design. Equivalent axle-load factors (EALFs) will be derived and will be proposed for included in the design approach.

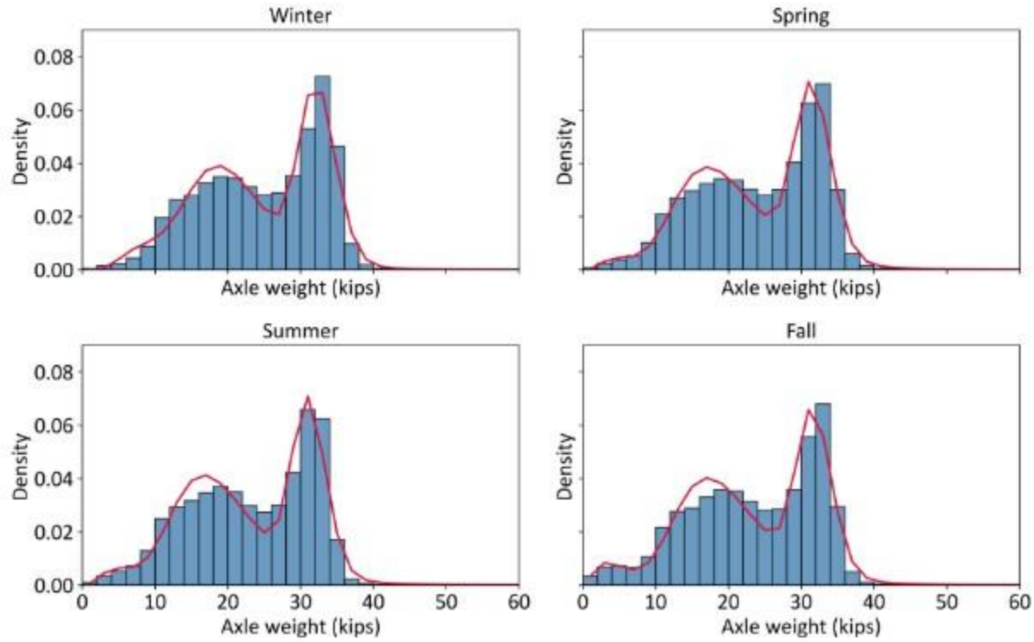

Figure 2: *Seasonal tandem axle load spectra for Cluster 3 (heavy freight).*

5 References

iQC, 2025. Traffic Data Quality Check System Operator’s Manual. Accessed February 12, 2025. https://vi2m.irdinc.com/documentation.

Li, Q., Wang, K. P., Eacker, M., & Zhang, Z. (2017). Clustering Methods for Truck Traffic Characterization in Pavement ME Design. ASCE-ASME Journal of Risk and Uncertainty in Engineering Systems, Part A: Civil Engineering, 3(2), F4016003. https://doi.org/10.1061/AJRUA6.0000881

Sayyady, F., Stone, J. R., Taylor, K. L., Jadoun, F. M., & Kim, Y. R. (2010). Clustering Analysis to Characterize Mechanistic–Empirical Pavement Design Guide Traffic Data in North Carolina. Transportation Research Record: Journal of the Transportation Research Board, 2160(1), 118–127. https://doi.org/10.3141/2160-13

VI2M, 2025 . VI2M Operator’s Manual. Accessed February 12, ://vi2m.irdinc.com/documentation.

Precision analyses of deflection measurements in FWD proficiency tests

José Neves
CERIS, Department of Civil Engineering, Architecture and Environment, Instituto Superior Técnico, Universidade de Lisboa, Avenida Rovisco Pais, 1049-001 Lisboa, Portugal

Abstract

The falling weight deflectometer (FWD) is one of the most widely used non-destructive tests for monitoring the bearing capacity of pavements. This simple and quick test measures the deflections on the pavement surface caused by the impact of the test load. These measurements allow for estimating the mechanical properties of the pavement layers and soil subgrade through a retro-analysis process. It is well known that deflection measurements significantly influence the quality of the analysis and could affect decision-making and pavement rehabilitation design. This paper describes a proficiency test scheme (PTS) conducted in 2023, involving four entities and three different equipment models. The PTS was performed on a flexible pavement, utilizing a methodology that enabled the analysis of precision in the deflections measured under various conditions of repeatability and reproducibility. Based on statistical analysis of the results, the paper presents values for the limits of repeatability and reproducibility of the deflections. In particular, the paper presents better reproducibility than that obtained in previous studies.

Keywords: FWD, precision, deflection, proficiency tests

1 Introduction

The falling weight deflectometer (FWD) is one of the most widely used non-destructive testing devices for evaluating the structural capacity of pavements. The quality of the deflection measurements obtained from FWD testing strongly influences the results of back-analysis procedures, as even small variations in deflection values may lead to significant differences in back-calculated layer moduli and, consequently, in engineering judgement. Neves and Cardoso (2017, 2019) investigated the precision and uncertainty of FWD deflection measurements through proficiency testing schemes (PTS) conducted in accordance with ISO/IEC 17043 on asphalt and concrete pavements. By comparing three FWD devices, those studies showed that, although individual equipment generally exhibits good repeatability, significant variability may occur in terms of reproducibility between devices from different manufacturers. Building on these findings and aiming to further examine the reproducibility of FWD measurements under field conditions, a new proficiency test was conducted in 2023, involving four entities and three different FWD equipment models on an asphalt pavement section. This paper presents the repeatability and reproducibility limits of FWD deflection measurements obtained from the 2023 proficiency test, evaluated using the statistical methodology defined in ISO 5725.

2 Methodology

The evaluation of FWD measurement precision was based on a PTS organised in accordance with ISO/IEC 17043. The FWD tests were conducted on 21 November 2023 on an asphalt pavement, following the procedures defined in ASTM D 4694. The main test configurations included a loading plate with a diameter of 300 mm and deflection sensors located at 0, 30, 45, 60, 90, 120, 150, 180, and 210 cm from the load centre. Each FWD device performed tests at four measurement locations. At each location, three target load levels (40, 65, and 90 kN) were applied sequentially, with a time interval of approximately five minutes between successive load applications. Three tests were repeated for each load level.

Figure 1 illustrates the four FWD units involved in the proficiency test. Table 1 summarises the main technical specifications of each device, namely the load range and the load pulse duration. With respect to deflection sensing systems, the Carl Bro PRI 2100 was equipped with seismometers, whereas the remaining devices employed geophones. The load cells and deflection sensors of all devices had been calibrated within the previous year. Air and pavement surface temperatures were monitored throughout the tests.

***Figure 1**: FWD equipment participating in PTS.*

3 Results and discussion

The statistical analysis of the collected deflection data was carried out in accordance with the ISO 5725 series, namely Parts 2 and 3, which define the accuracy (trueness and precision) of measurement methods. Neves and Cardoso (2017) derived the relationships for the repeatability and reproducibility limits shown in Figure 2 based on the PTS carried out in 2016. The analysis of the results obtained from the PTS conducted in 2023 made it possible to establish relationships of the same type, expressed as a function of the measured deflection and also presented in Figure 2. The repeatability limit is slightly higher and exhibits greater dispersion, whereas the reproducibility limit is significantly lower, despite also showing increased dispersion. Overall, the 2023 proficiency tests are highly beneficial, as they not only confirm previously identified trends but also yield results that are more acceptable and more representative of realistic conditions of FWD tests.

***Table 1**: Specifications of the FWD equipment.*

Equipment	Manufacturer and model	Load range (kN)	Load pulse time (milliseconds)
1	Dynatest FWD 8000	30 – 240	30
2	Dynatest HWD 8082	30 – 320	30
3	Carl Bro PRI 2100	7 – 250	20 – 30
4	Sweco Danmark PRIMAX 3500	7 – 120	20 – 30

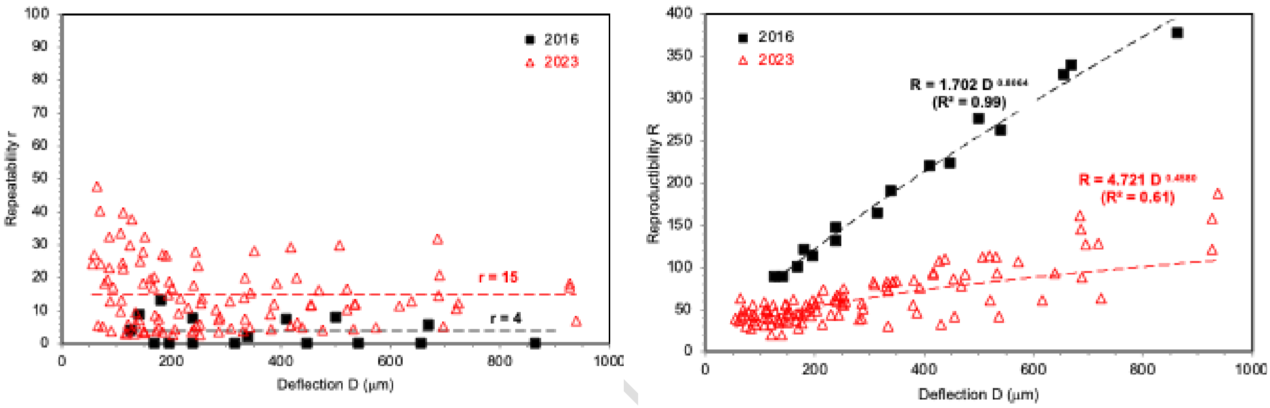

a) Repeatability limit

b) Reproducibility limit

***Figure 2**: Repeatability and reproducibility limits.*

4 Conclusions

The 2023 proficiency test confirmed reasonable repeatability of FWD deflection measurements and identified reproducibility between different devices as the main source of variability. The observed trends are consistent with previous studies and provide more realistic estimates of measurement precision, also reinforcing the importance of proficiency testing to support reliable pavement structural evaluation based on FWD tests.

5 References

ASTM D 4694. 2020. Standard Test Method for Deflections with a Falling-Weight-Type Impulse Load Device. ASTM International, US.

ISO 5725-2. 2025. Accuracy (trueness and precision) of measurement methods and results. Part 2: Basic method for the determination of repeatability and reproducibility of a standard measurement method. International Organization for Standardization, Switzerland.

ISO/IEC 17043. 2023. Conformity assessment – General requirements for proficiency testing. International Organization for Standardization, Switzerland.

Neves, J. & Cardoso, E. 2017. Uncertainty evaluation of deflection measurements from FWD tests on road pavements. Proceedings of the 7th International Conference on Engineering Surveying (INGEO 2017), Lisbon, Portugal, pp. 59-68, ISBN 978-972-49-2300-0.

Neves, J. & Cardoso, E. 2019. Influence of FWD uncertainty on back-calculated flexible pavement layer moduli. Proceedings of the GeoChina 2018, Z. Hossain et al. (eds.), Solving Pavement and Construction Materials Problems with Innovative and Cutting-Edge Technologies, Sustainable Civil Infrastructures, pp. 153-163 https://doi.org/10.1007/978-3-319-95792-0_13.

Impact of Moisture Content on Light Weight Deflectometer (LWD) Response for Quality Control of Compacted Subgrade & Base Material

Xiaogang Guo
Mansour Solaimanian
Larson Transportation Institute, Pennsylvania State University, University Park, PA 16802, USA

Abstract

The Light Weight Deflectometer (LWD) is widely used to evaluate the stiffness of subbase and base layers in the field. However, its measurements are significantly influenced by moisture content (MC), which may reduce the reliability of the results. This study aimed to investigate the effect of MC on LWD responses using small-scale laboratory testing and to establish relationships among MC, dry density, and the elastic modulus (ELWD) measured by LWD.

Five representative materials—2A, 2RC, open-graded aggregate, AASHTO A-4 soil, and AASHTO A-6 soil—were tested at four moisture levels. Specimens were compacted in 150-mm molds in accordance with AASHTO T 99 / AASHTO T 180, and deflections were measured using LWD. Gradation characteristics, moisture–density relationships, and LWD results were analyzed. Statistical methods were applied to evaluate the sensitivity of ELWD to variations in moisture content.

The results indicate that fine-grained soils exhibit complex, nonlinear behavior with changing MC, whereas coarse-grained materials are less sensitive to moisture content. Stiffness generally reaches its maximum at the optimum moisture content, although exceptions exist, particularly for silty soils. Results indicate that laboratory LWD testing provides valuable insights into soil behavior and compaction quality, serving as a practical tool for improving quality control protocols in the field.

Keywords: LWD; moisture content; soil stiffness; Proctor mold; compaction quality; soil types

1 Introduction

The Light Weight Deflectometer (LWD) is a widely used non-destructive testing device for evaluating the in-situ stiffness of compacted subgrade soils and base materials (Schwartz et al., 2021). Its portability, rapid testing capabilities, and relatively simple operation make it ideal for on-site quality control/quality assurance during pavement construction. However, despite its growing adoption in both research and practice, LWD measurements are significantly affected by the moisture content (MC) of the tested material, particularly in fine-grained or cohesive soils (Hossain and Apeagyei, 2010). Variations in moisture content can alter soil structure, suction, and pore pressure conditions, which in turn influence the stiffness and deformation behaviour of compacted layers (Sotelo et al., 2014).

This study was undertaken to investigate the influence of varying moisture contents on LWD responses through controlled laboratory-scale testing. The primary objective was to establish reliable correlations between MC, dry density, and the LWD-derived elastic modulus (ELWD), in order to provide a scientific basis for interpreting LWD results and improving compaction quality control protocols in the field. Ultimately, the findings are expected to support the development of performance-based specifications for subgrade and base compaction and construction.

2 Methods

Five commonly used subgrade and base materials were selected for testing. These materials were designated as 2A aggregate (well-graded crushed stone), 2RC recycled aggregate, Open Graded Stone (OGS), AASHTO A-4 soil (silty soil), and AASHTO A-6 soil (clayey soil). Each material was tested at four distinct moisture content levels. The specimens were compacted in a Proctor mold in accordance with AASHTO Test Standards T 99-11 and T 180-11. Gradation characteristics of the materials were documented, and dry density–moisture content relationships were established. An LWD device was employed to conduct deflection tests on the surface of each compacted specimen according to ASTM E2583-07. This LWD has a geophone as central transducer to capture velocity. Although the device supports two external geophones via an extended arm, this research focused solely on the central geophone. Size gradation of all five tested materials were documented through sieve analysis, showing a wide range of particle size distributions from well-graded to open-graded structures (Figure 1). For each compaction condition, corresponding moisture content, dry density, and LWD-measured modulus (ELWD) were systematically recorded. These parameters enabled the establishment of dry density–moisture–modulus relationships and the identification of material-specific trends. Comparative plotting was applied to evaluate the sensitivity of ELWD to moisture variation across different soil types.

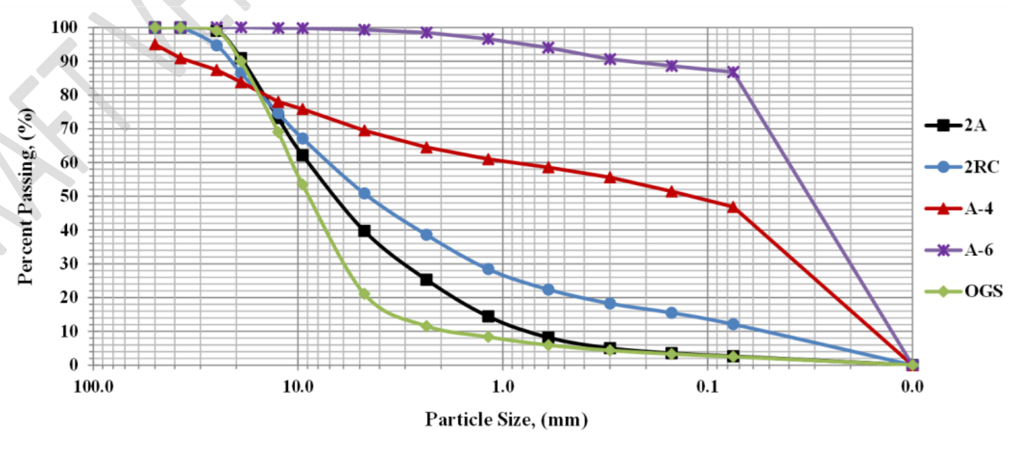

Figure 1*: Example of Gradation for 2A, 2RC, A-4, A-6 and OGS materials.*

3 Results and Discussion

The test results highlight the relationships between moisture content, dry density, and LWD responses for various soil types. As shown in Figure 2, the dry density of all tested materials followed typical compaction behavior, increasing with moisture up to the Optimum Moisture Content (OMC), then declining beyond that point. Figure 3 illustrates the corresponding LWD deflection values, which generally decreased as dry density increased, reflecting higher stiffness at OMC. However, the degree of sensitivity to moisture content varied substantially among different materials:

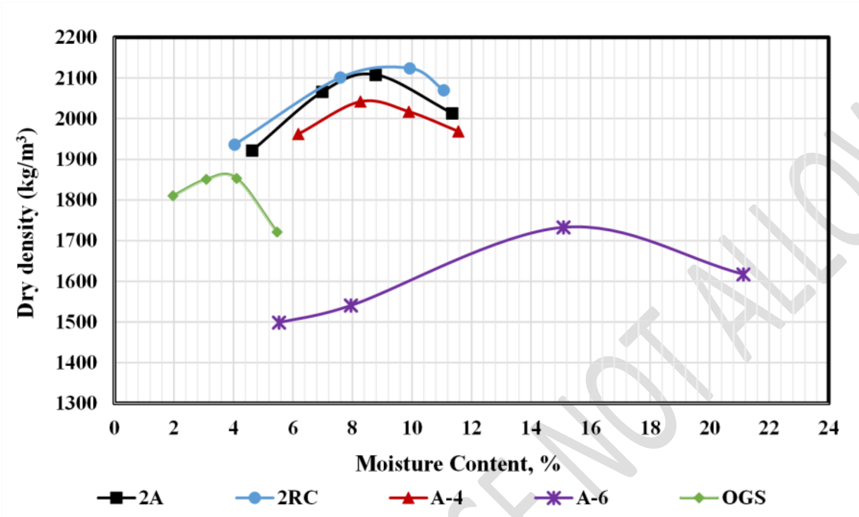

Figure 2: *Variation of dry density with moisture content for different soils.*

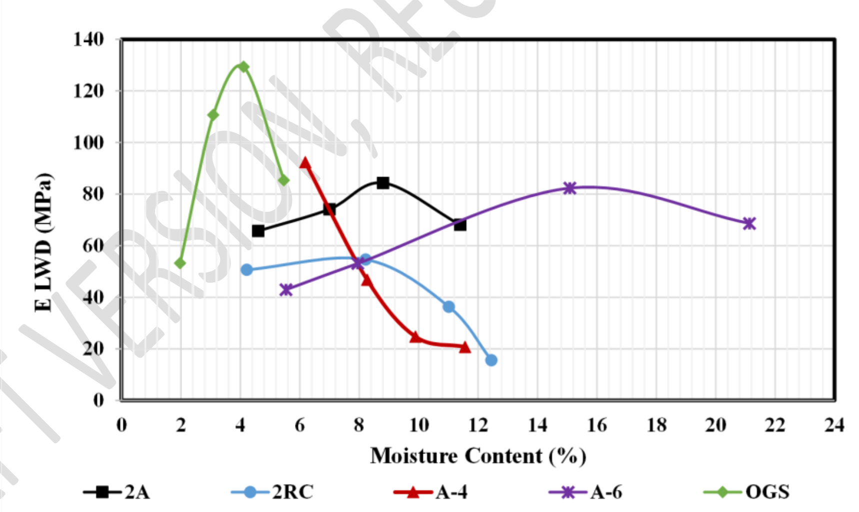

Figure 3: *LWD Deflection Values Measured on Proctor Mold Samples at Different Moisture Contents.*

– Fine-Grained Soils (e.g., A-6) exhibit complex responses to changes in moisture content. As moisture increases, the deflection response may initially increase due to reduced stiffness. However, at very high moisture levels, the deflection decreases slightly, indicating a non-linear relationship influenced by factors such as pore pressure.
– Coarse-Grained Soils (e.g., 2A and Open Graded Stone) are less sensitive to moisture content variations. The deflection response remains relatively stable across different moisture levels, indicating that their stiffness is less affected by moisture changes compared to finer soils.
– At optimum moisture content (OMC), soils generally achieve their maximum dry density, which corresponds to the highest stiffness and lowest deflection in LWD measurements. However, for some soils

like A-4, as indicated by LWD test response, the soil modulus may continue to decrease even when the moisture content is increased to the OMC level. This phenomenon is believed to be due to the dominance of moisture-induced softening over density-induced stiffening.

- Correlation Establishment: Small-Scale Laboratory LWD Tests help link the measured deflection response to the soil conditions and the quality of compaction, offering practical insights for field assessments. The results indicate that LWD tests in the Proctor mold can aid in developing standards for quality control in construction.

These observations emphasize the importance of considering both soil type and moisture condition when interpreting LWD measurements. While coarse materials may tolerate a wider moisture range during compaction, fine or intermediate soils require closer control to ensure consistent stiffness. In summary, moisture content has a material-dependent influence on LWD responses. Fine-grained soils are highly sensitive and show non-linear behavior, whereas coarse aggregates respond more consistently. Understanding these trends can help guide field compaction practices and improve the interpretation of LWD test results under varying moisture conditions.

4 Conclusions

The study highlights the critical role of moisture content in LWD measurements. By establishing correlations between LWD measurements and soil conditions, the study provides a foundation for optimizing field testing protocols and improving the accuracy of in-situ soil property evaluations. The findings underscore the potential of using LWD tests in the Proctor mold to establish standards or protocols for quality control in construction conditions. The study indicated that using deflection as the criterion for quality control of compaction is viable, as it is a direct and tangible response from the LWD device.

5 Acknowledgements

This work was conducted as part of a research study sponsored by Pennsylvania Department of Transportation.

6 References

American Association of State Highway and Transportation Officials. 2011. Standard Methods of Test for Moisture–Density Relations of Soils (T 99/T 180). Washington, DC: AASHTO.

ASTM International. 2020. ASTM E2583-07(2020): Standard Test Method for Measuring Deflections Using a Portable Impulse Plate Load Test Device. West Conshohocken, PA: ASTM International.

Schwartz, C., Zhang, X., Siddiki, N., & Dawson, A. 2021, September 29. Ensuring Construction Quality Assurance with Light Weight Deflectometers [Webinar]. Transportation Research Board, National Academies of Sciences, Engineering, and Medicine. https://www.trb.org/

Hossain, M. S., & Apeagyei, A. K. 2010. Evaluation of the Lightweight Deflectometer for In-situ Determination of Pavement Layer Moduli (VTRC 10-R17). Charlottesville, VA: Virginia Transportation Research Council. https://rosap.ntl.bts.gov/view/dot/19407

Sotelo, M. J., Mazari, M., Garibay, J., & Nazarian, S. 2014. Variability of Moisture Content Measurement Devices on Subgrade Soils. In Geo-Congress 2014: Geo-characterization and Modeling for Sustainability (pp. xxx–xxx). Reston, VA: American Society of Civil Engineers. https://doi.org/10.1061/9780784413272

Sensitivity evaluation of temperature correction techniques for TSD data

Ramez Hajj
Department of Civil and Environmental Engineering, The Grainger College of Engineering, University of Illinois Urbana-Champaign, USA

Abstract

The Traffic Speed Deflectometer (TSD) is an important technology being widely deployed for structural testing of pavements. One issue when it comes to implementing this technology, however, is the requirement to correct the results for temperature. While several procedures have been developed and utilized, it is unclear how sensitive these temperature models are to different factors. This study explores two case studies in terms of effects on TSD results, one at a temperature relatively close to the reference and one at a very high surface temperature, on similar pavement sections on the same road. The findings indicate that TSD testing at high temperatures can yield unrealistic modulus values when shifted to a reference temperature. Furthermore, the findings indicated that speed does have a substantial effect, especially at higher temperatures, but that this will not change the analysis much if the speed is reasonably close to the reference.

Keywords: traffic speed deflectometer (TSD); pavement structural testing; temperature correction; nondestructive pavement evaluation

1 Introduction

Traffic Speed Deflection Devices (TSDDs) represent an important advancement in the art of pavement structural evaluation. The idea of these devices is straightforward; they can measure pavement deflections due to an applied tire load while moving at traffic speed, allowing for comprehensive analysis of pavement structural condition at the network level. This is a substantial advancement over Falling Weight Deflectometer (FWD) technologies, which are restricted to stationary loads and therefore cannot be used for network-level assessment. Over the past decade and a half, several TSDDs have been developed (Katicha et al., 2022), with one known as the Traffic Speed Deflectometer (TSD) becoming prominent. The TSD utilizes doppler laser measurements when the load is applied, for which the velocities can be integrated to convert them to pavement deflections. However, one of the key issues remaining when it comes to analysis of TSD data is the lack of data at multiple temperatures. Since the TSD passes over a pavement section quickly, there is not multiple temperature data, which limits its application in pavement management systems (PMS). However, some researchers have developed methods to correct the pavement temperatures to a reference temperature. The present study identifies some of these methods and compares them with respect to a data set from TSD measurements recently collected in Illinois, USA.

2 Temperature models

This paper evaluates several temperature models in the existing literature. The models selected are briefly described below. One very simply model is the stiffness adjustment model (Rada et al., 2016; Nasimifar et al., 2020). This method uses an empirical function to compute strain at the bottom of the asphalt layer based on the surface curvature index (SCI) reported by the TSD. The second method studied herein is the work of Zhang et al. (2023), who proposed a method for both speed and temperature correction of TSD data based on the Arrhenius equation. Since these models require the pavement temperature at mid-depth, the BELLS3 equation was used for computing the mid-depth pavement temperature (Equation 1). In Equation 1, T_d is the temperature at a specific depth, IR is the pavement surface temperature, d is the depth at which temperature is computed, 1day is the average air temperature the day before testing, and h_{18} is the time of the measurements during the day.

$$T_d = 0.95 + 0.892 * IR + (\log(d) - 1.25)(-0.448 * IR + 0.621 * 1day + 1.83 * \sin(h_{18} - 15.5)) + .042 * IR * \sin(h_{18} - 13.5) \quad (1)$$

3 Data

The data used in this study was collected using a TSD on Interstate 57 in Champaign County and Coles County in Illinois. Two datasets which were collected on separate dates were selected to capture a wide range of temperature conditions. The first date was a relatively cold day for pavement structural testing, with surface temperatures around 11°C. The second date was much warmer with surface temperatures around 40°C. These two datasets were selected because the first represents mid-depth pavement temperatures very close to the selected reference temperature of 20°C, while the second represents a major need for correction due to the very high temperature at collection. However, it was notable that deflections were not too different in the two sections, likely due to the very thick pavement design which involves a full-depth asphalt layer of 40.6 cm. Data points with missing values were in some cases removed from the analysis. Further information about the sections can be found in Table 1. For the Zhang et al. (2023) method, reference speed was 88.5 kph while the actual speed was higher in both cases.

4 Results and Discussion

A sample of the results are shown in Table 1. The back-calculated moduli values are much higher, when temperature-adjusted, for very similar sections simply as an artifact of the test temperature. It should also be noted that values of 23 GPa for modulus of asphalt concrete are not reasonable. Therefore, it is recommended not to perform structural testing at such high temperatures for very thick pavements, where deflections will still be low and outside reasonable bounds for approximation. With respect to speed, it is interesting that adjusting for speed had a non-negligible impact, even though the difference from the reference speed was less than 10 kph.

***Table 1**: Sections and results.*

Parameter	Champaign County	Coles County
Surface temperature	11.6℃	44.1℃
Number of data points	761	399
Testing time	10:00	16:45
Back-calculated temperature-adjusted modulus (Rada et al., 2016 method)	7864 MPa	23650 MPa
Back-calculated temperature-adjusted modulus (Temperature/speed correction from Zhang et al., 2023 method)	7723 MPa	23041 MPa

5 Conclusions

This study examined several methods for computing pavement temperature adjusted modulus from TSD results and presented the results of two of them herein. For these two methods, it was clear that speed does have some impact on the back-calculated modulus, although it is limited for speeds relatively close to a reference speed of 55 kph. It was also further concluded that it is not advisable to perform very large temperature adjustments for thick pavements tested at high temperatures. This is because these measurements will still result in low deflections and will lead to exceptionally high computed moduli which are not realistic.

6 Acknowledgement

This publication is based on the results of ICT-R27-SP75, Development of Pavement Temperature Measurement System for ICART. ICT-R27-SP75 was conducted in cooperation with the Illinois Department of Transportation and Illinois Center for Transportation. The contributions of the technical review panel are acknowledged. The contents do not reflect the official views or policies of the Illinois Department of Transportation or Illinois Center for Transportation.

7 References

Katicha, S., Flintsch, G., & Diefenderfer, B. (2022). Ten years of traffic speed deflectometer research in the United States: a review. *Transportation research record*, *2676*(12), 152-165.

Nasimifar, M., Chaudhari, S., Thyagarajan, S., & Sivaneswaran, N. (2020). Temperature adjustment of surface curvature index from traffic speed deflectometer measurements. *International Journal of Pavement Engineering*, *21*(11), 1408-1418.

Rada, G. R., Nazarian, S., Visintine, B. A., Siddharthan, R. V., & Thyagarajan, S. (2016). *Pavement structural evaluation at the network level* (No. FHWA-HRT-15-074). United States. Department of Transportation. Federal Highway Administration. Office of Infrastructure Research and Development.

Knowledge from the evaluation of visco-elastic behaviour of asphalt pavements

Zsolt Boros
Filip Buček
prof. Jozef Komačka
TPA Society for Quality Assurance and Innovation, member of STRABAG concern, Slovakia

Abstract

The paper describes the results of evaluation of visco-elastic behaviour of pavements based on the time delay of central deflection behind the applied force, which was determined from FWD deflectometer measurements. The time delay values are presented for different temperature conditions and intensity of traffic load. Using evaluations of measurements made during the construction of a pavement, it was found, the time delay of previously constructed portion of pavement changes after the addition of asphalt layers. The measurements on an experimental section confirmed that time delay values are influenced by duration of loading impulse. Next findings are that temperature and repeated loading (fatigue) does not have a significant effect on time delays. This was also confirmed by results determined from 11 years of measurements on five long-term monitored sections of Slovak road network.

Keywords: FWD; time; history; pavement; deflection; phase; angle; temperature; fatigue

1 Introduction

Asphalt layers of pavements must be able to withstand impacts of vehicle loading under variable climatic conditions. Therefore, the combined effect of these factors must be considered when designing the asphalt mix for the relevant pavement layer and the design of the asphalt mix must be done in such a way as to avoid undesirable damage to the layer and to the entire pavement.

The suitability of an asphalt mix for a given location is usually demonstrated by its properties under two contrasting temperature conditions (low winter and high summer temperatures). These properties are dominantly influenced by parameters of bitumen as one of the asphalt mixture components. The selection of a suitable bitumen is very important and is emphasized in various asphalt mix design methods (AASHTO, 2017; Asphalt Institute, 2003; Hunter et al., 2015). The aim is to prevent two main types of damage to asphalt pavements, namely low temperature cracking (Mugume and Kakoto, 2020) and permanent deformations (rutting) occurring at high temperatures of asphalt mixtures in summer.

One of approaches used to verify the suitability of bitumen in terms of the resistance of asphalt mixture to permanent deformation is based on the evaluation of complex shear modulus and phase angle resulting from tests in a dynamic shear rheometer. The phase angle, determined from the time delay between an applied force and resultant deformation of test specimen, is considered as a parameter representing the visco-elastic behaviour of bitumen. Together with the complex shear modulus, it allows to distinguish the susceptibility of bitumen to plastic (permanent) deformation.

Phase angle and complex modulus are used not only in the evaluation of the viscoelastic behaviour of bitumen but also of asphalt mixtures. These parameters are determined using different test methods (uniaxial or triaxial tests on cylindrical specimens or stiffness and fatigue tests on specimens of different shapes). The values of the complex modulus and phase angle vary depending on the frequency of loading and test temperature. Research results indicate that phase angle values increase with increasing temperature or decreasing frequency. However, in the research (Clyne et al., 2003), it was shown that at 40°C and 54°C, the value of phase angle decreased with increasing temperature.

In laboratory tests focused on determining parameters characterizing visco-elastic behaviour, test specimens form asphalt mixtures are tested separately, which does not correspond to real conditions in a pavement when all asphalt layers interact. In addition, in a pavement, asphalt layers are supported by subbase layers and subgrade. Also, the load generated by wheel(s) of passing vehicles creates a stress condition that differs from that used in laboratory tests. Considering this, a question is what behaviour of whole asphalt pavement is and what is an influence of visco-elastic behaviour of asphalt layers on behaviour of whole pavement.

To investigate (verify) this issue, a phase angle is a crucial input. To get it, a pavement load test enabling continuous record of load force and pavement response (deflections of pavement surface) in the same time axis is inevitable. This type of test is made possible by Falling Weight Deflectometers (FWD). Therefore, these devices were used to perform diagnostics of different pavement structures (pavement in different stages of construction, pavements in service). Time delays between peaks of load force and central deflection (the main factor predetermining the value of phase angle) were analysed and used to determine an effect of:

a) asphalt layers on visco-elastic behaviour of whole pavement (change in the visco-elastic behaviour of pavement after asphalt layers have been constructed/added);
b) loading impulse duration (comparison of FWD KUAB and Dynatest measurements);
c) asphalt layers temperature and repeated loading (fatigue).

2 Change in time delay of peak of force and deflection after asphalt overlays

Measurements for this purpose were carried out on a semi-rigid pavement composed of three asphalt layers with a total thickness of 200 mm (40 mm SMA 11 PMB 45/80-75, 60 mm AC 16 PMB 25/55-65, 100 mm AC

22 35/50), lying on a 200 mm cement bound course (CBGM). Beneath this was the subgrade, the top 400 mm of which was treated/improved by addition of lime.

Measurements were taken using a FWD KUAB deflectometer after two phases of pavement construction:

a) on the CBGM layer 7 days after its placement (applied loading forces of 25 kN and 50 kN);
b) on the wearing course 3 months after laying the CBGM layer (loading force of 50 kN applied).

Based on the time delays between the peak of central deflection and the peak of applied force for the measurements in both stages (Figure 1), it can be noted that there is a difference in the values along the length of the section, namely between the measurements on the CBGM layer at 25 kN and 50 kN forces, and also a difference between the measurements on the CBGM layer and the asphalt wearing course.

The largest time delays for the measurements on asphalt wearing course can be considered as a manifestation of the influence of the visco-elastic behaviour of asphalt layers on the overall behaviour of asphalt pavement. The differences (about 1 - 1.5 ms when compared to the measurements on the CBGM layer) imply a difference in phase angles of about 4 - 6 degrees (assuming an average FWD KUAB loading time of 45 ms), while the phase angle of the whole asphalt pavement for an average time delay value of 5 ms is 20 degrees (according to the relation given in (Biligiri et al., 2010) for a loading impulse in the shape of a half-sinusoid - similar to the shape of loading impulse of FWD deflectometer). This value corresponds to the equivalent frequency of FWD Kuab loading impulse (according to Ligang, 2011 it is 10 - 15 Hz) and the average temperature of asphalt layers at time of measurement (13 - 15 °C). When compared with the phase angle values determined for these boundary conditions by laboratory tests (19 - 24° according to Clyne et al. (2003) and Ambassa (2013)); 10 - 16° according to Guo et al. (2021) and Xu and Solaimanian (2009)), a relatively good agreement can be stated.

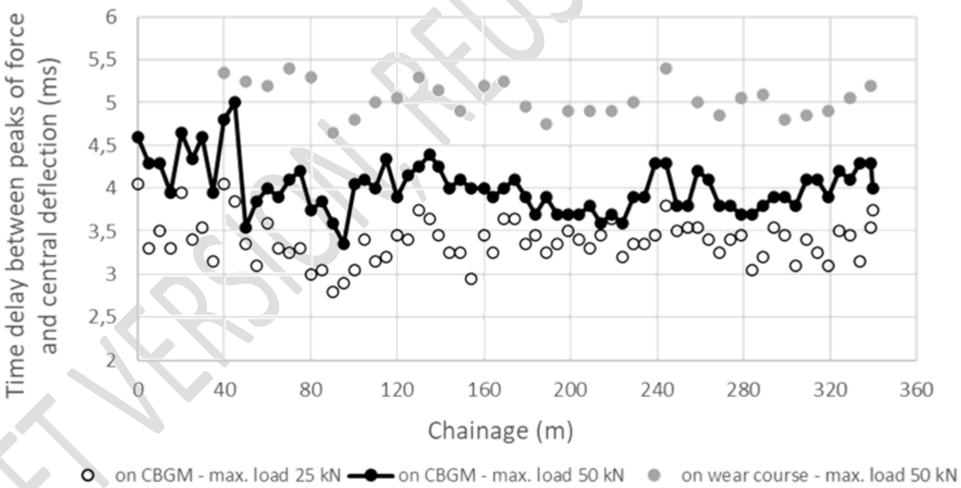

Figure 1: *Time delays of peaks of force and central deflection at different construction stages of pavement.*

3 Effect of temperature and fatigue at different loading impulse duration

The pavement of the 300 m long road section was tested with FWD KUAB and Dynatest deflectometers, which have different loading impulse duration (approx. 45 ms vs. 25 ms respectively). In the longitudinal and transverse directions, there was a slight difference in the position of tested points for all measurements (even when measured with the same FWD during repeated measurements within a day).

Since the section has been in operation for many years and the heavy vehicles intensity is relatively high (more than 5500 HV/24 h), measurements with both deflectometers were made in the right wheel track of passing vehicles and between the wheel tracks to evaluate the effect of long-term loading (fatigue).

In each trace, measurements were taken three times per day at different asphalt pavement surface temperatures (Table 1). It allows to monitor the effect of temperature of asphalt layers. The spacing of the deflectometers during the measurements within a given time interval was kept to a minimum so that the measurements at a given point were taken at the same temperature.

Table 1: *Measurement intervals and pavement surface temperature.*

Position	Right wheel track			Between the wheel tracks		
Time	7.00-8.00	10.00-11.00	13.00-14.00	8.00 - 8.30	11.00-11.30	14.00-14.30
Temperature of pavement surface	20 - 22 °C	28 - 31 °C	34 - 40 °C	23 - 27 °C	30 - 33 °C	37 - 42 °C

The time delay of the deflection peak behind the force peak was greater for the KUAB deflectometer measurements (Figure 2). The differences in the delays were approximately the same for measurements at all time intervals and for both measured traces (Figure 3), with coefficient of variation values well below the 0.3-0.35 value that is usually considered as the boundary between homogeneous and inhomogeneous sets of values.

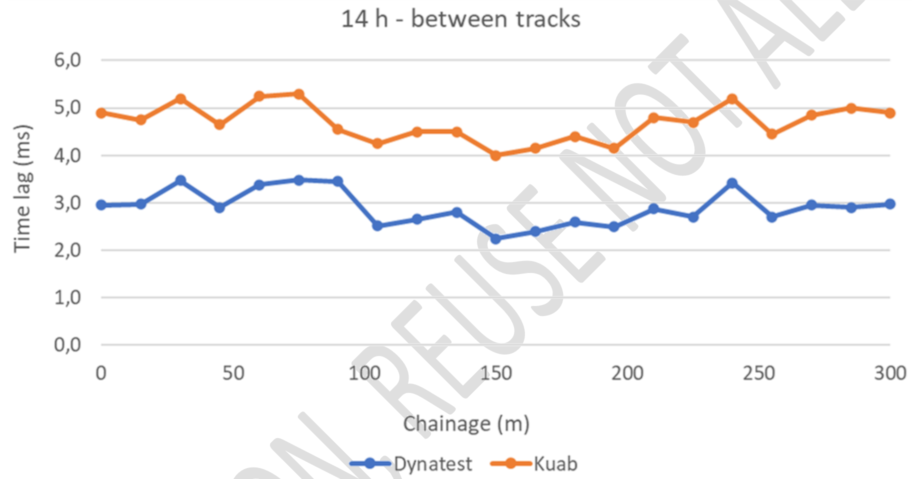

Figure 2: *Differences in time delays for FWD KUAB and Dynatest measurements.*

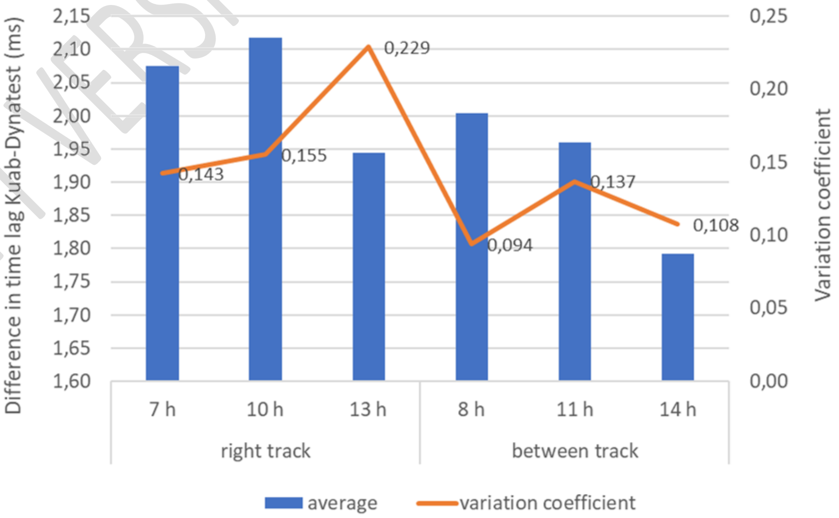

Figure 3: *Variability in time delays for FWD KUAB and Dynatest measurements.*

Based on the evaluations of the measurements, it can be concluded that the shorter duration of the Dynatest loading impulse (i.e. the higher frequency of the loading impulse) results in a shorter time delay of the peak values of force and deflection - a more elastic behaviour of tested pavement.

The different asphalt layer temperatures during the intraday measurements were not reflected in the time delay values. They were approximately the same at each measurement time (Figure 4), although the average asphalt layer temperatures determined according to (TP 031, 2009) were in the range of 22-31 °C (right wheel track at the beginning of the section) and 26-38 °C (between the wheel tracks at the end of the section). This contradicts the knowledge of the effect of temperature on the phase angle values (at the same loading frequency, it is essentially an effect on the change in the time delay between the applied force and the resultant deformation) resulting from laboratory tests of asphalt mixtures.

Figure 4 also demonstrates that for both deflectometers, the time delays between the peaks of load force and central deflections are in the same range in the right wheel track and between wheel tracks. This means that repeated road loading (fatigue) has no effect on the change in time delay values. The same conclusions follow from laboratory fatigue tests of asphalt mixtures (the time delay between the applied force and the resultant deformation is almost constant during testing of a single specimen at a given frequency and temperature).

Figure 4: *Effect of temperature and fatigue on time delays in KUAB and Dynatest FWD measurements.*

The influence of temperature and repeated loading was also evaluated using periodic measurements by FWD KUAB, which the Slovak Road Administration has been carrying out on long-term monitored sections since 2005. The values of the time delay between the peaks of load and central deflection for five sections with different geographical location and climatic conditions (Figure 5) confirm the above-mentioned findings resulting from the measurements on the 300 m long road section.

The time delay values on the individual sections do not vary with the average temperature of the asphalt layers but stay in a narrow range (about 0.5 ms). With an average FWD KUAB loading impulse duration of 45 ms, this implies a difference in phase angles of up to 2 degrees. This is a significant difference compared to the temperature effect when visco-elastic behaviour is tested in a laboratory on asphalt mix specimens.

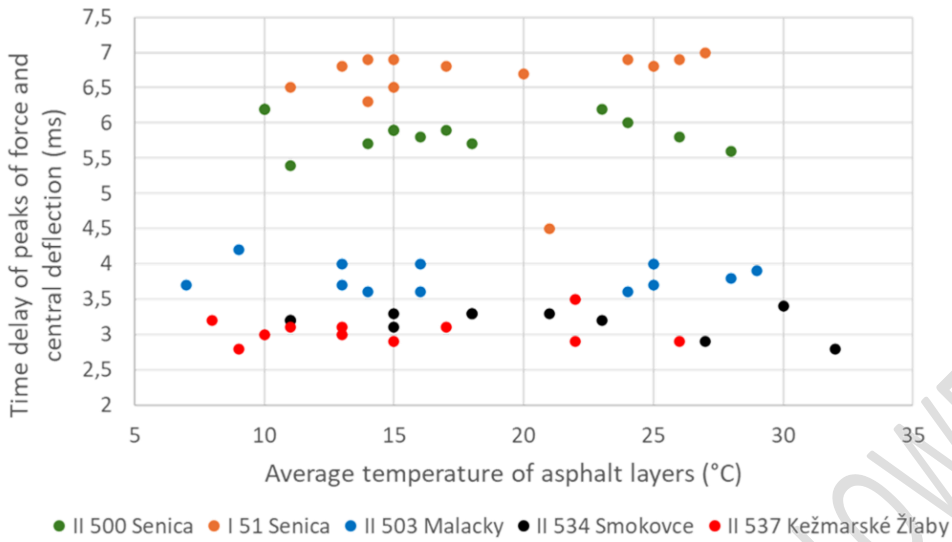

Figure 5: *Time delays on long term monitored sections.*

The time delays in Figure 5 are determined from measurements between 2010 and 2021 (Boros et al., 2022). During the 11 years of operation, there has not been a significant change in the time delays on any section. Thus, it can be concluded that fatigue of asphalt pavements due to repeated loading by wheels of passing vehicles does not affect the change in the visco-elastic behaviour of asphalt pavements.

Figure 5 also shows the difference in the values of time delays one individual sections. As there are no changes in the time delays because of repeated loading or the effect of temperature of asphalt layers, it can be considered that each pavement has its own characteristics of visco-elastic behaviour, which are determined by its composition and the properties of its layers, and which it maintains from the time of its construction throughout its service life. Thus, different pavement structures have different visco-elastic behaviour, which can affect the rate of damage. For the pavements in Figure 5, the maximum difference in time delays between pavements is about 3.5 ms (II/537 and I/51). For the same duration of the FWD KUAB loading impulse (45 ms), this implies a difference in phase angle values up to 14 degrees. Such a difference is considered significant when comparing and evaluating the visco-elastic behaviour of asphalt mixtures.

4 Conclusions

Evaluations of measurements focused on monitoring the visco-elastic behaviour of asphalt pavements revealed the following findings:

- As the visco-elastic behaviour of hydraulically bound materials (in this case, CBGM layer) should not be temperature-dependent, the larger time delay of peaks of load force and central deflection observed in measurements on top asphalt layer (compared to the measurements on the CBGM layer) should reflect the more viscous behaviour of asphalt mixtures, which predominantly predicts visco-elastic behaviour of asphalt pavement;
- The duration of loading impulse affects the time delay of peaks of load force and central deflection (shorter duration of loading impulse (i.e. the higher frequency of loading impulse) results in a shorter time delay of peak values of force and central deflection - a more elastic behaviour of tested pavement); this gives a possibility to suggest that visco-elastic behaviour of asphalt pavements will be different at different moving vehicle speeds;
- Temperature and repeated loading (fatigue) of asphalt layers does not have a significant effect on time delays characterizing the visco-elastic behaviour of asphalt pavements;
- Each pavement has its own visco-elastic behaviour characteristics, which it maintains from the time of construction throughout its service life;

- Different pavement structures have different visco-elastic behaviour, and the differences can be significant;
- Based on time delays between the peak of load force and central deflection and the assumed average loading impulse time of KUAB deflectometer (45 ms), the phase angles values of the tested pavements ranged from 12° to 28°, which corresponds to the ranges found in the laboratory tests of the asphalt mixtures.

Time delay of peaks of load force and deflections is usually ignored in procedures commonly used to evaluate the bearing capacity of asphalt pavements (including back-calculation procedures). In principle, this does not affect the results of the calculations, as determined values are of the nature of a complex modulus that includes both elastic and plastic constituent. The differences in time delays of peaks (predetermining value of phase angle) indicate only differences in the proportional distribution of the constituents of complex modulus. This is useful in estimating the resistance of a given pavement to cracking and permanent deformation (rutting).

5 References

AASHTO M 320, 2017. Standard Specification for Performance-Graded Asphalt Binder. Washington, DC: American Association of State Highways and Transportation Officials.

Asphalt Institute, 2003. Superpave performance graded asphalt binder specification and testing: Superpave series No.1 (Third Revision). Asphalt Institute.

Hunter, R. N., Self, A. & Read, J. 2015. London. The Shell Bitumen Handbook (Sixth edition). ICE Publishing.

Mugume, R. & Kakoto, D., 2020. Effect of Inappropriate Binder Grade Selection on Initiation of Asphalt Pavement Cracking. Sustainability 2020, 12(15), 6099, doi.org/10.3390/su12156099.

Boros, Z., Komačka, J., 2022. Indication of viscoelastic behaviour of asphalt pavements using FWD time history data. Bearing capacity of roads, railways and airfields. Trondheim, CRC Press/Balkema, Volume III, pp. 45-53. ISBN 978-1-032-12044-7, DOI: 10.1201/9781003222880.

Biligiri, K. P., Kaloush, K. & Uzan, J. 2010. Evaluation of asphalt mixtures' viscoelastic properties using phase angle relationships. International Journal of Pavement Engineering, 11(2), 143–152. doi:10.1080/10298430903033354

Ligang L. 2011. Backcalculation of asphalt concrete complex modulus curve by layered viscoelastic solution. Dissertation thesis. Michigan State University, 2011. ISBN 978112459700311245970OX. doi.org/doi:10.25335/rbfr-0g22.

Clyne, T.R., Li, X., Marasteanu, M.O. & Skok, E.L. 2003. Dynamic and resilient modulus of MN/DOT asphalt mixtures. Report MN/RC – 2003-09. University of Minnesota. 2003.

Ambassa, Z. 2013. Vers la modélisation du comportement a la fatigue des chaussées bitumineuses routieres sous chargement réel. PhD thesis. Université de Limoges. 2013.

Guo, L., Xu, Q., Zeng, G., Wu, W., Zhou, M., Yan, X., Zhang, X. & Wei, J. 2021. Comparative Study on Complex Modulus and Dynamic Modulus of High-Modulus Asphalt Mixture. Coatings 2021, 11, 1502. https://doi.org/10.3390/coatings11121502.

Xu, Q. & Solaimanian, M. 2009. Modelling linear viscoelastic properties of asphalt concrete by the Huet–Sayegh model. International Journal of Pavement Engineering, 2009, vol. 10, No. 6, pp. 401-422.

TP 031 (1/2009) Measurements and evaluation of asphalt pavements bearing capacity by FWD KUAB. Technical conditions. MDPT SR, 2009 (in Slovak).

Boros, Z., Dancs, N. Buček, F. & Benkó, Z. 2022. Software application for long-term monitoring and assessment of pavement serviceability and performance in Slovakia. The 9th symposium on pavement surface characteristics. Milano.

Global Initiatives to Advance Comprehensive Pavement Assessment

Jerry Daleiden
ARRB Systems

Abstract

Technologies for more efficient structural assessment are changing the way Agencies evaluate pavements. Agencies are now actively seeking more effective means for incorporating this data into their decision-making process. These advancements have brought about a greater awareness of the true resource needs for better managing infrastructure in a proactive manner, while significantly reducing the costs for gathering the data needed. Having a more comprehensive assessment, incorporating both surface and structural data (collected simultaneously), enables road asset managers to better understand the true condition of their network. Road agencies around the world are now using these tools to more efficiently collect the desired pavement performance properties.

Combining pavement structural and surface data, enables the identification and cause of pavement deterioration, providing a powerful tool, in managing pavement condition and providing a solid background for robust infrastructure maintenance strategies. The unique capability of continuous high accuracy and high-resolution data enables infrastructure managers to pinpoint areas of concern and initiate identification of remediation needs.

This presentation will highlight some of the initiatives currently underway to advance the application of these comprehensive pavement assessments, including QA/QC, standards development, system wide assessments, project treatment design, airfield testing

1 Introduction

Technologies for more efficient structural assessment are changing the way Agencies evaluate pavements. Transportation Agencies are shifting from sampled surface assessments to very detailed functional and structural assessments, collected continuously, and at traffic speeds. In addition to the efficiency and safety considerations, these more detailed assessments provide for a better understanding of the variability of condition, as well as treatment needs.

These advancements have brought about a greater awareness of the true resource needs for better managing infrastructure in a proactive manner, while significantly reducing the costs for gathering the data needed. Having a more comprehensive assessment, incorporating both surface and structural data (collected simultaneously), enables road asset managers to better understand the true condition of their network. Road agencies around the world are now using these tools to more efficiently collect the desired pavement performance properties.

Combining pavement structural and surface data, enables the identification and cause of pavement deterioration, providing a powerful tool, in managing pavement condition and providing a solid background for robust infrastructure maintenance strategies. The unique capability of continuous high accuracy and high-resolution data enables infrastructure managers to pinpoint areas of concern and initiate identification of remediation needs.

While Agencies are eager to apply these improved assessments, they must address how best to manage the increased volume of data, and complexities of the inherent variability documented with such capabilities. This presentation is intended to highlight some of the initiatives currently underway to support this implementation process.

2 Quality Assurance & Quality Control

As Agencies increasingly seek to contract for collection of the comprehensive data sets, the need for more robust quality assurance and quality control procedures is growing. Fortunately, most are drawing from previous experience with QA/QC for other data collection vendors (like longitudinal profile collection). Agencies are having data collected on instrumented sites along with comparisons against other methods of structural assessment. Research is underway to establish other options for verification and validation of these data collection technologies.

3 Standards Development

Similarly, standards are needed to facilitate the procurement process. Standards have been prepared (and balloted) to describe the technology desired, and test methodologies for collection of the data desired. It is envisioned that ultimately, such standards might also include details for data formatting.

4 System Wide Assessment

Significant work has previously been documented in this area (Flintsch et al., 2013, Maser et al., 2017, Plati and Loizos, 2023, Jansen et al., 2023, Kressirer, 2020, Murekye et al., 2024) Significant work has previously been documented in this area (Flintsch et al., 2013, Maser et al., 2017, Plati and Loizos, 2023, Jansen et al., 2023, Kressirer, 2020, Murekye et al., 2024). Tools are being deployed to facilitate review and interpretation of these comprehensive data sets. Data filters, graphical visualization capabilities, segmentation tools; the aim is to support efficient implementation in the decision-making process. Additional Studies are also ongoing to identify metrics best suited to further aid in the decision-making process.

5 Project Treatment Design

As network level applications become more widely accepted, the focus is shifting to Project treatment applications (Weitzel et al., 2023). With the ability to report data with very high resolution (i.e. 5cm), isolation of areas of concern is now being explored more frequently. The ability to highlight discontinuities (along with their structural response signature), is generating greater interest in assessing a wider array of pavements for treatment design.

6 Airfield Testing

Interestingly, even though current technology has been integrated into tractor trailors, interest is now actively growing to apply similar concepts for airfield testing. Develop work is ongoing to explore alternative (more appropriate) platforms for the airfield application.

7 Conclusions

Comprehensive and continuous pavement assessments are closing the gap between system wide evaluations and project specific treatment designs. Such practices are not only safer and more efficient, but they are now being reported to generate significant cost savings as well.

8 References

Flintsch, G., Katicha, S., Bryce, Ferne, J.B., Nell, S., Diefenderfer, B. 2013. Assessment of Continuous Pavement Deflection Measuring Technologies. SHRP 2 Rep., no. S2-R06F-RW-1.

Maser, K., Schmalzer, P., Shaw, W., Carmichael, A. 2017. Integration of Traffic Speed Deflectometer and Ground-Penetrating Radar for Network-Level Roadway Structure Evaluation. Transp. Res. Rec., Vol. 2639/1: 55-63.

Plati, C., Loizos, A. 2023. An Approach to Combine Structural and Functional Testing to Optimize Condition Assessment of Flexible Pavements TRB Annual Meeting

Jansen, D., Podolski, C., Kalantari, M., Rahimi, M. 2023. ME-SAS Aus- und Bewertung – Stufe 1. BASt report (unpublished)

Kressirer, B. 2020. Pilotprojekt Tragfähigkeitsmessung in Bayern als Baustein des Erhaltungsmanagements. Straße und Autobahn, Kirschbaum-Verlag, Heft 10/2020: 813-820

Murekye, A., Flintsch, G., Katicha, S., Diefenderfer, B., Urbaez, E.P. 2024. A Pilot Study to Incorporate Network-Level Structural Condition into Agency Pavement Management Practices. TRB Annual Meeting

Weitzel, N.D., Pierce, L.M., Caroll, E., Thompson, J.U. 2023, Use of Traffic Speed Deflectometer Data in Project-Level Pavement Rehabilitation Design. Transportation Research Record, Vol. 2678/6: 1-12

Assessment of Load-Deflection Linearity Between 40 kN and 50 kN in Falling Weight Deflectometer Measurements

Andrejs Taranovs
Road Competence Centre, Latvian State Roads, Riga, Latvia

Abstract

The Latvian road management system has historically lacked a scientifically grounded methodology for interpreting Falling Weight Deflectometer (FWD) data. One candidate approach is the Caltrans methodology, which defines deflection threshold values at a 40 kN load level. Since the standard test load in Latvia is 50 kN, this study investigates whether Caltrans thresholds can be reliably scaled using a linear factor of 1.25. FWD measurements were collected from the Latvian road network with paired 40 kN and 50 kN drops at each location. Following data filtering and normalization, Bland–Altman agreement analysis was applied to 848 paired observations. Results reveal a systematic negative bias (Bias = –8.4 µm), with 78.54% of observations falling below the 1.25 linear scaling reference line. The observed sub-linear pavement response may be partly attributed to stress-dependent behaviour of unbound pavement layers, although the dataset did not allow for a full quantitative assessment of measurement repeatability and other contributing factors. Caution is therefore recommended when scaling FWD deflection thresholds between load levels using linear assumptions.

Keywords: falling weight deflectometer; load-deflection linearity; pavement structural assessment; Bland–Altman analysis; stress-dependent behaviour

1 Introduction

In the Latvian road management system, a unified and scientifically grounded methodology for evaluating pavement structural capacity using the Falling Weight Deflectometer (FWD) has long been lacking. Although FWD equipment has been used in the country for several decades, the analysis of collected data—which would enable reliable estimation of remaining service life and determination of required rehabilitation measures—has not been a standardized practice.

To address this gap, the recently developed pavement rehabilitation guidelines incorporated the use of FWD data evaluation, suggesting the adaptation of the internationally recognized Caltrans methodology. The Caltrans approach is based on deflection threshold values at a 40 kN load (Caltrans, 2004); however, this raised concerns about its suitability under Latvian conditions. Historically, considering the legal axle load limits, a 50 kN test load has been applied as the standard in Latvia. This discrepancy raises the question of whether Caltrans deflection thresholds can be reliably adjusted to a higher load level without compromising interpretation accuracy.

Scientific literature has repeatedly emphasized that the response of pavement layers to increasing load is not linear. For example, Mehta and Roque (2003) note that elastic layered analysis only approximates real pavement behavior, as actual pavement materials often display nonlinear or viscoelastic characteristics. This has a significant impact on the reliability of backcalculation results, particularly when deflection basin matching is performed without accounting for structural variability and material properties. Similarly, Nabizadeh et al. (2017) point out that the behavior of unbound pavement layers, particularly the subgrade, is strongly stress-dependent, and that this nonlinear behavior can be reflected in FWD measurements when multiple load levels are applied. The authors emphasize that such stress-dependent responses may influence the interpretation of pavement performance and that simple linear load–deflection assumptions may not always be sufficient.

Given the above, the objective of this study is to practically assess the applicability of Caltrans deflection threshold values at a 50 kN load using data from the Latvian road network. To achieve this, the FWD testing setup was extended by including an additional 40 kN drop alongside the standard 50 kN measurements, thereby enabling direct comparison between the two load levels. The analysis focuses on evaluating the relationship between deflection responses at 40 kN and 50 kN in order to determine whether Caltrans deflection thresholds can be reliably adapted to higher load conditions and subsequently incorporated into Latvia's pavement rehabilitation guidelines. A similar multi-load-level approach is recommended in international practice. FHWA guidelines indicate that routine FWD testing should be performed at multiple load levels, as this allows evaluation of potential nonlinear pavement material behavior (FHWA, 2016). The inclusion of an additional load level in this study is therefore consistent with established testing protocols and enables verification of whether pavement response remains linear within the investigated load range.

2 Methodology

2.1 Data Collection and Quality Control

The dataset comprised FWD measurements collected from six state road sections in Latvia — P8, P64, P69, P77, P124, and P126 — all scheduled for reconstruction or structural strengthening at the time of testing. The total length of the surveyed sections was approximately 40 km, covering a range of aged flexible pavement structures representative of Latvia's rural road network. Measurements were conducted as part of routine pre-design pavement evaluation; for the purposes of this study, the standard testing protocol was extended to include an additional 40 kN load drop alongside the standard 50 kN drops, enabling direct load-level comparison. A total of 946 measurement points were recorded prior to filtering.

To ensure the reliability and consistency of the analysis, a rigorous data filtering procedure was applied to exclude low-quality or non-representative measurements. Only measurements where the target load levels of 40 kN and 50 kN were achieved within a ±10% tolerance were retained, in accordance with internationally recognized FWD testing standards (FHWA, 2006). Measurements were further excluded if the deflection basin did not exhibit a monotonic decrease with increasing sensor distance from the load plate, a criterion widely accepted as an indicator of physically plausible pavement response.

The importance of such filtering is well documented in the literature. Mehta and Roque (2003) highlight that deflection data can be strongly influenced by structural anomalies, temperature effects, and equipment variability, and that meaningful interpretation requires verification of both physical plausibility and consistency across multiple load drops. Similarly, FHWA guidelines explicitly recommend excluding data that fails to meet load precision and deflection basin shape criteria, as such measurements may lead to erroneous modulus estimation and unreliable rehabilitation decisions (FHWA, 2006).

Figure 1 illustrates the distribution of deflection values before and after data filtering. The comparison demonstrates that the applied filtering procedure effectively removes extreme and physically implausible measurements while preserving the overall characteristics of the dataset required for subsequent comparative analysis.

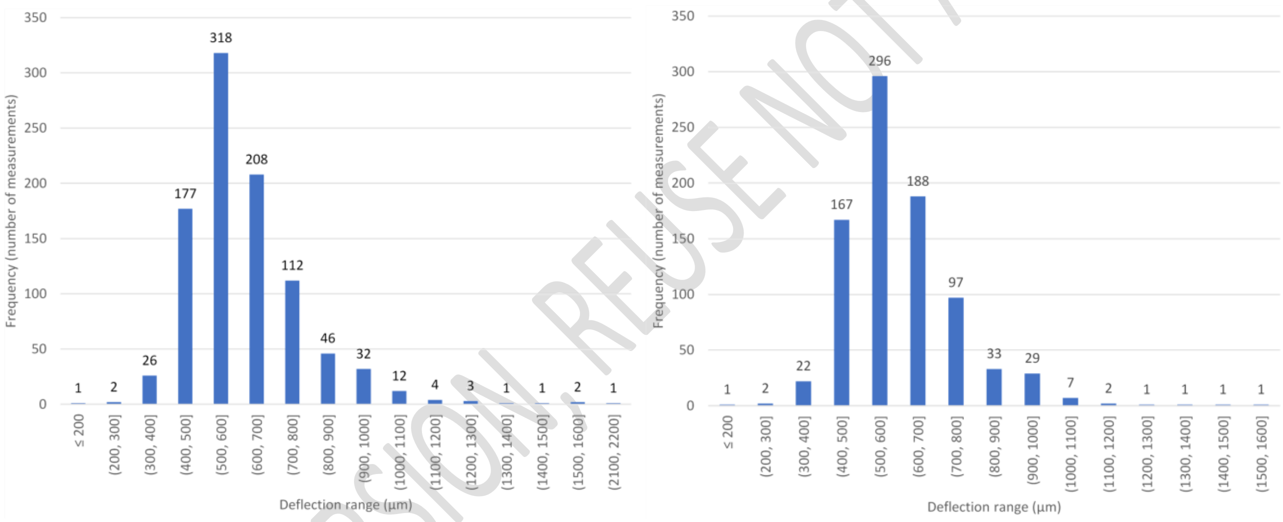

Figure 1: *Distribution of deflection values before filtering (left, N = 946) and after filtering (right, N = 848).*

2.2 Data Processing and Statistical Methodology

2.2.1 Deflection Normalization

To mitigate the influence of minor variations in the applied load and ensure precise comparability between measurements, all central deflection values (D_1) were normalized to a target reference stress. This procedure, which corrects for actual load deviations from the set pulse level, is a fundamental prerequisite for the consistent interpretation of Falling Weight Deflectometer (FWD) data (FHWA, 2006).

For each recorded measurement point, the normalized central deflection was calculated using the following equation:

$$D_{\mathrm{norm}} = \frac{D_1}{P_{\mathrm{actual}}} \cdot P_{\mathrm{ref}} ,$$

Where:

- D_{norm} – normalized deflection (µm);

- D_1 – measured deflection under the load plate (μm);
- P_{actual} – actual applied stress (kPa);
- P_{ref} – reference stress (566kPa for 40 kN, 707kPa for 50 kN).

2.2.2 Linear Scaling and Deviation Analysis

To evaluate whether 40 kN measurements can be linearly extrapolated to 50 kN conditions, a theoretical normalized deflection at 50 kN was calculated from the normalized 40 kN data, assuming ideal linear material behavior:

$$D_{50\text{kN}}^{\text{theoretical}} = D_{40\text{kN}}^{\text{norm}} \cdot \frac{P_{50\,\text{kN}}}{P_{40\,\text{kN}}},$$

Where:

- $D_{50\text{kN}}^{\text{theoretical}}$ – interpolated deflection at 50 kN (μm);
- $D_{40\text{kN}}^{\text{norm}}$ – normalized deflection at 40 kN (μm);
- $P_{50\,\text{kN}}$ – reference stress 707 (kPa);
- $P_{40\,\text{kN}}$ – reference stress 566(kPa).

The discrepancy between the actually measured normalized 50 kN deflection ($D_{50\text{kN}}^{\text{norm}}$) and the theoretically predicted value was quantified using the absolute difference (ΔD) and the relative Error (%):

$$\Delta D = D_{50\text{kN}}^{\text{norm}} - D_{50\text{kN}}^{\text{theoretical}},$$

$$\text{Error (\%)} = \frac{D_{50}^{\text{norm}} - D_{50}^{\text{theoretical}}}{D_{50}^{\text{norm}}} \cdot 100,$$

Where:

- ΔD – difference between actual and interpolated deflection (μm);
- $D_{50\text{kN}}^{\text{norm}}$ – normalized deflection at 50 kN (μm);
- $D_{50\text{kN}}^{\text{theoretical}}$ – interpolated deflection at 50 kN (μm).

2.2.3 Statistical Agreement Analysis

The agreement between the measured and interpolated values was assessed using the Bland–Altman method. This approach allows for the determination of the mean difference (Bias), the standard deviation of the differences (s_{Δ}), and the 95% Limits of Agreement (LOA):

$$Bias = \left(\frac{1}{n}\right) \sum_{i=1}^{n} \Delta D_i,$$

$$SD_{diff} = \sqrt{\left(\frac{1}{n-1}\right) \sum_{i=1}^{n} (\Delta D_i - Bias)^2},$$

$$LOA = Bias \pm 1.96 \cdot SD_{diff},$$

Where:

- $Bias$ – the estimated mean of the differences (ΔD) between the theoretically calculated and the measured values;

- ΔD_i – the difference for an individual pair of measurements (D_measured−D_theoretical);
- SD_{diff}– the standard deviation of those differences;
- LOA – 95% Limits of Agreement;

The resulting distributions and statistical indicators of agreement are presented and analyzed in the Results and Analysis section below.

3 Results and Analysis

3.1 Agreement between Interpolated and Measured 50 kN Deflections

Figure 2 illustrates the distribution of the absolute difference (ΔD) and the corresponding Bland–Altman plot comparing the theoretically calculated $D_{50\text{kN}}^{\text{theoretical}}$ and the actually measured $D_{50\text{kN}}^{\text{norm}}$ (N = 848 paired observations).The results exhibit a systematic negative bias (Bias = -8.4 µm), indicating that the theoretical linear scaling (factor of 1.25) consistently overestimates the actual pavement response at the 50 kN load level. While the majority of measurements are concentrated near zero difference, the Limits of Agreement (LOA from –39.57 to +22.85 µm) reveal a significant variation in individual data points. Notably, observations at higher deflection values (>500 µm) show a tendency toward increased dispersion, which may be attributed to the non-linear nature of weaker pavement sections.

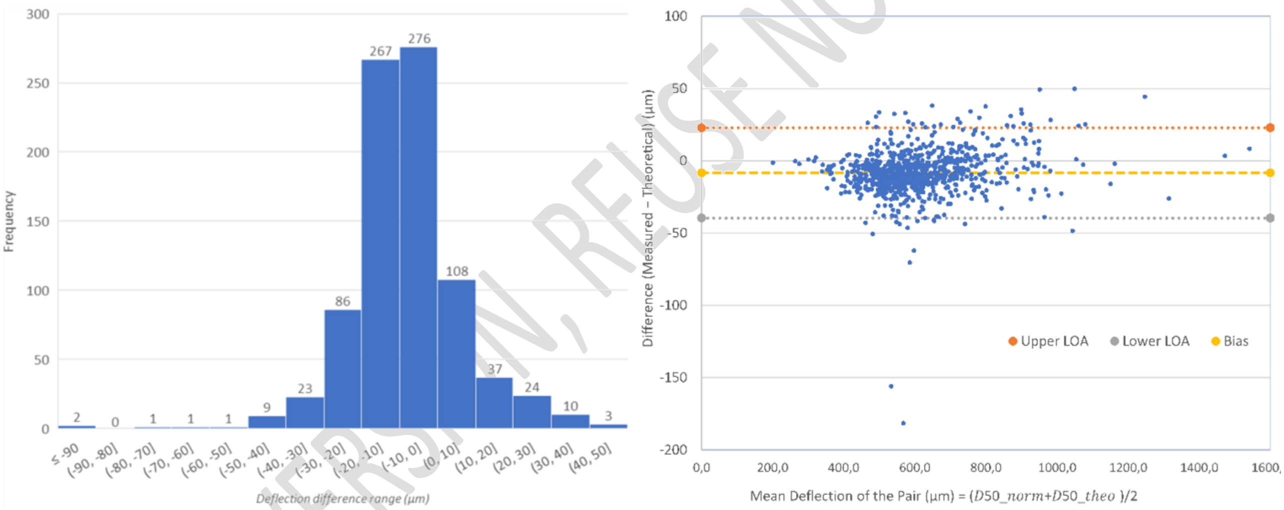

Figure 2: *Frequency distribution of deflection differences (left) and the corresponding Bland-Altman plot for agreement analysis (right).*

3.2 Distribution of Relative Error and Scaling Trends

Figure 3 (left) shows the distribution of the relative error in 1% intervals. The histogram is markedly asymmetric and skewed in the negative direction, confirming that the calculated value $D_{50\text{kN}}^{\text{theoretical}}$ exceeds the measured value in the vast majority of cases. This trend is further visualized in Figure 3 (right), where measured 50 kN deflections are plotted against their 40 kN counterparts. Using the 1.25 scaling line as a reference, the data were categorized into two groups: Below (where $D_{50}^{\text{norm}} < D_{50\text{kN}}^{\text{theoretical}}$ and At/Above (on or above the reference line). According to this classification, 672 out of 848 observations (78.54%) fall below the reference line. This statistically confirms that simple linear extrapolation is not fully representative of the actual structural behavior under increasing load levels.

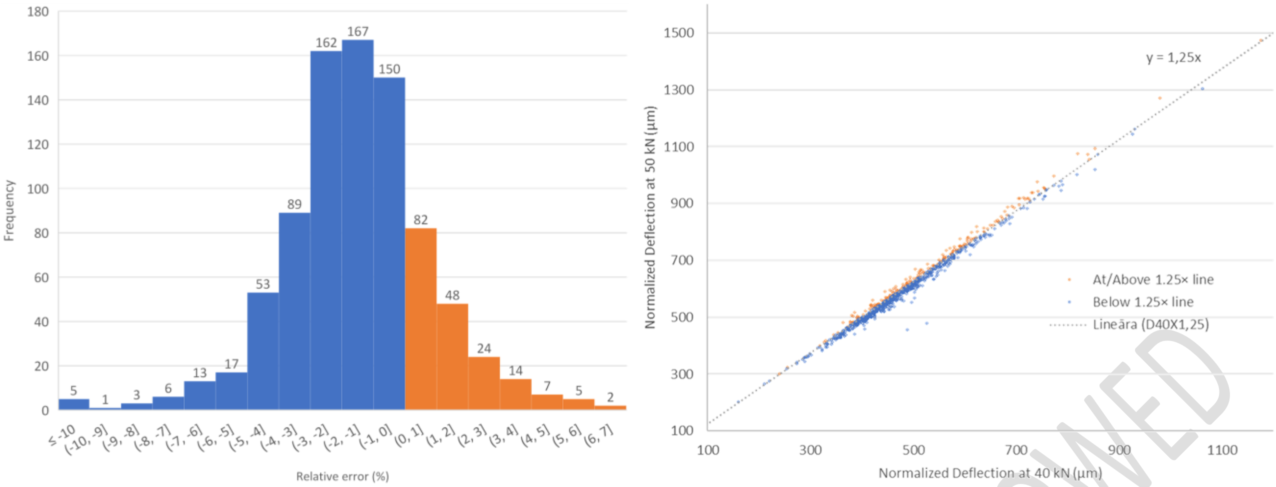

***Figure 3**: Relative error distribution (left) and 50 kN measured deflections vs. 40 kN values with a 1.25 scaling reference line (right).*

3.3 Mechanical Interpretation of the Results

The observed systematic bias—where the actual deflection at 50 kN is lower than theoretically predicted—may be partly explained by the stress-dependent stiffness behaviour of the unbound pavement layers (base and subgrade). This interpretation is consistent with the stress-hardening behaviour of granular materials documented in literature (Li et al., 2017), although the present dataset did not allow for independent verification of this mechanism. Consequently, the deflection response is sub-linear: as the load increases by 25% (from 40 to 50 kN), the resulting deflection increases by a factor smaller than 1.25. This study underscores that accounting for these non-linear effects is critical when interpreting FWD data across different load levels to avoid inaccurate bearing capacity assessments.

4 Conclusions

This study addresses a practical engineering challenge: the adaptation of Caltrans deflection thresholds for a transition from the 40 kN load level to the 50kN level standard in Latvian engineering practice. Bland–Altman analysis results reveal a systematic negative bias of -8.4 µm (LOA from –39.57 to +22.85 µm), with 78.54% of observations falling below the 1.25 linear scaling line. This demonstrates that a linear recalculation of threshold values is associated with a "non-conservative" decision-making risk. Since the pavement structure response is sub-linear — a behaviour consistent with the stress-dependent stiffness of unbound materials, though not independently verified within this dataset — the 1.25 linear coefficient raises the allowable deflection threshold higher than the actual structural response permits, creating a risk of misclassifying inadequate bearing capacity as acceptable.

The study also highlights significant methodological limitations. The dataset, obtained within the framework of routine pavement maintenance evaluations, primarily included structurally weak sections under relatively uniform weather conditions. This restricted the diversity of deflection responses and may have obscured more complex non-linear behavior at varying stiffness levels.

In the future, to conduct a higher-quality study on non-linearity, it would be beneficial to transition to multi-level load sequences with several repeated drops at each level, following the LTPP (*Long-Term Pavement Performance*) methodology. Such an approach would ensure higher data reliability by allowing for the assessment of measurement repeatability and clearly distinguishing true mechanical non-linearity from measurement noise or the initial seating effect. Although this increases the duration of field testing, this logistical trade-off is necessary to obtain a representative dataset required for a more accurate characterization of material non-linearity.

5 References

California Department of Transportation, Division of Engineering Services. 2004. Sacramento. Methods of Test to Obtain Flexible Pavement Deflection Measurements for Determining Pavement Rehabilitation Requirement. California Test 356. Transportation Laboratory.

Federal Highway Administration. 2006. McLean, VA. LTPP Manual for Falling Weight Deflectometer Measurements. FHWA-HRT-06-132. Turner-Fairbank Highway Research Center.

Federal Highway Administration. 2016. McLean, VA. Using Falling Weight Deflectometer Data with Mechanistic-Empirical Design and Analysis, Volume III: Guidelines for Deflection Testing, Analysis, and Interpretation. FHWA-HRT-16-011. Turner-Fairbank Highway Research Center.

Li, M., Wang, H., Xu, G. & Xie, P. 2017. Finite element modeling and parametric analysis of viscoelastic and nonlinear pavement responses under dynamic FWD loading. Construction and Building Materials, 141, pp. 23–35.

Mehta, Y. & Roque, R. 2003. Evaluation of FWD Data for Determination of Layer Moduli of Pavements. Journal of Materials in Civil Engineering, 15(1), pp. 25–31.

Nabizadeh, H.; Hajj, E.Y.; Siddharthan, R.V.; Elfass, S. & Nimeri, M. 2017. Athens. Application of falling weight deflectometer for the estimation of in-situ shear strength parameters of subgrade layer. In: Loizos, A., Al-Qadi, I. & Scarpas, T. (Eds.) Bearing Capacity of Roads, Railways and Airfields – Proceedings of the 10th International Conference (BCRRA 2017). Taylor & Francis Group, pp. 743–759.

FWD Comparison - an update and basis for discussions

Dirk Jansen
BASt – Federal Highway and Transportation Research Institute

Abstract

For over 10 years now, BASt has been carrying out an annual international comparison of FWD devices. This event has now established itself in Europe. Around 20 FWDs now take part each year. Different model years, types and manufacturers are represented. Building on the BCCRA contribution 2022 'FWD quality assurance in Germany', the current status of the comparative measurements will be presented and the general conclusions and requirements that can be drawn from them based on the COST 336 action will be discussed. In addition, a valuable and extensive database is now available, the possibilities for extended use of which will also be discussed here.

Keywords: FWD, quality, comparison, rodeo

1 Introduction

The first Falling Weight Deflectometers (FWD) were put into operation in Germany in the early 1990s. The scientific introduction took place in 1996. A series of working papers for the planning, implementation and evaluation of bearing capacity measurements has been established and being used. In the working paper Bearing Capacity, part B2.1 (FGSV, 2008) recommendations are given for the own and external monitoring of the measuring equipment as well as for the execution of interlaboratory comparisons.

In 2015, 2016 and 2018, the first comparative tests were therefore carried out on the BASt premises in the present form (Jansen and Čicković, 2017), with the aim of creating the basis for a permanent and recurring organization for comparative measurements. This was based on many years of experience in the Netherlands (Van Gurp, 2013), which was also incorporated into the report on COST Action 336 (COST, 2005).

Results and demand or the reactions of the participants clearly spoke for an annual repetition. Since then, the measurements have been offered regularly. The Federal Highway and Transportation Research Institute (BASt), in its role as a quality assurance body for a number of measurement methods used in the road sector and as a client for FWD measurements within the framework of research projects, is very interested in carrying out comparative measurements for FWD in Germany.

The data from eight events is now available in anonymized form and can be made available to the research community for research and development ideas.

2 Comparative tests

The design of the experimental programme is closely aligned with the European consensus elaborated in COST Action 336. The experimental program pursues the following core points:

- Examination of repeatability (each FWD separately),
- Examination of comparability (comparison between the FWDs),
- Investigation of the precision of temperature measurements.

In order to act as independently as possible from the aspects of traffic safety, only measuring points on the BASt site are considered. To a certain extent, this can ensure that repeated measurements are carried out from year to year in the same situation.

A total of 21 measurement points are available per measurement round. Two measurement rounds are carried out, one in the morning and one in the afternoon. In general, the FWDs should be equipped in accordance with the FGSV Working Paper Bearing Capacity, Part B.2 [1] and brought into operational readiness as for the performance of regular measurements. All deviations from this are documented.

3 Database

To protect the economic interests of FWD operators, the results of comparison measurements are kept anonymous. This allows for broad use of the database for research and development.

As said the database includes data from at least eight comparative events. The number of participating FWDs was initially around 10 and has risen to around 20 in recent years. By 2025, data from a total of 110 FWDs (many of which have of course participated multiple times, but have nevertheless been added up here) will be available at 21 measuring points. This corresponds to a theoretical sample size of 2,310.

Each dataset contains the following:

- load
- deflection at load centre and at each geophone position
- air temperature (if available)

- surface temperature (if available)
- pavement temperature (drill hole) (one per measuring round)

Some of the datasets also contain time history data.

4 Conclusions

Both the experience gained from regularly conducting international comparative measurements and the resulting database represent a valuable source of information. Joint discussions will focus on the further development of standards and such measurements, as well as their use as a contribution to research and development.

5 References

FGSV. 2008. Köln. Arbeitspapier Tragfähigkeit, Teil B2.1: Falling-Weight-Deflectometer (FWD) – Beschreibung, Messdurchführung – Asphaltbauweisen. FGSV-Verlag.

Jansen, D. & Čičković, M. 2017. Bonn. Qualitätssicherung von FWD-Tragfähigkeitsmessungen. Straße und Autobahn, 8/2017. Kirschbaum-Verlag.

European Cooperation in the Field of Scientific and Technical Research (COST). 2005. Brussels. Use of Falling Weight Deflectometers in Pavement Evaluation. Final Report. European Commission.

Van Gurp, C. 2013. Ede. FWD Correlation Trial 2013. CROW-report D13-05. CROW.

Incorporation of Structural Response in Pavement Management

Jerry Daleiden
Neil Mastin
ARRB Systems
Dirk Jansen
BASt – Federal Highway and Transportation Research Institute, Germany

Abstract

Pavements have historically been managed by their functional (or surface) conditions. This was largely the result of limitations in technology and the relatively slow speed of data collection. Such limitations have generally necessitated a reactive approach to road maintenance with related negative effects. Road managers typically wait for distress to occur prior to acting and such action is based on the surface distress. Much of the more detailed structural information needed to make proactive informed decisions had to be collected on a sample basis and required extensive traffic control and delays to the traveling public.

Ideally, road managers would have access to co-located structural and functional data to make the most informed decisions possible and to maximize the benefit of limited funding. Technologies for traffic speed assessment of structural response continue to advance and gain acceptance and agencies are now actively seeking effective means for incorporating this data into their decision-making process. These advancements have brought about a greater awareness of the true resource needs for better managing our infrastructure in a proactive manner, while significantly reducing the costs for gathering the data needed. This holds the potential to dramatically improve decision making for managing the road network and drives inclusion in pavement management systems.

This robust information set provides a more complete and accurate assessment of pavement condition. The resulting data is better suited for both project and network level applications. Continuous data provides for a more detailed assessment within a project, and helps to avoid concerns associated with assigning "average" condition for treatment selection and design. Discrete sections can also be identified with greater confidence and accuracy. Isolated repairs can be performed in advance of larger rehabilitation projects to produce a more homogeneous structure, for more cost-effective designs and improved performance.

1 Introduction

Agencies conduct pavement management to systematically plan maintenance and repair and with a goal of optimizing the condition of their entire network. As technology for data collection is rapidly evolving, the role of "Pavement Management" is shifting from collecting some data to report current condition of a pavement network to analysis of more detailed assessments to facilitate optimizing treatment decisions and designing optimal solutions for the specific treatments.

Transportation Agencies are shifting from sampled surface assessments to very detailed functional and structural assessments, collected continuously, and at traffic speeds. In addition to the efficiency and safety considerations, these more detailed assessments provide for a better understanding of the variability of condition, as well as treatment needs. Details on the technologies used, the evaluation approaches, and case studies can be found in the following literature sources, for example: (Flintsch et al., 2013), (Maser et al., 2017), (Plati and Loizos, 2023), (Jansen et al., 2023), (Kressirer, 2020), (Weitzel et al., 2023), (Murekye et al., 2024).

While Agencies are eager to apply these improved assessments, they must address how best to manage the increased volume of data, and complexities of the inherent variability documented with such capabilities.

2 Applications

Applications of these integrated pavement assessment systems rely heavily on using user-friendly tools for:

- Graphical visualization capabilities;
- Data filters;
- Segmentation capabilities;
- Driving decision in Pavement Management Systems with cross-referenced data

2.1 Graphical Visualization

Graphical visualization tools enable multiple data types to be portrayed simultaneously to facilitate review and interpretation. The ultimate objective is to identify deficiencies (as efficiently as possible) to support treatment needs and designs. Figure 1 demonstrates an example of multiple data types on one plot.

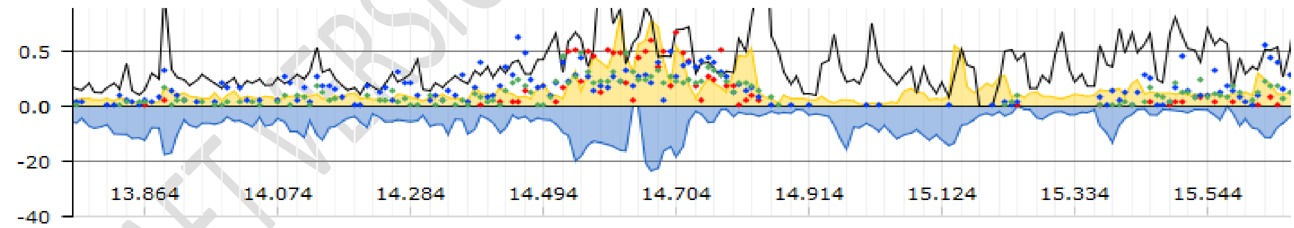

Figure 1: *Example of Simultaneous Data Visualization.*

2.2 Data Filters

Data filters are particularly useful for identifying and highlighting segments that correspond to specific parameters. Again, this helps to efficiently identify areas of concern for further review and potential treatment. Figure 2 demonstrates potential filter combinations needed to identify sections using multiple filters at once.

2.3 Segmentation Capabilities

These continuous data sets also are very helpful in addressing variability within a network. By identifying parameters of interest (structural response, ride, rutting, etc.), along with applicable thresholds, networks can be categorized into segments of comparable performance. This ultimately helps to support more cost-effective designs and treatment applications. Algorithms can be applied in reporting tools or within pavement management systems to identify sections with commonality.

Filters:
- IRI > 120
- Rutting > 0.3 in
- WP Cracking > 50%
- D0 > 21 mils

Figure 2: *Example of Filtering.*

2.4 Improving Decision Making Capabilities in Pavement Management Systems

While new data collection methods and reporting are key, they must also be used at the network level. This can be accomplished by combining surface distress and structural information in a decision tree within pavement management systems. Figure 3 provides a very simple example of a decision tree using surface distress combined with structural criteria.

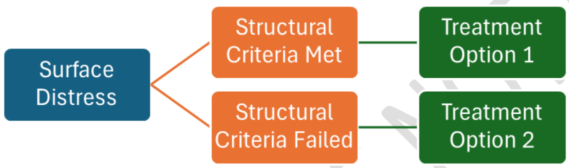

Figure 3: *Simple Decision Tree.*

3 Case Studies

Closing this gap between network level and project level evaluations is generating:

- Greater value and applicability of the data collected;
- The ability to better optimize network performance and
- Improve the efficiency and effectiveness of project specific treatments.

As will be seen from the case studies, the ability to conduct more comprehensive assessments is capable of significantly impacting the ability to identify the correct remedial solutions and optimization (and application) of Agency pavement funds.

In Case 1, the common belief is that structural issues will manifest themselves in surface deterioration, eventually. While this may typically be true (eventually), it is not always the case and therefore structural assessment helps to confirm the presence of structural deterioration before treatments are planned.

For Case 2, continuous structural capacity assessment, can reveal isolated/discrete portions of highways that may appear acceptable from the surface, but (for a multitude of potential reasons) are not able to provide the same structural support as adjacent portions of the same highway.

With Case 3, observations have been made of sections of pavement that exhibit extensive surface deterioration, that would traditionally lead one to believe that extensive repairs are required. Continuous structural assessment can highlight locations where such deterioration is only surficial, offering significant cost savings.

And Case 4, When sections of pavement appear to have limited surface deterioration, it is beneficial to be able to confirm that these sections truly require no work for the foreseeable future with simultaneous structural assessment.

4 Conclusions

Comprehensive and continuous pavement assessments are closing the gap between system wide evaluations and project specific treatment designs. Such practices are not only safer and more efficient, but they are now being reported to generate significant cost savings as well.

5 References

Flintsch, G., Katicha, S., Bryce, Ferne, J.B., Nell, S., Diefenderfer, B. 2013. Assessment of Continuous Pavement Deflection Measuring Technologies. SHRP 2 Rep., no. S2-R06F-RW-1.

Maser, K., Schmalzer, P., Shaw, W., Carmichael, A. 2017. Integration of Traffic Speed Deflectometer and Ground-Penetrating Radar for Network-Level Roadway Structure Evaluation. Transp. Res. Rec., Vol. 2639/1: 55-63.

Plati, C., Loizos, A. 2023. An Approach to Combine Structural and Functional Testing to Optimize Condition Assessment of Flexible Pavements TRB Annual Meeting

Jansen, D., Podolski, C., Kalantari, M., Rahimi, M. 2023. ME-SAS Aus- und Bewertung – Stufe 1. BASt report (unpublished)

Kressirer, B. 2020. Pilotprojekt Tragfähigkeitsmessung in Bayern als Baustein des Erhaltungsmanagements. Straße und Autobahn, Kirschbaum-Verlag, Heft 10/2020: 813-820

Weitzel, N.D., Pierce, L.M., Caroll, E., Thompson, J.U. 2023, Use of Traffic Speed Deflectometer Data in Project-Level Pavement Rehabilitation Design. Transportation Research Record, Vol. 2678/6: 1-12

Murekye, A., Flintsch, G., Katicha, S., Diefenderfer, B., Urbaez, E.P. 2024. A Pilot Study to Incorporate Network-Level Structural Condition into Agency Pavement Management Practices. TRB Annual Meeting

Real-Time Rockfall Monitoring for Street Safety Using Pulse-Doppler Radar at the Example for the E652 at Tržič, Slovenia

Richard Koschuch
IBTP Koschuch e.U., Langegg 31 8463 Leutschach, Austria
Suzana Svetličič
DRI Investment Management Ltd, Kotnikova 40, 1000 Ljubljana, Slovenia

Abstract

The E652 Road at Tržič, Slovenia (G2-101/0232 MP LJUBELJ - BISTRICA(TRŽIČ) has been affected by ongoing rockfall activity in 2022 so that a rapid need for action has been required. Until permanent protection through active construction measures comes into force, automatic alarm systems can reduce the risk of the public traffic, of exposed infrastructure, of inhabited properties and work activities in the hazardous area. The pulsed Doppler Radar offers a reliable variant in every weather situation and every visibility to automatically trigger traffic lights and send alarms to the street authorities within a second.

This example underscores the effectiveness of real-time monitoring for adaptive hazard mitigation during high-risk situations to keep the infrastructure working for the public and give the authorities time to plan the construction solution to reduce the risk.

Keywords: rockfall; rockfall detection; alarming system; street safety

1 Introduction

The E652 road near Tržič, Slovenia (G2-101/0232 MP LJUBELJ – BISTRICA (Tržič)), serves as a crucial link between Ljubljana, Slovenia, and Klagenfurt, Austria. Closing this road would cause major traffic disruptions, as alternative routes are already heavily congested. To avoid prolonged closures, the road administration DRI Investment Management Ltd. together with TERRAS Zdenka Popović s.p.h sought an innovative interim solution. In collaboration with ESFERA d. o. o., they implemented a temporary protection and monitoring system combining video surveillance and Pulse Doppler radar from IBTP Koschuch e.U. The video system detects subtle slope movements over time, while the radar provides real-time detection of sudden rockfalls or landslides. Together, these technologies significantly reduce the risk, minimizing it to an acceptable residual level.

2 Initial Situation and Solution

Figure 1 illustrates the condition of the landslide hazard on the E652 near Tržič, both prior to and following the implementation of urgent remedial measures. The affected area, located between km 11+505 and km 11+525, revealed a landslide scarp approximately 23 meters above the road level.

a) b)

***Figure 1:** Initial situation of the landslide hazard on the E652 near Tržič before (a) and after (b) the urgent remedial measures (Foto: DRI).*

To stabilize the slope and mitigate further risk, the following urgent measures were undertaken:

- Cessation of slope creep
- Extensive deforestation of the surrounding area
- Removal of unstable rock masses from the embankment
- Installation of eight horizontal drainage wells
- Reinforcement of the slope with a high-strength steel mesh (load capacity: 150 kN)

Following these rapid interventions, a Pulse Doppler Radar system was installed to provide real-time detection and alerting. In the event of a sudden landslide, the radar system automatically activates traffic lights positioned several meters ahead of the hazard zone to halt incoming traffic immediately. Additionally, the site is continuously monitored via a video surveillance system, enabling the observation of minor slope movements and providing direct visual feedback in case of an alert.

This solution gave DRI time until a final fortification of the danger area could be planned and carried out using massive construction measures.

3 Technical description of the Pulse Doppler Radar

The Pulse Doppler Radar emits some electromagnetic pulses through a parabolic antenna which are then reflected by the objects in the illuminated area and the reflected beam is picked up again with the antenna. If there are moving objects, there is a frequency shift according to the well-known Doppler effect. In the receiver part of the Radar the incoming frequency and intensities are digitalised and streamed to the PC to analyse the data. The raw data then passes there an algorithm specifically developed for natural hazards like avalanches, rockfalls, debris flow (Hübl et al., 2017; Schimml et al., 2017; Koschuch et al., 2015). This algorithm distinguishes these natural hazards from other movements such as rain, animals, etc. with high precession.

So, in the case of the Tržič Radar we are looking for a rockfall/landslide which would block the road. In case of such an event the Radar would detect it in the first second, when this occurs and would trigger the traffic lights located before the hazard place. Additionally, the competent bodies and authorities are informed via email and SMS.

4 Conclusions

In this example, we have been able to clearly demonstrate how one can react quickly to such rockfall and landslide hazards and how one can reopen an important road to traffic in a very short time. In principle, only one mast and a power supply of 40W are necessary to install such a solution. This gives you time to think about and plan a permanent solution, or if the situation is not so critical, you can use this solution alone to defend safety for public transport.

5 References

Hübl, J., Koschuch, R., Brauner, M. & Jocham, P. 2017. Multifunctional RADAR-system in alpine mass movement monitoring. Conference Paper, EGU General Assembly 2017, Vienna.

Schimmel, A., Hübl, J., Koschuch, R. & Reiweger, I. 2017. Automatic detection of avalanches: evaluation of three different approaches. Natural Hazards, 87(1), pp. 83–102.

Koschuch, R., Jocham, P. & Hübl, J. 2015. One Year Use of High-Frequency RADAR Technology in Alpine Mass Movement Monitoring: Principles and Performance for Torrential Activities. In: Lollino, G., Arattano, M., Rinaldi, M., Giustolisi, O., Maréchal, J.-C. & Grant, G.E. (eds.) *Engineering Geology for Society and Territory – Volume 3*. Cham: Springer, pp. 69–72.

Impact of Wetting and Drying Cycles associated with Climate Change on Soil Erodibility: Novel Insights for Embankments Supporting Transport Infrastructure

Michael Atukunda
Ana Heitor
Duncan Borman
School of Civil Engineering, University of Leeds, United Kingdom
Genoveva Burca
Diamond Light Source, Harwell Campus, Didcot, United Kingdom

Abstract

Internal erosion remains a major threat to the long-term stability of geotechnical assets such as embankments supporting transport infrastructure. Despite its importance, the effect of wetting and drying (W-D) cycles on soil erodibility has been poorly investigated in geotechnical engineering.

This study examines how repeated W-D cycles, driven by weather variations associated with climate change, affect the erosion behaviour of compacted soils commonly used in civil engineering structures, such as embankments supporting roads, railways and airfields. Although these soils are compacted to engineering standards during construction, some are naturally prone to internal erosion, particularly when exposed to seasonal cycles. In addition, such embankments have not been designed to retain water caused by extreme flood events associated with climate change.

In the study, a moderately erodible soil was selected and subjected to a series of W-D cycles, followed by erodibility testing using a modified pinhole erosion test to determine its erosion behaviour. Pinhole erosion testing is essential for the laboratory simulation of the internal erosion potential of a water-retaining structure. A key parameter, the critical shear stress, was determined and used to quantify the extent of erodibility as the number of W-D cycles increased. It was found that the first four W-D cycles increased erodibility, with stability observed between the 4th and 8th cycles.

Overall, the study raises awareness of the impact of seasonal weather variations driven by climate change on soil aggregate stability over time. It is instrumental in assessing the resilience of existing infrastructure to frequent flooding.

Keywords: wetting and drying cycles; erodible soils; pinhole test; critical shear stress

1 Introduction

Internal erosion is a critical geotechnical phenomenon that poses a significant threat to the long-term stability and serviceability of infrastructure systems, particularly embankments supporting Transport Infrastructure. These structures, which form the backbone of transportation networks, are increasingly exposed to environmental stressors exacerbated by climate change. Among these, wetting-drying (W-D) cycles driven by seasonal and climatic variability have emerged as a key factor influencing the erosion susceptibility of compacted soils used in embankment construction. Despite their significance, the influence of wetting–drying cycles on soil erodibility remains poorly characterised within geotechnical engineering and the broader transportation infrastructure context.

This study presents a first-of-its-kind integration of wetting–drying cycle effects with internal erosion assessment specifically tailored to transport embankments. It addresses a critical knowledge gap by investigating the influence of repeated W–D cycles on the internal erosion behaviour of compacted soils commonly employed in embankments. The research is particularly relevant to the BCRRA community, as it provides novel insights into the long-term performance and resilience of road, railway, and airfield embankments under changing climatic conditions. The increasing frequency of extreme weather events, including intense rainfall by more than 22% in the last 50 years within Europe (European Environment Agency, 2025), necessitates a deeper understanding of how these cycles affect the structural integrity and bearing capacity of transport infrastructure that has not been designed to retain water arising from extreme flood events (see Figure 1).

A collapsed bridge in Stahovica village, near the town of Kamnik (Slovenia, 2023) (Public Domain)

Flooded railway track in Herefordshire, Wales. (Network Rail, 2019) (Public Domain)

***Figure 1**: Photos showing extreme wash-out failures of roads and railway embankments in a) Slovenia and b) UK.*

2 Methodology

A moderately erodible soil (Briaud et al., 2019; Briaud et al., 2017; Wan and Fell, 2002; Hanson et al., 2010), representative of materials commonly used in embankment construction, was selected for this investigation. The soil was subjected to a series of controlled W-D cycles in a laboratory setting to simulate the environmental conditions anticipated under future climate scenarios. Each cycle comprised fully saturating the soil sample to simulate heavy rainfall or flooding, followed by drying to replicate arid conditions. This process was repeated for up to 8 cycles to capture the progressive effects of hydraulic loading at hydraulic heads of 180mm, 380mm, and 1020mm. After every two (2) W–D cycles, the soil specimens were assessed for erodibility using a modified pinhole erosion test (Figure 2) after Sherard (1976). The Pinhole erosion test method evaluates the internal erosion potential of compacted soils under hydraulic gradients. A key parameter derived from this test is the critical shear stress, which quantifies the threshold hydraulic force required to initiate the detachment and transport of soil particles.

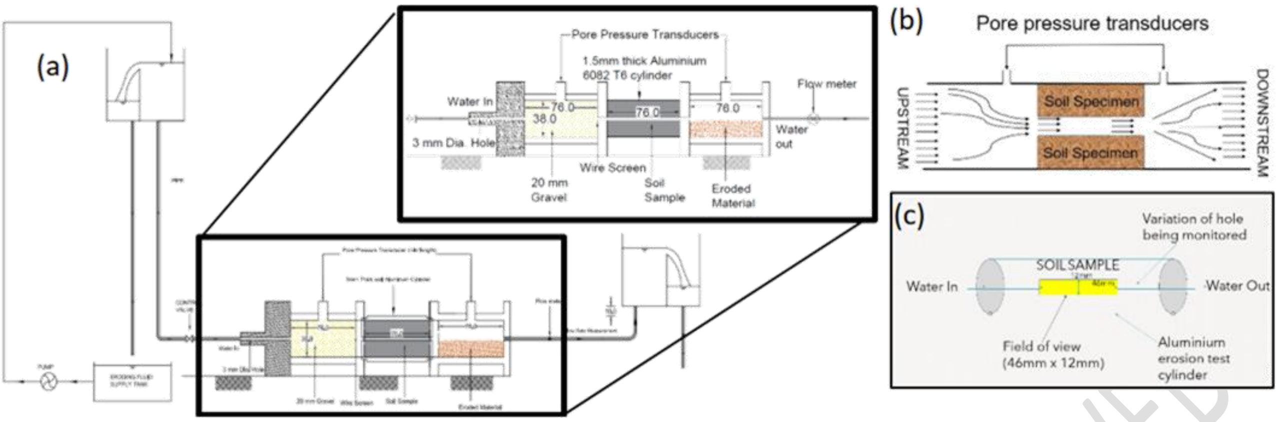

Figure 2: *a) Modified Pinhole erosion test apparatus, b) Flow through Pinhole cavity and c) Synchrotron X-ray Computed Tomography field of view.*

3 Results

The experimental results revealed a clear trend in the evolution of soil erodibility with increasing W–D cycles (Figure 3). Notably, the first four cycles resulted in a significant reduction in the critical shear stress (Figure 3a), indicating increased susceptibility to internal erosion. This degradation is attributed to the breakdown of interparticle bonds and the formation of preferential flow paths, which compromise the soil's structural integrity. Beyond the fourth cycle, however, erosion parameters plateaued, suggesting stabilisation of the soil structure at each hydraulic head. This behaviour implies that the most substantial changes in erodibility occur during the initial cycles, after which the soil may reach a new equilibrium.

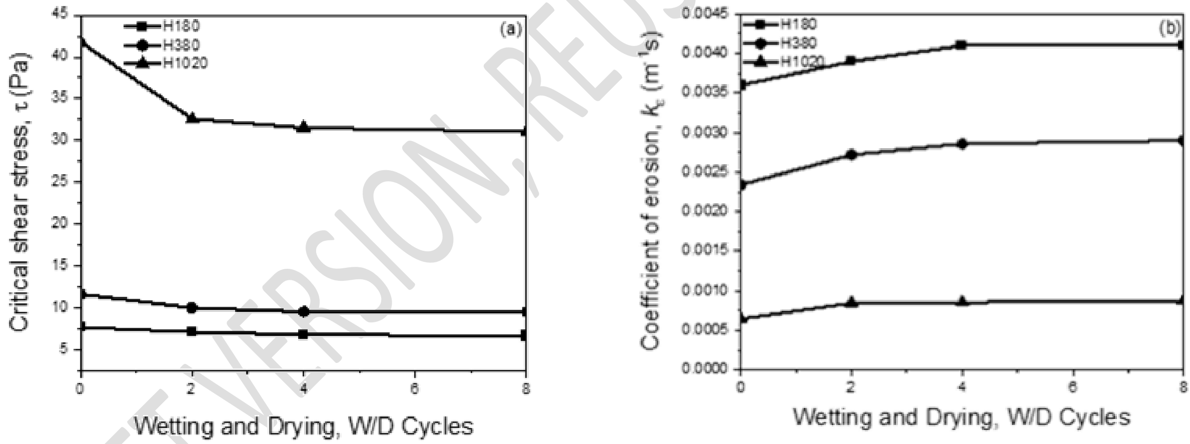

Figure 3: *a) Critical shear stress and b) Coefficient of erosion, against wetting and drying cycles (Atukunda et al. 2026).*

4 Implications for embankments supporting transport infrastructure

The implications of these findings are profound for the design, construction, and maintenance of embankments supporting Transport Infrastructure. In regions experiencing increased climatic variability, the frequency and intensity of W-D cycles are expected to rise, thereby elevating the risk of internal erosion. This study underscores the importance of incorporating erosion-resistance criteria into the geotechnical design of embankments, particularly in areas prone to extreme flooding.

5 Conclusions

In conclusion, this research provides a comprehensive and novel evaluation of the impact of climate change-induced wetting and drying cycles on the erodibility of compacted soils used in transportation embankments.

The study's unique contributions include: (1) the first integration of W-D cycles effects with internal erosion assessment for transport embankments, and (2) new insights into climate-change-induced degradation mechanisms relevant to long-term bearing capacity. These findings are directly applicable to the BCRRA community, offering valuable guidance for the design and maintenance of road, railway, and airfield embankments amid evolving climatic challenges. A major limitation is the reliance on a single soil type, which restricts application.

Some future work to be carried out is to apply wetting and drying cycles to various soil types and to incorporate soil stabilisation before erodibility testing.

6 References

Atukunda, et al. 2026. Impact of wetting and drying cycles on soil erodibility and microstructure under different hydraulic heads: implications for water-retaining structures. Under preparation.

Briaud, J.-L., et al. 2019. Relationship between erodibility and properties of soils

Briaud, J.-L., et al. 2017. Erosion charts for selected geomaterials. Journal of Geotechnical and Geoenvironmental Engineering, 143.

Wan, C. F. & Fell, R. 2002. Investigation of internal erosion and piping of soils in embankment dams by the slot erosion test and the hole erosion test – Interpretative report.

Hanson, G. J., et al. 2010. Erodibility characteristics of embankment materials. Association of State Dam Safety Officials Proceedings.

Sherard, J. L., et al. 1976. Pinhole test for identifying dispersive soils. Journal of the Geotechnical Engineering Division, 102, 69–85.

Development of Markov Decision Process for GPR-Optimized Asphalt Concrete Rolling Pattern

Lama Abufares
Imad L. Al-Qadi
University of Illinois Urbana-Champaign , USA

Abstract

In the United States, rolling pattern for asphalt concrete (AC) pavements is usually determined based on contractor experience (for small projects), or by preparing test strips (for large projects). Test strips are tested using a nuclear gauge after each roller pass to determine the required number of passes to achieve desired density. However, nuclear gauge only provides a spot check. Additionally, several variables in the field might affect the needed compaction effort. These variables include changes in weather conditions, produced materials, and temperature of the paved mix. Based on AC paved quality, agencies may incur extra costs due to future maintenance and rehabilitation or save costs when the pavement life is extended. Hence, contractors may receive incentives when surpassing target density or are subjected to penalties otherwise. A roller-mounted ground penetrating radar (GPR) was developed at the Illinois Center for Transportation and proven capable of monitoring AC density progression with roller passes, while covering nearly the entire AC mat. The AC density progression data may be utilized for real-time decision-making on rolling patterns. In this study, the AC rolling pattern is formulated as a Markov Decision Process (MDP) to account for in-situ AC density variability and uncertainty in GPR density prediction. Solving this problem dynamically, decisions of stopping or continuing compaction could be made instantaneously after each roller pass. The recommended decision is based on an optimization of penalty/incentive cost versus construction operational cost. The proposed approach was validated using field data and considering agency incentive programs.

Keywords: ground-penetrating radar; density; rolling pattern; asphalt concrete; decision-making

1 Introduction

In the United States, state highway agencies (SHAs) use various programs to accept products delivered by contractors. For asphalt concrete (AC), Illinois Department of Transportation (IDOT) developed two AC performance-related acceptance programs: Quality control for performance (QCP) and pay for performance (PFP). QCP specifications are usually applied to smaller projects with 1,200 to 8,000 tons of AC, whereas PFP specifications are applied to larger projects with 8,000 tons or more of AC (IDOT, 2019a; IDOT, 2019b). The goal of these programs is to improve the long-term performance of pavements. For accepted AC products, contractor's pay adjustment (pay factor) could be an incentive in case of superior product quality, or a disincentive in case of inferior quality. However, in the case of unaccepted product quality, the contractor might face monetary deductions up to the contracted amount. Disincentives are a major concern for contractors; for example, in the years 2015-2016, 55% of QCP projects and 44% PFP projects were penalized in Illinois. These penalties averaged around $20,000 per project (Al-Qadi et al., 2021).

Conventionally, to determine the rolling pattern, contractors either rely on their experience or construct control strips at the beginning of large projects. The strips are compacted by rollers, and density is monitored using nuclear gauges after each roller pass. Nuclear gauge measurements are calibrated against cores. Coring serves as the ground truth measurement for AC density. However, it is performed in sparse locations and after compaction. Mat density is dependent on several factors including roller characteristics, mix compaction temperature, ambient conditions, lift thickness, and underlying support (Hughes, 1989). Most of these parameters are variable throughout the project.

Ground-penetrating radar (GPR) may be used for real-time AC compaction monitoring. It is a nondestructive device that emits low-energy electromagnetic (EM) waves. GPR reflected signals are recorded and analyzed to infer material properties. GPR signals may be used to predict the dielectric constant. Afterwards, the Al-Qadi Lahouar Leng (ALL) density prediction model may be used to predict pavement density (*Leng et al., 2011*). In a recent study, GPR was mounted on a roller compactor and used to predict density progression curves for several test sections (*Abufares et al., 2025*). In that study, advanced singal corrections were applied and the final predicted densities were validated using cores.

Reporting AC density should be followed by real-time decision-making to avoid under- and over-compaction based on the agency's specified density limits. Moreover, compaction operational costs may be another limiting factor for extended rolling. In this study, the rolling pattern is formulated as a Markov Decision Process (MDP) to optimize compaction to achieve target density with minimal operational costs. MDP is a mathematical model for sequential decision-making problems when outcomes are uncertain (Puterman, 1990). An MDP is defined as a 4-tuple (S, A, P, R) as shown in Figure 1, where S is the set of possible states (s_1, s_2), A is the set of possible actions (a_1, a_2), P is a tensor of transition probabilities from one state (s_t) to another (s_{t+1}) given an action (a_t) = $P_r(s_{t+1}| s_t, a_t)$, for example, $P_r(s_2| s_1, a_2)$= 0.5, and R is the set of expected immediate rewards received after transitioning from s_t to s_{t+1} using action a_t, which is -10 for the mentioned transition.

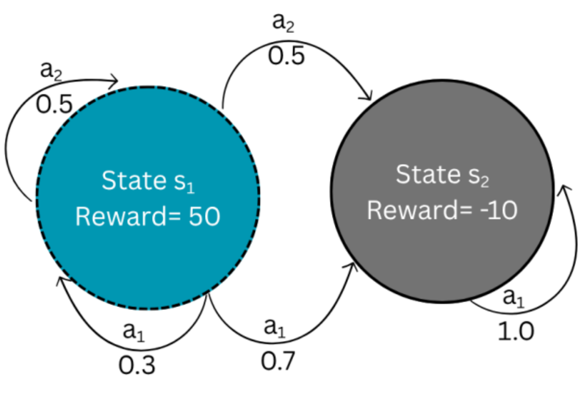

Figure 1: *Schematic of a two-state Markov Decision Process.*

Solving an MDP means finding an optimal sequence of actions. The optimal action is found by maximizing the total reward, which is the sum of immediate rewards and all expected future rewards. This total reward is often referred to as "utility" and is computed by solving Bellman's equation:

$$u(s) = \max_{a} \sum_{s'} P_r(s_{t+1} = s' | \, s_t = s, a)(r(s, a, s') + \gamma u(s')) \, ,$$

Where:

- $u(s)$ – utility of state s;
- $r(s, a, s')$ – reward for a transition from state s to s' using action a;
- γ – discount factor (< 1) indicating the value of future rewards compared to immediate rewards.

2 MDP Formulation

The following observations/assumptions are made to formulate the MDP for rolling pattern:

- Each lane was divided longitudinally into segments. An average segment length of 220ft was used.
- Each lane was divided transversly into sub-lanes. Three sub-lanes were assumed.
- For MDP decisions, only number of roller passes was considered, although roller operator may consider additional parameters (e.g., roller speed and vibration frequency and amplitude).

The MDP elements for rolling pattern optimization are defined as follows:

- States: Defined as tuples of the integer densities of three passes including the current pass, e.g., the tuple (85,87,90). States are defined for densities $d \in [82, 98]$.
- Actions: The possible actions at each state are to continue (perform one more pass) or to stop compaction: $A = \{\text{stop}, \text{continue}\}$.
- Transition probabilities: The model estimates $P_r\big(d_n | (d_{n-1}, d_{n-2}, d_{n-3})\big)$; where n is number of passes, and d_m is density after the m^{th} pass. A 3-point linear regression model was chosen.
- Rewards: Operational costs (labor/equipment) were used to estimate cost/roller pass. Incentives/ disincentives costs were based on IDOT's specifications while considering GPR uncertainty (Figure 2).

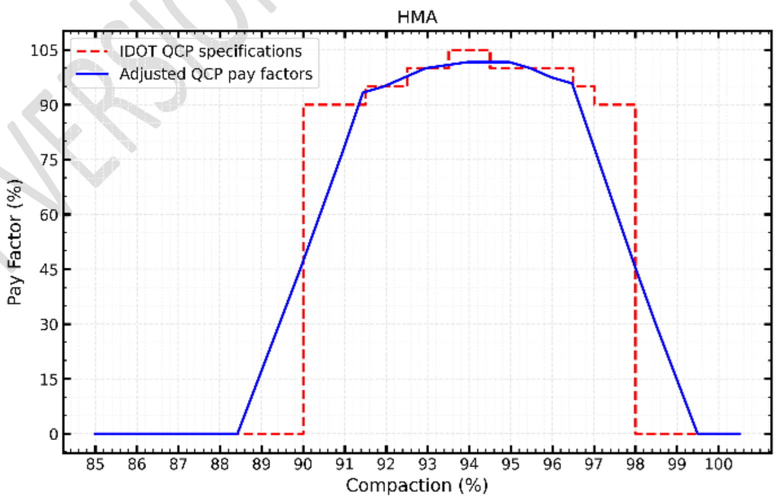

Figure 2: *Adjusted QCP pay factors for MDP rewards for AC mixes.*

3 MDP Demonstration

Figure 3 shows an example of applying the MDP to data collected from a real project around Bourbonnais, IL. For the project inputs, the estimated roller pass cost was around $20 and the value of each segment was

$619. The pay factor (Figure 2) is multiplied by the segment value to estimate the expected reward. Compared to an experienced roller operator who performed eight passes, the MDP decision was to stop after the fifth pass. This decision was based on: MDP predicting the density progression to be minimal using the transition model (black crosses), operational costs, and IDOT QCP density limits for AC mixes.

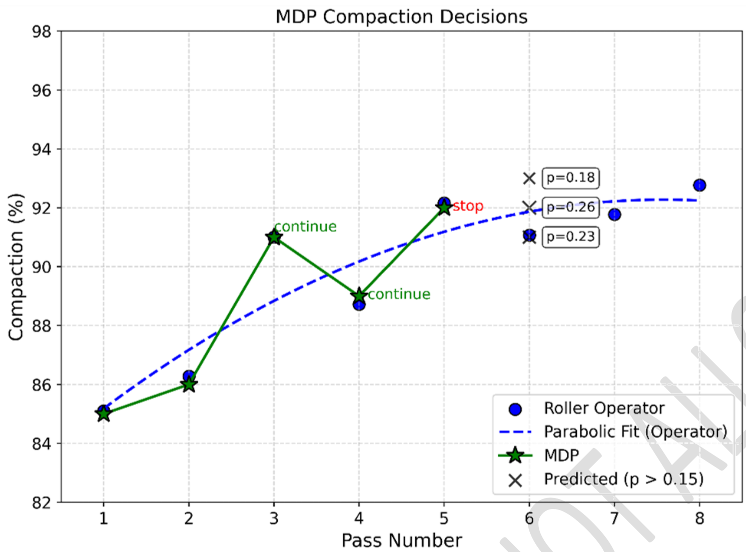

Figure 3: *MDP decision vs roller operator for an example segment near Bourbonnais, IL.*

4 Conclusions

Optimizing compaction rolling pattern during newly constructed AC pavements would avoid over- and under-compaction. In this study, a Markov Decision Process (MDP) was used to model the rolling pattern and recommend decisions to roller operators based on operational costs and acceptance limits by agencies. The developed MDP shows promising results in achieving target densities with minimal operational costs and may be applied to other scenarios. Time and cost savings may also be quantified.

5 References

Abufares, L., Chen, Y., & Al-Qadi, I.L. 2025. Asphalt Concrete Density Monitoring During Compaction Using Roller-mounted GPR. Automation in Construction, 174.

Al-Qadi, I. L., Rivera-Perez, J. J., García Mainieri, J. J., & Sayeh, W. 2021. Illinois' Experience Using Quality Control for Performance and Pay for Performance to Determine Pay for Hot-mix Asphalt. Report No. FHWA-ICT-21-018. Illinois Center for Transportation, Rantoul, IL.

Hughes, C. S. 1989. Compaction of asphalt pavement. National Cooperative Highway Research Program, Synthesis of Highway Practice 152.

Illinois Department of Transportation (IDOT). 2019. Internal Memorandum 80347: Special Provision for Hot-Mix Asphalt- Pay for Performance Using Percent within Limits- Jobsite Sampling. Springfield, Illinois.

Illinois Department of Transportation (IDOT). 2019. Internal Memorandum 80383: Special Provision for Hot-Mix Asphalt- Quality Control for Performance. Springfield, Illinois.

Leng, Z., Al-Qadi, I.L., & Lahouar, S. 2011. Development and Validation for in-situ Asphalt Mixture Density Prediction Models. NDT & E, 44(4), 369-375.

Puterman, M. L. 1990. Markov Decision Processes. Handbooks in operations research and management science, 2, 331-434.

Overview of thermal data collected during accelerated pavement testing

Mohamed Belmokhtar
Univ Gustave Eiffel, MAST-LAMES, F-44344 Bouguenais, France
Martin Souop
Esigelec, Rouen, France
Armelle Chabot
Juiliette Blanc
Univ Gustave Eiffel, MAST-LAMES, F-44344 Bouguenais, France
Katia Chancibault
Univ Gustave Eiffel, GERS-LEE, F-44344 Bouguenais, France

Abstract

This work takes place in the context of global warming, where there is a strong need to analyse the climate resilience of motorways, airports and urban roads. In parallel, the global digital transition enables the collection of large amounts of data and the development of new automated models using statistics and machine learning. Environmental data, such as thermal temperature, serves as a key input to the models, making them more realistic and reliable in addressing challenges related to road bearing capacity. This work presents a new database that collects temperature data from various research projects carried out at the Gustave Eiffel University fatigue test track. Main of these tests includes topics such as performance of sustainable and innovative materials, maintenance and rehabilitation solutions, smart and multi-functional pavements… The database aims to cover a range of materials, structures, mechanical and environmental loads. These variables are collected in a format that is optimally structured for data and pavement structural analysis. A thorough data management process is carried out to synchronise the collected data with meteorological information. These efforts will allow efficient structuring, manipulation and visualisation of the data for further studies. The final objective of the database is to provide a tool that uses a standard architecture and is applicable to urban environments.

Keywords: climate, big data, temperature, pavements, accelerated pavement testing

1 Context

It is well established that the mechanical behaviour of pavements is highly sensitive to temperature variations, especially in a context of global climate change (Sias et al., 2025). Such knowledge is essential not only for evaluating the long-term mechanical performance of conventional pavements (Freitas et al., 2025), but also for emerging technologies such as electrified roadways and urban pavements (Mazhoud et al., 2025; Tormos et al., 2025), and for the development of advanced monitoring strategies. The increasing availability of big data now provides new opportunities for empirical and statistical investigations of pavement thermal states, an approach that has been adopted in several recent research initiatives (Roberts et al., 2023; Podolsky et al., 2023).

The Université Gustave Eiffel is equipped with a large-scale accelerated pavement testing facility which named fatigue carousel (Figure 1). Since its commissioning in 1982 (Autret et al., 1987), numerous accelerated loading tests have been conducted to establish design coefficients (Corte and Goux, 1996) and to evaluate the durability of French pavement structures. Over the past several years, temperature data have also been systematically collected and processed at this facility, enabling analyses of their effects on pavement behavior (Homsi et al., 2017; Barreira et al., 2020; Chabot et al., 2020). The present study is part of the French I-Site Future "CADILLAC" project, which aims to automatically acquire and centralize thermal data from the pavements tested by the Université Gustave Eiffel's fatigue carousel into a freely accessible web-based database. This initiative is intended to support both researchers and practitioners in the field of pavement engineering by providing open-access data for design, monitoring, and modelling applications.

***Figure 1**: Photo of one of the four arms of the Université Gustave Eiffel's accelerated pavement testing facility: Fatigue carousel.*

2 Methods and tools used to develop the database

For the development of the database, we relied on the archived temperature datasets generated from the accelerated pavement testing campaigns at the Université Gustave Eiffel. A comprehensive review of these archives highlighted the diversity of available information, which could be systematically categorized into distinct classes: project name, localization, climatic condition (from the French governmental public server https://www.data.gouv.fr/datasets/donnees-climatologiques-de-base-horaires/public server), structural and layers information, site observation, information about the temperature sensor and raw data collected. This classification enabled the establishment of a coherent framework for data organization and subsequent analysis. Each class is refined by the integration of descriptive attributes that can be data and metadata. To ensure robustness and interoperability, the database was implemented following an SQL relational model. In this model, tables were designed to represent the main classes, while logical relationships between them were established through the use of primary and foreign keys. The conceptual model of the database is illustrated in Figure 2, which presents the Unified Modelling Language (UML) schema.

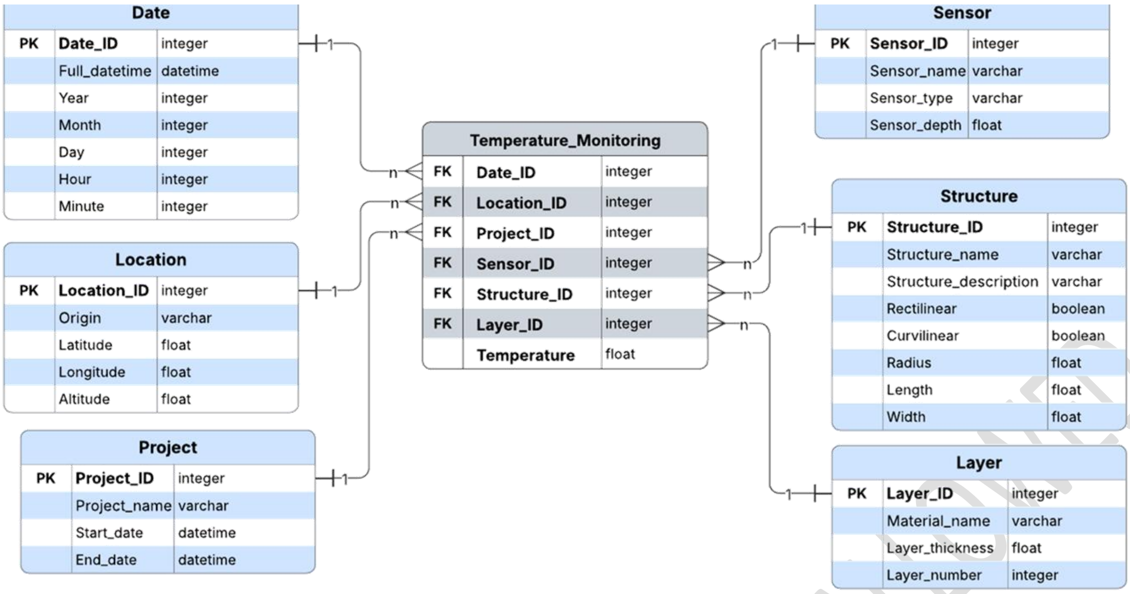

***Figure 2**: UML schema of the tables with attributes and their relationships: Data Warehouse (Khelifi, 2026).*

More generally, Figure 3a illustrates the overall data organization adopted including two primary servers: (i) a server dedicated to raw data and metadata collected from the instrumentation, and (ii) a server containing publicly accessible meteorological data obtained from online repositories. These two sources jointly feed a third, hybrid server, which consolidates the information into standardized *.csv* tables. Data integration in this hybrid server is achieved through both automated pipelines and manual inputs, ensuring flexibility while maintaining consistency across datasets.

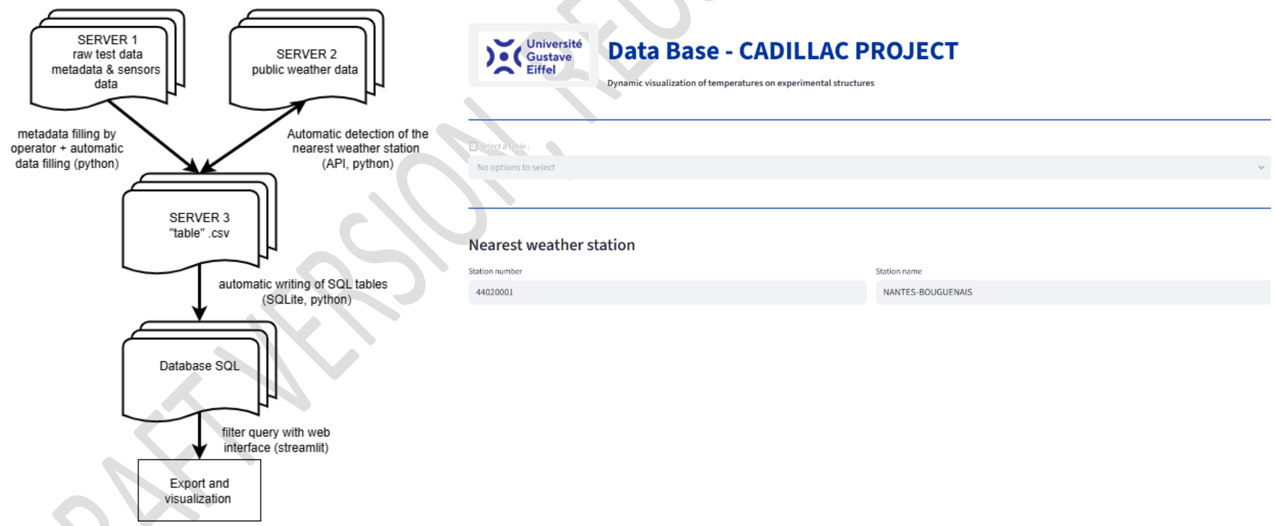

(a) *(b)*

***Figure 3:** CADILLAC Database (a) Data architecture with used programming tools (b) Web interface developed for data visualization.*

The database is designed to support the efficient execution of queries, enabling the extraction and visualization of temperature-related information through a web-based interface. The interface incorporates filtering functionalities based on the attributes defined in Figure 2. It allows targeted analyses (Figure 3.b).

3 Prospects

This work facilitates both data integrity and query efficiency, while providing a scalable structure for future extensions of the database. Specifically, the long-term objective of this tool is to include not only accelerated pavement testing data, but also datasets from other types of pavement, particularly those related to urban and airfield areas.

Furthermore, the proposed methodology has been conceived with sufficient flexibility to be applied to additional types of measurements, such as deformation monitoring or non-destructive testing results. This scalability ensures that the database can progressively evolve into a comprehensive resource, capable of supporting a wide range of applications in pavement research, design, and monitoring. Particularly, the French design method is based on an annual equivalent temperature of 15°C. The objective of collecting this temperature data is, firstly, to compile a comprehensive database of temperature data for pavement materials and structures, regardless of whether they are subjected to loading during APT projects (Khelifi, 2026). Ultimately, the aim is to improve the French design method by conducting a thermomechanical study based on the data.

4 References

Autret, P., de Boissoudy, A. B., Gramsammer, J. C. 1987. *The circular test track of the Laboratoire Central des Ponts et Chaussées – first results*. In: Proceedings of 6th International Conference on Structural Design of Asphalt Pavements, Ann Arbor, 13–17 June 1987, vol. 1, pp. 550–561

Barriera, M., Blanc, J., Chailleux, E., Pouget, S., Van Rompu, J., Lebental, B. 2020. *Procedure for Temperature Correction of Strains Measured in a Road Pavement*. In: Chabot, A., Hornych, P., Harvey, J., Loria-Salazar, L. (eds) Accelerated Pavement Testing to Transport Infrastructure Innovation. Lecture Notes in Civil Engineering, vol 96. Springer, Cham. DOI: 10.1007/978-3-030-55236-7_50

Chabot, A., Hornych, P., Harvey, J., Loria-Salaza, L. G. (eds) 2020. *Accelerated Pavement Testing for Transport Infrastructure Innovation*. Lecture Notes in Civil Engineering, Vol. 96. Springer International Publishing. Doi: 10.1007/978-3-030-55236-7.

Corte, J. F., Goux, M. T. 1996. *Design of pavement structures: the French technical guide*. Transp Res Rep 1539 (1), pp. 116–124. Doi: 10.1177/0361198196153900116.

Freitas, M., Hornych, P, Belmokhtar, M., Noel, R. 2026. *Asphalt pavements' temperature profile prediction combining a numerical model with weather data: a French case study.* In: Proceedings of 12th International conference on Bearing Capacity of Roads, Railways, and Airfields

Homsi, F., Bodin, D., Chabot, A., Hornych, P., 2017. *Effect of temperature on asphalt pavement strain responses: APT data and thermo-viscoelastic pavement modelling*. 17th AAPA International Flexible Pavements Conference & Exhibition, 13-16 August, Melbourne, Australia

Khelifi R., 2026, *Extrapolation à l'urbain des données préliminaires de Cadillac pour l'analyse de la résilience des chaussées urbaines au climat*. Master thesis, ISG Tunis, Tunisia

Mazhoud, B., Gabet, T., Bouron, S., Belmokhtar, M., 2025. *Development of a Thermal Fatigue Test to Assess eRoads.* Journal of Testing and Evaluation. DOI: 10.1520/JTE20240191

Podolsky, J., Bautista, E., Velasquez, R., Worel, B., 2023. Leveraging Thermal Couple Data at MnRoad. Data Science for Pavements Symposium, https://pavementdatascience.com/2023-presentations

Roberts, R., Menant, F., Broutin M. 2023. *Towards efficient airfield pavement surface condition monitoring using Deep Learning models*. Roads and Airports Pavement Surface Characteristics - Proceedings of the 9th International Symposium on Pavement Surface Characteristics, SURF 2022Conference Paper2023. DOI: 10.1201/9781003429258-85

Sias, J. E., Dave, E. V., Underwood, B. S. et al. 2025. *Climate change impacts on roadways*. Nat Rev Earth Environ, 6, pp. 555–573. Doi: 10.1038/s43017-025-00711-9.

Tormos, S., Chabot, A., Dave, E. V. 2024. *A Review of Urban Heat Island-Reducing Pavement Types and Thermal Properties*. In: Carter, A., Vasconcelos, K., Dave, E. (eds) 14th International Conference on Asphalt Pavements ISAP2024 Montreal. ISAP APE 2024. Springer, Cham. Doi: 10.1007/978-3-031-67252-1_35.

Integrating Automatic Layer Detection with Visco-Elastic Back-calculation from TSD-Based Deflection Data

Magnus H. Jørgensen
Greenwood Engineering, Danmark

Abstract

The Traffic Speed Deflectometer (TSD) enables continuous measurement of pavement response under a moving axle load, offering new possibilities for network-level structural evaluation. However, reliable backcalculation of material properties from TSD data requires accurate layer thickness information, which is often limited when relying on sparse bore cores or construction records. In this study, a U-Net-based deep learning model is applied to Ground Penetrating Radar (GPR) data to automatically extract pavement layer interfaces. The detected layer information is integrated with synchronized TSD measurements and used in a viscoelastic backcalculation framework. Two scenarios are compared: one using continuously estimated layer thicknesses and another simulating traditional bore core spacing. Results from a case study in Romania demonstrate that incorporating continuous layer information leads to higher estimated asphalt moduli, while subgrade and base layers remain relatively insensitive. The findings highlight the importance of accurate, spatially resolved layer data for reducing bias in backcalculated pavement properties. Key limitations, limited dataset size and restricted GPR penetration depth.

Keywords: deep learning; pavement evaluation; GPR; back calculation

1 Introduction

The Traffic Speed Deflectometer (TSD) is a continuous measurement device capable of capturing the road response under a moving 10-ton axle load and are used in network level pavement evaluation (Shresta et al., 2022). The measured deflection response can be used in back-calculation software to inversely estimate structural characteristics of the pavement, such as elastic moduli (E-moduli). Traditionally, such calculations have been performed using Falling Weight Deflectometer (FWD) data, where bore cores are often available at the measurement locations.

With TSD providing continuous measurements, bore cores or construction schematics may, in many cases, lead to inaccurate assumptions during back-calculation, as subsurface conditions can vary significantly along the road.

A U-Net architecture (Ronneberger et al., 2015) was developed to automatically extract layer information from Ground Penetrating Radar (GPR) radargrams. The network was trained exclusively on radargrams obtained using a GSSI 2 GHz air-coupled horn antenna. Validation metrics indicated moderate performance (IoU at 0.49, precision at 0.66); however, visual inspection showed that the model produced very few false positives and successfully identified dominant (high-amplitude) layer interfaces.

A commonly used index for assessing the condition of the upper pavement layer is the Surface Curvature Index (SCI-300), which quantifies curvature near the load using deflection values. Since TSD does not measure deflection directly, a derived index, SCI-TSD, has been introduced (Pehrsson et al., 2025):

$$SCI_{TSD} = \frac{(S_{Front} - S_{behind}) * l}{2}$$

where S_{front} and S_{behind} are the slope values in front and behind the axle load, respectively, and l m is the distance between the two points. Both SCI-300 and SCI-TSD quantify curvature near the load and are therefore highly correlated.

2 Methods

A case study is presented in which a trained model is applied to GPR data collected using a GSSI 2 GHz air horn antenna system mounted on a TSD operated by Greenwood Engineering A/S. The data were recorded near Bucharest, Romania, in 2025. The extracted layer information was synchronized with the TSD measurements and used as input for Greenwood's in-house viscoelastic back-calculation software (Nielsen, 2019), developed specifically for TSD data.

Two back-calculation scenarios were evaluated. In the first, layer thicknesses were obtained from the automated GPR-based layer detection. In the second, layer thicknesses were sampled at only four locations to simulate the use of bore core data, with these values applied to the nearest measurement points. A three-layer structure was used, consisting of an asphalt layer, a base layer (0.4 m), and a subgrade of infinite thickness. The base and subgrade thicknesses were held constant across all datasets.

3 Results and Discussion

Figure 1 shows the GPR radargram with detected layer interfaces overlaid, along with the corresponding SCI-TSD profile. The stars indicate the location used for bore core layers thickness. The dataset is 4 km long and is sampled every 1 meter. The SCI-TSD shows that the section looks relatively homogenous, with some spikes and deterministic structure. The same is seen with the GPR radargram, but the structure is more dynamic.

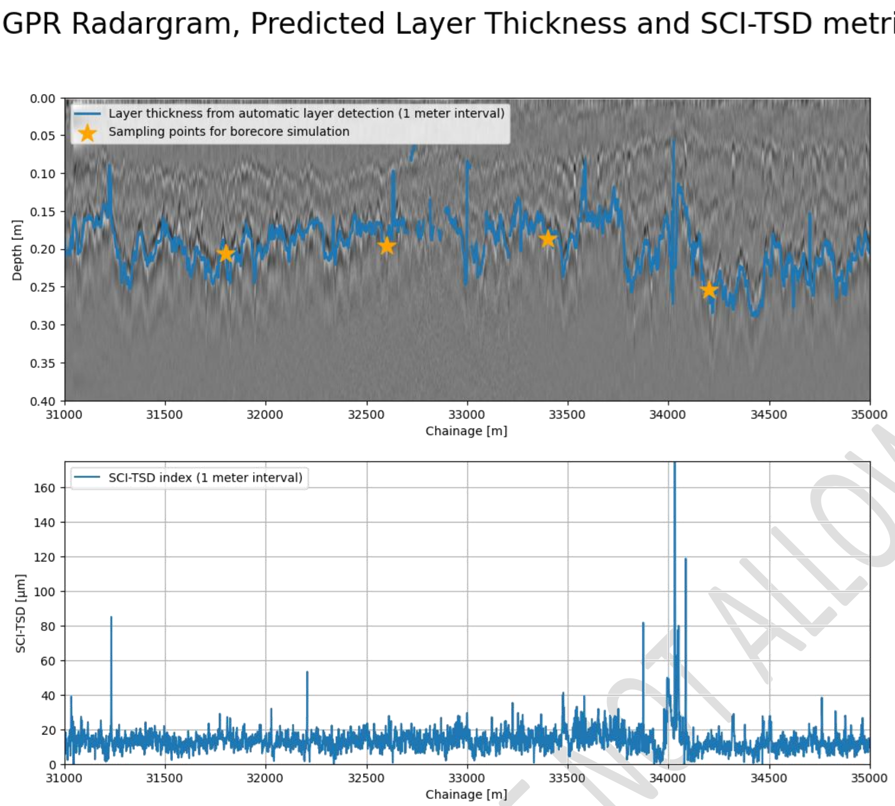

Figure 1: *Top) Calculated Layer thickness from automatic layer detection overlaid on the GPR radagram, Y-axis have been scaled such that the two datasets coincide with each other. Orange stars indicate position of 'bore cores' used for second dataset calculation.*

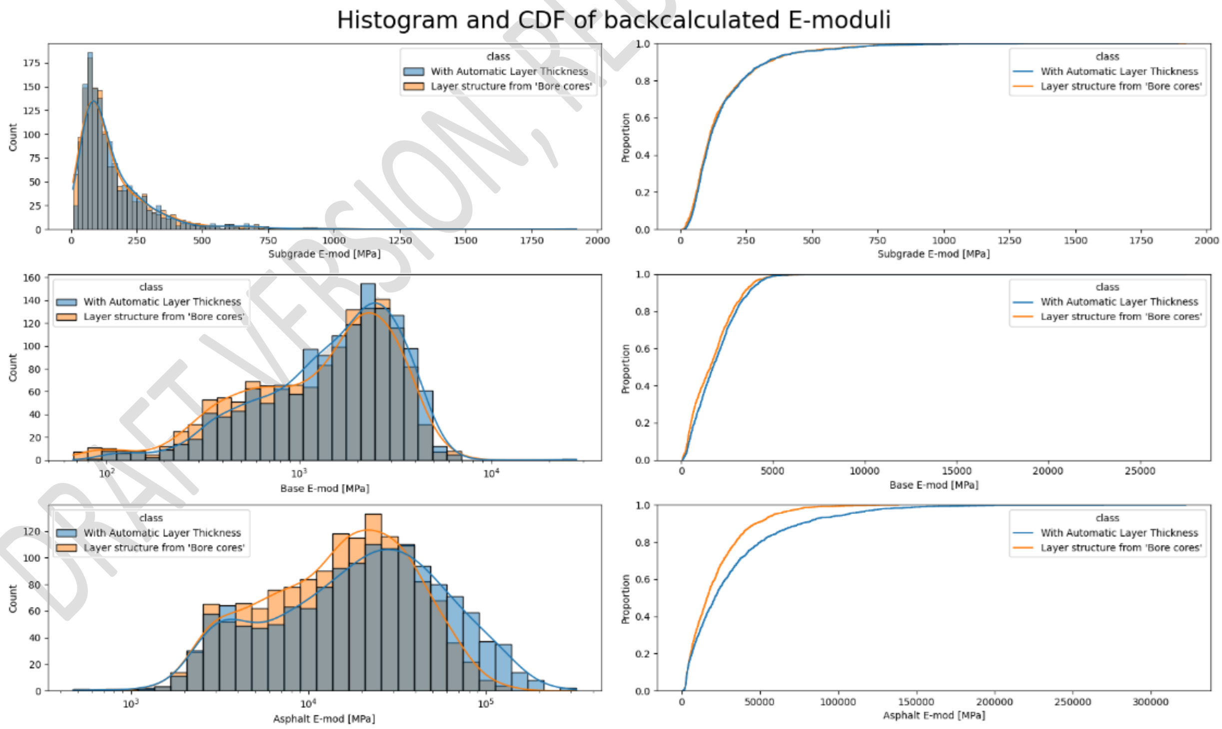

Figure 2: *Plots of histograms and Cumultive Distribtution Functions (CDF) of the back-calculated values generated from the two datasets with full layer information and the other with 'bore core' information only.*

Figure 2 shows that the estimated E-moduli of the subgrade and base layers are relatively insensitive to the assumed layer thickness. This is expected, as these parameters were held constant in both scenarios. In contrast, a clear difference is observed in the cumulative distribution function (CDF) of the asphalt layer modulus.

When using continuously estimated layer thicknesses, the distribution exhibits a heavier upper tail compared to the bore core-based approach. This suggests that neglecting spatial variation in layer thickness leads to a systematic underestimation of the asphalt modulus.

4 Conclusions

This research showed the need for the better layer information for back-calculating the E-moduli of pavement structures, and using automatic layer detection in GPR is a good approach to obtain the information for continuous structural data. Several uncertainties should be noted. The dataset is relatively small and was selected based on clear and interpretable layer structures, which may limit generalizability. Other sections exhibited discontinuities and ambiguous layers that were challenging for both manual interpretation and automated detection. Finally, GPR penetration depth is limited, which may result in inaccurate estimation of deeper layers such as the base. These limitations should be addressed in future studies.

5 References

Shresta, S. Katicha, S. Flintsch, G. & Diefenderfer, B. 2022. Implementing Traffic Speed Deflection Measurements for Network Level Pavement Management in Virginia, Journal of Transportation Engineering, Part B: Pavements, Volume 148, Issue 2.

Ronneberger, O. Fischer, P. Brox, T. 2015. U-Net: Convolutional Networks for Biomedical Image Segmentation. Medical Image Computing and Computer-Assisted Intervention. pp. 234-241

Pehrsson, H. Malmgren-Hansen, D. Arokia, M. Grønskov, L. 2025. SCITSD: A New Structural Curvature Index for Strain Analysis of Large Road Networks. Transport Transitions: Advancing Sustainable and Inclusive Mobility. TRA Conference 2025. pp. 104-110

Nielsen, C. P., 2019. Visco-elastic back-calculation of traffic speed deflectometer measurements. Transportation research records, 2673(12). pp. 439-448

Domain adaptation of modern large language models in pavement engineering through advanced information retrieval

Mason Smetana
Igor Sukharev
Lev Khazanovich
Department of Civil and Environmental Engineering, University of Pittsburgh, USA

Abstract

Recent advancements in artificial intelligence have ushered in a wave of large language model (LLM) assistants, such as ChatGPT and Gemini, that are reshaping professional workflows. Within the realm of pavement engineering and other civil engineering disciplines alike, these tools have a unique potential to assist with document understanding, specification adherence, knowledge management/transfer, and employee training. This study, in collaboration with state and local agencies of Pennsylvania, U.S., seeks to minimize the gap in LLM understanding of pavement design, construction, and maintenance information, providing a more deterministic approach to question answering in the domain. By applying an advanced retrieval technique, queries related explicitly to pavement knowledge embedded in industry documentation can be addressed with high confidence and transparency. An artificial dataset of over 10,000 question-answer pairs was generated and evaluated to test the proposed system. Early findings indicate that this approach outperforms traditional Retrieval-Augmented Generation (RAG) by at least 20%.

Keywords: pavement engineering; artificial intelligence; large language models; knowledge management; information retrieval

1 Introduction

Large language models (LLMs) continue to improve in general knowledge capability and complex comprehension tasks (Lightman et al., 2023); however, proprietary model providers tend to neglect the gap in domain expertise for niche areas of science and engineering. Many models also persistently struggle with "hallucinations," or the generation of factually inconsistent content, which is inherently a product of their probabilistic nature. While general-purpose models like ChatGPT are commonly used for everyday tasks, domain-specific models still need to be crafted to better capture professional knowledge. This study seeks to close this gap by building upon our previous work on improving LLM performance with pavement engineering knowledge and dually promoting more deterministic, traceable output from generative models (Smetana et al., 2025).

Retrieval-Augmented Generation (RAG) stands as an attractive alternative to increase pre-trained LLM performance on various tasks without resource-intensive finetuning. It is lightweight, adaptive, and relatively easy to implement on industry documentation. Based on the results of our previous study, the combination of open-source models, which have some degree of out-of-the-box understanding of pavement-related content, and RAG could improve pavement engineering question answering by as much as 29%. However, most of these retrieval techniques rely on an unrepresentative similarity metric of cosine, which has been questioned by various researchers regarding its actual meaning and accuracy (Steck et al., 2024). Additionally, most retrieval systems will supply top-k relevant texts to the model, with no resolution on conflicting information.

2 Advanced Retrieval Mechanism & Preliminaries

Based on the limitations of cosine similarity in RAG systems, we introduce an adaptation of a lightweight multi-layer perceptron (MLP) classifier, similar to the model proposed in (Li et al., 2025). This classifier is trained on over 10,000 LLM-generated question-answer pairs from PennDOT Publication 242 (PennDOT, 2025), with each pair containing important metadata information, including its parent chapter and subsection. Traditional cosine retrieval answers these questions with an accuracy of approximately 47%, whereas the MLP classifier approach shows preliminary accuracy of 70% – a marked increase over naïve methods. Furthermore, the devised methodology, which is agnostic of LLM selection, can be used in conjunction with most open-source models to combat potential data privacy and security concerns.

The classifier demonstrates generalization abilities for questions outside of training data, including the capability of providing the most relevant information from specifications (with exact reference text) and surfacing uncertainty in answering ambiguous questions, where most flagship LLMs don't exhibit this behavior. For example, the query "how to calculate k-value?" could be answered by two independent sections of Pub 242, depending on design type: chapter 10.4 for overlay of JPCP or chapter 8.6 for new rigid pavement.

Figure 1 illustrates the retriever output for the k-value query, with word saliency scores (Yoo et al., 2024), probabilities of relevant sections, and each word's impact on prediction per chapter/subsection: blue (+) guides prediction and red (−) derails. A higher saliency indicates that the model considers a word as more important for prediction. In this example, the word "k-value" has the highest saliency (+0.93), pulling the retriever toward both 10.4 and 8.6, which is why the model predicts a 77% and 21% probability for each section, respectively. These distributions indicate that follow-up information regarding the type of pavement design (overlay or new) will be required to accurately answer this question and retrieve relevant specification text. Due to this ambiguity conflict, even when supplemented with the entire specification PDF, proprietary models such as ChatGPT or Gemini tend to guess an answer based on one design type and may not ask the user to clarify their intention.

		Chapter.Subsection (Process)					
Token (w_i)	**Score$_i$**	**1.3 (1)**	**6.2 (6)**	**8.6 (1)**	**8.9 (1)**	**10.4 (2)**	**10.4 (3)**
how	**+0.19**	0.0	-0.01	-0.15	0.0	0.00	+0.15
to	+0.01	0.0	0.00	-0.01	0.0	0.00	+0.01
calculate	**+0.70**	0.00	+0.01	-0.55	-0.01	0.00	+0.54
k-value	**+0.93**	-0.01	+0.01	+0.21	+0.01	-0.41	+0.72
?	-0.03	0.00	0.00	+0.02	0.00	0.00	-0.02
Probabilities (z_i), %		0.00	0.93	**21.2**	0.12	0.02	**76.9**

***Figure 1:** Average MLP probabilities and chapter/subsection saliency for the k-value query.*

3 Conclusion

Many engineering specifications and industry documents are written in dense, highly technical language that presumes specialized domain expertise. With recent advancements in large language models (LLMs), new opportunities have emerged to enhance document understanding and productivity in professional engineering workflows. However, while modern models perform well in general-purpose applications, their effectiveness in niche scientific and engineering domains remains limited. Consequently, information retrieval techniques such as Retrieval-Augmented Generation (RAG) offer a practical solution to this limitation.

This study presents the early findings of an advanced retrieval approach designed to improve LLM performance on pavement engineering specifications, including documents such as PennDOT Pub 242. The proposed multi-layer perception (MLP) classifier, trained on more than 10,000 question-answer pairs, outperforms traditional retrieval techniques by as much as 20%. Preliminary results further demonstrate that the classifier generalizes to questions outside of the training corpus and more effectively resolves ambiguities in cases involving conflicting or context-dependent specification requirements, such as the k-value query example. Future work will expand the corpus of industry documents used to train the retriever, which will naturally result in a much larger, comprehensive pavement engineering knowledge base. An important byproduct of this approach will enable future chatbots to be more deterministic and transparent in responses, which is critical for engineering applications.

4 References

Lightman, H., Kosaraju, V., Burda, Y., et al. 2023. Let's Verify Step by Step. arXiv Preprint. https://doi.org/10.48550/arXiv.2305.20050

Pennsylvania Department of Transportation. 2025. Publication 242 Pavement Policy Manual, October 2025 Edition, Change No. 10. PennDOT, Harrisburg, PA, USA.

Li, K., Dong, C., Fang, X., & Li, D. 2025. Automated Text Classification of Construction Inspection Report: A Small Samples Training Approach. Proceedings. Sixth International Conference on Civil and Building Informatic, ICCBEI2025, 22, pp. 543-557, Kapla Publications in Computing, Hong Kong, China.

Smetana, M., Sukharev, I., & Khazanovich, L. 2025. Evaluating Expertise of Concrete Pavement Construction in Modern Large Language Models. Transportation Research Record, 2679(11), pp. 805-821.

Steck, H., Ekanadham, C., & Kallus, N. 2024. Is Cosine-Similarity of Embeddings Really About Similarity?. Proceedings. ACM Web Conference, WWW'24, pp. 887-890, Association for Computing Machinery, Singapore, Singapore.

Yoo, B., Kim, J., Park, S., Ahn, C. R., & Oh, T. 2024. Harnessing Generative Pre-Trained Transformers for Construction Accident Prediction with Saliency Visualization. Applied Sciences, 14(2), pp. 664.

Influence of Reduced Lateral Wandering by Connected and Automated Vehicles on Rutting and Fatigue of Elastic Pavements

Taavi Tõnts
Estonian Transport Administration (ETA) Road Design Expert Development Department, Estonia

Abstract

Connected and automated vehicles (CAVs), as well as vehicles equipped with advanced driver-assistance systems (ADAS), are engineered to maintain an almost constant lateral position within a traffic lane. Although this improves safety, the resulting reduction in lateral wandering concentrates wheel loads and can create a "rail-type" damage pattern that accelerates rutting and fatigue in elastic pavements. This effect is likely to be compounded by the European Commission's draft revision of Directive 96/53/EC, which would raise the allowable single-driving-axle load for zero-emission vehicles (ZEVs) to 12.5 t. Because the European Union maintains roughly 5 million km of roads valued at more than €8 trillion, the combined influence of reduced lateral wandering and higher axle loads could significantly shorten pavement service lives and erode the value of public road assets. This paper quantifies these impacts through various mechanistic–empirical modelling analyses, calibrated with long-term pavement performance data, and incorporates the perspectives of road authorities on these emerging risks.

Keywords: connected and automated vehicles; lateral wandering; rutting; fatigue; flexible pavements; zero-emission vehicles

1 Introduction

The transition toward connected and automated vehicles (CAVs) is reshaping the design requirements of road infrastructure. Existing pavement design methods assume random lateral wandering by heavy vehicles, which distributes traffic loads across the lane. CAVs, however, travel with precise lane-keeping systems, leading to much more concentrated loading paths. Combined with higher axle loads of zero-emission vehicles (ZEVs), these trends may significantly shorten the design life of flexible pavements.

Europe’s 5 million km of roads, valued at more than €8,000 billion, represent a critical public asset. Even in smaller countries such as Estonia, with only 40,000 km of highways (asset value of approximately €5 billion), the cumulative effect of CAV traffic could reduce pavement service lives by 20–50%. Therefore, understanding and mitigating these impacts is essential.

2 Impact on Flexible Pavements

2.1 Rutting and fatigue caused by reduced wandering

Traditional driver behaviour results in relatively wide lateral wandering, which reduces rutting and fatigue. Studies show that, in the absence of wander (CAVs with strict lane keeping), rutting may increase by 30–56%, while fatigue damage may accelerate by a factor of 2–3 (see Figure 1; K. Georgouli et al., 2021).

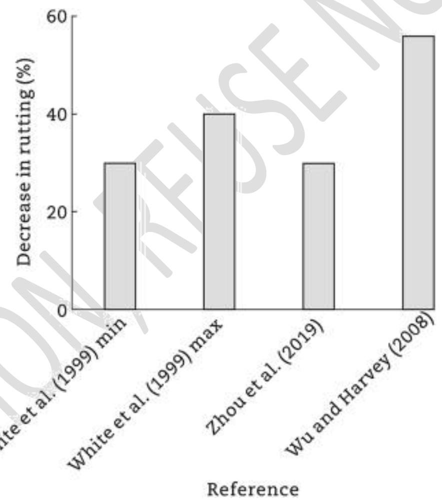

Figure 1: *Impact of wheel wander on rutting.*

2.2 Platooning effects

Platoons of CAV trucks further concentrate loading. With inter-truck gaps as short as 0.5 s and high pavement temperatures (approximately 35 °C), service life reductions of up to 79% have been observed (see Figure 2; P. Leiva-Padilla et al., 2024).

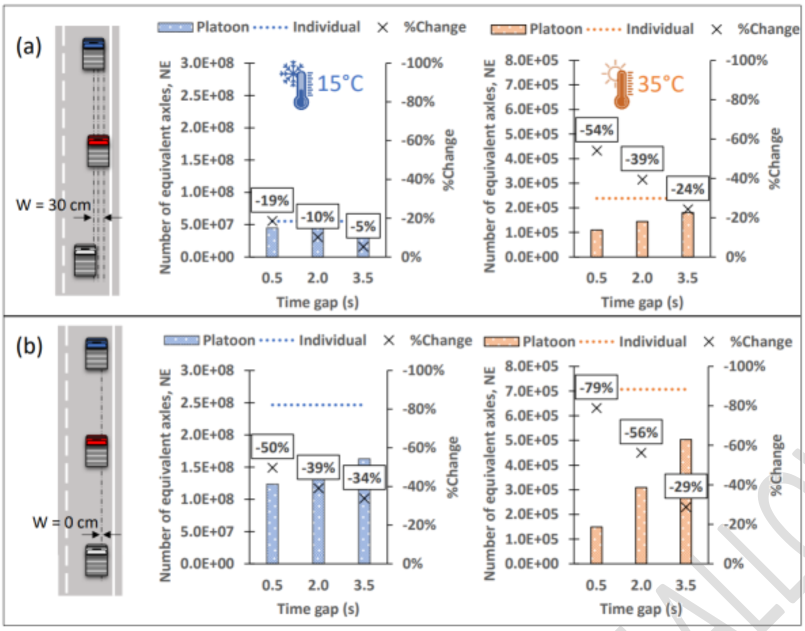

Figure 2: *Pavement service lives, expressed as the number of equivalent axles (NE), for 3-truck platoons at 80 km/h.*

2.3 Effect of higher axle loads (ZEV 12.5 t)

The proposed revision of Directive 96/53/EC would allow ZEVs to operate with 12.5 t drive axles, compared with the current 11.5 t. According to the fourth power law, this additional tonne increases pavement stress by approximately 40% (Table 1). For example, in the case of a two-axle ZEV bus, the average impact, including the front axle, increases by more than 30% (Schmidt et al., 2021).

Table 1*: Fourth power law.*

Axle load, t	Ratio to 10 t standard axle	Fourth-power impact
10	1.00	1.0
11.5	1.15	1.7
12.5	1.25	2.4
	Increase from 11.5 t to 12.5 t:	0.69
	Additional ESAL (stress) on roads:	**40%**

Under the fourth power law, an additional one-tonne load on an 8 t axle (i.e., the average load on a trailer's tridem axle) means a 60% stress increase for the existing pavement. The average stress from a five-axle ZEV could rise by more than 40% under the fourth power law. Road owners should compensate for this increase by constructing thicker pavements in good time.

2.4 Mitigation Strategies

Road authorities have three main options:
- Reactive approach: maintain pavements more frequently as deterioration accelerates;
- Proactive approach: design thicker pavements (e.g., base layers) today, anticipating future traffic;
- Smart and proactive approach: implement Intelligent Access (IA), where CAV behaviour (lateral wander, platoon gaps and speed) adapts dynamically.

European standards should start addressing new types of vehicles such as CAVs. From the road owner's point of view, one option is to standardize a minimum lateral wandering amplitude for CAVs and a minimum spacing between vehicles, depending on external conditions (weather, surrounding traffic, etc.). It may also be possible to standardize, for example, a random offset from the lane centre for each platoon truck and a minimum distance between trucks, so that CAV traffic simulates the annual average lateral deviation curve of human-driven traffic.

3 Conclusions

CAVs introduce new challenges for pavement performance by reducing lateral wandering and, in combination with ZEV axle loads, intensifying rutting and fatigue damage. Studies suggest reductions in pavement service life of between 30% and 70%. The most promising solution is the early adoption of European-level standards that regulate CAV lane positioning, inter-vehicle distances and axle load allowances. Coupled with Intelligent Access, such measures can help ensure sustainable pavements.

4 References

K. Georgouli, C. Plati, and A. Loizos, “Autonomous vehicles wheel wander: Structural impact on flexible pavements”, J. Traffic Transp. Eng. Engl. Ed., vol. 8, no. 3, pp. 388–398, June 2021, doi: 10.1016/j.jtte.2021.04.002.

P. Leiva-Padilla, J. Blanc, O. Chupin, A. Salgado, F. Hammoum, and P. Hornych, “Effect of different platoon configurations on strains and fatigue performance of flexible pavements”, Road Mater. Pavement Des., vol. 25, no. sup1, pp. 153–165, June 2024, doi: 10.1080/14680629.2023.2192814.

Schmidt, F., Tõnts, T., Asp, T., and Aarts, L. (2025). Impact on infrastructure of reduced lateral wandering by CAVs. HVTT18 Proceedings.

Design of the main apron at Ljubljana Airport

Brecelj Matija
go-plan, projektivni biro d.o.o., Slovenia
Stanič Dalibor
go-plan, projektivni biro d.o.o., Slovenia
Frelih Dunja
Fraport Slovenija d.o.o., Slovenia

Abstract

In 2026, Fraport Slovenija d.o.o. will carry out rehabilitation works on the main airport apron covering a total area of approximately 37,400 m². The rehabilitation includes the replacement of the existing asphalt pavement structure with a new concrete slab at aircraft parking positions, as well as the construction of a flexible asphalt pavement structure on the remaining surfaces. The works also include the installation of airfield lighting and navigation system elements.

Prior to the design phase, investigations of the composition and quality of the existing pavement structures were conducted, based on which appropriate technical solutions were developed. In the concrete apron area, a 38 cm thick slab is planned, divided into individual panels of up to 22 × 22 m, subsequently saw-cut into a 5.5 × 5.5 m grid. On the asphalt surfaces, the pavement structure will consist of three layers of high-modulus asphalt with a total thickness of 24 cm.

As European regulations do not provide sufficient support for the design of airfield pavements, the FAA methodology and Faarfield software were used for the design of the concrete slabs, while SOFiSTiK was employed for additional verification using the finite element method. The paper presents the pavement design process and the key solutions ensuring the functionality and durability of the new apron.

Keywords: concrete apron; Faarfield; SOFiSTiK; finite element method; slab curling

1 Introduction

The main airport apron at Ljubljana Airport, designated GLP 3 and GLP 4, represents a critical part of the infrastructure that supports daily aircraft operations. Parts of the apron were originally built in 1963 and last comprehensively reconstructed in 1978 and 1989. Since then, the pavement has been subjected to increasingly heavy traffic, including larger aircraft of ICAO/EASA categories E and F.

Over the years, significant deterioration has been observed. The asphalt wearing course shows fatigue cracking, block cracking, and ravelling, while local rutting and depressions are visible at parking positions where aircraft main gear loads are concentrated. Some areas were previously rehabilitated through overlays, but reflective cracking and progressive fatigue damage persisted.

In the context of Fraport Slovenia's long-term investment plan, a full rehabilitation of approximately 37,000m² of the apron has been scheduled. The project requires not only surface renewal but also structural upgrading, especially on parking stands, where rigid concrete pavements are considered more appropriate due to repeated high wheel loads.

Although European standards provide certain recommendations for the design of airfield pavements, they often do not offer sufficient guidance for practical application in large-scale projects. Therefore, international practices, particularly the FAA guidelines, are frequently applied as a reference.

The aim of this paper is to present the design process of the main apron rehabilitation, including the selection of pavement types, the applied calculation methods, and the use of specialized software tools. Special attention is given to the dimensioning of rigid concrete pavement structures and the verification of results using finite element analysis.

2 Background and history review

Globally, in addition to Jointed Plain Concrete Pavements (JPCP), Continuously Reinforced Concrete Pavements (CRCP) are also utilized; however, design approaches for the latter have not been established in Slovenia. Consequently, the majority of concrete pavements are designed as Jointed Plain Concrete Pavements (JPCP). The following section provides a general overview of Slovenian, European, and international legislation and guidelines for the design of JPCP pavements.

In Slovenia, we rely heavily on the Technical Specifications for Roads (TSC). Although these are generally not mandatory, some investors include them as a compulsory part of their projects. Concrete pavements are addressed by two guidelines: TSC 06.420:2003 (Bound Wear-Resistant Layers – Cement Concrete) and TSC 06.530:2009, which covers the design of cement concrete pavements. Both guidelines were prepared exclusively for road traffic and cannot be directly applied to the design of airfield surfaces. Furthermore, the TSC in question does not provide recommendations for joint execution or the planform dimensions of the slabs between joints.

Similar principles and procedures for determining appropriate thicknesses were also implemented in the JUS standards, according to which the existing concrete apron was designed and constructed. Cement concrete pavements were covered by the JUS U.E3.020 standard from 1987. This standard specified minimum concrete slab thicknesses based on traffic load (e.g., 20 cm for very heavy traffic), and also provided well-defined joint details and maximum planform dimensions for individual slabs.

At the European Union level (and other European countries), there is no unified method for the dimensioning of concrete pavements. Each country employs its own methods; most countries use empirical methods (the so-called German method), while a smaller number of countries utilize analytical methods (the so-called Dutch method). Opinions on which method is more appropriate are divided, but the most effective approach is likely a combination of both. Therefore, the ACR – PCR method has become the established standard in the field of airfield surfaces.

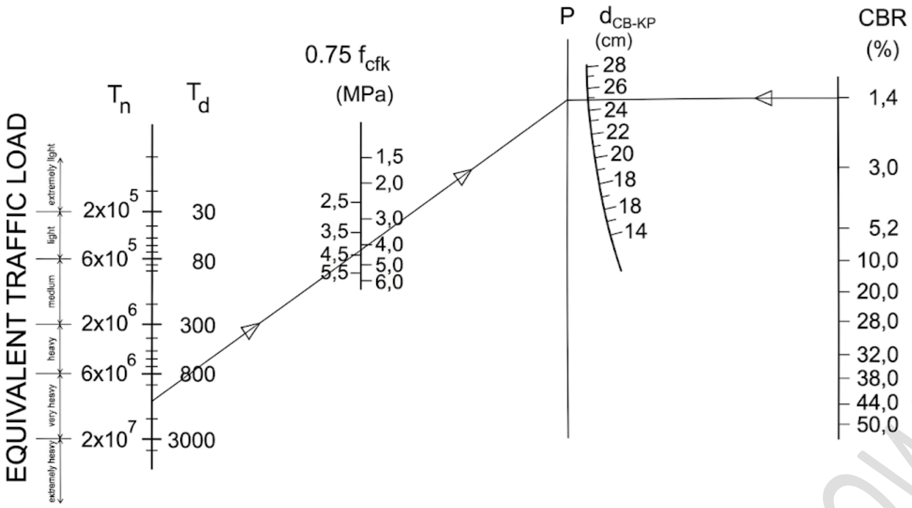

Figure 1: Nomogram for determining the thickness of the cement concrete wearing course (Republika Slovenija Ministrstvo za promet: 2009).

A common weakness of all methods and recommendations for the design of unreinforced concrete airfield surfaces is the determination of appropriate planform dimensions of the slabs, which are significantly influenced by thermal effects that are not accounted for in these methods.

3 Design methodology and technical basis

The aim and purpose of the design was to determine the required concrete slab thickness and joint spacing for airfield main apron.

The design approach combined empirical-analytical and numerical methods:

- **FAARFIELD 2.1.1 (FAA)** was used to determine the required pavement thickness based on cumulative aircraft traffic, load spectra, and fatigue damage models. The governing aircraft was identified as the Airbus A321XLR, whose load contributions dominated the cumulative damage factor.
- **SOFiSTiK** finite element software was employed to simulate stresses and strains in the pavement under different load scenarios. The model considered self-weight, rheological effects (creep and shrinkage of concrete), temperature gradients, and aircraft loads. Special attention was given to the interaction between slab geometry, joint spacing, and subgrade reaction.

Input data:

- Concrete class C30/37 with elastic modulus 32,837 MPa, density 25 kN/m³, and thermal expansion coefficient 1.0×10^{-5}.
- Reinforcement steel B500B with modulus 200,000 MPa (for new concrete slabs).
- Subgrade reaction modulus kv ≈ 84,000 kN/m³, derived from plate load tests and correlations with CBR values.
- Joint friction coefficient conservatively set to 1.5 due to the presence of slip layers (2 x PE foil).
- Joint spacing: 7.5 × 7.5 m (existing slabs), 5.5 × 5.5 m (proposed).

Both existing slabs (26 cm concrete + 14 cm overlay) and newly designed slabs were analyzed to assess performance.

4 Results

4.1 Existing slab

The analysis of the overlaid slab (total thickness 40 cm) revealed tensile stresses at the bottom surface of up to 5.28 MPa under combined load scenarios. Given that the original material properties are uncertain and likely degraded over time, this stress level is considered unsafe. Reflective cracking observed in practice supports this conclusion, as the fatigue resistance of the old concrete is already exhausted.

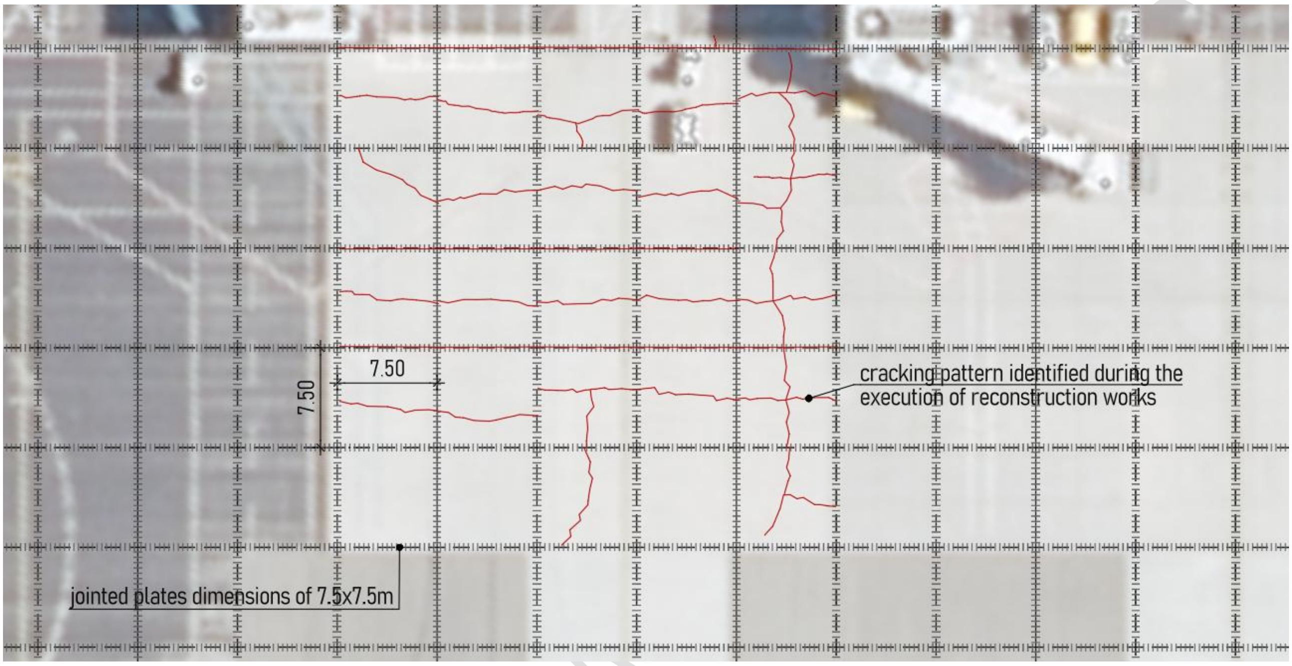

Figure 2: *Elevation view section of old concrete slabs area with recorded cracking pattern during execution of reconstruction works (Aerodrom Ljubljana, d.d.: 2011).*

4.2 New slab design

FAARFIELD determined a required slab thickness of 379 mm, rounded to 380 mm, for a 40-year design life. FEM analysis confirmed that stresses under critical load combinations remained below allowable limits for both the ultimate limit state (ULS) and the serviceability limit state (SLS).

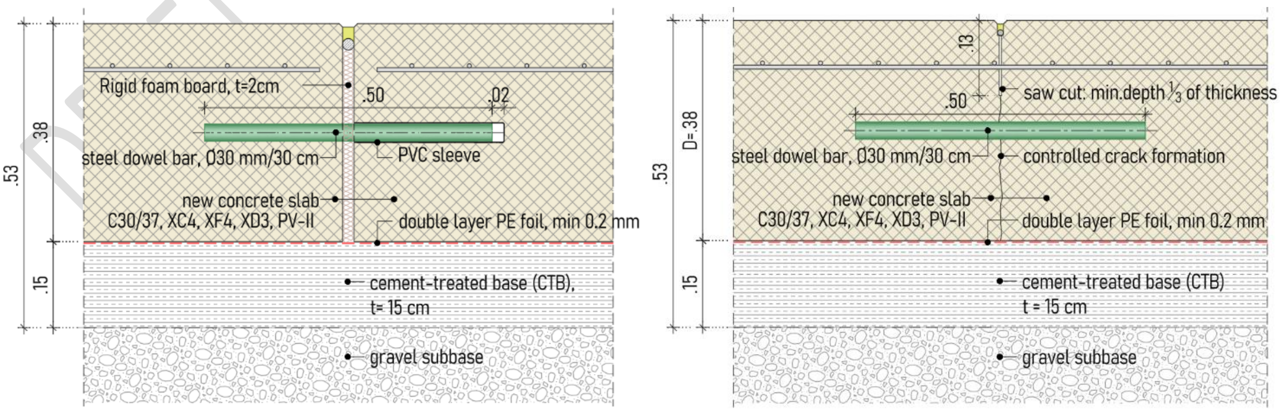

***Figure 3**: Joint section view. Left is expansion joint, right is contraction/control joint (go-plan d.o.o.: 2024).*

- **Joint spacing effect:** Reducing the joint grid from 7.5 m to 5.5 m significantly lowered tensile stresses and minimized curling effects from thermal gradients.
- **Temperature gradients**: Thermal analysis considered uniform shifts of ±24 °C and linear gradients of ±10 °C, both of which remained within acceptable stress margins.
- **Rheological effects:** Long-term shrinkage deformation was estimated at 0.308 ‰ over 50 years. FEM modelling confirmed that differential shrinkage between adjacent slabs is effectively mitigated with the proposed joint configuration.

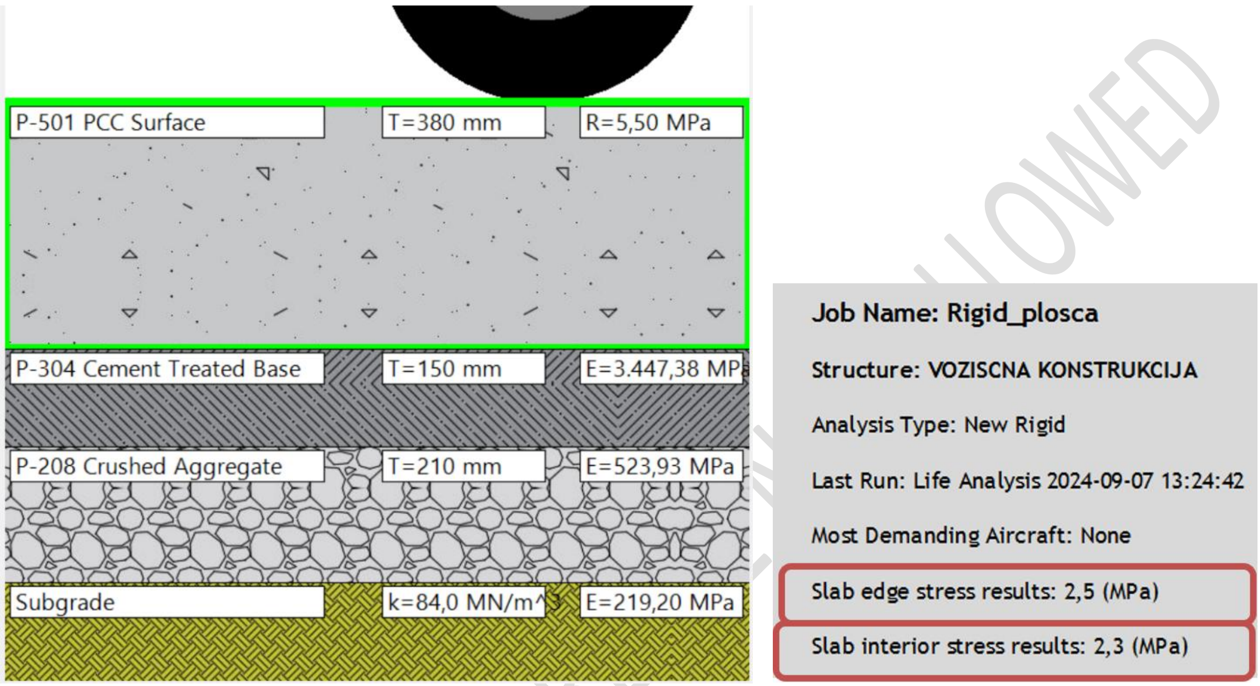

Figure 4: Proposed structure and results of concrete slab design from Faarfield.

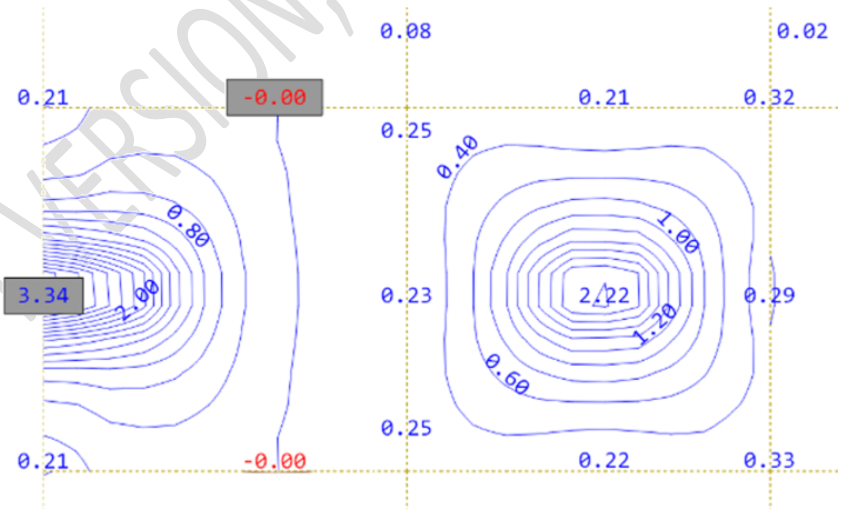

Figure 5: Stresses (in MPa) on bottom surface of slabs for regular loading – aircraft load on edge of slab, calculated using SOFiSTiK.

5 Discussion

The results demonstrate the importance of combining mechanistic-empirical FAA-based pavement design with detailed finite element simulations. While FAARFIELD ensures compliance with international standards for thickness design, FEM provides insight into stress concentrations, joint performance, and thermal effects, which are crucial for durable apron performance.

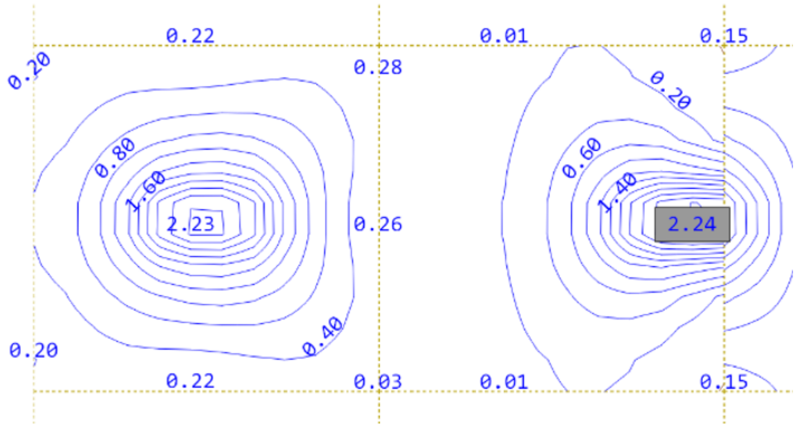

***Figure 6**: Stresses (in MPa) on bottom surface of slabs for regular loading – aircraft load at center of slab length, calculated using SOFiSTiK.*

The comparison between existing and new slabs highlights that simple overlays cannot ensure long-term serviceability. Instead, full replacement with a new 380 mm thick rigid pavement is the only sustainable solution. The proposed joint grid and reinforcement detailing (including dowel bars and weak reinforcement with PP fibres) will further enhance crack control and durability.

6 Conclusions

The structural analysis confirmed that the existing apron structure is no longer adequate for heavy aircraft operations at Ljubljana Airport. The newly designed 380 mm concrete pavement with optimized joint spacing meets all design requirements for a 40-year service life. This solution provides improved resistance to fatigue, rutting, and thermal cracking, ensuring safe and reliable operation of the airport infrastructure.

A particular added value of this study lies in the application of finite element modelling using SOFiSTiK. While FAARFIELD provided the baseline slab thickness according to FAA standards, the FEM analysis enabled a much more detailed assessment of stresses, temperature gradients, shrinkage, and joint behaviour. This dual approach not only verified the adequacy of the design but also gave deeper insights into the mechanisms of slab performance, especially in terms of long-term durability and serviceability. Such integration of FEM methods into pavement engineering represents a significant step forward in ensuring robust and reliable airfield infrastructure. It has been demonstrated that the temperature load gradient and the slab dimensions are critical factors in determining the adequacy of the assumed slab thickness. In particular, more attention should be devoted to thermal loads in future research, and the findings should be integrated into dedicated software for design of JPCP (e.g., FAARFIELD).

7 References

FAA, FAARFIELD 2.1.1. User Manual.

Igmat d.d. (2024). Elaborat za izvedbo obnovitvenih del glavne letališke ploščadi na delih GLP 3 in GLP 4.

go-plan d.o.o. (2024). Projektna dokumentacija PZI: Obnova voziščne konstrukcije.

Republika Slovenija Ministrstvo za promet (2003). TSC 06.420:2003 Vezane obrabnonosilne plasti – Cementni beton.

Republika Slovenija Ministrstvo za promet (2009). TSC 06.530:2009 Projektiranje Dimenzioniranje novih cementnobetonskih voziščnih konstrukcij.

SFRJ (1987). JUS U.E3.020 Tehnički uslovi za izradu cementnobetonskog kolovoza.

Karst Phenomena and the Use of BIM in the Construction of the Second Track Railway Line Divača – Koper

Franc Švegl
2TDK d.o.o., Ljubljana, Slovenia
Jure Česnik
Elea iC d.o.o., Ljubljana, Slovenia
Mitja Prelovšek
ZRC SAZU, Karst Research Institute, Postojna, Slovenia

Abstract

The alignment of the second track of the Divača–Koper railway line traverses one of the most intensely karstified regions in Slovenia, characterized by numerous caves, karstified lithological contacts, sinkholes, and groundwater occurrences. These features pose significant geotechnical challenges during construction, as they are difficult to predict in advance and can substantially affect ground bearing capacity, tunnel stability, and the long-term durability of the infrastructure.

During the excavation of the Lokev Tunnel (T1, length 6,714 m) and the Beka Tunnel (T2, length 6,017 m), a total of 77 karst caves were encountered, requiring detailed speleological investigation and site-specific adaptation of construction and bridging solutions, including hydrological measures.

This paper presents in detail the approach adopted to address complex karst phenomena, using the case of cave 2TDK-080, discovered during the excavation of Tunnel T2. The cave comprises laterally enlarged passages (caverns) containing collapse debris, groundwater sediments, and periodically active water flows, representing a direct risk to construction stability, site safety, and potential contamination of drinking water resources.

Specialized technical solutions were implemented, including separation of the tunnel from cave passages using blind lining systems, reinforced concrete bridging structures, and hydrological bypass arrangements. A key component of the project was the implementation of BIM technology, which enabled the integration of geological, geophysical, hydrological, speleological, and construction data into a unified 3D model. This approach ensured improved data transparency, enhanced visualization, faster identification of karst features, and more efficient communication among designers, contractors, the client, and geological, geotechnical, and karst supervision teams.

The upgraded 4D/5D BIM model further enabled real-time monitoring of the impact of karst cavities on construction scheduling and costs. The experience gained from documenting and bridging karst phenomena along the second track confirms that the combination of speleological supervision and digital modeling is essential for effective risk management in karst environments. The integration of multidisciplinary data into the BIM framework provided a robust basis for safe construction execution and the development of long-term sustainable solutions, which will also be valuable for future infrastructure projects in similar geological settings.

1 Introduction

Karst terrain between Divača and Koper represents one of the most challenging construction environments in Slovenia. The Divača–Koper second railway track (2TDK) spans approximately 27 km, with over 75 % of its length running underground (https://drugitir.si). The longest tunnels, double-tube Lokev (T1, 6714 m) and Beka (T2, 6017 m), mostly pass through highly karstified limestones formations with old relict caves, vertical pits, and active stream caves (Prelovšek & Knez, 2024). While their location can be generally foreseen on the basis of detailed geological survey and geophysics (Fux et al., 2024), exact location and characteristics are known not earlier than during tunnel excavation. Previous highway projects conducted in the same area revealed an exceptionally high density of caves in this area (Knez & Slabe, 2016). However, while predictive reliability decreases with depth, proximity of water table increases risk of flooding in deep tunnels. Structural impact of a single cave on tunnel stability may be critical for the whole track. The main challenge in tunnelling is unpredictability and bridging of caves, where engineers must ensure structural stability, prevent inflows of water and sediments, and guarantee construction safety. Additionally, all water courses in caves have to be retained since the area serves as the main source of drinking water for Slovene and Italian coastal cities nearby. Conventional mitigation measures such as backfilling with coarse material and shotcrete support are often insufficient and, due to obstruction of underground water flow, inappropriate bridging solutions.

During construction of the Lokev (T1, 6714 m) and Beka (T2, 6017 m) tunnels, 77 caves have been discovered, requiring extensive speleological survey, documentation and continuous adaptation of engineering bridging solutions. This paper presents a comprehensive approach of bridging complex karst phenomenon, namely cave 2TDK-080, which was discovered during the excavation of the Beka tunnel. The cave consists of passages and chambers with complex geometry partly filled with breakdown material, fluvial sediments, and calcite speleothems. While active water courses have been discovered in the lower section, cave sections at the tunnel level indicate relatively frequent flooding creating direct risks for construction site stability and safety. Specific technical measures were implemented, including reinforced concrete arches, hydraulic bypasses, and geotextile lining to protect cave calcite deposits and underground water.

The selection of a suitable engineering solution required a clear understanding of the cave geometry and its relationship to the tunnel alignment. This has been achieved by detailed geolocated 3D cave survey (using Disto X2 and terrestrial 3D scanner) providing point cloud and triangle mesh. Here, BIM modelling played a decisive role by integrating geological surveys, 3D laser scanning, and speleological survey into a unified digital model (Česnik et al., 2023). BIM enabled spatial visualization of caves relative to already performed and planned excavation, testing of alternative structural solutions, and their scheduling and cost optimization (4D/5D) (Švegl, 2024). BIM 4D/5D modeling was performed in the Bexel Manager software environment. (https://bexelmanager.com/). All participants have immediate access to the latest, most up-to-date information, including all technical documentation within the digital platform Dalux (CDE - Common Data Environment), which is the Single Source Of Truth on the Second Track project. This approach marked a significant step forward in reducing geotechnical risks, ensured higher safety, transparency, and efficiency throughout the construction process.

2 Karst Mitigation Measures - Case Study: Cave 2TDK-080

Cave 2TDK-080 is the longest (>600 m) semihorizontal cave developed at the level of the Beka tunnel (Figure 2). Whereas lower cave passages were hydrologically active during exploration, presence of oil flakes of unknown source not connected with Beka tunnel excavation below and at the tunnel level shows occasional water flow and possible flooding of the tunnel. Parts of the cave are directly related to the Škrklovica thrust fault, where caves have been already discover from the surface and during Kastelec highway tunnel construction (Prelovšek & Knez, 2024). Along the fault, limestone was crushed and cracked up to the rock mass quality class of RMR 42–62 and GSI 40–60, indicating fair to poor conditions. Laboratory tests confirmed high variability in strength parameters. The geotechnical analysis recommended consideration of possible cavity flushing during the service life, meaning voids could re-open after initial backfilling. Additional problem is length of tunnel-cave interaction connected with highly acute intersection angle.

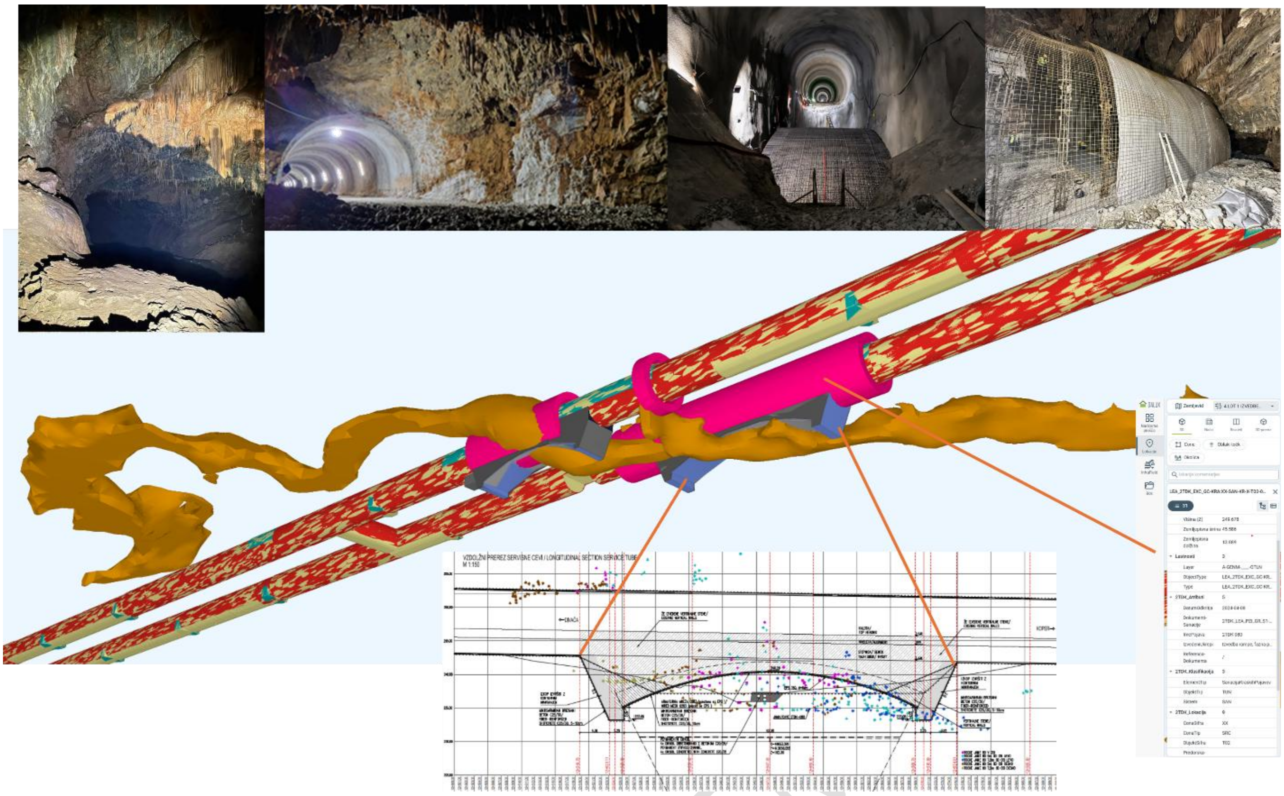

***Figure 1**: Presentation of BIM 3D model of cave 2TDK-080 and construction elements of the cave 2TDK-080 mitigation measures. (https://build.dalux.com).*

The engineering approach included a set of tailor-made mitigation measures based on speleological survey, 3D laser scanning, hydrogeological monitoring, additional exploratory boreholes with GPR survey, and real-time BIM model updates. Key mitigation measures included:

- **Bridging structures in both tunnel tubes:** Reinforced concrete arches and slabs were used to span larger cave voids.
- **Hydrological bypasses:** High-density polyethylene (PE) pipes were laid at the tunnel-cave intersection, embedded in reinforced concrete, ensuring flood resilience while maintaining the structural integrity of the tunnel lining and allowing for undisturbed water courses.
- **Geotextile and shotcrete protections:** Tunnel face, sides and bottom were sealed with geotextile prior to spraying concrete linings and drilling, minimizing shortcrete dispersion, water and cave pollution as well as biological disturbance.
- **Environmental documentation:** Detailed cave mapping and environmental documentation were conducted under the karstological supervision, ensuring documentation of cave characteristics before application of mitigation measures.

2.1 Structural solution – cave 2TDK-080 service pipe

The adopted engineering solution composed of reinforced concrete arch structure spanning 45 m, with a clear width of 9 m and arch radius of 52.8 m. Arch thickness varied from 1.4 m at the crown to 2.2 m at the footings. Foundations were placed on concrete blinding layers and supported by cement-stabilized limestone ground. The cavity was partially backfilled with compacted limestone blocks and excavation spoil, separated by geotextile layers to prevent leakage of drilling mud, erosion and mixing with natural sediments. Four PE pipes DN 400–500 were installed as a permanent hydraulic bypass below service tube, encased in C20/25 concrete to ensure durability against uplift and hydraulic loads. Due to space and other technical limitations a vertical pit had to be excavated before construction of the arch bridge. Shotcrete layers (C25/30, 15 cm thick) reinforced with Q283 meshes, rock bolts, and lattice girders provided immediate support to the vertical pit walls during construction.

2.2 Structural analysis and design verification

A FEM model was prepared in Sofistik, considering non-linear soil–structure interaction based on a Winkler foundation model. The analysis included self-weight, tunnel lining loads, cement stabilization weight, and railway traffic loading according to EN 1991-2 (LM71 and SW/2). Dynamic amplification factors were applied according to TSI INF. Reological effects such as shrinkage and creep were incorporated, with shrinkage equivalent to a temperature drop of 9.9 °C. Seismic verification was carried out with horizontal and vertical design spectra. Results confirmed structural safety for ULS and SLS, with crack widths below serviceability limits and long-term durability ensured for a 100-year design life. Ultimately, the allowed deformation of the structure under maximum railway traffic load at maximum speed proved to be the limiting factor.

2.3 Role of BIM integration

BIM served as a central platform to combine geological mapping, geophysical surveys, laser scanning of caves, and structural design data. The 3D model of the tunnel excavation combined with cave 2TDK-080 allowed for visualization of the arch structure relative to the tunnel alignment and integration of speleological survey data. During the design additional geological boreholes were conducted which provided further information regarding the geological conditions under the tunnel. The geological model was updated accordingly, and the initial design solution had to be adapted (enlarged span and omission of micro-pilots). Time-dependent construction stages were simulated (4D), and cost implications of different design solutions were analyzed (5D). This facilitated transparent communication between designers, contractors, and karstologists, reducing risks during construction and ensuring robust decision-making.

3 Outcome and conclusions

The remediation of cave 2TDK-080 demonstrates how geometrically and hydrologically unfavorable karst phenomena can be successfully bridged using a combination of geotechnical investigations, advanced numerical modelling, and BIM-supported structural solutions. The reinforced concrete arch and hydraulic bypass system ensured safe continuation of tunnelling works and long-term reliability of the infrastructure. The approach provides a reference case for similar projects in karst regions worldwide.

4 References

https://drugitir.si (accessed 04 September 2025)

Prelovšek M., Knez M., 2024. Odkrivanje kraških pojavov na trasi drugega tira. V: Erčulj M. (Editor). Gradnja drugega tira: dosedanje izkušnje in prihodnji načrti. Ljubljana, 2TDK, Družba za razvoj projekta, d.o.o.: 38-48.

Fux J., Schmidt M., Kusnirak D., 2024. Geofizikalne preiskave za zaznavanje kraških pojavov na trasi drugega tira. V: Erčulj M. (Editor). Gradnja drugega tira: dosedanje izkušnje in prihodnji načrti. Ljubljana, 2TDK, Družba za razvoj projekta, d.o.o.: 26-37.

Knez, M., Slabe, T. (Editors), 2016. Cave Exploration in Slovenia. Springer.

Švegl F., 2024. BIM v dimenzijah na 2. tiru. V: Erčulj M. (Editor). Gradnja drugega tira: dosedanje izkušnje in prihodnji načrti. Ljubljana, 2TDK, Družba za razvoj projekta, d.o.o.: 51-61.

https://bexelmanager.com/ (accessed 04 September 2025)

Česnik J., Žigon A., Žibert M., 2023. Izdelava projektne dokumentacije za izvedbo gradnje v okolju BIM. DRUGI tir : nova železniška proga Divača-Koper, 2TDK, Družba za razvoj projekta, d.o.o.

https://build.dalux.com/client/297514/location/default (accessed 04 September 2025)

Impact of ICAO Code E Aircraft on Airport Pavement PCI Values

Zsolt Boros
Filip Buček
TPA Society for Quality Assurance and Innovation, member of STRABAG concern, Slovakia

Abstract

As part of the modernization and strategic development of M. R. Štefánik Airport (BTS) in Bratislava, regular flights by aircraft with an ICAO code E, including the Airbus A350-900, resumed in 2024. These aircraft, with a significantly larger main landing gear span (~10.6 m), generate different load patterns compared to traditional Category C aircraft landing gear span (~5.6 m). Due to the expected redistribution of stresses and potential degradation, a comprehensive visual inspection was conducted prior to the introduction of these aircraft and one year thereafter. The objective was to assess surface damage and determine the impact of wide-body aircraft operations on Portland Cement Concrete (PCC) slabs, as well as the behaviour of the slabs on cross-runways.

Keywords: airfields; increased load influence; visual inspection; pavement condition index; rate of change

1 Introduction

M. R. Štefánik Airport in Bratislava (ICAO code: LZIB) is the largest international airport in the Slovak Republic with two operational runways (RWY 13-31 and RWY 04-22). In 2024, the airport introduced regular operations of ICAO Code E aircraft, including e.g. Airbus A350-900. That decision was applied after extensive calculations and studies to analyse the impact of Type E aircraft on existing pavement structures. Compared to traditional narrow-body Category C aircraft such as Boeing 737, which have a main gear span of approximately 5.5–6.0 meters, Category E aircraft have a significantly wider main gear span of around 10.6 meters. This change has the potential to shift and widen the zones of maximum pavement stress (PCC slabs). As a preventive measure, the airport initiated a two-phase PCI assessment (2024 and 2025) to monitor the evolution of pavement defects and assess the resilience of existing concrete surfaces under new loading conditions.

2 Methodology and Visual Inspection Procedure

The inspection procedure followed the ASTM D5340-20 and UFC 3-260-16 guidelines. Visual diagnostics were conducted in 2024 and 2025 across all operational runways (RWY 13-31, RWY 04-22) and taxiway (TWY F) surfaced with PCC slabs. Trained personnel documented defect types, severity levels (L-M-H), and recorded observations on standard PCI survey sheets. Data were processed using the certified PAVER 7.1 software to compute Pavement Condition Index (PCI) scores for individual sampling units.

Defects monitored included:

- Shrinkage cracks and cracks across full slab width;
- Broken or damaged slab corners and edges;
- Joint seal damage;
- Small and large patches;
- Surface spalling and disintegration;
- Faulting (vertical step at joints).

Defects were geolocated and compared between 2024 and 2025, allowing analysis of the change rate in pavement condition.

The data outputs obtained from the PCI survey included not only the standard PCI value maps, both at the local level for the 20 selected slabs and at the global level for the entire pavement area, but also several additional analytical outputs that go beyond common practice. For each individual defect type identified and described in the previous chapter, a dedicated occurrence map was developed for the entire airport pavement area. These thematic maps provide airport administrators with a more detailed overview of the spatial distribution of individual defects and significantly support more effective maintenance planning and prioritization of repair interventions. Figure 1 presents an example of the distress map for the broken slab corner defect. A colour spectrum is used to indicate the severity level of the distress, where yellow represents low severity, orange medium severity, and red high severity.

3 PCI Change and Impact of Aircraft Category E

Table 1 summarizes average overall PCI values before and after the introduction of Category E operations on selected areas.

Between 2024 and 2025, PCI values remained largely stable across most airfield sections. RWY 13/31 showed a negligible improvement (+0.1) caused by effective maintenance, while RWY 04/22 experienced a slight decline (−0.8), both indicating consistent pavement condition. Taxiway F also saw a minimal decrease (−0.6), suggesting no immediate concern. Overall, the data reflect steady conditions with localized issues requiring targeted intervention.

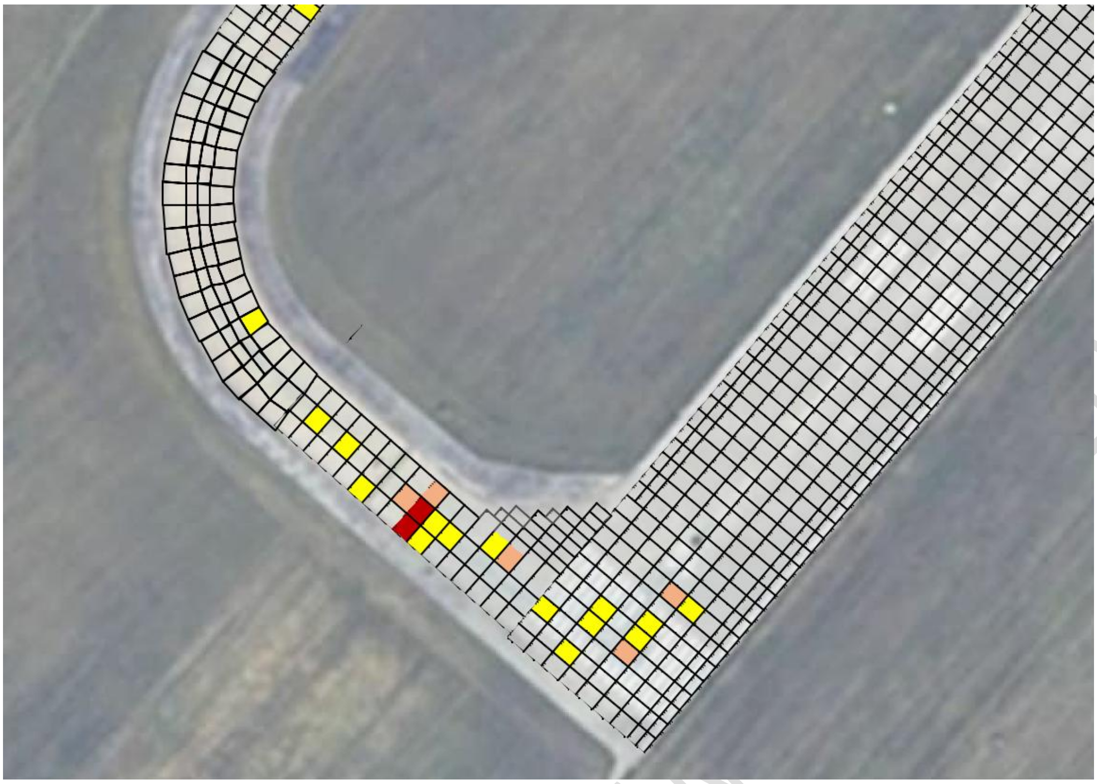

***Figure 1**: Broken slab corner defect occurrence map.*

***Table 1**: PCI value change between 2024 and 2025.*

Section	PCI 2024	PCI 2025	Change
RWY 13/31 main part	67.4	67.5	+0.1
RWY 04/22 main part	72.2	71.4	-0.8
TWY F	63.1	62.5	-0.6

4 Cross-Runway Pavement Behaviour

To better understand lateral loading effects, PCI changes were mapped on both runways transversely along slab strip A through H, with slab width of 7,5 m. Aircraft with large main gear spans introduce edge loading in strips C and F, which are not usually affected by narrower gear footprints. This was confirmed by measurable PCI decreases in these strips.

On RWY 13-31, the most significant PCI drops occurred in strips C (-1.36) and F (-1.17), while strips D and E—located under the direct load path—remained stable or improved. This supports the hypothesis that Category E aircraft, due to their wider gear base, contribute to deterioration not only in the central wheel path, but also in adjacent lanes due to lateral drift or touchdown offset during landings.

On RWY 04-22, the pattern was even more pronounced. Strip F dropped by -2.17 points to a critical PCI of 50.69. Strip C also declined by -1.67. These are attributed to Category E aircraft approaching and landing in lateral offset conditions. This observation is consistent with operational practice and aircraft geometry.

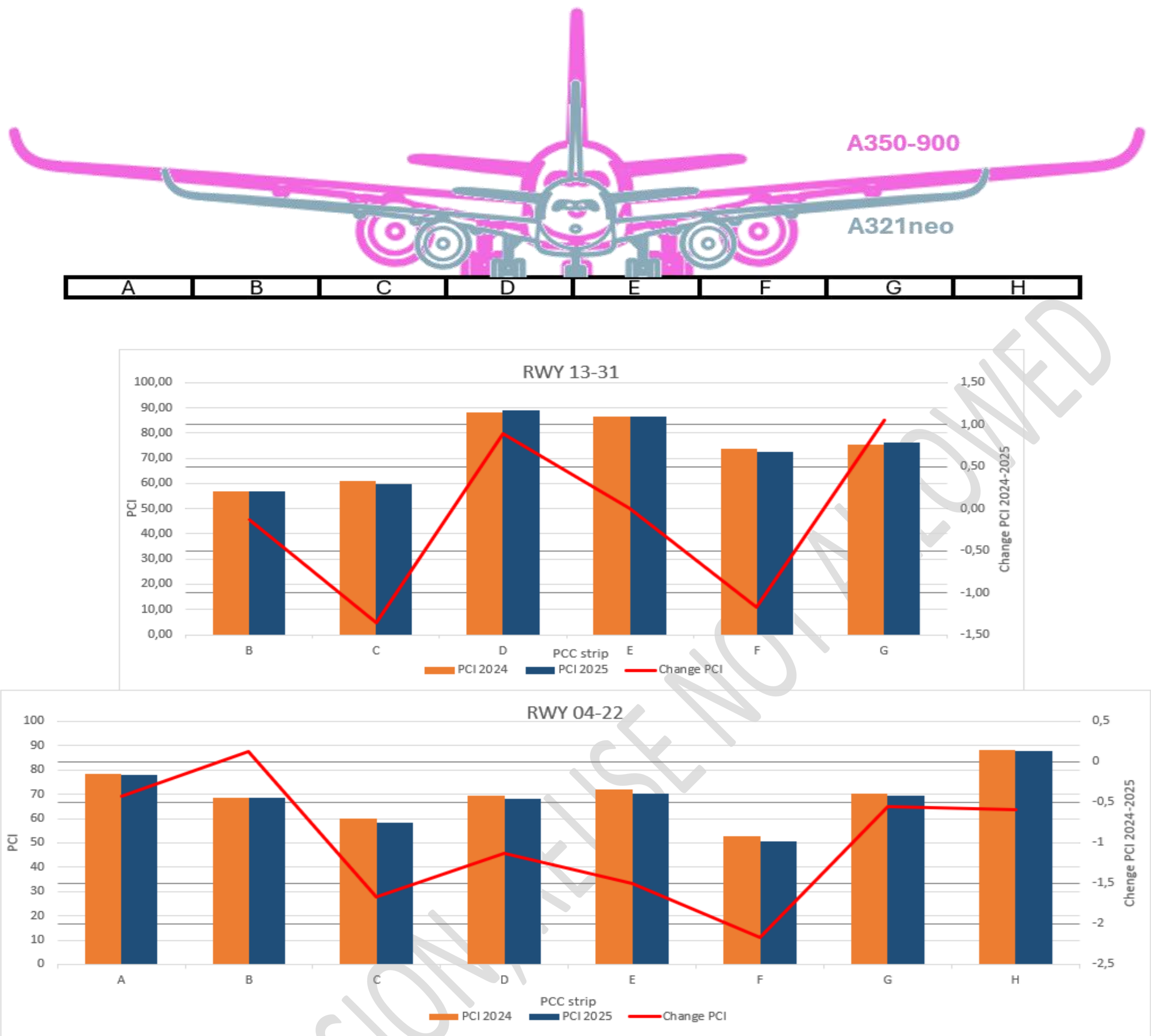

Figure 2: PCI Change in Crosswise Slab strips on RWY 04-22.

Possible reasons for higher PCI drops in strips C and F than in strips D and E are:

- Localized repairs and maintenance in the most exposed strips in 2024 – strips D and E;
- Significant parts of strips D and E consist of new replaced slabs;
- Lower initial PCI values in strips C and F – values of PCI are lower than 70, which is a breakpoint, when accelerated deterioration starts (fig. 3), while strips D and E are above PCI 70.

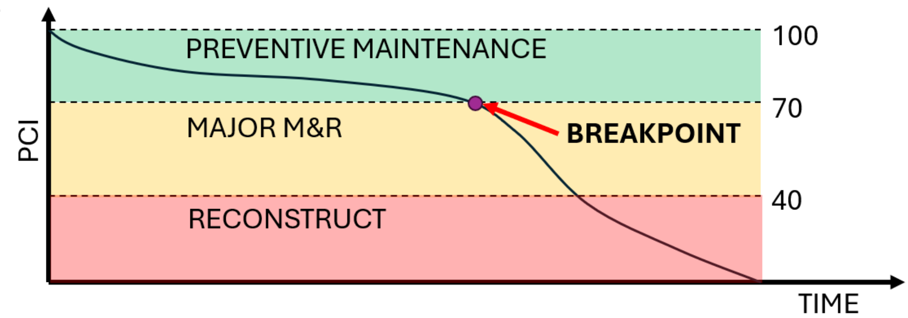

***Figure 3**: Deterioration model of PCI.*

5 Conclusions

One year after the launch of Category E aircraft operations at BTS, a PCI-based comparison confirms that overall pavement conditions remain stable in primary load zones, while minimal increases in surface degradation are present in adjacent slab strips. The key findings include:

- Localized PCI drops in slab strips adjacent to main gear loads of wide-body aircrafts (strips C and F);
- The importance of preventive maintenance of selected slab strips and slab repairs in resisting new aircraft loads.

Despite the introduction of wide-body aircraft in Category E to the serviced fleet, wear trends on the runways remain minimal, though still measurable. The deployment of aircraft such as the Airbus A350-900 has a quantifiable impact on load distribution across the pavement. While the main landing gear of this aircraft primarily loads central slabs D and E, its gear span (approximately 10.6 m) causes lateral movement during landing, extending the load into slabs C and F. These areas show the most notable PCI decreases on both runways, supporting the hypothesis of load spread beyond traditional zones.

The study validates the hypothesis that wider gear configurations redistribute load paths and lead to measurable degradation outside standard wheel tracks. It is recommended to continue periodic PCI monitoring, particularly in transition zones, to support preventive maintenance and asset management.

6 References

ASTM International. 2020. ASTM D5340-20. Standard Test Method for Airport Pavement Condition Index Surveys. ASTM International, West Conshohocken, PA.

UFC 3-260-16. Airfield Pavement Condition Evaluation. United States Department of Defense, Unified Facilities Criteria.

TPA. 2024. Bratislava. PCI Report: Letisko M. R. Štefánika – Bratislava, 2024.

TPA. 2025. Bratislava. PCI Report: Letisko M. R. Štefánika – Bratislava, 2025.

Investigation of structural capacity and surface defects on municipal roads in metropolitan area of Stockholm, Sweden

Calle Ossbahr
Martin Wiström
Ramboll RST, Sweden

Abstract

The introduction of TSDD (Traffic Speed Deflectometer Device) measurements has created new opportunities for large-scale network investigations. This paper presents the findings from a large-scale investigation of the main municipal road network in the metropolitan area of Stockholm, Sweden. The project demonstrates how network-wide investigations can be carried out within a short time frame, with no traffic interruption and improved traffic safety compared with traditional stationary measurement methods. The investigation included structural data from a TSDD and GPR (Ground Penetrating Radar) measurements, together with surface condition and crack data from LCMS (Laser Crack Measurement System) and Laser RST (Road Surface Tester). The combined dataset was cross-analysed to support long-term planning of resurfacing and reinforcement measures, identify potential risk sections in relation to current and future traffic loading, and assess the implications of allowing 74-tonne transports on parts of the network. The data were aggregated and automatically segmented into homogeneous road sections to provide an interpretable basis for maintenance planning, prioritization, and assessment of economic effects. The results showed limited direct correlation between structural capacity and surface characteristics based on a single measurement campaign. Nevertheless, the dataset provided a robust basis for establishing a baseline for future condition monitoring, estimating the maintenance backlog, proposing measures and indicating where certain investments would provide the greatest benefit for the available funding. The project demonstrates the value of combining structural capacity, surface condition, and traffic loading data to support proactive pavement management at the municipal level.

Keywords: TSDD (Traffic Speed Deflectometer Device); RAPTOR; GPR (Ground Penetrating Radar); LCMS (Laser Crack Measurement System); laser RST (Road Surface Tester); network-wide investigations; structural capacity, surface characteristics; correlation

1 Introduction

Ramboll RST has an ongoing project with Stockholm City with the aim to support them in making data-driven decisions based on objective measurement data for planning maintenance and reinforcement measures on Stockholm's road network.

For the goal to be achieved, the city's main roads have been mapped with TSDD, GPR, and Laser RST/LCMS. A total of 375 km of roads were measured in both directions divided into about 250 links over a week in mid-July 2025. Measurements were carried out at night to minimize both the impact on other traffic and vice versa minimize the impact on the measurements due to traffic. Some of the measurements are more sensitive to start and stop and it is desirable to maintain an even speed during measurement, which can be difficult in an urban environment. The investigations were carried out with two separate vehicles shown in Figure 1. The left side shows a Laser RST equipped with dual 360 cameras, LiDAR-scanners for the road corridor, and LCMS that scan the road surface for transversal/longitudinal evenness and automated surface defect detection. The right side shows Ramboll RAPTOR (TSDD) equipped with GPR antennas that measure the structural condition of the roads.

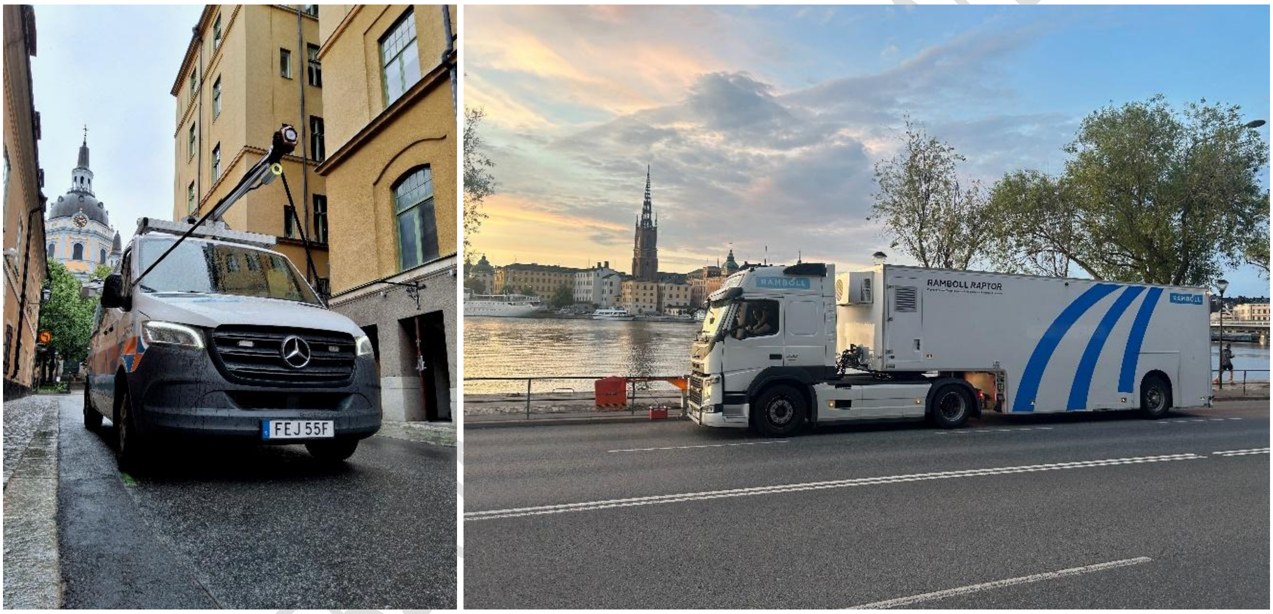

Figure 1: *Utilised equipment for road scanning to the left and Ramboll RAPTOR to the right.*

2 Results

After data collection, the data was processed and quality controlled. Approximately 1% of the total measured length was deemed invalid for various reasons, including starts and stops, sharp turns, and off-track measurements. This is considered a successful outcome for this type of measurement in an urban environment. Covering an entire main road network with such a high level of detail in both surface condition and structural capacity provides a comprehensive basis for analysis. If a corresponding investigation had been carried out using traditional methods, such as FWD (Falling Weight Deflectometer) testing instead of traffic-speed deflection measurements and manual visual damage mapping instead of LCMS, the fieldwork would likely have taken several months. In addition to the time savings, the traffic-speed approach also reduced disruption to other traffic and improved traffic safety. The measured road network is shown in Figure 2.

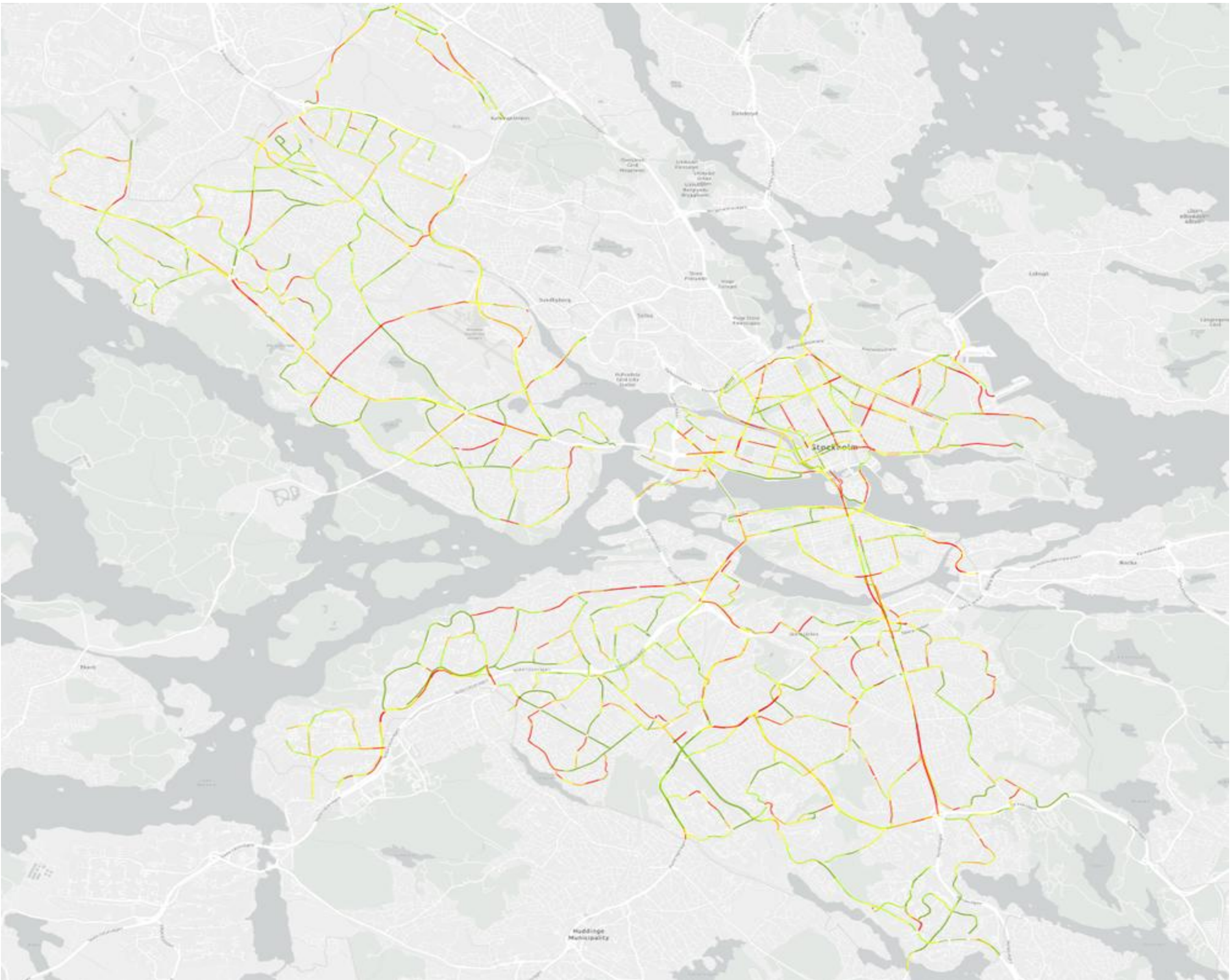

Figure 2: *The measured road network in Stockholm.*

During the initial analyses, parameters such as surface modulus and subgrade modulus from the deflection measurements were studied. The GPR measurements provided after interpretation valuable information on asphalt thickness, overall structural thickness and the risk of tar- or bitumen-saturated macadam containing carcinogenesis PAH (Polycyclic Aromatic Hydrocarbons). From the initial analysis of the road surface measurements, the main parameters used were rut depth, longitudinal evenness (IRI), and cracking. The data were averaged before being divided into homogeneous sections.

To provide an overview of the condition of the municipal road network, the distributions of these parameters are presented as pie charts in Figure 3.

To relate bearing capacity to traffic loading, the required reinforcement was calculated using two methods. The first measure, referred to as RamOverlay, is based on asphalt strain derived from the deflection basin. Using mechanistic-empirical reference calculations (Trafikverket, 2022), asphalt is added until the strains reach the required level corresponding to the Swedish definition of “bearing capacity class 1” for the relevant traffic loading (Trafikverket, 2019). The second measure, referred to as FinOverlay, is based on the surface modulus and Odemark’s method of equivalence, in which the entire road structure is converted into a single equivalent material. Target moduli were defined based on traffic loading, and asphalt is added to the structure until the target modulus is reached (Odemark, 1949).

To assess the relationships between the different measured parameters, a correlation analysis was performed; the results are presented in Figure 4. Both total traffic volume and total heavy traffic volume were included in the analysis.

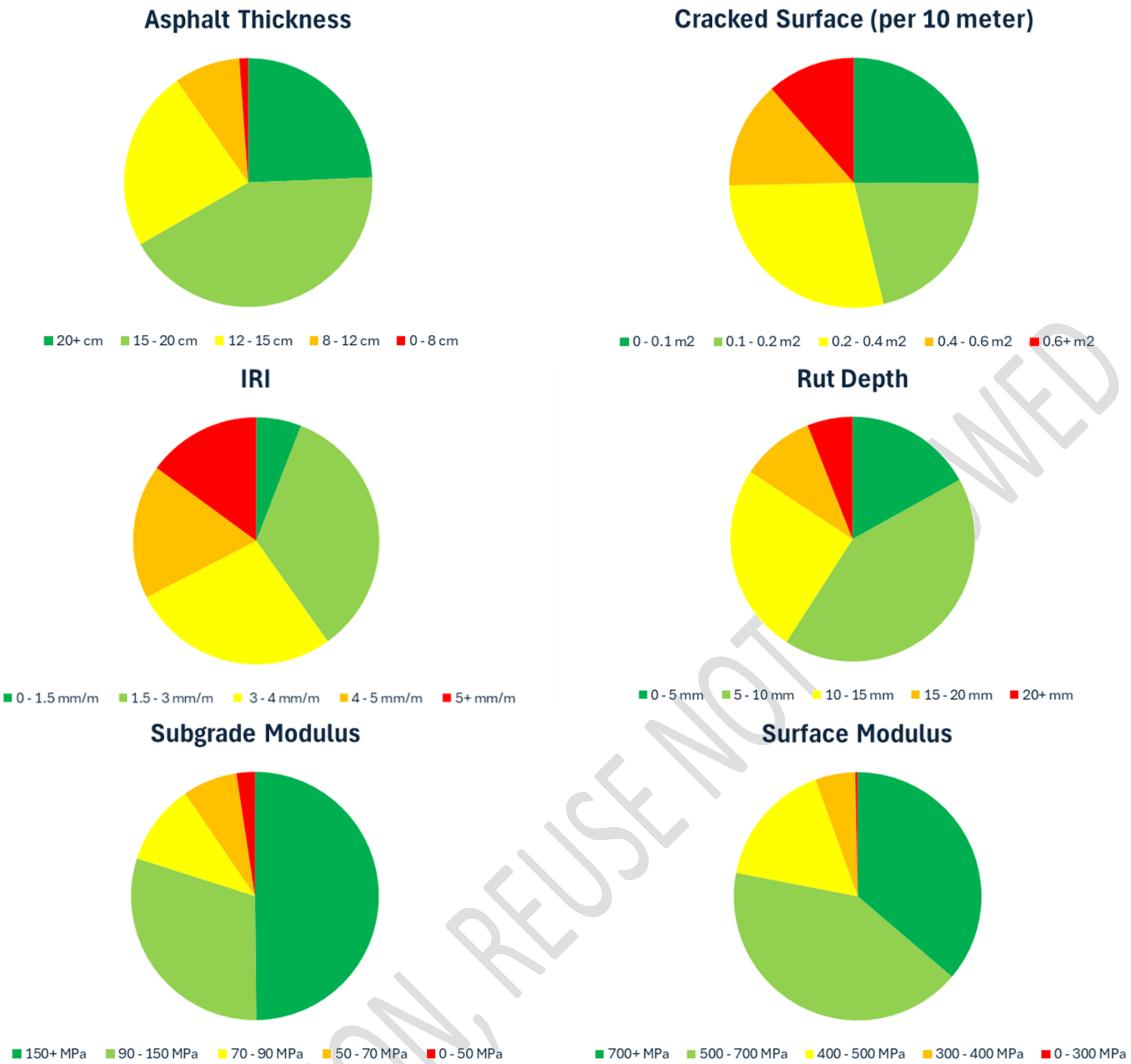

Figure 3: *Distribution of selected measured parameters in Stockholm City.*

	Surface modulus	Subgrad modulus	Asphalt thickness	Risk of PAH	IRI Max	Rut depth	Cracking	Traffic Volume	Heavy Traffic Volume	Reinforcement (FinOverlay)	Reinforcement (RamOverlay)
Surface modulus	-										
Subgrad modulus	70%	-									
Asphalt thickness	26%	1%	-								
Risk of PAH	6%	5%	5%	-							
IRI Max	18%	14%	12%	1%	-						
Rut depth	3%	4%	1%	8%	24%	-					
Cracking	2%	1%	5%	2%	8%	23%	-				
Traffic Volume	32%	19%	28%	3%	27%	9%	19%	-			
Heavy Traffic Volume	15%	11%	13%	2%	8%	1%	8%	18%	-		
Reinforcement (FinOverlay)	37%	25%	6%	1%	1%	8%	8%	17%	10%	-	
Reinforcement (RamOverlay)	39%	2%	32%	3%	4%	4%	10%	26%	15%	37%	-

Figure 4: *Correlation between parameters from the Stockholm City dataset.*

It is notable that there is almost no direct correlation between the bearing capacity parameters and the surface characteristics. This was not unexpected, as the unknown time elapsed since the most recent maintenance or rehabilitation measure complicates the interpretation of these relationships. Weak correlations could, however, be observed within the structural capacity parameters, within the surface characteristic parameters, and in relation to traffic loading.

To investigate the surface characteristics in greater detail, a further analysis of the LCMS data was performed. The previously aggregated cracking parameter was disaggregated into several more detailed parameters, including the total area of cracks grouped by width, together with two additional parameters used to identify ravelling, potholes, and alligator cracking. Manholes and curb drops were excluded from the data. The delivered dataset consists of five views for each section, showing, from top to bottom: 1) the total volume missing from a flat reference profile and its location, 2) the area affected by probable ravelling, 3) an intensity image of the road surface with the LCMS analysis overlay, 4) an intensity image of the road surface, and 5) a crack grid coloured according to crack width. These views were delivered to the client in GIS for every 10-metre section of the measurement.

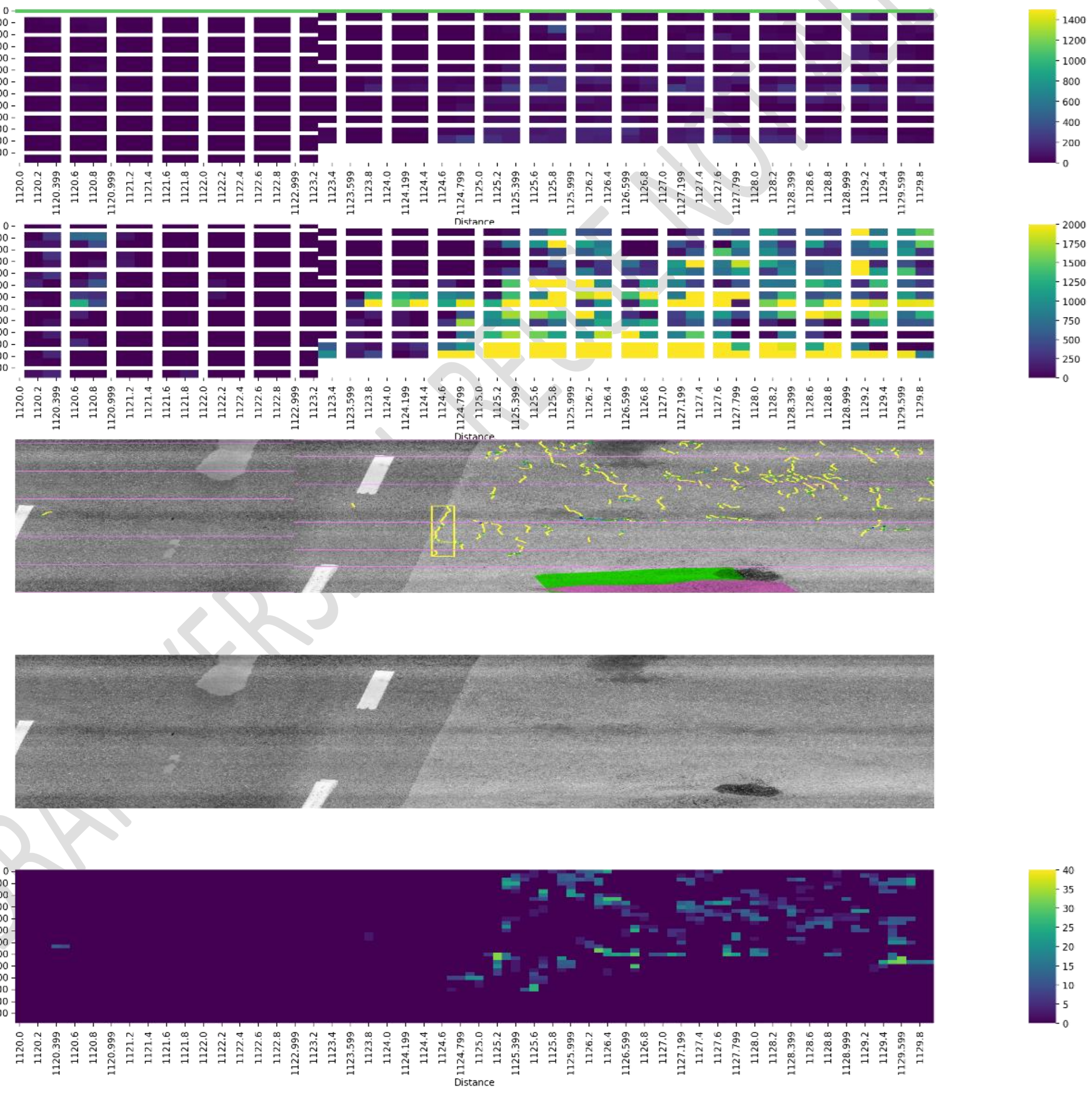

Figure 5: *Five views used for the LCMS data analysis.*

A second correlation analysis was performed using the more detailed classification of cracks and surface defects. The results are presented in Figure 6.

	Surface modulus	Subgrade modulus	Asphalt thickness	Risk of PAH	Reinforcement (FinOverlay)	Reinforcement (RamOverlay)	IRI Max	Rut depth	Cracking Area	Ravelling Area	Ravelling Volume	Small Cracks	Medium Cracks	Large Cracks
Surface modulus	-													
Subgrade modulus	69%	-												
Asphalt thickness	28%	2%	-											
Risk of PAH	6%	5%	4%	-										
Reinforcement (FinOverlay)	37%	25%	8%	0%	-									
Reinforcement (RamOverlay)	40%	2%	34%	2%	38%	-								
IRI Max	18%	14%	11%	1%	1%	3%	-							
Rut depth	6%	7%	1%	9%	9%	6%	23%	-						
Cracking Area	1%	1%	3%	1%	9%	11%	9%	23%	-					
Ravelling Area	8%	7%	5%	0%	3%	1%	23%	24%	16%	-				
Ravelling Volume	10%	4%	8%	2%	5%	7%	11%	9%	29%	20%	-			
Small Cracks	1%	1%	5%	3%	6%	9%	0%	16%	66%	3%	28%	-		
Medium Cracks	9%	6%	7%	1%	5%	4%	22%	27%	48%	19%	11%	53%	-	
Large Cracks	9%	6%	7%	0%	4%	2%	21%	22%	36%	24%	6%	35%	61%	-

Figure 6: *Extended correlation analysis between parameters from the Stockholm City dataset.*

No new correlations between structural capacity and surface characteristics could be identified. However, a stronger correlation was observed between rutting and medium to large cracks than between rutting and small cracks. This is not surprising, as greater rut depth may indicate a longer time since the last resurfacing, allowing more time for cracks to develop.

The assessment indicated that 74-tonne transports are unlikely to pose a major challenge across most of the investigated road network, due to generally favourable structural conditions, including thick pavement structures and good bearing capacity.

3 Data-Driven Support for Maintenance and Reinforcement Planning

A central objective of the project was to transform the extensive measurement data into practical decision support for the client. This required identifying how the measurements could create value for the municipality, how the most important findings could be highlighted, how the data could be aggregated without losing relevant detail, and how the results could be summarised in a form suitable for maintenance and reinforcement planning.

The data was aggregated and automatically segmented into homogeneous sections to make the results easier to interpret and apply in the planning process.

To make the best use of the investigation results, the data were primarily analysed with the aim of identifying road sections requiring one of the following types of measure: 1) resurfacing, 2) patching and crack sealing, or 3) more extensive reconstruction to improve structural capacity.

1. The need for resurfacing was primarily determined through a combined assessment of rut depth, IRI, and the overall road surface condition derived from the LCMS data.
2. Sections suitable for patching and crack sealing, rather than full resurfacing, were identified with particular emphasis on cracking and surface characteristics. These were preferably sections with relatively low rut depth, where resurfacing would otherwise be required mainly to improve ride quality.
3. Sections requiring reinforcement due to low structural capacity in relation to traffic loading were identified and analysed together with other candidate sections. The classification was based on how the structural capacity varied at different depths, using the RamOverlay and FinOverlay measures. These sections were primarily considered potential investments for reducing long-term maintenance costs across the road network.

To support the selection of appropriate measures, field studies were carried out together with the client, and each road section's history and priority were also considered in the assessment.

To help distinguish between road sections in poorer and better condition, automated signal processing using the PELT ruptures python function (Truong et al., 2020) was applied to create a clearer basis for decision-making. Figure 7 presents an example of how the original 10-metre data were converted into homogeneous sections.

Figure 7: *Example of data segmentation, showing 10-metre data on the left and automatically segmented homogeneous sections on the right.*

4 Conclusions

One of the main conclusions is that the direct correlation between structural capacity and surface characteristics is limited when based on a single measurement campaign. A one-time measurement does not provide the temporal dimension required to establish strong relationships between structural condition, surface defects, and deterioration over time. Repeated LCMS measurements of the road surface, combined with repeated bearing capacity measurements, would provide a stronger basis for predicting pavement deterioration and optimising future resurfacing and reinforcement planning.

Stockholm City currently lacks a Pavement Management System (PMS) that documents current and historical road conditions or previous rehabilitation measures in a structured way. The measurements carried out in this project therefore provide an important baseline for future monitoring of condition changes across the road network. Where historical information was available, it was also possible to study condition development on selected sections and use this information to support the interpretation and calibration of the measurement data.

A Road Status Index is being implemented to combine several key parameters into a single aggregated and easily interpretable indicator. This will provide the city's maintenance planners with a practical basis for comparing road sections, identifying priorities, and communicating the overall condition of the network.

Involving the client throughout the development and analysis of the data was important for ensuring that the results were relevant, understandable, and applicable in practice. This collaborative process also helped create a sense of ownership of the data and increased the likelihood that the results will be used effectively in future planning.

For the results to support decision-making, the large amount of detailed measurement data had to be aggregated and presented in a form that was easy to interpret. The choice of aggregation and segmentation method can influence how the condition of the network is perceived, making transparency in the processing method important.

Overall, the measurement results supported budgeting and maintenance planning by providing the client with an estimate of the maintenance backlog, as well as indications of where investments are likely to generate the greatest benefit for the available funding. The project thereby demonstrates the value of combining structural capacity, surface condition, and traffic loading data to support more proactive and cost-effective pavement management at the municipal level.

5 References

Trafikverket, 2019. TDOK 2019:0463 – Utvärdering av vägkonstruktioners bärighet med fallviktsapparat. Borlänge: Trafikverket.

Trafikverket, 2022. PMS-Objekt. Borlänge: Trafikverket. https://bransch.trafikverket.se/for-dig-i-branschen/teknik/Tekniska-dokument/Vagteknik/PMS-Objekt/ [dostop 1. 2. 2022].

Odemark, N., 1949. Undersökning av elasticitetsegenskaperna hos olika jordarter samt teori för beräkning av beläggningar enligt elasticitetsteorin. Stockholm: Statens Väginstitut.

Truong, C., Oudre, L. & Vayatis, N., 2020. Selective Review of Offline Change Point Detection Methods. Signal Processing, 167, 107299. doi:10.1016/j.sigpro.2019.107299.